Methods in Molecular Biology 1336

Springer Protocols

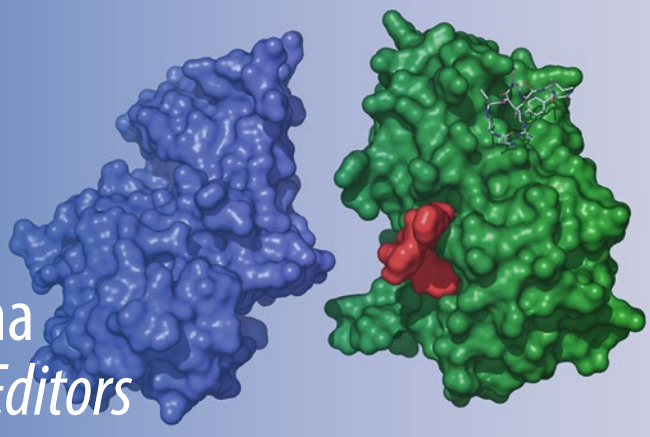

Mar Orzáez
Mónica Sancho Medina
Enrique Pérez-Payá *Editors*

Cyclin-Dependent Kinase (CDK) Inhibitors

Methods and Protocols

Humana Press

METHODS IN MOLECULAR BIOLOGY

Series Editor
John M. Walker
School of Life and Medical Sciences
University of Hertfordshire
Hatfield, Hertfordshire, AL10 9AB, UK

For further volumes:
http://www.springer.com/series/7651

Cyclin-Dependent Kinase (CDK) Inhibitors

Methods and Protocols

Edited by

Mar Orzáez

Medicinal Chemistry, Centro de Investigación Príncipe Felipe, Valencia, Spain

Mónica Sancho Medina

Medicinal Chemistry, Centro de Investigación Príncipe Felipe, Valencia, Spain

Enrique Pérez-Payá

IBV-CSIC and Centro de Investigacion Príncipe Felipe, Valencia, Spain

Humana Press

Editors
Mar Orzáez
Medicinal Chemistry
Centro de Investigación Príncipe Felipe
Valencia, Spain

Mónica Sancho Medina
Medicinal Chemistry, Centro de Investigación Príncipe Felipe
Valencia, Spain

Enrique Pérez-Payá
IBV-CSIC and Centro de Investigacion Príncipe Felipe
Valencia, Spain

ISSN 1064-3745 ISSN 1940-6029 (electronic)
Methods in Molecular Biology
ISBN 978-1-4939-2925-2 ISBN 978-1-4939-2926-9 (eBook)
DOI 10.1007/978-1-4939-2926-9

Library of Congress Control Number: 2015944984

Springer New York Heidelberg Dordrecht London

Printed on acid-free paper

Humana Press is a brand of Springer
Springer Science+Business Media LLC New York is part of Springer Science+Business Media (www.springer.com)

Preface

Proliferation of eukaryotic cells is under control of a series of concerted molecular mechanisms defined as the cell division cycle whose progression is tightly governed by members of the cyclin-dependent kinase family (CDKs). At different phases of the cell cycle, the CDKs associate with specific cyclins. These particular CDK/cyclin pairs preferentially phosphorylate sets of largely distinct substrates triggering the progression through the cell cycle phases. For example, CDK2/cyclin E mediated phosphorylation of the tumor suppressor protein pRb is required for inactivation of the protein and for the subsequent release of E2F transcription factor, altering the status of E2F-regulated genes from fully repressed to induced and leading progression through G1 to S phases.

Deregulation of CDK function is a hallmark of cancer. Aberrations in CDK activity have also been observed in viral infections, neurological diseases, ischemia, and some proliferative disorders. This has led to the intensive research on CDK inhibitors for therapeutic applications.

Several strategies have been used to inhibit these complexes such as development of ATP-competitive inhibitors, molecules targeting the CDK/cyclin interaction surfaces or inhibitors mimicking natural CDK inhibitor proteins (CKIs). However, clinical development has not been as successful as expected. More precise details of how inhibitors behave in different disease models remain to be elucidated and more specific inhibitors with improved pharmacological characteristics still need to be developed.

Protocols to develop screening assays or to identify novel CDK inhibitors have been compiled in the first part of the book. Future work in this area will reveal novel targets for pharmacological interference and could lead to more specific urgently needed cell cycle inhibitors. The second part of the book describes elaborate procedures to evaluate activity and mechanism of action of new and/or already identified CDK inhibitors. A number of expert laboratories have developed specific techniques to study many aspects of CDK inhibitors activity in cell culture and in vivo models. The book also compiles protocols to evaluate metabolomics changes associated with inhibitor treatment. Moreover, drug delivery strategies focused on nanoparticle development to provide alternative internalization systems for increasing inhibitor efficacy have been also described. We hope this collection will be a relevant source of information for drug discovery in cell cycle research.

This project would not have been possible without the help of some key people. Thank you to Dr. John Walker and Anna Rakovsky for providing support along the way. We would like to thank all the authors for their excellent contributions throughout this project. These protocols and the notes shared by each author will form a worthwhile tool for scientists interested in this research field. Finally, we would like to dedicate the book to the memory of Professor Enrique Pérez-Payá.

Valencia, Spain

Mar Orzáez
Mónica Sancho Medina

Contents

Contributors

Deepak Adhikari • *Department of Chemistry and Molecular Biology, University of Gothenburg, Gothenburg, Sweden*

Daniel Alvira • *Centre Mediterranéen de Médecine Moléculaire (C3M), Biology and pathology of melanocyte cells: from skin pigmentation to melanomas, Institut National de la Santé et de la Recherche Médicale (INSERM), Nice, France*

Oriol Bachs • *Department of Cell Biology, Immunology and Neurosciences, University of Barcelona, Barcelona, Spain; Institut d'Investigacions Biomèdiques August Pi i Sunyer (IDIBAPS), Barcelona, Spain*

Ilaria Dutto • *Genome Stability Group, Department of Biology and Biotechnology, Istituto di Genetica Molecolare del CNR, University of Pavia, Pavia, Italy*

Rosa Farràs • *Oncogenic Signaling Laboratory, Centro de Investigación Príncipe Felipe de Valencia, Valencia, Spain*

Jennifer M. Felton • *MRC Centre for Inflammation Research, The Queen's Medical Research Institute, The University of Edinburgh, Edinburgh, UK*

Edurne Gallastegui • *Department of Cell Biology, Immunology and Neurosciences, University of Barcelona, Barcelona, Spain; Institut d'Investigacions Biomèdiques August Pi i Sunyer (IDIBAPS), Barcelona, Spain*

Anna Gortat • *Department of Anatomical Pathology, Pharmacology and Microbiology, University of Barcelona, Barcelona, Spain*

Asterios I. Grigoroudis • *Department of Biochemistry, Veterinary School, University of Thessaly, Karditsa, Greece*

Tatiana Guevara • *Laboratory of Peptide and Protein Chemistry, Centro de Investigación Príncipe Felipe, Valencia, Spain*

Hiroshi Hirai • *Taiho Pharmaceutical Co. Ltd., Tsukuba Research Center, Tsukuba, Ibaraki, Japan*

Laura J. Hoodless • *MRC Centre for Inflammation Research, The Queen's Medical Research Institute, The University of Edinburgh, Edinburgh, UK*

Karthiga Arumugasamy • *Computer Aided Drug Designing and Molecular Modeling Lab, Department of Bioinformatics, Alagappa University, Karaikudi, Tamil Nadu, India*

George Kontopidis • *Department of Biochemistry, Veterinary School, University of Thessaly, Karditsa, Greece*

Kui Liu • *Department of Chemistry and Molecular Biology, University of Gothenburg, Gothenburg, Sweden*

José L. Mascareñas • *Centro Singular de Investigación en Química Biolóxica e Materiais Moleculares (CIQUS), Departamento de Química Orgánica, Universidade de Santiago de Compostela, Santiago de Compostela, Spain*

Laura Mondragón • *Centre Mediterranéen de Médecine Moléculaire (C3M), Biology and pathology of melanocyte cells: from skin pigmentation to melanomas, Institut National de la Santé et de la Recherche Médicale (INSERM), Nice, France*

Yoko Nakatsuru • *Taiho Pharmaceutical Co. Ltd., Tsukuba Research Center, Tsukuba, Ibaraki, Japan*
Martina Palomino-Schätzlein • *Structural Biochemistry Laboratory, Advanced Therapies Program, Centro de Investigación Príncipe Felipe, Valencia, Spain*
Elena Pazos • *Centro Singular de Investigación en Química Biolóxica e Materiais Moleculares (CIQUS), Departamento de Química Orgánica, Universidade de Santiago de Compostela, Santiago de Compostela, Spain*
Beatriz Pérez-Benavente • *Oncogenic Signaling Laboratory, Centro de Investigación Príncipe Felipe de Valencia, Valencia, Spain; Biochemistry and Molecular Biology Department, Universidad de Valencia, Valencia, Spain*
Enrique Pérez-Payá • *IBV-CSIC and Centro de Investigación Príncipe Felipe, Valencia, Spain*
Antonio Pineda-Lucena • *Structural Biochemistry Laboratory, Advanced Therapies Program, Centro de Investigación Príncipe Felipe, Valencia, Spain*
Reena Pinhero • *Department of Molecular Biology and Genetics, University of Guelph, Guelph, ON, Canada*
Ennio Prosperi • *Genome Stability Group, Department of Biology and Biotechnology, Istituto di Genetica Molecolare del CNR, University of Pavia, Pavia, Italy*
Sanjiv Risal • *Department of Chemistry and Molecular Biology, University of Gothenburg, Gothenburg, Sweden*
Calum T. Robb • *MRC Centre for Inflammation Research, The Queen's Medical Research Institute, The University of Edinburgh, Edinburgh, UK*
Adriano G. Rossi • *MRC Centre for Inflammation Research, The Queen's Medical Research Institute, The University of Edinburgh, Edinburgh, UK*
Poonam Singh • *Division of Toxicology, CSIR-Central Drug Research Institute, Lucknow, India*
Sanjeev Kumar Singh • *Computer Aided Drug Designing and Molecular Modeling Lab, Department of Bioinformatics, Alagappa University, Karaikudi, Tamil Nadu, India*
Micol Tillhon • *Genome Stability Group, Department of Biology and Biotechnology, Istituto di Genetica Molecolare del CNR, University of Pavia, Pavia, Italy*
Sunil Kumar Tripathi • *Computer Aided Drug Designing and Molecular Modeling Lab, Department of Bioinformatics, Alagappa University, Karaikudi, Tamil Nadu, India*
Carl S. Tucker • *BHF Centre for Cardiovascular Science, The Queen's Medical Research Institute, The University of Edinburgh, Edinburgh, UK*
M. Eugenio Vázquez • *Centro Singular de Investigación en Química Biolóxica e Materiais Moleculares (CIQUS), Departamento de Química Orgánica, Universidade de Santiago de Compostela, Santiago de Compostela, Spain*
Krassimir Yankulov • *Department of Molecular Biology and Genetics, University of Guelph, Guelph, ON, Canada*

Chapter 1

Immunoprecipitation of Cdk–Cyclin Complexes for Determination of Kinase Activity

Edurne Gallastegui and Oriol Bachs

Abstract

Cyclin-dependent kinases (Cdks) belong to a family of key regulators of cell division cycle and transcription. The activity of some of them is deregulated in tumor cells and to find specific inhibitors is an important goal to be achieved. We report here the current methods to determine their in vitro activity in order to facilitate the identification of specific inhibitors. Mainly, the activity can be determined by using immunoprecipitates from cell samples with antibodies against specific Cdks as a source of the enzymes.

Key words Cdk2, Cdk4, Cdk6, Cdk1, Cyclin A, Cyclin B, Cyclin D, Kinase assay

1 Introduction

Cyclin dependent kinases (CDKs) are serine/threonine kinases characterized by needing a regulatory subunit (cyclin) that by associating with the enzyme provides domains necessary for the catalytic activity [1]. This family of kinases includes 20 members that recently have been renamed as Cdk1 through to Cdk20 [2]. From the functional point of view this family of kinases participates in two major cellular roles: cell division cycle and transcription. The analysis of evolutionary expansion of the Cdk family in mammals allows to classify these enzymes into three cell-cycle related subfamilies: Cdk1, Cdk4, and Cdk5 and five transcriptional subfamilies: Cdk7, Cdk8, Cdk9, Cdk11, and Cdk20 [3]. Most of these Cdks bind one or a few cyclins that confers to these specific complexes a functional specialization [1]. The cyclin family (the regulatory subunits of Cdks) contains approximately 29 proteins in humans clustered in three major groups: cyclin B group, mostly associated to cell cycle related Cdks, the cyclin I group, the partners of Cdk5 and the cyclin C group, the major partners of transcriptional Cdks. Thus, a significant number of specific Cdk–cyclin complexes can be generated and it is assumed that each one of

Mar Orzáez et al. (eds.), *Cyclin-Dependent Kinase (CDK) Inhibitors: Methods and Protocols*, Methods in Molecular Biology, vol. 1336, DOI 10.1007/978-1-4939-2926-9_1,

these complexes have, at least in some degree, specific substrate specificity [1]. As a consequence, the different Cdk–cyclin complexes play specific roles in cellular functions. In addition to the regulation by cyclins, Cdk activity is also regulated by other mechanisms that include phosphorylation of specific amino acid residues, acetylation, and binding to proteins called Cdk-inhibitors (CKIs) [4, 5]. A relevant phosphorylation that directly affects Cdk activity is that of the threonine residue 160 in Cdk2 (or its equivalent in other Cdks) by CAK (Cdk activating kinase). This phosphorylation stabilizes the activated form of the kinase heterodimer. However, this is not general and for instance Cdk5 does not require this phosphorylation for full activity [6]. A second relevant regulatory phosphorylation is that occurring at specific residues Thr14 and Tyr15 in Cdk2 (or their equivalents in the other Cdks). These phosphorylations are performed by Wee1 and Myt1 kinases and inhibit the activity of several family members [7]. Another regulatory mechanism of Cdk activity is acetylation. It has been reported that at least Cdk2 can be acetylated by the acetyltransferase PCAF at a specific Lys residue of the catalytic center and the kinase activity is inhibited because this Lys residue is critical for the interaction with ATP [5]. This acetylation has not been demonstrated to occur in all Cdks. However, because it is a conserved residue it can be hypothesized that acetylation of this residue can be a general mechanism of Cdk inhibition [8].

Finally, the cell cycle related CDKs can also be negatively regulated by binding to low molecular weight proteins of the INK4 or Cip/Kip families of inhibitors [9]. INK4 proteins ($p16^{INK4a}$, $p15^{INK4b}$, $p18^{INK4c}$, and $p19^{INK4d}$) are specific for the Cdk4 subfamily and interact with the monomeric Cdks preventing the activation by the D-type cyclins or by CAK. Members of the Cip/Kip family of inhibitors ($p21^{Cip1}$, $p27^{Kip1}$, and $p57^{Kip2}$) associate with both the Cdk and the cyclin subunits and inhibit the kinase activity by introducing a domain into the catalytic center of the Cdks, thus blocking ATP association [9]. It has been shown that p27 and p21 can be phosphorylated at specific Tyr residues by members of the Src family of protein kinases. When phosphorylated at these Tyr residues, p27 and p21 associated with Cdk–cyclin complexes cannot fully inhibit Cdk activity. Thus, under these conditions the complexes remain partially activated [10, 11]. All these aspects of the regulation of Cdk activity have to be taken into account when its activity has to be determined.

In this chapter we describe a general protocol to determine in vitro Cdk activity by using Cdk–cyclin complexes obtained by immunoprecipitation (IP) of cell samples with antibodies against specific Cdks or cyclins as a source of the enzymes. When the activity has to be analyzed after IP of Cdk–cyclin complexes the first aspect to be considered is the antibody that has to be used for the IP. When a Cdk can associate with several cyclins, the use of the

antibody against the Cdk will allow determining the activity of all complexes containing this Cdk. On the contrary, to only analyze the activity of a specific Cdk–cyclin complex, the antibody against the specific cyclin of the complex has to be used. However, in some cases a specific cyclin can bind to several Cdks. For instance, cyclin A can associate with both Cdk2 and Cdk1. Thus, in these cases it is better to use antibodies against the Cdk or to perform several determinations using antibodies against the Cdk and additionally also antibodies against each cyclin and then with all results the interested activity can be calculated. Another consideration is that on depending of the status of the cell cultures used for the IPs a percentage of Cdk–cyclin complexes can be associated with CKIs. Additionally, these associated CKIs (more specifically p27 and p21) can be Tyr phosphorylated. Thus, immunoprecipitates may contain a heterogeneous population of free Cdk or free cyclin (on depending of the antibody used), free Cdk–cyclin complexes and complexes associated with CKIs that can be Tyr phosphorylated or not. Finally, Cdks in the immunoprecipitates can be acetylated or phosphorylated at T160 or/and T14/Tyr15.

We describe here the protocols for the in vitro determination of the activities of relevant Cdk–cyclin complexes involved in cell cycle regulation as Cdk1, Cdk2, and Cdk4/6. These activities will be determined by using complexes obtained by IP of cellular extracts by using antibodies against Cdks.

2 Materials

2.1 Immunoprecipitation and Kinase Assay for Determination of Cdk2 Activity

1. *HAT buffer + Inhibitors*: 50 mM Tris–HCl pH 8, 50 mM KCl, 0.1 mM EDTA pH 8, 5 % glycerol, 0.5 % NP-40, 0.5 μg/ml aprotinin, 10 μg/ml leupeptin, 1 mM PMSF, 0.1 mM Na_3VO_4.
2. *10× Kinase buffer Cdk2*: 250 mM HEPES pH 7.4, 100 mM $MgCl_2$.
3. *1× Kinase buffer Cdk2*: 25 mM HEPES pH 7.4, 10 mM $MgCl_2$.
4. *Kinase assay reaction buffer*: 2 μg Histone H1 (Cdk2 substrate), 12.5 μM ATP, kinase buffer 10×, 1 μCi [γ-^{32}P], 2 mM DTT, Milli-Q water.
5. *4× Loading buffer*: 40 mM NaPi pH 7.0, 40 % glycerol, 10 % SDS, 2 mg/ml DTT, 0.67 mg/ml bromophenol blue.
6. *Coomassie Blue staining*: 2.5 mg/ml Coomassie Brilliant Blue, 45 % methanol, 10 % acetic acid.
7. *Destaining solution*: 50 % methanol, 10 % acetic acid.
8. *Bradford reagent.*
9. *Protein A/G Agarose Beads.*

10. *Antibodies*: Cdk2 (Santa Cruz, sc-163), Cyclin A (Santa Cruz, sc-596), Cyclin E (Santa Cruz, sc-481).
11. *X-ray Films.*
12. *Sonicator* (Bioruptor).
13. *Microcentrifuge.*

2.2 Immunoprecipitation and Kinase Assay for Determination of Cdk4/6 Activity

1. *Lysis buffer D4+ Inhibitors*: 50 mM HEPES pH 7.5, 150 mM NaCl, 2.5 mM EGTA, 1 mM EDTA, 0.1 % Tween 20, 10 % glycerol, 1 mM DTT, 10 mM β-glycerol phosphate, 0.1 mM Na_3VO_4, 1 μg/ml aprotinin, 10 μg/ml leupeptin, 1 mM PMSF.
2. *10× Kinase buffer Cdk4/6*: 500 mM HEPES pH 7.4, 100 mM $MgCl_2$, 25 mM EGTA, 10 mM DTT.
3. *1× Kinase buffer Cdk4/6*: 50 mM HEPES pH 7.4, 10 mM $MgCl_2$, 2.5 mM EGTA, 1 mM DTT.
4. *Kinase assay reaction buffer*: 3 μg GST-pRB (aa. 379–928) (Cdk4/6 substrate), 15 μM ATP, kinase buffer 10×, 2 μCi [ɣ-^{32}P], 1 mM DTT, Milli-Q water.
5. *4× Loading buffer*: 40 mM NaPi pH 7.0, 40 % glycerol, 10 % SDS, 2 mg/ml DTT, 0.67 mg/ml bromophenol blue.
6. *Coomassie staining*: 2.5 mg/ml Coomassie Brilliant Blue, 45 % Methanol, 10 % Acetic acid.
7. *Destaining solution*: 50 % Methanol, 10 % Acetic acid.
8. *Bradford reagent.*
9. *Protein A/G Agarose Beads.*
10. *Antibodies*: Cdk4 (Santa Cruz, sc-260), Cdk6 (Santa Cruz, sc-7181).
11. *X-ray Films.*
12. *Sonicator* (Bioruptor).
13. *Microcentrifuge.*

2.3 Immunoprecipitation and Kinase Assay for Determination of Cdk1 Activity

1. *HAT buffer+ Inhibitors*: 50 mM Tris–HCl pH 8, 50 mM KCl, 0.1 mM EDTA pH 8, 5 % glycerol, 0.5 % NP-40, 0.5 μg/ml aprotinin, 10 μg/ml leupeptin, 1 mM PMSF, 0.1 mM Na_3VO_4.
2. *10× Kinase buffer Cdk1*: 200 mM HEPES pH 7.4, 100 mM magnesium acetate.
3. *1× Kinase buffer Cdk2*: 20 mM HEPES pH 7.4, 10 mM magnesium acetate.
4. *Kinase assay reaction buffer*: 2 μg Histone H1 (Cdk2 substrate), 12.5 μM ATP, kinase buffer 10×, 1 μCi [ɣ-^{32}P], 2 mM DTT, Milli-Q water.
5. *4× Loading buffer*: 40 mM NaPi pH 7.0, 40 % glycerol, 10 % SDS, 2 mg/ml DTT, 0.67 mg/ml bromophenol blue.

6. *Coomassie Blue staining*: 2.5 mg/ml Coomassie Brilliant Blue, 45 % methanol, 10 % acetic acid.
7. *Destaining solution*: 50 % methanol, 10 % acetic acid.
8. *Bradford reagent*.
9. *Protein A/G Agarose Beads*.
10. *Antibodies*: Cdk1 (Abcam, ab32384).
11. *X-ray Films*.
12. *Sonicator* (Bioruptor).
13. *Microcentrifuge*.

3 Methods

3.1 Immunoprecipitation and Kinase Assay for Determination of Cdk2 Activity

3.1.1 Cell Lysis

1. Cells are lysed using HAT buffer + inhibitors for 30 min on ice (*see* **Note 1**).
2. After incubation, centrifuge the samples and clarify at 11,700 × *g* for 10 min at 4 °C.
3. Transfer the supernatants containing whole cell protein extract to new tubes.
4. Protein concentration of each sample is quantified using the Bradford assay.

3.1.2 Immunoprecipitation

1. Immunoprecipitate 500 μg of whole cell proteins with 2 μg of Cdk2, Cyclin A, or Cyclin E antibody for 16 h. IgG antibody (2 μg) is used as a negative control. The final volume of each IP is 500 μl in HAT buffer + inhibitors.
2. After antibody incubation, add 30 μl of protein A-Sepharose or protein G-Sepharose (*see* **Note 2**) to the samples that are subsequently incubated for 1 h at 4 °C on rotation.
3. Wash the beads three times with HAT buffer. At this step, each sample (including the beads) is split in two tubes; one of them is used to perform the kinase assay and the other one to perform a western blot to detect the amount of immunoprecipitated Cdk2.
4. Wash the tubes used for the kinase assay once with 1× kinase buffer.

3.1.3 Kinase Assay

1. Add 30 μl of kinase assay reaction buffer, prepared as explained above (*see* Subheading 2), to each tube (*see* **Note 3**).
2. Perform the kinase assay at 30 °C for 30 min and then stop the reaction by adding 10 μl of 4× loading buffer.
3. Centrifuge the samples for 30 s at 2000 × *g* to remove the beads.

3.1.4 Polyacrylamide Gel Electrophoresis and Coomassie Blue Staining

1. Run the samples in a 12 % polyacrylamide gel at 120 V for 1 h and 15 min.
2. Stain the gel with Coomassie Blue staining solution for 15 min in a glass tray and then remove this solution and replace with Coomassie destaining solution for 16 h (overnight) in a shaker machine (*see* **Note 4**).
3. Place on the top of the gel a maximum resolution film recommended for ^{32}P detection (Kodak Biomax) and expose between 2 and 24 h (*see* **Note 5**) at −80 °C to detect ^{32}P-H1.
4. After exposing the film, develop it in a developer machine.

The amount of immunoprecipitated Cdk2 protein in the western blot and the amount of H1 protein (Cdk2 substrate) observed in the Coomassie stained gel are used as a loading control for the kinase assay.

3.2 Immunoprecipitation and Kinase Assay for Determination of Cdk4/6 Activity

3.2.1 Cell Lysis

1. Cells are lysed using lysis buffer D4 + inhibitors for 30 min on ice (*see* **Note 6**).
2. Sonicate the samples twice for 10 s at 4 °C.
3. After sonication, centrifuge the samples and clarify at 11,700 × *g* for 10 min at 4 °C.
4. Transfer the supernatants containing whole cell protein extract to new tubes.
5. Protein concentration of each sample is quantified using the Bradford assay.

3.2.2 Immunoprecipitation

1. Immunoprecipitate 500 μg of whole cell proteins with 2 μg of Cdk4 or Cdk6 antibody for 16 h. IgG antibody (2 μg) is used as a negative control. The final volume of each IP is 500 μl in lysis buffer D4 + inhibitors.
2. After antibody incubation, add 30 μl of protein A-Sepharose or protein G-Sepharose (*see* **Note 2**) to the samples that are subsequently incubated for 1 h at 4 °C on rotation.
3. Wash the beads three times with lysis buffer D4. At this step, each sample (including the beads) is split in two tubes; one of them is used to perform the kinase assay and the other one to perform a western blot to detect the amount of immunoprecipitated Cdk4/6.
4. Wash the tubes used for the kinase assay once with 1× kinase buffer Cdk4/6.

3.2.3 Kinase Assay

1. Add 30 μl of kinase assay reaction buffer, prepared as explained above (*see* Subheading 2), to each tube (*see* **Note 3**).
2. Perform the kinase assay at 30 °C for 30 min and then stop the reaction by adding 10 μl of 4× loading buffer.
3. Centrifuge the samples for 30 s at 3000 rpm to remove the beads.

3.2.4 Polyacrylamide Gel Electrophoresis and Coomassie Staining

1. Run the samples in a 10 % polyacrylamide gel at 120 V for 1 h and 15 min.
2. Stain the gel with Coomassie Blue staining solution for 15 min in a glass tray and then remove this solution and replace with Coomassie destaining solution for 16 h (overnight) in a shaker machine (*see* **Note 4**).
3. Place on the top a maximum resolution film recommended for ^{32}P detection (Kodak Biomax) and expose between 2 and 24 h (*see* **Note 5**) at −80 °C to detect ^{32}P-GST-pRB (379–928).
4. After exposing the film, develop it in a developer machine.

The amount of immunoprecipitated Cdk4/6 proteins in the western blot and the amount of GST-pRB (aa. 379–928) protein (Cdk4/6 substrate) observed in the Coomassie stained gel are used as a loading control for the kinase assay.

3.3 Immunoprecipitation and Kinase Assay for Determination of Cdk4/6 Activity

Kinase assay of Cdk1 is performed like Cdk2 kinase assay with an exception: 500 μg of whole cell proteins is immunoprecipitated with 1 μg of Cdk1 or Cyclin B1 antibody for 16 h and 1 μg of IgG antibody is used as a negative control.

4 Notes

1. We use 200 μl of HAT buffer to lyse one million cells. For each IP, 500 μg of protein is used. Thus, the number of starting cells depends on the cell type. The HAT buffer can be prepared and stored at 4 °C, but the inhibitors must be added at the beginning of the protocol (0.5 μg/ml aprotinin, 10 μg/ml leupeptin, 1 mM PMSF, 0.1 mM Na_3VO_4).
2. Protein A-sepharose or protein G-sepharose would be used depending on the species of the antibody we use (Table 1).

Table 1
Protein A/G binding affinities

Species	Protein A	Protein G
Human	++++	++++
Mouse	++	–
Rat	–	++
Rabbit	++++	+++
Goat	–	++
Sheep	+/–	++

3. Half-life of ^{32}P is around 15 days. This means that every 2 weeks, the amount of radioactivity that it is needed for kinase assays, has to be doubled. This has to be taken into account when the kinase assay reaction buffer is prepared.
4. Coomassie Blue staining and destaining solutions can be reused several times before been wasted.
5. Time of exposure will depend on the amount of Cdk2 or Cdk4/6 and their activity in the cells we are studying. We recommend to do a short exposure and according to the result, next step would be to increase this time.
6. We use 200 μl of lysis buffer D4 buffer to lyse one million cells. For each IP, 500 μg of protein is used. Thus, the number of starting cells depends on the cell type. The lysis buffer can be prepared and stored at 4 °C but DTT and the inhibitors must be added at the beginning of the protocol (10 mM β-glycerol phosphate, 0.1 mM Na_3VO_4, 1 μg/ml aprotinin, 10 μg/ml leupeptin, 1 mM PMSF).

References

1. Malumbres M (2014) Cyclin-dependent kinases. Genome Biol 15:122–131
2. Malumbres M, Harlow E, Hunt T, Hunter T, Lahti JM, Manning G, Morgan DO, Tsai L-H, Wolgemuth DJ (2009) Cyclin-dependent kinases: a family portrait. Nat Cell Biol 11:1275–1276
3. Cao L, Chen F, Yang X, Xu W, Xie J, Yu L (2014) Phylogenetic analysis of CDK and cyclin proteins in premetazoan lineages. BMC Evol Biol 14:10
4. Morgan DO (1997) Cyclin-dependent kinases: engines, clocks, and microprocessors. Annu Rev Cell Dev Biol 13:261–291
5. Mateo F, Vidal-Laliena M, Canela N, Zecchin A, Martínez-Balbás M, Agell N, Giacca M, Pujol MJ, Bachs O (2009) The transcriptional co-activator PCAF regulates Cdk2 activity. Nucleic Acids Res 37:7072–7084
6. Echalier A, Endicott JA, Noble MEM (2010) Recent developments in cyclin-dependent kinase biochemical and structural studies. Biochim Biophys Acta 1804:511–519
7. Malumbres M, Barbacid M (2005) Mammalian cyclin-dependent kinases. Trends Biochem Sci 30:630–641
8. Russo AA, Jeffrey PD, Patten AK, Massagué J, Pavletich NP (1996) Crystal structure of the p27Kip1 cyclin-dependent-kinase inhibitor bound to the cyclin A-Cdk2 complex. Nature 382:325–331
9. Pavletich NP (1999) Mechanisms of cyclin-dependent kinase regulation: structures of Cdks, their cyclin activators, and Cip and INK4 inhibitors. J Mol Biol 287:821–828
10. Grimmler M, Wang Y, Mund T, Cilensek Z, Keidel E-M, Waddell MB, Jäkel H, Kullmann M, Kriwacki RW, Hengst L (2007) Cdk-inhibitory activity and stability of p27Kip1 are directly regulated by oncogenic tyrosine kinases. Cell 128:269–280
11. Chu I, Sun J, Arnaout A, Kahn H, Hanna W, Narod S, Sun P, Tan C-K, Hengst L, Slingerland J (2007) p27 phosphorylation by Src regulates inhibition of cyclin E-Cdk2. Cell 128:281–294

Chapter 2

Expression and Purification of Recombinant Cyclins and CDKs for Activity Evaluation

Edurne Gallastegui and Oriol Bachs

Abstract

Cyclin-dependent kinases (Cdks) belong to a family of key regulators of cell division cycle and transcription. Their activity is mainly regulated by association with regulatory subunits named cyclins but their activities are also regulated by phosphorylation, acetylation, and the association with specific inhibitory proteins (CKIs). The activity of different Cdks is deregulated in many different type of tumors, and thus, Cdks are considered targets for antitumoral therapy. For large screenings of inhibitors the use of purified recombinant Cdks and cyclins is recommended. We report here the current methods to determine their in vitro activity for large screenings of inhibitors.

Key words Cdk1, Cdk2, Cyclin A, Cyclin B, Kinase assay

1 Introduction

Regarding cell cycle regulation, the most important cyclins are the D-type cyclins that include three members (cyclins D1, D2, and D3), cyclin E, cyclin A, and cyclin B [1]. During cell cycle progression different Cdk–cyclin complexes are generated each one operating at specific moments along the cell cycle [2]. Specifically, Cdk4/6–cyclins D complexes are activated during the G_1 phase of the cell cycle and they are responsible of phosphorylating members of the pocked proteins family (pRb, p107, and p130) that are in transcriptional repressor complexes [3]. Subsequent phosphorylation of these complexes, by Cdk2–cyclin E, disrupts them inducing the transcription of genes encoding proteins necessary for DNA replication and mitosis [4]. Cdk2–cyclin E complexes are also involved in the triggering of DNA replication. Cdk2–cyclin A are subsequently activated and are necessary for the progression of DNA replication during the S phase of the cell cycle. Finally, Cdk1–cyclin A and Cdk1–cyclin B participate in the triggering and progression of mitosis [5].

Mar Orzáez et al. (eds.), *Cyclin-Dependent Kinase (CDK) Inhibitors: Methods and Protocols*, Methods in Molecular Biology, vol. 1336, DOI 10.1007/978-1-4939-2926-9_2,

The activities of different Cdks are deregulated in many different types of tumors, so they are considered relevant targets for antitumoral therapy [6]. To identify specific Cdk inhibitors, protocols to determine their activity have been developed. The in vitro Cdk activity is mainly determined by two general protocols. The first is by using Cdk–cyclin complexes obtained by immunoprecipitation (IP) of cell samples with antibodies against specific Cdks or cyclins as a source of the enzymes (Chapter 1). The second is by using purified recombinant Cdks and cyclins. When performing kinase assays using purified recombinant proteins, a more defined composition of the complexes can be achieved. When proteins are expressed in and purified from bacteria, the post-translational modifications (phosphorylation and acetylation) of Cdks are not produced and additionally no CKIs are associated. However, because the activating phosphorylation at T160 is not produced, the activity of the complexes that need this phosphorylation for full activity only would display a reduced activity. This problem can be solved by in vitro phosphorylating this T160 residue by incubation of the purified Cdk with the CAK enzyme previously to mix the Cdk with the selected cyclin. Finally, in vitro association of specific Cdks with their cyclin partners in some cases might be highly inefficient. For instance, the association of Cdk4 with D-type cyclins is one of these cases. The CKIs p21 and p27 can work as adaptor proteins that stimulate the interaction between both subunits [7]. However, because p21 and p27 also work as inhibitors of these complexes the in vitro activity of these complexes using purified recombinant proteins is difficult.

We describe here the protocols to determine Cdk1 and Cdk2 activities by using recombinant proteins expressed in and purified from bacteria. These protocols are recommended when the aim is to screen high amount of products on trying to identify specific inhibitors of these complexes. To analyze the activity of other Cdk–cyclin complexes, specific modifications of the protocols have to be done.

2 Materials

2.1 Expression and Purification of Recombinant Cyclins and Cdks for Determination of Kinase Activity

1. *LB* (*Luria–Bertani*) *medium*: 1 % tryptone, 0.5 % yeast extract, 0.5 % NaCl (Autoclave before use).
2. *Antibiotics*: ampicillin (final concentration: 50 μg/ml) and chloramphenicol (final concentration: 20 μg/ml).
3. *Bacteria strain*: BL21 (DE3).
4. *IPTG*.
5. *Lysis buffer NETN+Inhibitors*: 20 mM Tris–HCl pH 8, 100 mM NaCl, 1 mM EDTA, 0.5 % NP-40, 0.5 μg/ml aprotinin, 10 μg/ml leupeptin, 1 mM PMSF, 0.1 mM Na_3VO_4.

6. *Glutathione-Sepharose-4B resin*.
7. *Elution buffer*: 50 mM Tris–HCl pH 9.6, 120 mM NaCl, 20 mM glutathione reduced.
8. *1× PBS*: 137 mM NaCl, 2.7 mM KCl, 10 mM Na_2HPO_4, 2 mM KH_2PO_4.
9. *Bradford reagent*.

3 Methods

3.1 Protein Expression

Cdk and cyclin cDNA must be cloned in a pGEX plasmid. This kind of plasmids is used to express high amounts of proteins fused to glutathione S-transferase (GST).

1. Transform pGEX plasmids containing cDNAs of interest in BL21 (DE3) and grow in LB medium with ampicillin and chloramphenicol at 37 °C with shaking to mid-log phase (OD_{600nm} 0.8).
2. Induce the expression by the addition of isopropyl 1-thio-d-galactopyranoside (IPTG) at a final concentration of 0.5 mM and incubate the culture for 4 h with shaking at room temperature.
3. To test the induction, run 30 μl of non-induced and induced bacteria culture in a polyacrylamide gel and stain with Coomassie Blue.

3.2 Protein Purification

1. Harvest the bacteria by centrifugation at 4000 × *g* at 4 °C for 10 min.
2. Suspend the pellet in NENT buffer + Inhibitors (*see* **Note 1**).
3. Froze the bacterial cells at −80 °C and thaw on ice three times.
4. Lyse the cells by sonication four times for 10 s.
5. Perform a centrifugation at 24,000 × *g* at 4 °C for 15 min.
6. Do the purification using affinity chromatography by incubating the supernatant with Glutathione-Sepharose-4B resin in a column. For every 5 mg of protein 1 ml of Glutathione-Sepharose-4B has to be used (*see* **Note 2**).
7. Incubate the mix with shaking at 4 °C for 1 h.
8. Wash three times with NENT (final volume of 100 ml).
9. At this point, GST from recombinant proteins can be removed if needed but to perform the kinase assay this step is not necessary (*see* **Note 3**).
10. Add 5 ml of elution buffer and incubate with shaking at 4 °C for 10 min.

11. Protein is obtained after centrifuging at 2000×*g* at 4 °C for 5 min and keeping the supernatant.
12. Dialyze the purified recombinant proteins against PBS and calculate the concentration by Bradford assay.

3.3 Kinase Assay

1. Mix 400 nM of Cdk protein and the same concentration of cyclin protein in a tube and incubate for 10 min on ice (as many tubes as reactions we want to perform are prepared at this step). If the effect of some inhibitor wants to be studied, it has to be added to the mix at this point.
2. Kinase assay and polyacrylamide gel electrophoresis are performed as previously described (*see* Chapter 1), depending on the Cdk–cyclin activity to be determined. For Cdk2, Cdk4/6, and Cdk1 activities *see* Subheadings 3.1, 3.2, and 3.3, respectively. For material related to Cdk2, Cdk4/6, and Cdk1 kinase assays *see* Subheadings 2.1, and Subheadings 2.2, and 2.3, from Chapter 1 (E. Gallastegui and O. Bachs).

4 Notes

1. The NETN buffer can be prepared and stored at 4 °C, but the inhibitors must be added at the beginning of the protocol (0.5 μg/ml aprotinin, 10 μg/ml leupeptin, 1 mM PMSF, 0.1 mM Na_3VO_4).
2. 5 mg of protein is equal to a starting volume of bacterial culture of 0.5–1 l, approximately.
3. If desired, GST can be removed from the GST fusion proteins by digestion with thrombin protease.

References

1. Malumbres M, Barbacid M (2005) Mammalian cyclin-dependent kinases. Trends Biochem Sci 30:630–641
2. Morgan DO (1997) Cyclin-dependent kinases: engines, clocks, and microprocessors. Annu Rev Cell Dev Biol 13:261–291
3. Malumbres M (2014) Cyclin-dependent kinases. Genome Biol 15:122–131
4. Rubin SM (2013) Deciphering the retinoblastoma protein phosphorylation code. Trends Biochem Sci 38:12–19
5. Lindqvist A, Rodríguez-Bravo V, Medema RH (2009) The decision to enter mitosis: feedback and redundancy in the mitotic entry network. J Cell Biol 185:193–202
6. Asghar U, Witkiewicz AK, Turner NC, Knudsen ES (2015) The history and future of targeting cyclin-dependent kinases in cancer therapy. Nat Rev Drug Discov 14:130–146
7. LaBaer J, Garrett MD, Stevenson LF, Slingerland JM, Sandhu C, Chou HS, Fattaey A, Harlow E (1997) New functional activities for the p21 family of CDK inhibitors. Genes Dev 11:847–862

Chapter 3

Expression and Purification of Recombinant CDKs: CDK7, CDK8, and CDK9

Reena Pinhero and Krassimir Yankulov

Abstract

Cyclin-dependent kinases have established roles in the regulation of cell cycle, in gene expression and in cell differentiation. Many of these kinases have been considered as drug targets and numerous efforts have been made to develop specific and potent inhibitors against them. The first step in all of these attempts and in many other biochemical analyses is the production of highly purified and reliable kinase, most frequently in a recombinant form. In this chapter we describe our experience in the cloning, expression, and purification of CDKs using CDK7/CycH, CDK8/CycC, and CDK9/CycT1 as an example.

Key words Cyclin-dependent kinases, CDK expression, CDK purification

1 Introduction

Cyclin-dependent kinases (CDKs) are Ser/Thr protein kinases, which are critically dependent on their association with a cyclin partner [1–3]. CDKs have a firmly established role as key regulators of the division of cells. Their cyclin partners are expressed and degraded in tightly regulated temporal fashion thus furnishing the orchestrated oscillating kinase activities required for the proper progression though the cell cycle. Other members of the CDK family play roles in gene transcription and in cell differentiation [3]. Some of the cyclins that couple with these kinases do not display oscillating abundance, but still remain critical for the activity of the kinase. Most cyclins associate with one or two kinases [3]; however, some of the budding yeast CDKs can associate with as many as nine cyclins [2].

In addition to association with cyclins, CDKs are regulated by a variety of mechanisms including phosphorylation, association with inhibitory proteins and assembly factors, and protein degradation [1]. In particular, the activity of many CDKs is dependent on their phosphorylation by CAK (CDK Activating Kinase). CAK itself is a CDK, CDK7/CycH [4]. The phosphorylation by CAK and other posttranslational modifications provide yet another layer

Mar Orzáez et al. (eds.), *Cyclin-Dependent Kinase (CDK) Inhibitors: Methods and Protocols*, Methods in Molecular Biology, vol. 1336, DOI 10.1007/978-1-4939-2926-9_3,

of complexity in the regulation of CDKs and pose challenges to the expression of active recombinant kinases that can be used in vitro.

Many studies on CDKs have been carried out with natural or epitope-tagged kinases that have been immunoprecipitated from cell extracts. This approach benefits from the natural environment for posttranslational modifications of the enzymes. Normally, the presence of contaminating kinase in such preps is addressed by testing for kinase activity in a blank control. Additional reassurance is provided through the use of specific kinase inhibitors or the use of multiple substrates. However, many CDKs exist in vivo in more than one complex (*see* below) and some of these complexes display substantial variations in their substrate preferences [5–9]. The uncertainty on the homogeneity of these kinase preparations often obfuscates the correct interpretation of the data. Clearly, these small-scale procedures have provided valuable insights, but are incompatible with large-scale analyses including the search and characterization of inhibitors and drug candidates.

Here we describe strategies for large-scale expression and purification of recombinant CDKs with a focus on CDK7/CycH, CDK8/CycC, and CDK9/CycT1 (*see* Fig. 1 for outline). These kinases do not directly regulate the progression through the cell cycle. CDK7 exits in several forms including a core tripartite CDK7/CycH/MAT1 complex known as CAK (CDK activating kinase) and as a component in the general pol II transcription factor TFIIH [10, 11]. CDK8/CycC exists as a bipartite complex, but has also been found in a variety of complexes that contain RNApol II and general RNApol II transcription factors [12]. CDK9 has been initially identified as P-TEFb (Positive Transcription Elongation Factor-b) [13, 14]. Independently, CDK9/CycT1 has been isolated as the HIV-tat associated kinase TAK [15, 16]. All these kinases have multiple targets, but share the carboxy-terminal domain (CTD) of RNA pol II as a common substrate [10].

As mentioned earlier, most CDKs are regulated by posttranslational modifications. The enzymes that exert these modifications are not available in prokaryotic cells. Consequently, the expression and/or assembly of CDKs in *E. coli* frequently generates inactive kinases. Practice has shown that insect cells, albeit more expensive and cumbersome, provide the proper environment for the expression of active CDKs. We recommend insect Sf9 cells and baculovirus vectors for the expression of these enzymes.

2 Materials

2.1 Growth and Maintenance of Sf9 Cells

1. 1× Grace's Medium; 100× yeastolate solution; 100× lactalbumin hydrolysate solution; 100× antibiotic/antimycotic solution; fetal bovine serum (*see* **Note 1**).

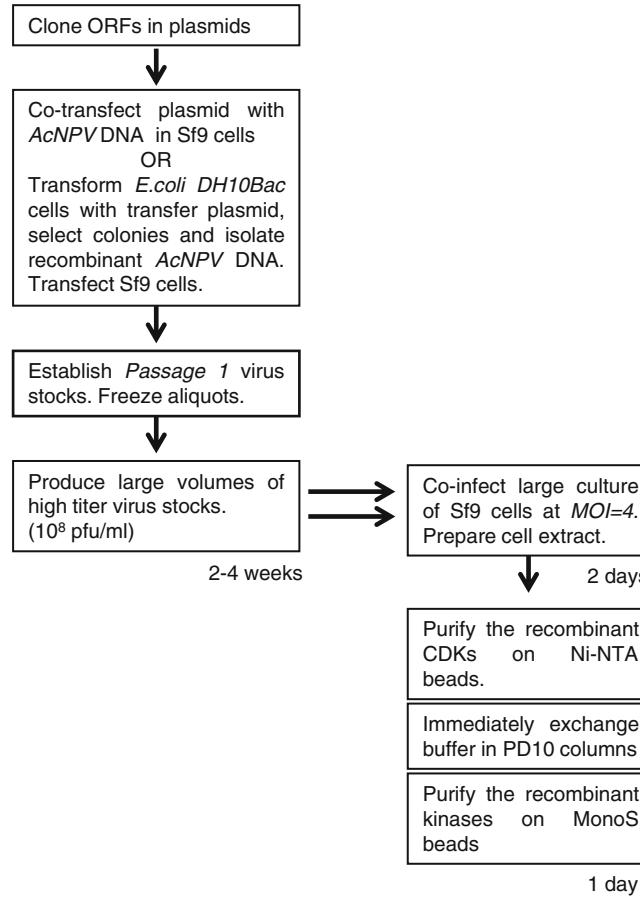

Fig. 1 An outline of the expression and purification of CDK complexes. Cloning of the proteins of interest in transfer plasmids and the production of recombinant AcNPV usually takes 2–4 weeks. The subsequent expression of the kinases takes 2 days. The purification of the kinases over Ni-NTA and MonoS resins should be performed in a single day

2. Tissue culture hood.
3. 28 °C incubator.
4. Tissue culture flasks (25, 175 cm^2).

2.2 Expression and Purification of Recombinant Kinases

1. Cell lysis buffer: 10 mM Tris–HCl pH 7.5, 10 mM NaCl, 2 mM β-mercaptoethanol, 0.5 mM EDTA, 10 mM 2-glycerophosphate, 0.5 mM Na-vanadate Na3VO4, 2 mM NaF. Add 2 μg/ml leupeptin, 2 μg/ml aprotinin, 2 μg/ml pepstatin (*see* **Note 2**), 0.2 % (v/v) NP-40. Add 50 μg/ml PMSF immediately before use.
2. 5 M NaCl.
3. 80 % glycerol.

4. 0.5 M imidazole–HCl pH 7.6.
5. Dounce homogenizer, 40 ml.
6. SW50.1 rotor and a compatible ultracentrifuge.

2.3 Purification of CDK Complexes by Ni^{2+}-NTA

1. Ni^{2+}-NTA Agarose.
2. Equilibration buffer: 10 mM Tris–HCl pH 7.6, 0.5 M NaCl, 5 mM imidazole, 10 % (v/v) glycerol. Add 50 μg/ml PMSF immediately before use.
3. Ni-NTA Elution buffer: 10 mM Tris–HCl pH 7.6, 100 mM NaCl, 10 % (v/v) glycerol. Supplement with 5, 15, 25, 100, and 400 mM imidazole–HCl as indicated. Add 50 μg/ml PMSF immediately before use.
4. Disposable 10 ml columns.

2.4 Purification of CDK Complexes by Mono S Chromatography

1. PD10 buffer exchange columns.
2. 5 ml Econo-Pac Mono S cartridge.
3. S-buffer: 25 mM Hepes.Na pH 7.6, 0.1 mM EDTA, 1 mM DTT, 5 % (v/v) glycerol, supplemented with 80 or 500 mM NaCl. Add 50 μg/ml PMSF immediately before use.

2.5 Expression and Purification of GST-CTD Substrate

1. Competent *E. coli BL21*(*DE3*)*lysS* cells.
2. LB (Luria Broth)/amp plates and LB/amp liquid medium.
3. Bacterial shaker/incubator set at 37 °C.
4. IPTG powder.
5. TEN buffer: 20 mM Tris–HCl pH 7.5, 5 mM EDTA, 200 mM NaCl. Add 50 μg/ml PMSF before use.
6. Protease inhibitors (pepstatin, leupeptin, aprotinin) at 1 mg/ml (*see* **Note 2**).
7. Glutathione-agarose beads.
8. 1 M glutathione reduced.
9. 10 % Triton X-100 (TX100).
10. Disposable 10 ml columns.
11. One 10 % SDS-PAGE gel.
12. A mid-speed centrifuge (*Sorvall Evolution RC* or similar), rotors (*Sorvall* SA300, SLA1500 or similar), 250 ml centrifuge bottles, 35 ml centrifuge tubes.
13. A sonicator, Misonix XL or similar.

2.6 Kinase Assays

1. Kinase buffer: 20 mM Tris–HCl, pH 8, 50 mM KCl, 7 mM $MgCl_2$, 5 mM 2-glycerophosphate, 100 μg/ml BSA, 10 μM ATP, 2 μCi (7.4×10^4 Bq) α-^{32}P-ATP.
2. 1 mg/ml GST-CTD.
3. 1 mg/ml myelin basic protein (MBP).

2.7 Other Equipment

1. Basic radiation safety equipment and Geiger counter.
2. Mini-PROTEAN II electrophoresis cell (Bio-Rad) or comparable mini-gel system.
3. Microcentrifuge, standard molecular biology equipment.

3 Methods

3.1 Production of and Handling of Recombinant Viruses

The viruses for expression of CDK7, MAT1 [17] and CycC [18] were gifts from Dr. D. Morgan and Dr. E. Lees, respectively. The virus for the expression of His_6-CDK9 and CycT1 was produced by pBAC4/CDK9/CycT1 plasmid [19] and the BacVector-3000 kit (Novagen) according to the instructions of the manufacturer (*see* **Note 3**). The virus for the expression of His_6-CycH was produced by cloning CycH into pBlueBac and the Bac-N-Blue transfection system (Invitrogen Life Technologies) (*see* **Note 3**). The recombinant virus was purified through three rounds of selection of blue plaques. His_6-CDK8 was produced by cloning CDK8 into pFastBacHTa and the BAC-to-BAC recombination system (Invitrogen Life Technologies) according to the instructions of the manufacturer (*see* **Note 3**). All three systems are reliable and produce viruses with equal success. Space limitations preclude extensive details on these procedures. However, we must note that in our hands Bac-to-Bac (Invitrogen Life Technologies) has been most user-friendly and least time-consuming.

3.2 Amplification of Recombinant Viruses

The initial preparations of recombinant baculovirus (termed Passage 1 virus stocks) typically contain low titer of the virus. For the viruses produced by the Bac-N-Blue system Passage 1 corresponds to the cell culture infected with a virus plaque that has been purified by three rounds of plaque selection. Passage 1 for the viruses produced by Bac-to-Bac or BacVector systems is the transfected Sf9 cultures themselves. High titer viral stocks are prepared from Passage 1 by two-step amplification as described below.

1. Infect 10 ml Sf9 cells at $0.1–0.3 \times 10^6$ cells/ml in a 25 cm^2 T-flask with 0.1 ml of virus Passage 1. The expected Multiplicity of Infection (MOI) is in the range of 0.05–1 (*see* **Note 4**).
2. Incubate for 4–6 days at 28 °C. At this point all cells should be in suspension (*see* **Note 5**).
3. Spin the culture at $275 \times g$ for 5 min in sterile 15 ml conical tubes and collect the supernatant. These supernatants contain $1 \times 10^6–1 \times 10^7$ plaque forming units per ml (pfu/ml).
4. Freeze 1 ml aliquots as Passage 2 and store at −80 °C (*see* **Note 6**).
5. Infect 75 ml Sf9 cells at $0.5–1 \times 10^6$ cells/ml in a 175 cm^2 flask (Sarsted) with 1 ml of the passage 2 stock. Incubate for 4 days

and collect the supernatant. These supernatants typically contain 1×10^8 pfu/ml.

6. Use the supernatants from **step 5** for large-scale protein expression. The viral stocks can be stored at 4 °C for several weeks.

3.3 Infection and Harvesting of Insect Cells

High levels of expression are achieved by the infection of high density Sf9 cells at high MOI. The gain of yields exceeds the concerns of superfluous virus recombination.

1. Grow Sf9 cells to $1.5–2 \times 10^6$ cells/ml in several (5–8) 175 cm^2 T-flasks or in a roller-flask.
2. Infect each flask with 2 ml of passage 4 of each of the appropriate viruses (MOI = 4) and incubate for 48 h at 28 °C (*see* **Note 7**). All cells must be floating (100 % infection) 30 h post infection. If less than 100 % infection is observed, do NOT proceed. Significantly lower yields of recombinant protein should be expected.
3. Harvest the cells after 48 h by spinning at $275 \times g$ for 5 min at 4 °C.
4. Pour off the supernatant, loosen the pellet by gently shaking it, and wash the pellets with 15 ml of chilled phosphate buffered saline.

3.4 Preparation of Cell Lysate

Cell lysis and chromatography must be performed on ice with prechilled buffers. Samples should be constantly kept on ice or in a 4 °C cold rooms.

1. Resuspend the cells in 3 pellet volumes of Cell lysis buffer. At this point the cells can be immediately processed or frozen at –80 °C (*see* **Note 8**).
2. Transfer the cell lysate to a Dounce homogenizer and break cells by ten strokes. Check for cell lysis under a microscope.
3. Add imidazole and NaCl to a final concentration of 5 mM and 0.5 M, respectively. Homogenize by two additional strokes.
4. Transfer the cell lysate to a 50 ml screw cap tube. Rock for 30 min in a cold room.
5. Spin at $75{,}000 \times g$ at 4 °C in SW50.1 rotor for 30 min.
6. Transfer the supernatant to a fresh prechilled tube; add glycerol and $MgCl_2$ to final concentrations of 10 % and 3 mM, respectively (*see* **Note 9**).

3.5 Ni^{2+}-NTA Chromatography

The Ni^{2+}-NTA and Mono S chromatography steps should be performed without any freezing and thawing of the samples. Buffer exchange should be in desalting columns rather than by dialysis (*see* **Note 10**). Several 10 % SDS–polyacrylamide gels should be

prepared prior to the chromatography for quick analysis of the fractions.

1. Equilibrate 1 ml Ni^{2+}-NTA agarose beads for 30 min with 10 ml of Equilibration buffer in a 50 ml screw cap tube. Swirl occasionally.
2. Spin the beads at 2000 rpm for 2 min and aspire the supernatant.
3. Add the cleared cell extract from 1 l of infected cells. Rock the tube for 1 h in a cold room.
4. Pellet the beads at 2000 rpm for 2 min, collect the supernatant (flow-through) and store at −80 °C. If there is any problem with the binding of proteins to the beads, the supernatant can be reused.
5. Add 10 ml of Ni-NTA Elution buffer supplemented with 5 mM imidazole. Swirl gently and transfer to a 15 ml disposable Bio-Rad column.
6. Wash the column with five aliquots of 2 ml Ni-NTA Elution buffer supplemented with 5 mM imidazole.
7. Elute the proteins as 5 × 1 ml fractions of each of the following buffers:
   - Ni-NTA Elution buffer, 15 mM imidazole.
   - Ni-NTA Elution buffer, 25 mM imidazole.
   - Ni-NTA Elution buffer, 100 mM imidazole.
   - Ni-NTA Elution buffer, 400 mM imidazole.
8. Run 10 µl of each fraction on 10 % SDS-PAGE and stain with Coomassie Brilliant Blue (*see* **Notes 11** and **12** and Fig. 2).
9. Pool the fractions that contain the proteins of interest and proceed to MonoS chromatography.

3.6 Mono S Chromatography

1. Equilibrate several disposable PD10 column with S-buffer/80 mM NaCl.
2. Attach a 5 ml Econo-Pac Mono S cartridges to a BioLogic DuoFlow system (*see* **Note 13**). Set the flow rate at 1 ml/min. Equilibrate as follows:
   - 10 ml of S-buffer with no NaCl.
   - 10 ml of 1 M NaCl in buffer A.
   - 5 ml of gradient 1 M–80 mM NaCl in buffer A.
   - 15 ml of 80 mM NaCl in buffer A.
3. In the meanwhile, exchange the buffer of the pooled Ni^{2+}-NTA chromatography fractions that contain the recombinant kinases. Process no more than 3 ml per column.

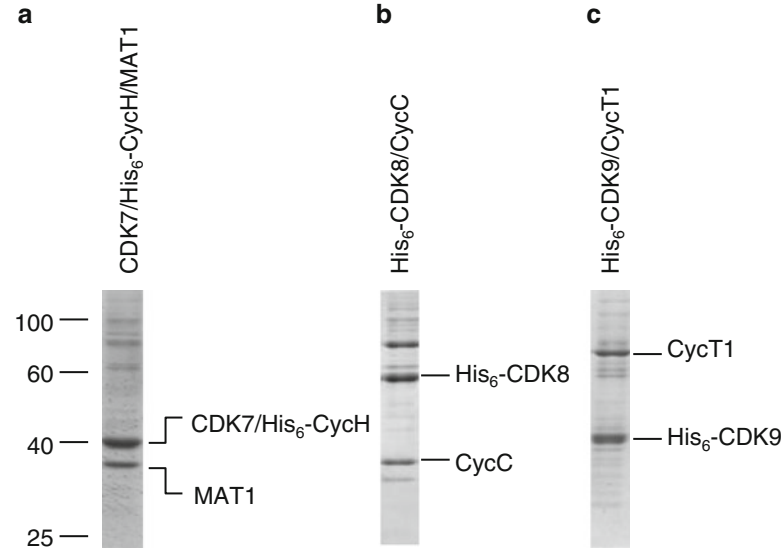

Fig. 2 Analysis of the recombinant peptides by SDS-PAGE. Coomassie stained gels from the peak fractions from the Ni^{2+}-NTA agarose chromatography are shown. (**a**) CDK7/His_6-CycH/MAT1; (**b**) His_6-CDK8/CycC; (**c**) His_6-CDK9/CycT1. The mobility of the molecular size standards is shown on the *left*. The position of the recombinant proteins is shown to the *right* of each lane. Their identity has been confirmed by Western blot (not shown)

4. Immediately load the buffer-exchanged fractions on the MonoS column at 1 ml/min. Collect the flow-through and save.
5. Wash the column with 5 ml of S-buffer/80 mM NaCl.
6. Elute with a 20 ml linear gradient of 80–500 mM NaCl in S-buffer A. Collect 1 ml fractions in 1.5 ml tubes that contain 100 µl of 80 % glycerol.
7. Vortex all fractions. Remove two 10 µl aliquots from each fraction for analysis by SDS-PAA electrophoresis and for kinase assays. Immediately freeze all fractions and aliquots at −80 °C. You can run the gels and stain/destain on the next day (*see* **Note 14**).

3.7 Expression and Purification of GST-CTD (1–52)

1. Transform pGEX-$CTD_{(1–52)}$ [20] in *E. coli BL21(DE3)lysS* cells and select colonies on LB/amp plates.
2. Inoculate 3 ml LB/amp with a single colony. Grow overnight at 37 °C.
3. Transfer the overnight culture to 400 ml LB/amp in a 2 l flask. Grow with vigorous shaking at 37 °C to $OD_{600} = 0.6$. bear in mind that the doubling time of this culture is about 20 min.

4. Transfer the culture to a 30 °C shaker. Add IPTG powder to 1 mM final concentration. Incubate with vigorous shaking for 3 h.
5. Transfer cells in two 250 ml centrifuge bottles and pellet cells at 5000 rpm in a SLA1500 rotor. Pour off supernatant. At this point you can proceed or freeze pellets at –80°C and process them later.
6. All subsequent steps are performed on ice with prechilled buffers. Resuspend the cells in 25 ml TEN buffer supplemented with protease inhibitors and fresh PMSF. Vortex to get an even suspension and transfer to a 35 ml centrifuge tube.
7. Sonicate with five bursts of 10 s at 30 % output with Misonix medium tip (*see* **Note 14**).
8. Rock for 30 min in a cold room. Spin the extract for 10 min at 15,000 rpm in a SA300 rotor.
9. In the meanwhile, mix 0.5 ml of Glutathione-Agarose beads with 25 ml of TEN buffer in a 50 ml screw cap tube. Rock for 5 min and pellet for 3 min at 1000 rpm in a bench top centrifuge. Pour off the buffer.
10. Using a 10 ml pipette, carefully remove the supernatant from **step 8** and add to the equilibrated Glutathione-Agarose beads. Add Triton X100 to 0.2 % and rock for 30 min in a cold room. Spin 3 min at 1000 rpm and remove the supernatant.
11. Wash beads three times with 25 ml of TEN buffer/0.2 % TX100. Transfer to a disposable 10 ml column.
12. Wash two times with 3 ml TEN buffer plus 0.2 % TX100.
13. Elute with ten aliquots of 1 ml Kinase buffer (*see* Subheading 2.6) supplemented with 10 mM Glutathione. Detect the peak of proteins by a standard Bradford assay.
14. Pool the fractions. Use PD10 columns to immediately exchange into Kinase buffer (*see* Subheading 3.8). Prepare 250 and 50 µl aliquots and freeze at –80 °C.
15. Run 10 µl on 10 % SDS-PAGE gel to assess the quality of the purified protein.

3.8 Kinase Assays

1. Use one of the 10 µl aliquots from Subheading 3.6 in SDS-PAGE gels to identify the fractions containing recombinant kinase (*see* **Note 15**).
2. After selecting the peak of kinase fractions, thaw the other 10 µl aliquots and use 1 and 5 µl in kinase assays.
3. The kinase assays are performed in 20 µl containing 20 mM Tris–HCl, pH 8, 50 mM KCl, 7 mM $MgCl_2$, 5 mM 2-glycerophosphate, 100 µg/ml BSA, 10 µM ATP, 2 µCi α-3^2P-ATP (ICN), 40 µg/ml GST-CTD or MBP for 30 min at 30 °C.

4. Terminate reactions by the addition of 5 μl 5× SDS-PAGE loading buffer and boil for 5 min. Load 12 μl on SDS-PAGE gels and run until the blue line of Bromo-Phenol-Blue dye leaves the gel. Use a Geiger counter to confirm that the unincorporated radioactive α-^{32}P-ATP has left the gel.
5. Discard the tank buffer according to the safety regulations of your institution.
6. Put the gel in 100 ml of 10 % methanol/10 % acetic acid and rock for 20 min. Repeat until no trace of radioactivity is detected in the wash buffer.
7. Dry the gel and expose to X-ray film or a Phosphorimager screen (if available).
8. If desired, the activity of the enzymes can be determined as incorporation of pmols ATP/min/mg of GST-CTD(1–52) or MBP (*see* **Note 16**).

3.9 Important Technical Considerations

1. *Expected yields of recombinant kinases. Infection with individual viruses versus co-infection.* Using the procedure outlined in Fig. 1, we purify between 115 μg and 1 mg of recombinant kinase from 1 l of co-infected Sf9 cells. The lowest yields are achieved with CDK7/His$_6$-CycH/MAT1. Nevertheless, the levels of co-expressed proteins are still slightly higher as compared to the levels produced by infection with individual CDK7, His$_6$-CycH, and MAT1 viruses. We suspect that co-expression and the formation of complexes in vivo stabilizes the individual peptides and so increases the yields. We must note that individual expression of cyclins and catalytic subunits and their subsequent assembly in vitro has been successfully used in the past [5, 18, 21–25]. We recommend co-expression as the more economical and efficient approach.
2. *Activity of the kinases.* The activities of the purified kinases have been assessed using GST-CTD as substrate [6]. In a standard kinase reaction, the CDK7/His$_6$-CycH/MAT1 preparations transferred about 1.5 nmol ATP/min/mg protein; the His$_6$-CDK8/CycC preparations transferred 0.1 nmol ATP/min/mg protein; His$_6$-CDK9/CycT1 transferred about 4 nmol ATP/min/mg protein. The kinases displayed distinct patterns of CTD phosphorylation that were reported elsewhere [6]. All kinases also efficiently phosphorylate MBP. In summary, the proposed expression and purification method produces highly active recombinant kinases with distinct substrate specificities.
3. *Background kinase activities.* The most haunting issue with in vitro kinase assays is the loose specificity of the enzymes and the adequacy of the observed phosphorylation events. Many CDKs phosphorylate a wide range of substrates in vitro,

including non-physiological "generic" substrates such as MBP, Histone H1, the carboxy-terminal domain of RNA pol II. Even worse, these "generic" substrates are also targeted by many of the contaminating kinases in the CDK fraction or in the substrate preparation itself. Hence, two important tests must be performed to determine background kinase activities for each substrate that will be used. The first one is a kinase assay(s) with parallel "blank" Ni-NTA and MonoS chromatography fractions from uninfected Sf9 cell cultures. The second important test is to perform kinase reactions with the substrate preparations only. If any of these tests show kinase activity towards the substrate of interest, additional purification of both the substrate and the kinase is needed.

4. *Autocatalytic activities.* Autocatalytic activities have been reported for many kinases including CDKs. These vary in magnitude relative to the substrates. In our hands, very low autocatalytic activity has been observed for CDK7/His_6-CycH/MAT1 (*see* Fig. 3). There is a clear auto-phosphorylation of His_6-CDK9 by His_6-CDK9/CycT1 (*see* Fig. 3). This could be a genuine auto-phosphorylation event or an artifact

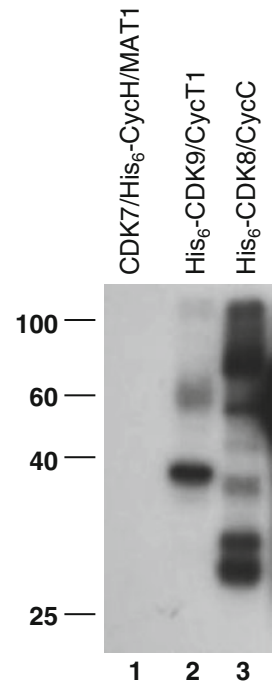

Fig. 3 Autocatalytic activity of the recombinant kinases. Peak fractions from the MonoS chromatography of the kinases shown on the top have been used in kinase reactions with no substrate. The reactions were run on SDS-PAGE gels and exposed for 2 days on X-ray films. The mobility of the molecular size standards is shown on the *left*

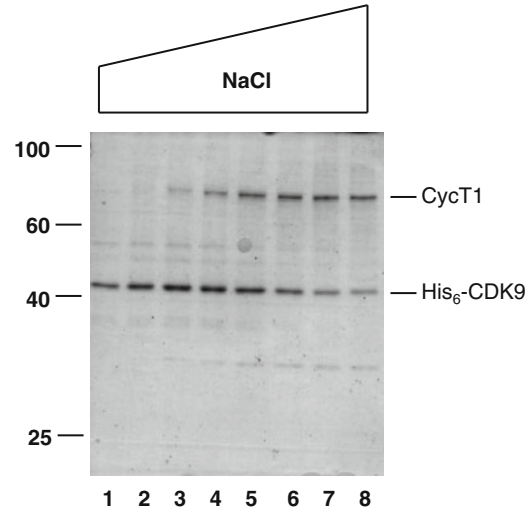

Fig. 4 Purification of His_6-CDK9/CycT1 on MonoS column. Pooled His_6-CDK9/CycT1 fractions from the Ni^{2+}-NTA chromatography were loaded on a 5 ml Mono S cartridge and eluted by linear 80–500 NaCl gradient. The 300–500 mM NaCl range is shown. Note the earlier elution of His_6-CDK9 monomers

because of the excess His_6-CDK9 in the prep (*see* **Note 15** and *see* Fig. 4). His_6-CDK8/CycC shows a broader pattern of auto-phosphorylation signals that include both His_6-CDK8 and CycC, but also other contaminating peptides (*see* Fig. 3).

The auto-phosphorylation signals in His_6-CDK8/CycC and His_6-CDK9/CycT1 preps have been detected upon long exposures of the gels. However, in cases of moderate phosphorylation of a substrate these auto-phosphorylation signals can impede the analysis of the data. In this situation a substrate molecule with an affinity tag can be useful. *See* **step 6** (GST-fusion proteins).

5. *Choice of substrate. Use of synthetic peptides.* If a contaminating kinase is detected in the substrate preparation, one can use short synthetic peptides (20 amino acids or so) that represent the phosphorylation site of interest. While most of the times these serve the purpose of measuring the activity of the CDK, they should be used with caution as they are not a true representative of the whole substrate.
6. *GST-fusion proteins.* We have found that, whenever possible, the best option for substrate is the natural target of the CDK, which is expressed as a GST fusion protein in *E. coli* (*BL21D*) cells. A variety of pGEX vectors can be used. Many GST-fusion proteins are soluble; they are produced at significant levels and can be easily purified by a one-step affinity chromatography on Glutathione-Agarose geads. Importantly, in our hands such preps are essentially free of contaminating kinase.

A disadvantage of this system is that sometimes the proteins are partially degraded. In this situation a gel filtration column that can enrich the preparation in full-length peptides should be considered.

GST-fusion proteins provide an important advantage in cases where the kinases display autocatalytic activities. In these situations the substrate can be pulled out of the kinase reaction by Glutathione-Agarose beads before analysis by SDS-PAGE [6]. Even if weak, only the signals from the phosphorylation of the substrate will be detected.

4 Notes

1. Comprehensive information on growth and maintenance of Sf9 cells plus extensive discussion on baculovirus expression vectors can be found in *Baculovirus and Insect Cell Expression Protocols* [26] and in *Baculovirus Expression Protocols* [27].
2. Commercial protease inhibitor cocktails can be used instead of the listed inhibitors.
3. We have used Bac-N-Blue (Invitrogen Life Technologies), Bac-to-Bac (Invitrogen Life Technologies), and BacVector-3000 system (Novagen) with equal success. We do not provide details on these procedures as point-by-point protocols are available on the manufacturers' websites. However, we mention some notes of consideration.

   In the Bac-N-Blue system a pBlueBac plasmid (it carries a cassette of the cloned gene of interest plus *LacZ*) is co-transfected with linearized *AcNPV* baculovirus DNA in Sf9 cells. The assembly of recombinant virus takes place in Sf9 cells to produce blue plaques while reconstituted wild type baculovirus produces translucent plaques. Normally, three rounds of purification of blue plaques are needed. This is a cumbersome, costly and time-consuming process that requires certain skills from the operator. Once established, the purified stock of the recombinant virus can be propagated and frozen stocks can last for years. The stock can be retested for the formation of only blue plaques to affirm its purity.

   The BacVector system (Novagen) uses a similar approach, but very efficiently suppresses the production of non-recombinant virus and confers more than 95 % of recombinant virus. Hence, no plaque purification is normally needed. The disadvantage of this convenient shortcut is that in a long run the contaminating non-recombinant viruses can outgrow the virus of interest. We recommend that the original preparation of recombinant virus is propagated to passage 2 and this stock is used for the expression of the protein. If more protein is

required, a fresh transfection with the plasmid and the pricey BacVector DNA should be performed.

The Bac-to-Bac system produces the recombinant baculoviral DNA by transposition in *E. coli* cells (*DH10Bac*) carrying the baculovirus genome as a bacmid (Bmon14272). The recombinant bacmid DNA is isolated from *E. coli* and is readily transfected into Sf9 cells. The produced viral stock is propagated to passage 2 and used for infection and expression of proteins. Again, there is no need for purification or selection of plaques. Importantly, more virus can be easily obtained by re-transfection with the bacmid. In our hands this is the most reliable and easy to handle procedure.

4. It is important to use low MOI during the amplification of the virus. This means that you need to have more cells than viral particles. Higher MOI generates the risk of multiple viruses infecting the same cell and recombining with each other.
5. Sf9 cells grow as monolayer, but lose adherence and change morphology upon infection. More details can be found in [26].
6. These small aliquots are handy if the expression of the proteins needs to be repeated. Their titer can decrease because of the freezing; however, they still can be used to directly proceed to the preparation of high titer viral stock.
7. In our hands MOI = 4 generates the highest level of expression for all the CDKs. Further increase in MOI does not yield more protein.
8. The cells should be quickly frozen using several small aliquots rather than one large aliquot. When thawing, gently swirl the tubes in ice bath until homogeneous suspension is produced. Do not leave on ice for prolonged periods of time.
9. You can freeze the extract or proceed directly to chromatography. If planning to load on N^{2+}-NTA agarose beads on the same day, do not add glycerol.
10. Freezing and thawing of proteins leads to denaturing and the formation of precipitates. Similarly, the dialysis of the Ni-NTA purified proteins causes extensive precipitation and significant loss of recombinant kinases. All these precipitates must be removed by high speed centrifugation. If not, such "cloudy" samples can clog the columns and compromise the purification. These complications and the loss of material can be avoided if the two chromatographies are performed in one long day.
11. The recombinant kinases typically elute in the 25 and 100 mM imidazole fractions. His_6-CycH and CDK7 co-migrate as a single band of 40 kDa while MAT1 is a single band of 36 kDa (*see* Fig. 2a). His_6-CDK8, CycC, and His_6-CDK9 and CycT1 are approximately 53 kDa, 36 kDa, 43 kDa, and 87 kDa, respectively (*see* Fig. 2b, c).

12. Stain with Coomassie Brilliant Blue for about 15 min on a rocking platform. Quick destaining of the gels can be achieved by adding a couple of Kimwipes (or other sturdy paper wipes) to the destaining container. We certainly prefer this fast and simple method of detection. Western blot or kinase assays could be more informative, but are significantly slower and can be very tricky because of the risk of using significant excess of kinase or antigen.
13. Any low-pressure gradient-making chromatography system can be used.
14. Avoid extensive sonication. Sonication breaks some of the cells and releases lysozyme, which continues to degrade the cell walls. If sonication is overdone, the cellular DNA is sheared in large pieces. This DNA is going to increase the viscosity of the extract and interfere with the subsequent affinity chromatography.
15. Sometimes the cyclin and the catalytic unit of the kinase are expressed at different levels. Purification by Ni-NTA agarose or other affinity resins will not reveal the unbalanced abundance of the peptides. The subsequent purification on MonoS (or other ion-exchange resins) can reveal fractions that contain the tagged subunit only. One such example is shown in Fig. 4. The tagged CDK9 elutes as an earlier peak as compared to the untagged CycT1, but then the peak trails and coincides with CycT1. The earlier CDK9 fractions contain significantly lower kinase activity as compared to the fractions that contain both subunits of the kinase (not shown). We have similar unbalanced expression in the case of His_6-CDK8/CycC (not shown).
16. The assessment of incorporation of ATP/min/mg of substrate gives a good idea of the activity of the kinase and can serve as cross-reference for different preparations. However, the measurement is inaccurate as very low proportion of the total ATP is incorporated. If such measurements are obligatory, details on the procedure can be found in [28].

Acknowledgements

We thank Drs. D. Morgan, E. Lees, and D. Price for providing baculoviruses and vectors for the expression of the recombinant kinases. MBP was a gift from Dr. G. Harauz. This study was supported by grants to K. Y. from the Natural Sciences and Engineering Research Council of Canada (NSERC #217548) and the Ontario Genomics Institute (OGI #043567).

References

1. Morgan DO (1997) Cyclin-dependent kinases: engines, clocks, and microprocessors. Annu Rev Cell Dev Biol 13:261–291
2. Andrews B, Measday V (1998) The cyclin family of budding yeast: abundant use of a good idea. Trends Genet 14:66–72
3. Gopinathan L, Ratnacaram CK, Kaldis P (2011) Established and novel Cdk/cyclin complexes regulating the cell cycle and development. Results Probl Cell Differ 53:365–389
4. Fisher RP (2005) Secrets of a double agent: CDK7 in cell-cycle control and transcription. J Cell Sci 118:5171–5180
5. Yankulov KY, Bentley DL (1997) Regulation of CDK7 substrate specificity by MAT1 and TFIIH. EMBO J 16:1638–1646
6. Pinhero R, Liaw P, Bertens K, Yankulov K (2004) Three cyclin-dependent kinases preferentially phosphorylate different parts of the C-terminal domain of the large subunit of RNA polymerase II. Eur J Biochem 271: 1004–1014
7. Bhaduri S, Pryciak PM (2011) Cyclin-specific docking motifs promote phosphorylation of yeast signaling proteins by G1/S Cdk complexes. Curr Biol 21:1615–1623
8. Pagliuca FW, Collins MO, Lichawska A, Zegerman P, Choudhary JS, Pines J (2011) Quantitative proteomics reveals the basis for the biochemical specificity of the cell-cycle machinery. Mol Cell 43:406–417
9. Koivomagi M, Valk E, Venta R, Iofik A, Lepiku M, Morgan DO, Loog M (2011) Dynamics of Cdk1 substrate specificity during the cell cycle. Mol Cell 42:610–623
10. Kobor MS, Greenblatt J (2002) Regulation of transcription elongation by phosphorylation. Biochim Biophys Acta 1577:261–275
11. Egly JM, Coin F (2011) A history of TFIIH: two decades of molecular biology on a pivotal transcription/repair factor. DNA Repair (Amst) 10:714–721
12. Galbraith MD, Donner AJ, Espinosa JM (2010) CDK8: a positive regulator of transcription. Transcription 1:4–12
13. Price DH (2000) P-TEFb, a cyclin-dependent kinase controlling elongation by RNA polymerase II. Mol Cell Biol 20:2629–2634
14. Cho S, Schroeder S, Ott M (2010) CYCLINg through transcription: posttranslational modifications of P-TEFb regulate transcription elongation. Cell Cycle 9:1697–1705
15. Ping YH, Rana TM (1999) Tat-associated kinase (P-TEFb): a component of transcription preinitiation and elongation complexes. J Biol Chem 274:7399–7404
16. Yankulov K, Bentley D (1998) Transcriptional control: tat cofactors and transcriptional elongation. Curr Biol 8:R447–R449
17. Fisher R, Jin P, Chamberlin H, Morgan D (1995) Alternative mechanisms of CAK assembly require an assembly factor or an activating kinase. Cell 83:47–58
18. Rickert P, Corden JL, Lees E (1999) Cyclin C/CDK8 and cyclin H/CDK7/p36 are biochemically distinct CTD kinases. Oncogene 18:1093–1102
19. Peng J, Zhu Y, Milton JT, Price DH (1998) Identification of multiple cyclin subunits of human P-TEFb. Genes Dev 12:755–762
20. Yankulov K, Yamashita K, Roy R, Egly JM, Bentley DL (1995) The transcriptional elongation inhibitor 5,6-dichloro-1-beta-D-ribofuranosylbenzimidazole inhibits transcription factor IIH-associated protein kinase. J Biol Chem 270:23922–23925
21. Matsuoka M, Kato JY, Fisher RP, Morgan DO, Sherr CJ (1994) Activation of cyclin-dependent kinase 4 (cdk4) by mouse MO15-associated kinase. Mol Cell Biol 14:7265–7275
22. Fisher RP, Morgan DO (1994) A novel cyclin associates with MO15/CDK7 to form the CDK-activating kinase. Cell 78:713–724
23. Larochelle S, Chen J, Knights R, Pandur J, Morcillo P, Erdjument-Bromage H, Tempst P, Suter B, Fisher RP (2001) T-loop phosphorylation stabilizes the CDK7-cyclin H-MAT1 complex in vivo and regulates its CTD kinase activity. EMBO J 20:3749–3759
24. Ramanathan Y, Rajpara SM, Reza SM, Lees E, Shuman S, Mathews MB, Pe'ery T (2001) Three RNA polymerase II carboxyl-terminal domain kinases display distinct substrate preferences. J Biol Chem 276:10913–10920
25. Rossignol M, Kolb-Cheynel I, Egly JM (1997) Substrate specificity of the cdk-activating kinase (CAK) is altered upon association with TFIIH. EMBO J 16:1628–1637
26. Murhammer DW (2007) Baculovirus and insect cell expression protocols, 2nd edn. Humana Press, Totowa, NJ
27. Richardson CD (1995) Baculovirus expression protocols. Humana Press, Totowa, NJ
28. Kikkawa U, Minakuchi R, Takai Y, Nishizuka Y (1983) Calcium-activated, phospholipid-dependent protein kinase (protein kinase C) from rat brain. Methods Enzymol 99: 288–298

Chapter 4

Preparation of CDK/Cyclin Inhibitor Complexes for Structural Determination

Asterios I. Grigoroudis and George Kontopidis

Abstract

The abundance of biochemical and structural knowledge on the Cyclin-Dependent Kinases (CDKs) has provided a comprehensive but not exhaustive insight into the molecular determinants that govern their function mechanisms. The implementation of structural and functional CDK models towards developing novel anticancer strategies that will specifically target individual or multiple CDKs remains a critical need.

More than 250 CDKs crystal structures are available to-date, including truncated or whole, modified or not, active or inactive forms, co-crystallized with the cyclins and/or their respective putative inhibitors, though, to our knowledge, there is no NMR solved structure available to date. We hitherto attempt to provide a useful guide from protein production to crystallization for CDK/Inhibitors complexes based on an overview of the already elucidated CDK structures, constructs and the preferable expression vectors in each case, in order to yield the respective crystals.

Key words CDK-inhibitors complexes, Cyclin-dependent kinases (CDKs), Cyclins, Protein crystallography, Structural determination

1 Introduction

1.1 Cyclin-Dependent Kinases Structural Insight

In terms of structural basis for regulation and inhibition, the CDKs have long been among the most extensively characterized [1]. Lolli's comprehensive review on CDKs gathered the majority of the then elucidated structures [2]. The CDK2 structure has been extensively analyzed in the inactive un-phosphorylated form, in the partially activated phosphorylated isoform in the partially and/or activated complex with Cyclin A. Numerous complexes have been solved in monomeric, cyclin partner and inhibitor bound forms [3–5] and the resulting information has enabled the discovery and optimization of highly potent ATP inhibitors of CDK2 [6]. CDKs are essentially inactive in monomeric form; being partially activated after binding to cyclins and fully after phosphorylation of the T-loop. CDKs remain the focus of intense efforts in drug

Mar Orzáez et al. (eds.), *Cyclin-Dependent Kinase (CDK) Inhibitors: Methods and Protocols*, Methods in Molecular Biology, vol. 1336, DOI 10.1007/978-1-4939-2926-9_4,

development and many inhibitors with activity against CDKs are under preclinical and clinical examination in cancer research [7].

Additional structures of CDKs, cyclins or CDK/Cyclin (CDK/C) complexes (CDK2/CE, CDK2/CB, CDK4/CD, CDK7, CDK9/CT) had already complemented others previously solved (CDK5/p25, CDK6/vCyc, and CDK6/INK4s). Since then, the CDK8 structure elucidation [8] revealed a unique Cyclin C recognition helix that explained the specificity of the CDK8/CC pair and discrimination among what is widely held as a highly promiscuous binding in the CDK/C family.

1.2 Similar Yet Different

CDKs are similar in terms of sequence and structure. Taking CDK2 as reference and comparing it with all other CDKs with known structure, sequence identity varies from 40 % for CDK7 to 60 % for CDK5 (with similarity between 58 and 74 %). However, a closer look at those structures highlights that while secondary structure elements are all very well conserved with minimal differences in terms of their length, structural deviations cluster in a few regions, which constitute the core of the interacting surfaces differentially used by CDKs to recognize their specific binding partners [2]. These elements also prove critical regarding the reproducibility of the crystallization process, as the disproportionally large number of CDK2 structures, compared to the rest of the CDKs, clearly demonstrates.

1.3 Construct That Yields Crystals

So the CDK sequence is the first and foremost concern when selecting the appropriate construct that will yield the crystal complexes with conformational stability. Flexible parts and vulnerable domains are truncated, while crucial amino acids are mutated omitted or retained. Choice of the crystallization partner and possible oligomerization CDK form also play their part. The construct type may also determine the purification procedure and the final purity of the protein sample. The level of the protein sample quality and level of purity is not the sole issue when determining a structural formation. The nature of the expression vector and protein source (prokaryotic or eukaryotic) should be taken under consideration as well, since CDK modifications—such as phosphorylation—can alternate their conformation from inactive to active and vice versa. The number of structures solved with the same crystal form and the accomplished resolution reflect the reproducibility and discretion of crystal yield. For drug design high resolution structures are required, as well as good number of crystals, in order to study a substantial number of ligands.

1.4 Tools Inventory

In an attempt to bridge the gap in recent bibliography, we gathered the majority of recently solved CDK/Cyclin/Inhibitor structures registered in the Protein Data Bank (PDB), and retrieved information—wherever available—regarding the respective constructs, expression

vectors, purification procedure, and crystallization conditions of the complexes. The expression systems and vectors—wherever available—are listed for each protein, followed by the respective multistep purification procedures. Crystallization conditions for each CDK complex with the putative inhibitors, as mentioned in the PDB files, together with the respective references, complement the CDK crystallization overview.

As demonstrated in Table 1, eukaryotic expression systems (Baculovirus transfected SF9 or SF21 cells) are preferable for production of CDKs in most cases, while expression in bacterial

Table 1
Construction, preparation, crystallization, and determination of most recent CDK-complex structures available

Protein construct (aa)	Expression	Purification procedure	Crystallization conditions	Reference
	System/Vector		Precipitant/ additive/pH	
CDK2 (299)	SF21/Baculovirus—*E. coli*/PGEX	SP-Sepharose/ ATP-agarose column	8–16 % PEG 3350/50–100 mM AMAC/7.5	[9]
-298	*E. coli*/PGEX6P-1		5 % PEG 3350/50 mM PHO (Na/K)/7.5	[10]
-298	*E. coli*/PPROEX	Double Ni affinity/ gel filtration	6 % PEG 3350/ 100 mM AMAC/7.8	[11]
-298	Hi5/Baculovirus		10 % PEG 3350/ AF/8.5	[12]
-298	SF9/Baculovirus	Ion exchange/ ATP-agarose/gel filtration	10 % PEG 3350/ NaF/7.0	[13]
-298	SF9/Baculovirus	DEAE/SP-Sepharose/ ATP-agarose/size exclusion	7 % PEG 3350/42.5 mM AMAC/7.4	[14]
-298	Hi5/Baculovirus	SP-Sepharose/ion exchange/gel filtration	10 % PEG 3350/ NaF/7.0	[15]
-300	*E. coli*/SF9/ Baculovirus	Ni-NTA/S-200 Sephacryl	14 % PEG 4000/50 mM AMAC/7.5	[16]
-299	SF21/Baculovirus	DEAE/SP-Sepharose/ ATP-agarose	8 % PEG 4000/50 mM AMAC/7.5	[17]

(continued)

Table 1
(continued)

Protein construct (aa)	Expression	Purification procedure	Crystallization conditions	Reference
-298	SF21/Baculovirus	DEAE/SP-Sepharose/ ATP-agarose	8 % PEG 4000/50 mM AMAC/7.5	[18]
-298	SF21/Baculovirus	DEAE/SP-Sepharose/ ATP-agarose	/30 mM NaCl/7.4	[19]
-299	SF21/Baculovirus	Affinity chromatography	8 % PEG 4000/50 mM AMAC/7.5	[20]
-299	SF9/Baculovirus	DEAE/SP-Sepharose/ ATP-agarose	8 % PEG 4000/50 mM AMAC/7.4	[21]
-306	*E. coli*/PGEX6P-1	Double GST-affinity/ size exclusion	15 % JEFFAMINE ED-2001/5 mM ANS/7.5	[22]
CDK2-CA (300–262)	SF9/ Baculovirus-*E. coli*	DEAE/SP-Sepharose/ ATP-agarose	1.1 M AMS/7.0/	[23]
(298–261)	SF9/ Baculovirus-*E. coli*	Ion exchange/ ATP-agarose/gel filtration	20–30 % PEG 3350 0.1 M TSC/7.8	[23]
(309–265)	Hi5/Baculovirus/ pVL1392— *E. coli*/PGEX	Double G-Sepharose/ gel filtration	20 % AMS–1 M KCl/7.0	[24]
(298–260)	SF/Baculovirus-*E. coli*	DEAE-Sepharose/ ATP-agarose/gel filtration-NiNTA	1.5 M SAC—100 mM SOC/6.7	[25, 26]
(298–264)	Hi5/Baculovirus/ pVL1392—*E. coli*	Double G-Sepharose/ gel filtration	AMS—KCl/7.0	[27]
CDK2-CB1 (289–260)	Hi5/Baculovirus— *E. coli*/pET28	Double G-Sepharose/ gel filtration	0.9–1.2 M AMS/6.0–6.5	[28]
CDK2-CE (298)	SF9/Baculovirus	NiNTA column	PEG 3350/-/8.0	[29]
CDK4-CD1 (271–306)	SF21/Baculovirus	Ni-NTA/ion exchange/gel filtration	10 % PEG 4000/200 mM AMS/7.0	[30]
CDK4-CD3 (308–306)			0–20 % MPD/6.0	
	SF9/pFastBac1	Glutathione Sepharose	15 % PEG 3350/10 % Tacsimate/6.6	[31]
CDK5-A (292–147)	SF9/Baculovirus	Ni-NTA/ion exchange/gel filtration	PEG 3350/200 mM KI (NaI)/7.6	[32]

(continued)

Table 1
(continued)

Protein construct (aa)	Expression	Purification procedure	Crystallization conditions	Reference
(292–149)	SF9/Baculovirus	Ni-NTA/ion exchange/gel filtration	PEG 3350/KI, BIS-TRIS PROPANE/7.0	[33]
CDK6 (307) CDK6-Ch (308–254)	Carna Biosciences Inc.	Commercially available	6–16 % PEG 3350/25–50 mM AMN/6.0	[34]
	SF9/Baculovirus/ pBSK-glob-CDK6	Co, Ni affinity/ion exchange/reverse phase	13 % PEG 3350/ NaCl, CAAC/8.0	[35]
CDK7 (346)	SF21/Baculovirus PVL1392	GSH-Sepharose/size exclusion	20 % PEG 4000/ NAC, NAAC, NDSB201/6.4	[36]
CDK 8-CC (405–285)	SF9/pFastBacHTa	GSH-Sepharose/ion exchange/gel filtration	20 % PEG 3350/0.2 M LiCl/6.8	[8]
CDK9-CT1 (331–259)	SF9-21/Baculovirus pVL1393	GSH-Sepharose/gel filtration	14 % PEG 1000/100 mM PHO (Na/K), 600 mM NaCl, 4 mM TCEP/6.2	[37]

AMAC ammonium acetate, *PHO* phosphate, *AF* ammonium fluoride, *ANS* anilinonaphthalene sulfonates, *SOC* sodium cacodylate, *AMS* ammonium sulfate, *AMN* ammonium nitrate, *CAAC* calcium acetate, *NAAC* sodium acetate, *NAC* sodium citrate, *NDSB* non-detergent sulfobetaine, *TCEP* tris (2-carboxyethy1) phosphine, *A* activator, *h* homolog

systems is a rare possibility. It also seems that a three-step purification procedure is mandatory to yield the appropriate quantity and quality for each complex, whereas the combination of 5–30 % PEG with selected precipitants, in a pH range of 6.0–8.0, generally consists the safest road to crystallization with the various inhibitors.

2 Methods

2.1 CDK2-Inhibitor Interactions

When determining crystallization conditions, one has to take under consideration the different ways in which CDKs and their putative inhibitors will behave in various soaking conditions. Many putative inhibitors, in most cases biologically interesting organic ligands, are more soluble in dimethylsulfoxide or alcohols and precipitate in aqueous solution. CDKs crystals on the other hand tend to crack or dissolve in these solutions, so some compromise must be reached. In many cases the ligand may be insoluble in the typical precipitant solution in which the CDK under

investigation crystallizes, and must be dissolved in solvents such as ethanol or DMSO to reproduce the experimental concentration. However, these solvents frequently have a detrimental effect on the crystals and result in poorer diffraction, so a different approach is required. In most cases the inhibitor's solubility is the limiting factor in obtaining a ligand complex structure. To maximize the formation of the CDK-inhibitor complex, the highest soluble ligand concentration is also needed with KD being the critical factor in this case. The above issues, as well as different strategies of soaking ligands are addressed by McNae et al. in detail in previous crystallography review: "Studying protein–ligand interactions using protein crystallography."

Obtaining structural data of selected CDK/Cyclin/Inhibitor complexes regarding most CDKs range from cloning to expression vectors and from purification techniques to crystallization conditions and X-ray data collection quoted in a manner to provide a thorough insight into the crystallization process, whereas the cited literature may provide with detailed descriptions. CDKs are listed according to their numerical order for guidance discretion and also to highlight the most comprehensive and widespread one, CDK2. The chief aim here is to give an overview of the experimental procedures widely used in the field, in order to present them to their full reproducible potential.

2.2 CDK2

Expression, purification, and crystallography of a CDK2-complex is reported by Betzi et al. in their recent work regarding crystal structure of CDK2/Cyclin A with various compounds [22], and was sampled for this chapter as a recent characteristic example of cloning, expression, purification, crystallization, and structural determination of CDK2.

2.2.1 Cloning and Expression

A bacterial expression system was implemented, not a typical choice for CDK complexes. The gene for human CDK2 (residues 1–298) was cloned into the pGEX6P-1 expression vector to provide an N-terminal GST-tag that was subsequently transformed into *E. coli* cells. Cultures were grown and induced as described [22].

2.2.2 CDK-Complex Purification

The authors followed a 3-column purification procedure, starting with resuspending the cells in 50 mM HEPES buffer (pH 7.5) containing 150 mM NaCl, 10 mM $MgCl_2$, 2 mM dithiothreitol (DTT), 1 mM EGTA, 0.5 mg/ml lysozyme, and 0.01 % Triton X-100 at 4 °C. After sonication and centrifugation, GST-affinity column chromatography was used. A second GST-affinity column removed the cleaved GST-tag, while CDK2 was loaded onto a gel filtration column, from where it was eluted with a 50 mM HEPES buffer (pH 7.5) containing 150 mM NaCl, 10 mM $MgCl_2$, 2 mM DTT, 2 mM EGTA, and 0.01 mM ADP. Purified CDK2 was concentrated to ~10 mg/ml. Cyclin A2 was also

purified by GST-affinity, the point here being the addition of an extra 100 mM $MgCl_2$ to fractions to prevent protein aggregation. After protease cleavage, the solution was applied to anion-exchange column, from which fractions containing cyclin A were pooled and concentrated to match double the CDK's. Activation of the CDK2-cyclin A complex was achieved in vitro [22]. Briefly, CDK2 was added to a solution of 30 mM Tris–HCl (pH 7.5), 10 mM $MgCl_2$, and 3 mM DTT containing the GST-CAK1 activator and 10 mM ATP. The mixture was incubated for 4 h at room temperature, then overnight at 4 °C, prior to addition of cyclin A, to yield the activated CDK2-cyclin A complex, suitable for crystallization.

2.2.3 CDK Complex Crystallography

For crystallization purposes, the purified CDK2 was transferred into a 100 mM Na/K phosphate buffer (pH 6.2) containing 2 mM DTT and was concentrated to 10 mg/ml as described. Crystallization of CDK2 was then performed at 19 °C using the hanging drop vapor-diffusion method. Initially, crystals of CDK2, as well as in the presence of several compounds (JWS648, SU9516, and ANS) were grown from 5 % (v/v) PEG 3350 in 50 mM HEPES/NaOH (pH 7.5) at a CDK2 concentration of ~5 mg/ml. While free CDK2 and complexes with inhibitors yielded crystals after 2 days, the CDK2-ANS crystals appeared after several weeks. To diminish the long crystallization interval, the authors suggested alternative crystallization conditions, using 15 % (v/v) Jeffamine ED-2001 and 50 mM HEPES, yielding co-crystals with ANS alone and in ternary complex with ANS and JWS648 after 2 days (1.5–5 mM of compound was added to the crystallization solution), conditions mentioned in the aforementioned table. Crystals were incubated for 24 h in 50 mM HEPES (pH 7.5), 50 mM phosphate (Na/K, pH 7.5), 7.5 % (v/v) PEG 3350, and 5–15 mM aqueous ANS, with or without 2 mM of compound JWS648 or SU9516. Prior to data collection, the cryoprotection mentioned is: 50 mM HEPES (pH 7.5), 50 mM phosphate (Na/K, pH 7.5), 7.5 % (v/v) PEG 3350, and 25 % (v/v) ethylene glycol, with the 0.5–2 mM respective inhibitor [22]. X-ray diffraction data were recorded in the Moffitt Cancer Center Structural Biology Core, while structural determination was carried out as described [22].

2.3 CDK4

The first attempt to solve the CDK4 structure was made by Takaki et al. [31]. They used CDK2 construct and specific mutations that mimic CDK4 binding site, since the overall homology between CDK2 and CDK4 is 45 %, presuming that both enzymes are folded in a similar fashion. According to authors, it was likely that sequence differences in the ATP binding pocket could affect the inhibitors' binding directly through different side chain residues. The binding pocket amino acid sequence of CDK2 was known to be FEFLHQDLKK, strikingly similar to the CDK4's FEHVDQDLRT,

indicating three non-conservative sequence differences at residues 82, 83, and 89. Thus, they synthesized CDK4 mimic CDK2 by site-directed mutagenesis that would possess the nucleotide sequence of CDK4 in the ATP binding pocket region. CDK4 mimic CDK2 was then expressed in Sf9 cells, producing a soluble protein as was the case with wild-type CDK2. This CDK4 mimic CDK2 also produced good crystals for X-ray crystallography under the same conditions used for crystallization of wild-type CDK2 [31].

2.3.1 CDK Complex Crystallography

Although the similarities between the ATP binding site of CDK2 and CDK4 are notable, drug design requires specific structural information. To identify structural differences of the inhibitor binding site of CDK4 and CDK2, the crystal structure of CDK4 mimic CDK2 bound to a specific "compound I" were determined and compared by the authors [31], with the structure of the compound I/wild-type CDK2 complex. Comparison indicated that CDK4 mimic CDK2 possesses additional space caused by differences in the size of the side chain of residue 89 (CDK2: Lys; CDK4: Thr). According to the X-ray structures, it seemed likely that the CDK4 structure had additional space to accommodate larger substituent parts for the inhibitors. Inhibitors designed to bind into this additional space should be selective for CDK4 without exhibiting analogous CDK2 activity.

The crystal structure of various mutated and/or truncated forms of the human CDK4 in complex with a D-type cyclin was elucidated in detail by Day et al. [30]:

2.3.2 Cloning and Expression According to Crystallization Tests

The authors' steps leading to the ideal complex for crystallization, with specific lengths for each protein is summarized here. Co-expression of full-length, CDK4 (residues 1–303), with a C-terminal 6-His tag and cyclin D1 (residues 1–295) in SF insect cells, yielded an active complex possessing heterogeneous phosphorylation of both CDK4 and cyclin D1, which nevertheless failed to crystallize [30]. The authors then decided to introduce the T172A (CDK4) and T286A (cyclin D1) substitutions which led to a non-phosphorylated complex, that failed to crystallize as well. Subsequently cyclin D1 was C-terminally truncated ($CycD_{11–271}$) in an attempt to remove the critical Thr-286 phosphorylation site and flexible poly-glutamate PEST region, where the hepta-glycine loop of CDK4 (residues 42–48) was replaced with the Gly42-Glu43-Glu44-Gly48 found in CDK6, resulting to what the authors named as: "$CDK4_{EE}$". The $CDK4_{EET172A}/CycD_{11–271}$ complex finally yielded crystals diffracting to 2.8 Å and enabled a—via molecular replacement—structure solution (described in detail by Day et al.). Novel crystallization conditions were also identified for $CycD_{11–271}$ in complex with a phospho-mimetic construct

$CDK4_{EET172D}$ and with a CDK4 construct containing phosphorylated T172 ($CDK4_{EET172Ph}$). Data were collected to 2.3- and 2.9-Å resolution for each complex respectively, which yielded equivalent structures. In all of these structures the N-terminal region of cyclin D1 caused disorder. Thus, a further truncation was applied ($CycD_{115–271}$) that, in combination with $CDK4_{EET172A}$, produced a complex that finally crystallized readily, even in the absence of precipitant, yielding a 2.5-Å resolution structure. The strategy described above and analyzed in their supporting material by Day et al. provides an excellent example of addressing crystallization issues by intervening in molecular level.

2.3.3 CDK-Complex Purification

Authors describe a typical CDK4 and cyclin D1 co-expression in SF21 insect cells. The complex was purified by using Ni-NTA affinity, ion exchange chromatography, and gel filtration. The purified complex was typically concentrated to a level of 10–12 mg/ml in 20 mM Tris–HCl (pH 8.0), 10 % glycerol, 150 mM NaCl, and 5 mM DTT for crystallization, as described in detail in the supplementary [30] information. Complex $CDK4_{EE(1–303/His6)}/CycD_{11–271}$ was also expressed, purified, and concentrated for crystallization in the same fashion. Concentration levels of 10 mg/ml seem to be sufficient for the majority of the works cited in this chapter.

2.3.4 CDK Complex Crystallography

The $CDK4_{EET172A}/CycD_{11–271}$ complex was concentrated to 12 mg/ml and mixed 1:1 with reservoir solution composed of 0.1 M Tris–HCl (pH 7.0), 10 % (w/v) PEG 4000, 0.2 M ammonium sulfate, and 1 mM AMP-PNP in sitting drops and incubated at 20 °C. Small plates appeared in 1–3 days. Crystals were cryoprotected in 0.1 M Tris–HCl (pH 7.0), 10 % (w/v) PEG 4000, 0.2 M ammonium sulfate, and 20 % (v/v) glycerol, before frozen in liquid nitrogen for data collection.

The mutated and/or truncated $CDK4_{EET172D}/CycD_{11–271}$, $CDK4_{EET172Ph}/CycD_{11–271}$, and $CDK4_{EET172A}/CycD_{115–271}$ complexes' purification and crystallization attempts are also described by the authors in their supplementary material. It is reported that all X-ray data were collected on beam lines ID23 and ID29, at the European Synchrotron Radiation Facility. The 2.85-Å dataset collected from crystals of construct $CDK4_{EET172A}/CycD_{11–271}$ were initially indexed as (a—57.15 Å, b—64.84 Å, c—188.97 Å) P22121, as stated in ref. [30].

Like an invention we previously commented on, Day et al. implemented a part of another similar CDK, the C-terminal domain of CDK6 (extracted from PDB ID code 1BLX, 1.9 Å) as a search model to determine translation function (TF) solutions, nevertheless with weak results for the CDK C-terminal domain model, while their extensive attempts to find solutions for the CDK4 N-terminal domain failed.

2.4 CDK5

2.4.1 Cloning and Expression

According to Tarricone et al. [32], the human p25 and CDK5 proteins were co-expressed in insect cells using a single Baculovirus vector. In order to avoid putative toxicity levels from unregulated CDK5 activity, residue Asp145, located in the conserved Asp-Phe-Gly motif, was mutated to Asn in order to deactivate the kinase. The full-length CDK5 sequence was then fused to a C-terminal 6-His tag, and the protein complex was purified by conventional chromatographic techniques as stated in detail in the experimental procedures of the aforementioned work. The complex is referred to crystallize in space group C2, with two p25-CDK5 complexes in the asymmetric unit.

2.4.2 CDK-Complex Crystallization and Structural Determination

Initial crystals of CDK5-p25 were generated by vapor diffusion at 20 °C using a reservoir buffer containing 20 % PEG3350 and 200 mM NaI with a protein concentration of 7 mg/ml and improved by micro-seeding. Crystals were gradually transferred to the appropriate cryo-buffer (10 % PEG 3350, 100 mM Tris–HCl [pH 7.6], 200 mM KI, 10 mM DTT, and 25 % glycerol) and were flash-frozen prior to data collection. X-ray diffraction data from a monoclinic crystal and two orthorhombic crystals were collected on a on beam line BW7A, at EMBL-DESY. Data processing was carried out by Tarricone et al. using DENZO and SCALEPACK computational calculations, the CCP4 (Collaborative Computational Project, 1994) and CNS suites, while molecular replacement was carried out using AMoRe (CCP4).

Another CDK5 form, $CDK5_{D144N}$/p25 [33] was initially crystallized in a monoclinic space group, and the structure was determined at 2.65 Å resolution. The authors also used the monoclinic crystals data for structural determination of the $CDK5_{D144N}$/p25/indirubin-3′-oxime complex, which, however, retained a plate-like morphology, tended to grow in very fragile stacks, making the handling for intensive screening of inhibitors a hard task [33]. A more robust crystal form was therefore attempted by Ahn et al., using primary seed stocks, derived from the monoclinic crystals. Seeding with the same seed stock yielded two different crystal forms depending on the composition of each drop. While the original monoclinic crystal grew when the protein concentration ranged between 7 and 10 mg/ml or the PEG concentration was lower than 12 % (w/v), when protein concentrations elevated up to 16 mg/ml and in the presence of 13–15 % PEG 3350 and 0.1 M Bis-Tris propane (pH 6.8–7.0), the authors reported growing of trigonal crystals instead. Repeated micro-seeding cycles performed with new seed stock generated by trigonal crystals reproducibly yielded new trigonal crystals of a considerable size which proved good enough for diffraction experiments and derivatization with inhibitory compounds. The trigonal crystals (space group $P3_221$), however, as the authors quote were much more reproducible, gave a better diffraction pattern, were more tolerant to DMSO

solubilizer and were suitable for screening. The structures were further solved by molecular replacement and refined as described within the manuscript.

2.4.3 Alternative CDK5-Generating Strategies

The mutant $CDK5_{D144N}$/p25 complex was produced by infecting cells with a single dual recombinant baculovirus and purified as described. Crystallization of p25/CDK5 was carried out by the hanging drop vapor diffusion technique using the streak-seeding method for crystal optimization. The original monoclinic crystals were used to generate stocks of seeds for micro-seeding: primary seed stocks were prepared by transferring a small crystal to 2 μl of reservoir solution and by crushing it with a sharp tip. This stock was serially diluted to 1:10, 1:100, and 1:300 and used to streak-seed drops pre-equilibrated for about 16 h. For inhibitor soaking, the crystals were harvested into a stabilizing solution of 13 % (w/v) PEG 3350, 100 mM KI, 100 mM Bis-Tris propane (pH 7), and 10 mM DTT supplemented with 1 μl of 10–100 mM inhibitor molecule previously dissolved in DMSO (4 % max). Soaks were carried out for 48–72 h, and crystals were subsequently cryoprotected by stepwise addition of stabilizing solution plus 50 % (w/v) glycerol up to a final concentration of 20 % glycerol before freezing in liquid nitrogen. Data were collected at beam lines ID14-1 and ID14-2 of the European Synchrotron Radiation Facility (ESRF). Data processing and reduction were carried out with the HKL package. The structure was determined by molecular replacement with the atomic coordinates of the CDK5/p25 complex (Protein Data Bank code 1H4L) as the search model, utilizing the program AMORE.

A new versatile protocol to characterize the structure of ATP-competitive inhibitors bound to the CDK5/p25 active site was the novelty in this interesting work. In particular, a very well diffracting crystal form of this complex was obtained, consistently providing X-ray diffraction data to high resolution. This new tool was thought to represent a very useful addition to crystals of CDK2 and of the CDK2/cyclinA complex, which had until then been the only way to address the mode of binding of CDK inhibitors to the CDK active site. According to the authors, CDK5/p25 crystals might provide an alternative to the CDK2 crystals for all those inhibitors whose co-crystallization with CDK2 proved impossible due to specific technical limitations. Furthermore, the collection of large datasets of crystallographic models of small molecule inhibitors bound into the active site of different members of the CDK family may eventually provide useful information on structural differences that should be exploited for the design of selective inhibitors.

Alternatively, the CDK5 was produced through a different route by Lim et al., [38]: mutants of p25nck5a were constructed using site-directed mutagenesis with corresponding oligonucleotide primers. Expression and preparation of recombinant proteins as well as the active kinase complexes were reconstituted from GST-CDK5

and GST-p25nck5a or its mutant proteins as described in ref. [39]. The recombinant pGEX plasmid constructs, encoding glutathione *S*-transferase (GST-26 kDa) fusion proteins, GST-p21, GST-p23, GST-p25, GST-Cdk5, and GST-cyclin D1, were individually expressed in *E. coli* strain BL21 (DE3) as described by the authors. Purification of the GST fusion proteins, crystallization attempts, and structural determination were carried out as described in ref. [32].

2.5 CDK6

In their attempt to characterize 4-(Pyrazol-4-yl)-pyrimidines as selective inhibitors of Cyclin-Dependent Kinase 4/6, Cho et al. managed to elucidate the CDK6 structure [34].

2.5.1 CDK-Complex Crystallography

Human CDK6/cyclin D3 was readily purchased. An equimolar complex of a compound and CDK6 at 5 mg/ml in buffer (25 mM Bis-Tris propane, 300 mM NaCl, 1 mM TCEP, pH 7.5, 20 % glycerol) was crystallized using the hanging drop vapor diffusion method. Mother liquor contained 100 mM MES pH 6.0, 25–50 mM NH_4NO_3, and 6–16 % PEG 3350. Crystals were frozen using glycerol as a cryoprotectant, and data were collected at beam line 17ID of the ArgonnePhoto Source (Chicago, IL). Authors opted to process data using the HKL200 package with CDK2 as the start model, while structures were solved employing the software suites from CCP428 and CNX29 and can be accessed in PDB (PDB ID: 3NUP, 3NUX).

2.6 CDK7

Lolli et al. [36] also reported in detail the expression and purification of human CDK7.

2.6.1 Cloning and Expression

A pBS-CDK7 vector was used as a template for a subsequent PCR. CDK7 was cloned into the vector pVL1392 modified with the insertion of GST and protease cleavage site. CDK7-expressing baculovirus was obtained by transfecting Sf21 cells with 2 μg of plasmid DNA and 0.5 μg of linearized baculovirus DNA for 5 days.

2.6.2 CDK-Complex Crystallography

Sitting drop crystallization trials were performed at 4 °C using a crystallization robot (CDK7 concentration up to 7 mg/ml), as described in the respective article. Drops were equilibrated by vapor diffusion. Final crystallization conditions were identified as 0.1 M Na Citrate (pH 6.4), 0.2 M Sodium Acetate (pH 6.4), 20 % PEG 4000, 10 % glycerol, 200 mM NDSB201 (to prevent excessive nucleation and promote crystal growth), and 2 mM ATP. The crystals were transferred to 0.1 M TCS (pH 6.4), 0.2 M Sodium Acetate (pH 6.4), 20 % PEG 4000, 20 % glycerol before freezing in liquid nitrogen.

Authors acquired two different data segments [36] which were indexed separately by computational programs, to which a more extensive reference will follow, since the findings were of great interest. Only 80 % overall completeness was achieved because of radiation damage, so it took the implementation of a combined data set

with addition of reflections in both the high and low resolution shells resulted in data that gave a successful structure solution.

The structure was solved (for a detailed description *see* [36]) by molecular replacement with the program MOLREP, as previously mentioned for other works cited in this overview, using a modified model of inactive as the search object, that yielded three copies, plus a fourth that was discovered by examination of the resulting electron density maps. It was initially suggested that there were two different conformations of CDK7 present within the asymmetric unit. However, upon rebuilding it became apparent that CDK7 differed from CDK2 in this region and the same backbone conformation was in fact present in all four copies. As a result, fourfold averaging was applied to maps during rebuilding followed by rounds of refinement, resulting in the final resolved structure.

2.7 CDK8

Schneider et al. [8] recently reported the structure of CDK8/CycC.

2.7.1 Cloning and Expression

CDK8 and CycC templates were commercially available for subsequent PCR. Besides the CDK8 full-length construct, the authors evaluated C-terminally truncated construct variants (Hs1-464, Hs1-424, Hs1-403, Hs1-377, and Hs1-348) and a kinase dead mutant (Hs1-464 D173A). CDK8 constructs were cloned into the pFastBacHTa vector, modified with the insertion of a glutathione *S*-transferase fusion with a protease cleavage site. CycC was cloned into the pFastBacHTa vector with additional thioredoxin fusion and S-tag fusion, including two cleavage sites. Expression of both proteins was performed as described, using the BAC-to-BAC system in Sf9 cells.

2.7.2 CDK-Complex Purification

Lysis buffer contained 20 mM Hepes/NaOH (pH 6.8), 500 mM NaCl, 10 % glycerol, and 1 mM Bis-Tris propane (2-carboxyethyl) phosphine (buffer A) and a protease inhibitor cocktail. The recombinant CDK8 protein was firstly purified through a GSH-Sepharose. Subsequently, cleaved protein was recovered by negative-affinity chromatography and further purified by size-exclusion. CycC was also purified in the same buffer, using affinity chromatography, with subsequent removal of thioredoxin fusion by thrombin protease overnight. Protein recovery was performed using negative-affinity chromatography, followed by SEC.

2.7.3 Crystallization, X-Ray Data Collection, Data Processing, and Structure Solution

More than 12 different CDK8/CycC constructs were evaluated, as stated by Schneider et al. [8]. Diffracting crystals were obtained from the constructs CDK8 (Hs1-403)/CycC (Hs1-283) at a concentration of ~11 mg/ml, co-crystallized with 10 μM of sorafenib. Crystallization trials were performed with the hanging drop setup in this case as well, at 20 °C within 20 mM Hepes/NaOH (pH 6.8), 210 mM NaCl, 5 % glycerol, and 1 mM Bis-Tris propane

(2-carboxyethyl) phosphine. The final crystallization condition included 20 % PEG 3350 and 0.20 M LiCl. Crystals were shock-frozen, with 15 % ethylene glycol as cryoprotectant. Data sets were collected at beam line X06SA of the Swiss Light Source to a 2.2 Å resolution. Data were computationally processed as described [8], with the objection of surprisingly good R-factors values compared to the corresponding electron density. The final structure solution was then achieved by a combination of manual building and improvement of the electron density. The authors highlighted that an excess of 93 % of all main-chain angles of non-glycine residues fell into the conformationally most favored or allowed regions of the Ramachandran plot. Their final model compromised CDK8 (Hs1-353) and CycC (Hs1-264), with two additional residues from the purification/expression tag (termed −1, 0, where 1 refers to Met1CDK8/Met1CycC according to the sequence in Swiss-Prot ID P49336/P24863).

2.8 CDK9

The CDK9 structure was determined in a procedure described by Baumli et al. [40] as follows:

2.8.1 Expression, Purification, and Crystallization

The pFast-BAC dicistronic vector containing both full-length CDK9 and CycT1 was used as template for PCR reactions. CDK9 and CycT1 constructs were separately cloned into the vector pVL1393, modified with the insertion of MBP or GST fusions and 3C protease cleavage sites. After transfection of Sf21 or Sf9 insect cells, complex expression was obtained by co-infecting insect cells with GST-CycT1 and MBP-CDK9 baculoviruses, as described [40]. The CDK9/CycT1 complex was purified using a GSH-Sepharose column, cleavage of GST and MBP fusions and further purification by size exclusion chromatography. Over 25 different constructs were evaluated. Diffracting crystals were obtained from the constructs CDK9 (residues 1–330)/CycT1 (residues 1–259) using 4.5 mg/ml CDK9/CycT1 with the precipitant solution 100 mM Tris–HCl, pH 8.5, 20 % PEG 1000, 500 mM NaCl, and 4 mM TCEP. The best diffracting crystals were obtained after in vitro autophosphorylation by incubation with ATP to achieve 100 % phosphorylation on Thr186. AMPPNP crystals were obtained in similar conditions by co-crystallizing CDK9/CycT1 in the presence of 2 mM AMPPNP and 2.4 mM $MgCl_2$. The complex with flavopiridol was obtained by co-crystallization with 100 mM flavopiridol in 100 mM Na/K-phosphate pH 6.2, 20 % PEG 1000, 200 mM NaCl, and 4 mM TCEP. Data were collected at ESRF beam lines and the CDK9/CycT1 structure was solved by molecular replacement using as independent search objects a truncated CDK2 model and the structure of free CycT1 (PDB: 2PK2), derived from a previously reported fusion complex with EIAV Tat. The CycT1 structure had been solved by molecular replacement from the CycT2 structure (2IVX), extensively reported in their paper.

Acknowledgments

We would like to thank Dr. Campbell McInnes, Associate Professor at USC for his scientific and financial support through a NIH-funded research project 5R01CA131368.

References

1. Pavletich NP (1999) Mechanisms of cyclin-dependent kinase regulation: structures of Cdks, their cyclin activators, and Cip and INK4 inhibitors. J Mol Biol 287(5):821–828. doi:10.1006/jmbi.1999.2640
2. Lolli G (2010) Structural dissection of cyclin dependent kinases regulation and protein recognition properties. Cell Cycle 9(8):1551–1561
3. Russo AA, Jeffrey PD, Patten AK, Massague J, Pavletich NP (1996) Crystal structure of the p27Kip1 cyclin-dependent-kinase inhibitor bound to the cyclin A-Cdk2 complex. Nature 382(6589):325–331
4. Vulpetti A, Pevarello P (2005) An analysis of the binding modes of ATP-competitive CDK2 inhibitors as revealed by X-ray structures of protein-inhibitor complexes. Curr Med Chem Anticancer Agents 5(5):561–573
5. Kontopidis G, McInnes C, Pandalaneni SR, McNae I, Gibson D, Mezna M, Thomas M, Wood G, Wang S, Walkinshaw MD, Fischer PM (2006) Differential binding of inhibitors to active and inactive CDK2 provides insights for drug design. Chem Biol 13(2):201–211
6. Wang S, Meades C, Wood G, Osnowski A, Anderson S, Yuill R, Thomas M, Mezna M, Jackson W, Midgley C, Griffiths G, Fleming I, Green S, McNae I, Wu SY, McInnes C, Zheleva D, Walkinshaw MD, Fischer PM (2004) 2-Anilino-4-(thiazol-5-yl)pyrimidine CDK inhibitors: synthesis, SAR analysis, X-ray crystallography, and biological activity. J Med Chem 47(7):1662–1675
7. McInnes C (2008) Progress in the evaluation of CDK inhibitors as anti-tumor agents. Drug Discov Today 13(19-20):875–881
8. Schneider EV, Bottcher J, Blaesse M, Neumann L, Huber R, Maskos K (2011) The structure of CDK8/CycC implicates specificity in the CDK/cyclin family and reveals interaction with a deep pocket binder. J Mol Biol 412(2):251–266. doi:10.1016/j.jmb.2011.07.020
9. Berg S, Bergh M, Hellberg S, Hogdin K, Lo-Alfredsson Y, Soderman P, von Berg S, Weigelt T, Ormo M, Xue Y, Tucker J, Neelissen J, Jerning E, Nilsson Y, Bhat R (2012) Discovery of novel potent and highly selective glycogen synthase kinase-3beta (GSK3beta) inhibitors for Alzheimer's disease: design, synthesis, and characterization of pyrazines. J Med Chem 55:9107. doi:10.1021/jm201724m
10. Martin MP, Zhu JY, Lawrence HR, Pireddu R, Luo Y, Alam R, Ozcan S, Sebti SM, Lawrence NJ, Schonbrunn E (2012) A novel mechanism by which small molecule inhibitors induce the DFG flip in Aurora A. ACS Chem Biol 7(4):698–706. doi:10.1021/cb200508b
11. Heathcote DA, Patel H, Kroll SH, Hazel P, Periyasamy M, Alikian M, Kanneganti SK, Jogalekar AS, Scheiper B, Barbazanges M, Blum A, Brackow J, Siwicka A, Pace RD, Fuchter MJ, Snyder JP, Liotta DC, Freemont PS, Aboagye EO, Coombes RC, Barrett AG, Ali S (2010) A novel pyrazolo[1,5-a]pyrimidine is a potent inhibitor of cyclin-dependent protein kinases 1, 2, and 9, which demonstrates antitumor effects in human tumor xenografts following oral administration. J Med Chem 53(24):8508–8522. doi:10.1021/jm100732t
12. Liu JJ, Daniewski I, Ding Q, Higgins B, Ju G, Kolinsky K, Konzelmann F, Lukacs C, Pizzolato G, Rossman P, Swain A, Thakkar K, Wei CC, Miklowski D, Yang H, Yin X, Wovkulich PM (2010) Pyrazolobenzodiazepines: part I. Synthesis and SAR of a potent class of kinase inhibitors. Bioorg Med Chem Lett 20(20):5984–5987. doi:10.1016/j.bmcl.2010.08.079
13. Wang S, Griffiths G, Midgley CA, Barnett AL, Cooper M, Grabarek J, Ingram L, Jackson W, Kontopidis G, McClue SJ, McInnes C, McLachlan J, Meades C, Mezna M, Stuart I, Thomas MP, Zheleva DI, Lane DP, Jackson RC, Glover DM, Blake DG, Fischer PM (2010) Discovery and characterization of 2-anilino-4- (thiazol-5-yl)pyrimidine transcriptional CDK inhibitors as anticancer agents. Chem Biol 17(10):1111–1121. doi:10.1016/j.chembiol.2010.07.016
14. Wyatt PG, Woodhead AJ, Berdini V, Boulstridge JA, Carr MG, Cross DM, Davis DJ, Devine LA, Early TR, Feltell RE, Lewis EJ, McMenamin RL, Navarro EF, O'Brien MA, O'Reilly M, Reule M, Saxty G, Seavers LC, Smith DM,

Squires MS, Trewartha G, Walker MT, Woolford AJ (2008) Identification of N-(4-piperidinyl)-4-(2,6-dichlorobenzoylamino)-1H-pyrazole-3-carboxamide (AT7519), a novel cyclin dependent kinase inhibitor using fragment-based X-ray crystallography and structure based drug design. J Med Chem 51(16):4986–4999. doi:10.1021/jm800382h

15. Krystof V, Cankar P, Frysova I, Slouka J, Kontopidis G, Dzubak P, Hajduch M, Srovnal J, de Azevedo WF, Jr OM, Paprskarova M, Rolcik J, Latr A, Fischer PM, Strnad M (2006) 4-arylazo-3,5-diamino-1H-pyrazole CDK inhibitors: SAR study, crystal structure in complex with CDK2, selectivity, and cellular effects. J Med Chem 49(22):6500–6509. doi:10.1021/jm0605740
16. Trujillo JI, Kiefer JR, Huang W, Thorarensen A, Xing L, Caspers NL, Day JE, Mathis KJ, Kretzmer KK, Reitz BA, Weinberg RA, Stegeman RA, Wrightstone A, Christine L, Compton R, Li X (2009) 2-(6-Phenyl-1H-indazol-3-yl)-1H-benzo[d]imidazoles: design and synthesis of a potent and isoform selective PKC-zeta inhibitor. Bioorg Med Chem Lett 19(3):908–911. doi:10.1016/j.bmcl.2008.11.105
17. Jones CD, Andrews DM, Barker AJ, Blades K, Daunt P, East S, Geh C, Graham MA, Johnson KM, Loddick SA, McFarland HM, McGregor A, Moss L, Rudge DA, Simpson PB, Swain ML, Tam KY, Tucker JA, Walker M (2008) The discovery of AZD5597, a potent imidazole pyrimidine amide CDK inhibitor suitable for intravenous dosing. Bioorg Med Chem Lett 18(24):6369–6373. doi:10.1016/j.bmcl.2008.10.102
18. Anderson M, Andrews DM, Barker AJ, Brassington CA, Breed J, Byth KF, Culshaw JD, Finlay MR, Fisher E, McMiken HH, Green CP, Heaton DW, Nash IA, Newcombe NJ, Oakes SE, Pauptit RA, Roberts A, Stanway JJ, Thomas AP, Tucker JA, Walker M, Weir HM (2008) Imidazoles: SAR and development of a potent class of cyclin-dependent kinase inhibitors. Bioorg Med Chem Lett 18(20):5487–5492. doi:10.1016/j.bmcl.2008.09.024
19. Lee J, Choi H, Kim KH, Jeong S, Park JW, Baek CS, Lee SH (2008) Synthesis and biological evaluation of 3,5-diaminoindazoles as cyclin-dependent kinase inhibitors. Bioorg Med Chem Lett 18(7):2292–2295. doi:10.1016/j.bmcl.2008.03.002
20. Finlay MR, Acton DG, Andrews DM, Barker AJ, Dennis M, Fisher E, Graham MA, Green CP, Heaton DW, Karoutchi G, Loddick SA, Morgentin R, Roberts A, Tucker JA, Weir HM (2008) Imidazole piperazines: SAR and development of a potent class of cyclin-dependent kinase inhibitors with a novel binding mode. Bioorg Med Chem Lett 18(15):4442–4446. doi:10.1016/j.bmcl.2008.06.027
21. Fischmann TO, Hruza A, Duca JS, Ramanathan L, Mayhood T, Windsor WT, Le HV, Guzi TJ, Dwyer MP, Paruch K, Doll RJ, Lees E, Parry D, Seghezzi W, Madison V (2008) Structure-guided discovery of cyclin-dependent kinase inhibitors. Biopolymers 89(5):372–379. doi:10.1002/bip.20868
22. Betzi S, Alam R, Martin M, Lubbers DJ, Han H, Jakkaraj SR, Georg GI, Schonbrunn E (2011) Discovery of a potential allosteric ligand binding site in CDK2. ACS Chem Biol 6(5):492–501. doi:10.1021/cb100410m
23. McIntyre NA, McInnes C, Griffiths G, Barnett AL, Kontopidis G, Slawin AM, Jackson W, Thomas M, Zheleva DI, Wang S, Blake DG, Westwood NJ, Fischer PM (2010) Design, synthesis, and evaluation of 2-methyl- and 2-amino-N-aryl-4,5-dihydrothiazolo[4,5-h]quinazolin-8-amines as ring-constrained 2-anilino-4-(thiazol-5-yl)pyrimidine cyclin-dependent kinase inhibitors. J Med Chem 53(5):2136–2145. doi:10.1021/jm901660c
24. Traquandi G, Ciomei M, Ballinari D, Casale E, Colombo N, Croci V, Fiorentini F, Isacchi A, Longo A, Mercurio C, Panzeri A, Pastori W, Pevarello P, Volpi D, Roussel P, Vulpetti A, Brasca MG (2010) Identification of potent pyrazolo[4,3-h]quinazoline-3-carboxamides as multi-cyclin-dependent kinase inhibitors. J Med Chem 53(5):2171–2187. doi:10.1021/jm901710h
25. Cheung M, Kuntz KW, Pobanz M, Salovich JM, Wilson BJ, Andrews CW 3rd, Shewchuk LM, Epperly AH, Hassler DF, Leesnitzer MA, Smith JL, Smith GK, Lansing TJ, Mook RA Jr (2008) Imidazo[5,1-f][1,2,4]triazin-2-amines as novel inhibitors of polo-like kinase 1. Bioorg Med Chem Lett 18(23):6214–6217. doi:10.1016/j.bmcl.2008.09.100
26. Stevens KL, Reno MJ, Alberti JB, Price DJ, Kane-Carson LS, Knick VB, Shewchuk LM, Hassell AM, Veal JM, Davis ST, Griffin RJ, Peel MR (2008) Synthesis and evaluation of pyrazolo[1,5-b]pyridazines as selective cyclin dependent kinase inhibitors. Bioorg Med Chem Lett 18(21):5758–5762. doi:10.1016/j.bmcl.2008.09.069
27. Bettayeb K, Sallam H, Ferandin Y, Popowycz F, Fournet G, Hassan M, Echalier A, Bernard P, Endicott J, Joseph B, Meijer L (2008) N-&-N, a new class of cell death-inducing kinase inhibitors derived from the purine roscovitine. Mol Cancer Ther 7(9):2713–2724. doi:10.1158/1535-7163.MCT-08-0080
28. Brown NR, Lowe ED, Petri E, Skamnaki V, Antrobus R, Johnson LN (2007) Cyclin B and cyclin A confer different substrate recognition

properties on CDK2. Cell Cycle 6(11): 1350–1359

29. Jorda R, Havlicek L, McNae IW, Walkinshaw MD, Voller J, Sturc A, Navratilova J, Kuzma M, Mistrik M, Bartek J, Strnad M, Krystof V (2011) Pyrazolo[4,3-d]pyrimidine bioisostere of roscovitine: evaluation of a novel selective inhibitor of cyclin-dependent kinases with antiproliferative activity. J Med Chem 54(8):2980–2993. doi:10.1021/jm200064p
30. Day PJ, Cleasby A, Tickle IJ, O'Reilly M, Coyle JE, Holding FP, McMenamin RL, Yon J, Chopra R, Lengauer C, Jhoti H (2009) Crystal structure of human CDK4 in complex with a D-type cyclin. Proc Natl Acad Sci U S A 106(11):4166–4170. doi:10.1073/pnas.0809645106
31. Takaki T, Echalier A, Brown NR, Hunt T, Endicott JA, Noble ME (2009) The structure of CDK4/cyclin D3 has implications for models of CDK activation. Proc Natl Acad Sci U S A 106(11):4171–4176. doi:10.1073/pnas.0809674106
32. Tarricone C, Dhavan R, Peng J, Areces LB, Tsai LH, Musacchio A (2001) Structure and regulation of the CDK5-p25(nck5a) complex. Mol Cell 8(3):657–669
33. Ahn JS, Radhakrishnan ML, Mapelli M, Choi S, Tidor B, Cuny GD, Musacchio A, Yeh LA, Kosik KS (2005) Defining Cdk5 ligand chemical space with small molecule inhibitors of tau phosphorylation. Chem Biol 12(7):811–823. doi:10.1016/j.chembiol.2005.05.011
34. Cho YS, Borland M, Brain C, Chen CH, Cheng H, Chopra R, Chung K, Groarke J, He G, Hou Y, Kim S, Kovats S, Lu Y, O'Reilly M, Shen J, Smith T, Trakshel G, Vogtle M, Xu M, Sung MJ (2010) 4-(Pyrazol-4-yl)-pyrimidines as selective inhibitors of cyclin-dependent kinase 4/6. J Med Chem 53(22):7938–7957. doi:10.1021/jm100571n
35. Schulze-Gahmen U, Kim SH (2002) Structural basis for CDK6 activation by a virus-encoded cyclin. Nat Struct Biol 9(3):177–181. doi:10.1038/nsb756
36. Lolli G, Lowe ED, Brown NR, Johnson LN (2004) The crystal structure of human CDK7 and its protein recognition properties. Structure 12(11):2067–2079. doi:10.1016/j.str.2004.08.013
37. Baumli S, Hole AJ, Noble ME, Endicott JA (2012) The CDK9 C-helix exhibits conformational plasticity that may explain the selectivity of CAN508. ACS Chem Biol 7(5):811–816. doi:10.1021/cb2004516
38. Lim HY, Seow KT, Li Q, Kesuma D, Wang JH, Qi RZ (2001) Structural Insights into Cdk5 activation by a neuronal Cdk5 activator. Biochem Biophys Res Commun 285(1):77–83. doi:10.1006/bbrc.2001.5086
39. Qi Z, Huang QQ, Lee KY, Lew J, Wang JH (1995) Reconstitution of neuronal Cdc2-like kinase from bacteria-expressed Cdk5 and an active fragment of the brain-specific activator. Kinase activation in the absence of Cdk5 phosphorylation. J Biol Chem 270(18): 10847–10854
40. Baumli S, Lolli G, Lowe ED, Troiani S, Rusconi L, Bullock AN, Debreczeni JE, Knapp S, Johnson LN (2008) The structure of P-TEFb (CDK9/cyclin T1), its complex with flavopiridol and regulation by phosphorylation. EMBO J 27(13):1907–1918. doi:10.1038/emboj.2008.121

Chapter 5

Fragment-Based *De Novo* Design of Cyclin-Dependent Kinase 2 Inhibitors

Sunil Kumar Tripathi, Poonam Singh, and Sanjeev Kumar Singh

Abstract

Cyclin-dependent kinases (CDKs) are core components of the cell cycle machinery that govern the transition between phases during cell cycle progression. Abnormalities in CDKs activity and regulation are common features of cancer, making CDK family members attractive targets for the development of anticancer drugs. One of the main bottlenecks hampering the development of drugs for kinase is the difficulty to attain selectivity. A huge variety of small molecules have been reported as CDK inhibitors, as potential anticancer agents, but none of these has been approved for commercial use. Computer-based molecular design supports drug discovery by suggesting novel new chemotypes and compound modifications for lead candidate optimization. One of the methods known as de novo ligand design technique has emerged as a complementary approach to high-throughput screening. Several automated de novo software programs have been written, which automatically design novel structures to perfectly fit in known binding site. The de novo design supports drug discovery assignments by generating novel pharmaceutically active agents with desired properties in a cost as well as time efficient approach. This chapter describes procedure and an overview of computer-based molecular de novo design methods on a conceptual level with successful examples of CDKs inhibitors.

Key words Cyclin-dependent kinases, De novo design, Genetic algorithm, High-throughput screening, X-ray crystallography

1 Introduction

In drug designing process the search for drug molecules with computational methods is frequently performed by molecular docking or to a lesser extent by de novo drug design approaches. While virtual screening relies on pre-existing compounds, de novo design approaches generate novel molecules out of building blocks consisting of single atoms or fragments [1]. The de novo design involves the design of novel structures based on the structure of binding site with which they are meant to interact, which can be identified from an X-ray crystallographic study of the receptor protein with bound ligand. By definition, de novo means "from the new" and involves the design of complex new molecules from

Mar Orzáez et al. (eds.), *Cyclin-Dependent Kinase (CDK) Inhibitors: Methods and Protocols*, Methods in Molecular Biology, vol. 1336, DOI 10.1007/978-1-4939-2926-9_5,

smaller constituent parts. The creation of any new chemical entity could be considered de novo design, while in practice the de novo design will be defined as the creation of novel chemical entities that are substantially different from any of the starting materials [2].

De novo design involves the design of novel structures based on the structure of binding site with which they have to interact. A drug can be designed which will have the correct size and shape to fit the space available with required functional groups to interact in binding sites [3]. The operator can carry out each of these procedures manually. Automated de novo design of bioactive molecules is one of the key aims in computational chemistry. To approach this idea, algorithms have to provide two principal tasks: First, the search space, i.e., the set of all algorithmically tractable molecules must be structured into regions of higher and lower quality to allow for prediction of desired properties (protein binding), and second, systematic search to make easy navigation in a high-dimensional chemical space [4].

One of the principal attractions of designing drug-like molecules starting from simpler building blocks is the potential to cover a larger fraction of the available compounds within the size range of interest. A relatively small number of fragments can be compiled to cover most of the possible shapes, features, and properties contained in a much larger set of drug-like compounds. This is in contrast to the very small amount of the accessible space that can be covered in a screening library for molecules of drug-like size [2, 5, 6]. Conceptually, Schneider and Fechner focused on three basic questions, which must be addressed by a de novo design program: (1) how to assemble the candidate compounds; (2) how to evaluate their potential quality; (3) and how to sample the search space effectively. All algorithmic decisions of a de novo design program are noticeably appraised by the quality of their outcome, which in turn crucially depends on a meaningful reduction of the search space [7].

In this chapter, we describe strategies and methods used in computer-based molecular de novo design methods on a conceptual level. The application of this approach is exemplified with a detailed description of the design of CDK2 and CDK4 inhibitors obtained by fragment-based de novo design program to identify promising scaffold candidates.

2 Materials

1. GANDI (Genetic Algorithm-based de Novo Design of Inhibitors).
2. Protein Data Bank (PDB) for protein structures.
3. Molinspiration Cheminformatics (www.molinspiration.com) to construct molecules and library of fragments design.

4. CORINA and Babel for conversion from SMILES strings to MOL2 format.
5. SEED software to dock fragment library into the receptor binding site.
6. LEGEND de novo design program.
7. MODELLER for homology or comparative modeling of protein three-dimensional structures.
8. CHARMm force field for model minimization.

3 Methods

The methods described here allow to the top ranking molecules to be involved in one to three hydrogen bonds with the backbone polar groups in the hinge region of CDK2, an interaction pattern observed in potent kinase inhibitors [1]. Crystallography has revealed that the ATP-binding site of CDK2 can accommodate a number of diverse molecular frameworks, exploiting various sites of interaction. In addition, residues outside the main ATP-binding cleft have been identified that could be targeted to increase specificity and potency [8]. For simplicity of reference the ATP-binding site is generally described by means of the ATP-binding mode as: The adenine pocket, the ribose pocket, and the phosphate groove. Figure 1 shows a schematic of the naming scheme incorporating two additional regions. An important feature in terms of drug design is that ATP does not occupy the total volume of the cleft and there are nonconserved regions that can be exploited in the development of inhibitors [9–11].

The search for drug molecules with computational methods is often performed by high-throughput docking or to a lesser extent by de novo drug design approaches [7]. The de novo procedures can also be done manually [4]; however this procedure would not be a good idea (*see* **Notes 1** and **2**). The de novo design approaches

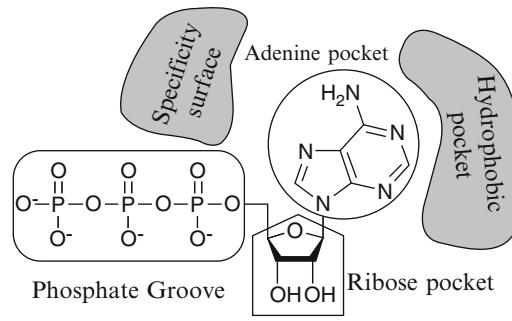

Fig. 1 Schematic presentation of ATP-binding site categorized according to ATP-binding mode in CDK2 with additional nonconserved regions

generate novel molecules out of building blocks consisting of single atoms or fragments. Because of the difficulty to predict synthetic accessibility, de novo drug design tools often generate molecules that demand synthesis [12]. Other important points could be also taken into consideration in de novo design (*see* **Notes 3–7**). Alternatively, there are many software packages available which will carry out the process automatically; some of de novo design programs are given in Table 1.

Table 1
Different de novo design programs with their scoring function

De novo design programs	Scoring function	References
GANDI	Force field	[1]
HSITE/2D Skeletons	Steric constraints and hydrogen bonds	[13]
Diamond Lattice	Steric constraints and hydrogen bonds	[14]
3D skeletons	Steric constraints and hydrogen bonds	[15]
MCDNLG	Potential energy	[16]
GrowMol	Simple empirical scoring function	[17]
MCSS & HOOK	Simplified van der Waals potential of nonpolar interactions	[18]
SPROUT	Solvent accessible surface, hydrogen bonds, electrostatic and hydrophobic interactions	[19]
GroupBuild	Force field	[20]
CONCEPTS	Empirical scoring function	[21]
GenStar	Steric constraints and ligand-protein contact	[22]
SPLICE	Pharmacophore based and steric constraints	[23]
NEWLEAD	Steric constraints	[24]
LUDI	Empirical scoring function	[25, 26]
LEGEND	Force field	[27]
Chemical Genesis	Combined score of shape, grid based and scalar constraints	[28]
PRO_LIGAND	Empirical scoring function	[29]
DLD	Potential-energy function without electrostatic interactions	[30]
SMoG	Knowledge-based scoring function	[31]
BUILDER	Steric constraints	[32]
CONCERTS	Force field	[33]
RASSE	Force field	[34]

(continued)

Table 1
(continued)

De novo design programs	Scoring function	References
PRO_SELECT	Empirical scoring function	[35]
SkelGen	Geometric, connectivity, and chemical constraints	[36]
Nachbar	Target-specific QSAR model based on topological connectivity descriptor	[37]
Globus	Molecular similarity based on all-atom-pairs-shortest-path descriptor	[38]
DycoBlock	Force field and solvent accessible surface	[39]
LEA	Target-specific QSAR model based on three-dimensional descriptors	[40]
LigBuilder	Empirical scoring function	[41]
TOPAS	Molecular similarity based on topological pharmacophore and substructure fingerprints	[3]
F-DycoBlock	Force field and solvent accessible surface	[42]
ADAPT	Weighted sum of DOCK score, clogP, MM, number of rotatable bonds and hydrogen bonds	[43]
CoG	Molecular similarity based on fingerprint descriptor	[44]
BREED	–	[45]
CCLD	Force field	[46]

3.1 Fragment-Based De Novo Ligand Design Strategy of CDK2 Inhibitors

In this section a novel approach for Genetic Algorithm-based de novo Design of Inhibitors (GANDI) is presented [1]. GANDI is a fragment-based method that generates molecules by joining pre-docked fragments with linkers with parallel genetic algorithm [47], employing the simultaneous evolution of multiple populations used in GANDI to search for feasible solutions. Only the pre-docked fragments are encoded by the genetic algorithm, while suitable linker fragments are efficiently evaluated with a tabu search [48–50]. GANDI is evaluated on CDK2, and it is able to suggest molecules with new scaffolds or substituents which preserve the main binding interaction motifs of known inhibitors of CDK2 [1].

3.1.1 GANDI Procedure for Design of CDK2 Inhibitors

In order to connect pre-docked fragments with linker fragments (*see* Fig. 2), GANDI uses a combination of two stochastic search procedures, namely (1) a genetic algorithm [51, 52] and a tabu search [48–50], which are as follows.

1. The genetic algorithm in GANDI is an island model, using the simultaneous, noninteracting evolution of multiple populations at the same time. The exchange of genetic material is

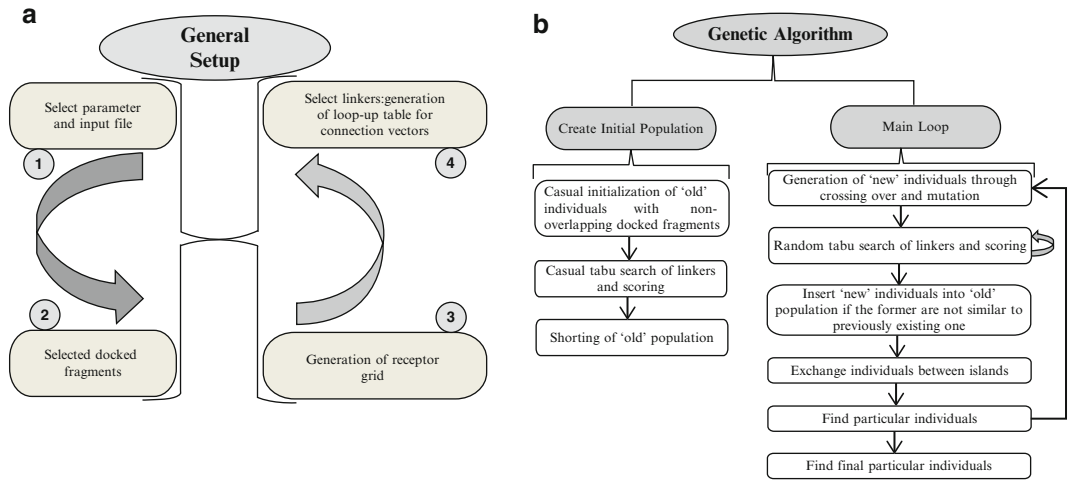

Fig. 2 Schematic illustration of GANDI with general procedure (**a**) from top to bottom including two iterative procedures, which are the main loop of the genetic algorithm and the random tabu search (**b**)

performed after a certain amount of optimization iterations by swapping individuals (i.e., molecules) between neighboring, all, or randomly picked islands as reported by Dey and Caflisch [1]. Every individual contains a single chromosome consisting of multiple genes. Contrary to classic genetic algorithms (*see* **Note 8**) [7, 53], the implementation in GANDI uses integers as gene values encoding indexes of docked fragments.

2. The next step involves linking the encoded fragments for each individual by a tabu search [48–50]. GANDI builds a look-up table containing all distances and angles of all pairs of linker fragment connection vectors. All possible connections of fragment pairs of an individual are generated with cutoff values and the look-up table. A connection solution is randomly picked, and the two fragments are joined with the linker [1].

3.1.2 3D-Similarity and Selection of Fittest Individuals

The detection of 3D-similarity between molecules may be measured as reported by several researchers [1, 54–56]. The scoring function implemented in GANDI is a linear combination, and force field-based energy function consists of van der Waals and electrostatic terms. The potentials of the receptor are calculated and stored on a grid [56] and used only for the linkers. The next term in the scoring function is a fingerprint-based 2D measure of similarity (2D similarity) as Dey and Caflisch have used the crystallographic structure of CDK2 with an oxindole-based inhibitor [1, 57] from the protein data bank (PDB ID: 1KE5). The crystallographic ligand can be prepared as described for the protein but minimized without any constraints inside the rigid protein binding site.

3.1.3 Selection of Fragment Library and Docking with SEED

In this step, library of fragments from Molinspiration Cheminformatics (*see* **Note 9**) is the source of constructed molecules (www.molinspiration.com). The library consisted of 20,000 fragments with one and 20,000 fragments with two connection points occurring in bioactive molecules. Both sets are converted from SMILES strings to MOL2 format with CORINA [58, 59] and Babel [60]. Then, all are docked into the receptor binding site with SEED, a program for docking mainly rigid fragments with evaluation of protein-fragment energy and electrostatic desolvation [56] (*see* **Note 10**).

3.1.4 Quality Assessment of Binding Modes

The quality of the binding modes generated by GANDI is further assessed with an in-house developed suite of programs for flexible ligand docking. First GANDI molecules were decomposed into fragments by DAIM [61]. DAIM prioritizes also the resulting fragments according to their suitability as anchors for the docking program FFLD [62]. In the present case study applied to CDK2, 2D similarity is used only for analysis (and not during GANDI runs) by Tanimoto coefficient based on normalized DAIM fingerprints [1, 61].

3.2 Generation of Potent CDK4 Inhibitors with De Novo Design Program LEGEND

This section presents the strategy of de novo design program LEGEND with structure-based design of novel and potent CDK4 inhibitors. To obtain the CDK4 protein structure, homology model is build, based on monomeric form of CDK2. It has been implemented a new de novo design strategy which combines the de novo design program LEGEND with in-house structure selection supporting system SEEDS to generate new scaffold candidates [63].

3.2.1 Homology Model Building of CDK4 Protein

According to the level of sequence homology between CDK4 and CDK2 (45 %), the CDK4 homology model has been constructed based on the CDK2 Protein (*see* **Note 11**). The model is minimized with the CHARMm force field [64] with the exception of the conserved region in CDK4 and CDK2. This minimized structure is used for scaffold design in the de novo design strategy.

3.2.2 Identification of New Scaffolds with Structural Requirements

In CDK2, the NH group in Leu83 is the most important in binding of the inhibitors because it serves as a hydrogen-bonding donor in every structure reported in earlier studies [11, 65]. The main chain carbonyl groups of Glu81 and Leu83 also seemed to be important because most inhibitors form hydrogen bonds with them. In CDK4, most of the residues that are important for hydrogen bonds interactions are conserved. Among the altered amino acid residues, those between Leu83 in CDK2 and Val96 in CDK4 would not be critical since only the main chain is used for hydrogen bond(s). Therefore, this information concerning structural requirements is also useful to find out new class of CDK4

inhibitors and is used to identify new scaffolds that satisfy these structural requirements [63]. LEGEND program is based on the atom-by-atom approach and is suitable for generation of drug molecules in cavity of the ATP-binding site [66]. The output structures from primary step could not be commercially available (*see* **Note 12**). In the case of CDK4, a diarylurea scaffold has been identified as appropriate for rapid construction of structurally diverse libraries [63]. The data obtained from LEGEND de novo design suggested that neighboring NH and CO in the diarylurea scaffolds form hydrogen bond(s) with the main chain(s) of Glu94 and Val96, and aromatic rings are supposed to be located in the hydrophobic regions of CDK4. According to these insights, Honma and his group also provided further strategy for constructing diarylurea informer libraries based on the structural requirements of Cdk inhibitors in the ATP-binding pocket of the Cdk4 mode. Further, docking study is performed to investigate the binding mode of Diarylurea in CDK4. Moreover, design and synthesis can be also executed based on the predicted binding mode. Finally, X-ray analysis could be done for confirmation of binding mode from de novo design.

4 Notes

1. In general, the structure of the binding site is identified from X-ray crystallography and it is possible that the designed molecule may not bind to the binding site exactly as predicted. If the projected fit is too rigid, a minor modification in the binding mode may prevent the molecule binding. It would be better to have a flexible structure in the first instance [4].
2. It is significant to leave possibility for variation and elaboration in the molecule, and this agrees on fine modification of the molecule's binding affinity and also on required pharmacokinetics.
3. Flexible molecules are better than rigid molecules, because the former are more likely to find an alternative binding conformation. This allows modification to be carried out based on the actual binding mode. On other hand, if rigid molecules fail to bind as predicted, it may not bind at all.
4. It is pointless designing molecules that are difficult or impossible to synthesize.
5. Similarly, it is pointless designing molecules that need to adopt an unstable conformation in order to bind.
6. Consideration of the energy losses involved in water desolvation should be taken into account.

7. There may be subtle differences in structure between receptors and enzymes from different species.
8. Evolutionary algorithms are based on the ideas described by Charles Darwin, which are population-based optimization algorithms that mimic biological evolution with the genetic operators. Mutation introduces new information into a population, whereas recombination exploits the information inherent in the population [7].
9. Molinspiration offers a broad range of cheminformatics software tools supporting molecule manipulation and processing, including SMILES and SDfile conversion, normalization of molecules, generation of tautomers, molecule fragmentation, calculation of various molecular properties needed in QSAR, molecular modeling and drug design, high quality molecule depiction, molecular database tools supporting substructure and similarity searches.
10. It is significant to note that in the Dey and Caflisch studies, 6882 fragments with two connection vectors were used also as linker fragments in GANDI. They have pointed out the protocol of GANDI which integrated three different parameter settings with 400 individuals in a single island, 4 islands of 100 individuals each, and 4 islands with 100 individuals exchanging 5 % of all individuals every 20th iteration with a randomly selected island. The minimized oxindole-based inhibitor co-crystallized with the protein (PDB code 1KE5) was used as a target structure [1].
11. De Bondt et al. in 1993 have solved the first X-ray structure and analysis of CDK2. Although the structures of the CDK6-p16 complex and CDK6-p19 complex were already reported, their cyclin binding region and the ATP-binding pocket in CDK6 were both largely altered by the endogenous inhibitors (p16 and p19). Therefore, despite a very high sequence identity between CDK4 and CDK6 (70%), CDK6 structural information could not be used for designing CDK4 inhibitors [63].
12. This difficulty appears to apply to most de novo design programs that build up structures sequentially. To overcome this disadvantage, one can use an in-house program SEEDS [63].

Acknowledgments

The authors thank the Department of Science and Technology (SR/FT/CS-66/2010), New Delhi, for financial support. One of the authors SKT gratefully acknowledges CSIR, New Delhi, for SRF.

References

1. Dey F, Caflisch A (2008) Fragment-based de novo ligand design by multi objective evolutionary optimization. J Chem Inf Model 48: 679–690
2. Loving K, Alberts I, Sherman W (2010) Computational approaches for fragment-based and de novo design. Curr Top Med Chem 10:14–32
3. Schneider G, Lee ML, Stahl M et al (2000) De novo design of molecular architectures by evolutionary assembly of drug-derived building blocks. J Comput Aided Mol Des 14: 487–494
4. Patrick GL (2009) An introduction to medicinal chemistry. Oxford University Press, New York
5. Fink T, Bruggesser H, Reymond JL (2005) Virtual exploration of the small-molecule chemical universe below 160 Daltons. Angew Chem Int Ed 117:1528–1532
6. Martin YC (1981) A practitioner's perspective of the role of quantitative structure-activity analysis in medicinal chemistry. J Med Chem 24:229–237
7. Schneider G, Fechner U (2005) Computer-based de novo design of drug-like molecules. Nat Rev Drug Discov 4:649–663
8. Davies TG, Pratt DJ, Endicott JA et al (2002) Structure-based design of cyclin-dependent kinase inhibitors. Pharmacol Ther 93:125–133
9. Toledo LM, Lydon NB, Elbaum D (1999) The structure-based design of ATP-site directed protein kinase inhibitors. Curr Med Chem 6:775–805
10. Cherry M, Williams DH (2004) Recent kinase and kinase inhibitor X-ray structures: mechanisms of inhibition and selectivity insights. Curr Med Chem 11:663–673
11. Furet P (2003) X-ray crystallographic studies of CDK2, a basis for cyclin-dependent kinase inhibitor design in anti-cancer drug research. Curr Med Chem Anticancer Agents 3:15–23
12. Böhm HJ, Banner DW, Weber L (1999) Combinatorial docking and combinatorial chemistry: design of potent non-peptide thrombin inhibitors. J Comput Aided Mol Des 13:51–56
13. Danziger DJ, Dean PM (1989) Automated site-directed drug design: a general algorithm for knowledge acquisition about hydrogen-bonding regions at protein surfaces. Proc R Soc Lond B236:101–113
14. Lewis RA (1990) Automated site-directed drug design: approaches to the formation of 3D molecular graphs. J Comput Aided Mol Des 4:205–210
15. Gillett VA, Johnson AP et al (1990) Automated structure design in 3D. Tetrahedron Comput Methodol 3:681–696
16. Gelhaar DK, Moerder KE, Zichi D et al (1995) *De novo* design of enzyme inhibitors by Monte Carlo ligand generation. J Med Chem 38: 466–472
17. Bohacek RS, McMartin C (1994) Multiple highly diverse structures complementary to enzyme binding sites: results of extensive application of a *de novo* design method incorporating combinatorial growth. J Am Chem Soc 116:5560–5571
18. Eisen MB, Wiley DC, Karplus M et al (1994) HOOK: a program for finding novel molecular architectures that satisfy the chemical and steric requirements of a macromolecule binding site. Proteins 19:199–221
19. Gillett VJ, Myatt G, Zsoldos Z et al (1995) SPROUT, HIPPO and CAESA: tools for *de novo* structure generation and estimation of synthetic accessibility. Perspect Drug Discov Des 3:34–50
20. Rotstein SH, Murcko MA (1993) GroupBuild: a fragment-based method for *de novo* drug design. J Med Chem 36:1700–1710
21. Pearlman DA, Murcko MA (1993) CONCEPTS: new dynamic algorithm for *de novo* design suggestion. J Comput Chem 14:1184–1193
22. Rotstein SH, Murcko MA (1993) GenStar: a method for *de novo* drug design. J Comput Aided Mol Des 7:23–43
23. Ho CMW, Marshall GR (1993) SPLICE: a program to assemble partial query solutions from three-dimensional database searches into novel ligands. J Comput Aided Mol Des 7:623–647
24. Tschinke V, Cohen NC (1993) The NEWLEAD program: a new method for the design of candidate structures from pharmacophoric hypothesis. J Med Chem 36:3863–3870
25. Böhm HJ (1992) The computer program LUDI: a new simple method for the de-novo design of enzyme inhibitors. J Comput Aided Mol Des 6:61–78
26. Böhm HJ (1992) LUDI: rule-based automatic design of new substituents for enzyme inhibitor leads. J Comput Aided Mol Des 6:593–606
27. Nishibata Y, Itai A (1991) Automatic creation of dug candidate structures based on receptor structure. Starting point for artificial lead generation. Tetrahedron 47:8985–8990
28. Glen RC, Payne AWR (1995) A genetic algorithm for the automated generation of molecules within constraints. J Comput Aided Mol Des 9:181–202

29. Clark DE, Frenkel D, Levy SA et al (1995) PRO-LIGAND: an approach to *de novo* molecular design. 1. Application to the design of organic molecules. J Comput Aided Mol Des 9:13–32
30. Miranker A, Karplus M (1995) An automated method for dynamic ligand design. Proteins 23:472–490
31. DeWitte RS, Shakhnovich EI (1996) SMoG *de novo* design method based on simple, fast, and accurate free energy estimates. 1. Methodology and supporting evidence. J Am Chem Soc 118:11733–11744
32. Roe DC, Kuntz ID (1995) BUILDERv.2: improving the chemistry of a *de novo* design strategy. J Comput Aided Mol Des 9: 269–282
33. Pearlman DA, Murcko MA (1996) CONCERTS: dynamic connection of fragments as an approach to *de novo* ligand design. J Med Chem 39:1651–1663
34. Luo Z, Wang R, Lai L (1996) RASSE: a new method for structure-based drug design. J Chem Inf Comput Sci 36:1187–1194
35. Murray CW, Clark DE, Auton TR et al (1997) PRO_SELECT: combining structure-based drug design and combinatorial chemistry for rapid lead discovery. 1. Technology. J Comput Aided Mol Des 11:193–207
36. Todorov NP, Dean PM (1997) Evaluation of a method for controlling molecular scaffold diversity in *de novo* ligand design. J Comput Aided Mol Des 11:175–192
37. Nachbar RB (2000) Molecular evolution: automated manipulation of hierarchical chemical topology and its application to average molecular structures. Genet Program Evolvable Mach 1:57–94
38. Globus A, Lawton J, Wipke WT (1999) Automatic molecular design using evolutionary algorithms. Nanotechnology 10:290–299
39. Liu H, Duan Z, Luo Q et al (1999) Structure-based ligand design by dynamically assembling molecular building blocks at binding site. Proteins 36:462–470
40. Douguet D, Thoreau E, Grassy G (2000) A genetic algorithm for the automated generation of small organic molecules: drug design using an evolutionary algorithm. J Comput Aided Mol Des 14:449–466
41. Wang R, Gao Y, Lai L (2000) LigBuilder: a multi-purpose program for structure-based drug design. J Mol Model 6:498–516
42. Zhu J, Fan H, Liu H, Shi Y (2001) Structure-based ligand design for flexible proteins: application of new F-DycoBlock. J Comput Aided Mol Des 15:979–996
43. Pegg SCH, Haresco JJ, Kuntz ID (2001) A genetic algorithm for structure-based *de novo* design. J Comput Aided Mol Des 15: 911–933
44. Brown N, McKay B, Gilardoni F, Gasteiger J (2004) A graph-based genetic algorithm and its application to the multiobjective evolution of median molecules. J Chem Inf Comput Sci 44:1079–1087
45. Pierce AC, Rao G, Bemis GW (2004) BREED: generating novel inhibitors through hybridization of known ligands application to CDK2, P38, and HIV protease. J Med Chem 47: 2768–2775
46. Caflisch A (1996) Computational combinatorial ligand design: application to human R-thrombin. J Comput Aided Mol Des 10: 372–396
47. Venkatasubramanian V, Chan K, Caruthers JM (1994) Computer-aided molecular design using genetic algorithms. Computers Chem Eng 18:833–844
48. Glover F (1986) Future paths for integer programming and links to artificial intelligence. Comput Oper Res 13:533–549
49. Glover F (1989) Tabu Search-Part I. ORSA J Comput 1:190–206
50. Glover F (1990) Tabu Search-Part II. ORSA J Comput 1:4–32
51. Holland JH (1975) Adaptation in natural and artificial systems. University of Michigan Press, Ann Arbor, MI
52. Goldberg DE (1989) Genetic algorithms in search optimization and machine learning. Addison-Wesley Longman Publishing, Boston
53. Darwin C (1859/1975) On the origin of species: facsimile of the first edition. Harvard University Press, Cambridge, MA
54. Cormen TH, Leiserson CE, Rivest RL et al (2001) Introduction to algorithms. MIT Press, Cambridge, pp 531–539
55. Kearsley S, Smith G (1990) An alternative method for the alignment of molecular structures. Maximizing electrostatic and steric overlap. Tetrahedron Comput Methodol 3:615–633
56. Majeux N, Scarsi M, Apostolakis J et al (1999) Exhaustive docking of molecular fragments on protein binding sites with electrostatic solvation. Proteins Struct Funct Genet 37:88–105
57. Bramson HN, Corona J, Davis ST et al (2001) Oxindole-based inhibitors of cyclin-dependent kinase 2 (CDK2): design, synthesis, enzymatic activities, and X-ray crystallographic analysis. J Med Chem 44:4339–4358
58. Momany FA, Rone R (1992) Validation of the general purpose QUANTA 3.2/CHARMm force field. J Comput Chem 13:888–900

59. Sadowski J, Gasteiger J (1993) From atoms and bonds to three-dimensional atomic coordinates: automatic model builders. Chem Rev 93:2567–2581
60. Guha R, Howard M, Hutchison G et al (2006) The Blue Obelisk- interoperability in chemical informatics. J Chem Inf Model 46:991–998
61. Kolb P, Caflisch A (2006) Automatic and efficient decomposition of two-dimensional structures of small molecules for fragment-based high-throughput docking. J Med Chem 49:7384–7392
62. Budin N, Majeux N, Caflisch A (2001) Fragment-based flexible ligand docking by evolutionary optimization. Biol Chem 382: 1365–1372
63. Honma T, Hayashi K, Aoyama T et al (2001) Structure-based generation of a new class of potent Cdk4 inhibitors: new de novo design strategy and library design. J Med Chem 44:4615–4627
64. Swaminathan S, Karplus M (1983) CHARMM: a program for macromolecular energy, minimization, and dynamic calculation. J Comput Chem 4:187–217
65. Tripathi SK, Singh SK, Singh P et al (2012) Exploring the selectivity of a ligand complex with CDK2/CDK1: a molecular dynamics simulation approach. J Mol Recognit 25:504–512
66. Murcko MA (1997) An introduction to *de novo* ligand design. In: Practical application of computer-aided drug design. Marcel Dekker, New York, pp 322–325

Chapter 6

Protein-Protein Interaction for the *De Novo* Design of Cyclin-Dependent Kinase Peptide Inhibitors

Karthiga Arumugasamy, Sunil Kumar Tripathi, Poonam Singh, and Sanjeev Kumar Singh

Abstract

The homology of the inhibitor binding site regions on the surface of cyclin-dependent kinases (CDKs) makes actual CDK inhibitors unable to bind specifically to their molecular targets. Most of them are ATP competitive inhibitors with low specificity that also affect the phosphorylation mechanisms of other non-target kinases giving rise to harmful side effects. So, the search of specific and potent inhibitors able to bind to the desired CDK target is still a pending issue. Structure based drug design minimized the erroneous binding and increased the affinity of the inhibitor interaction. In the case of CDKs their activation and regulation mechanisms mainly depend on protein-protein interactions (PPIs). The design of drugs targeting these PPIs makes feasible and promising towards the discovery of new and specific CDK inhibitors. Development of peptide inhibitors for a target protein is an emerging approach in computer aided drug designing. This chapter describes in detail methodology for use of the VitAL-Viterbi algorithm for de novo peptide design of CDK2 inhibitors.

Key words Molecular docking, Peptide inhibitors, Protein-protein interaction, Structure based drug design, VitAL-Viterbi

1 Introduction

Approximately 20 different chemical classes of CDK inhibitors are available; they are analogues of purine, pyrimidine, and natural metabolites isolated from microbial strains and their derivatives. Flavopiridol, roscovitine, stauroporins, purvalanol, and alsterpaullone are some of the potential drug candidates undergone clinical trials which inhibit the CDK activity. Specificity is the biggest problem in these currently available antagonists. They do not have the specificity to target only one CDK; most of these inhibitors have multiple CDK targets [1]. For example, R-Roscovitine inhibits CDK1, CDK2, CDK5, CDK7, and CDK9 [2]. To design specific kinase inhibitors is essential in order to minimize the

Mar Orzáez et al. (eds.), *Cyclin-Dependent Kinase (CDK) Inhibitors: Methods and Protocols*, Methods in Molecular Biology, vol. 1336, DOI 10.1007/978-1-4939-2926-9_6,

unnecessary side effects of these drugs. CDK inhibitors could be designed through two types of strategies, using either small organic molecules or peptides. Peptide inhibitors promise better specificity of interaction than small molecule ATP competitors.

In CDKs, inhibitor peptides could be derived from cyclin or negative regulators binding regions. Some peptide inhibitors are reported against the CDKs; for example, $p27^{KIP}$ inhibitor acts as model to design a peptide inhibitor of the CDK2/Cyclin A complex activation [3]. In vitro and in vivo studies encourage the potential of a peptide inhibitor derived from the $p21^{Waf1/cip1}$ protein that potently inhibits the CDK2/Cyclin E and CDK4/Cyclin D complexes [4]. Some previously reported complexes of CDK2/Cyclin A/peptide inhibitors are listed in Table 1.

There are different ways to design a specific peptide inhibitor against the active site of a protein. Diverse graphical user interfaces (GUI) and algorithms based software tools help to model the peptide sequence. In this chapter, we describe strategy and VitAL-Viterbi algorithm to design the CDK2 peptide inhibitor based on the protein active site.

Table 1
CDK2/Cyclin A complexed with different peptide chain derived from the natural regulator of cell cycle from PDB (http://www.rcsb.org)

PDB ID	Resolution (Å)	Peptide inhibitor derived from natural regulator	Position of the residues	Amino acid sequence	PubMed ID
1H24	2.50	E2F	Residues 87–95	Pro-Val-Lys-Arg-Arg-Leu-Asp-Leu-Glu	12501191
1H25	2.50	Retinoblastoma-associated protein	Residues 869–878	Pro-Lys-Pro-Leu-Lys-Lys-Leu-Arg-Phe-Asp	12501191
1H26	2.24	p53	Residues 376–386	Ser-Arg-His-Lys-Lys-Leu-Met-Phe-Lys	12501191
1H27	2.20	p27	Residues 25–35	Arg-Asn-Leu-Phe-Gly-Pro	12501191
1H28	2.80	p107	Residues 653–663	Gly-Ser-Ala-Lys-Arg-Arg-Leu-Phe-Gly-Glu	12501191
1URC	2.60	Synthetic derivative of p27	Leu-Phe-Gly motif region	Ace-Arg-Lys-Leu-Phe-Gly	15455144

2 Materials

1. Linux cluster system to execute the Viterbi algorithm coding and perform the molecular docking.
2. Protein Data Bank to retrieve the crystal structure of CDK protein associated with inhibitor or substrate proteins (p53, p21, p27, p107, etc.) given as input structure.
3. Hotpoint, web server (http://prism.ccbb.ku.edu.tr/hotpoint) to predict the interest of amino acid residues on the binding surface of protein.
4. AutoDock package for docking analysis and binding free energy calculation.
5. Hyperchem tool for preparation of peptide structure.
6. Coil library, web server (http://www.roselab.jhu.edu/coil) to determine the probabilities of the φ–ψ torsion angles of the peptides.

Prediction of peptide inhibitor through VitAL-Viterbi based algorithm is proved by other target enzymes which compared with their known peptide inhibitors and final peptides shows significant binding free energy [5]. AutoDock has been used to check the reliability of the binding interaction and HyperChem package for amino acids and possible dipeptides [6, 7]. Ramachandran plot have used to characterize the $\varphi\neg\psi$ propensities of the dipeptides. Acetyl-group have added at the N-terminal end of dipeptides for their stability.

3 Methods

The Viterbi algorithm based de novo peptide design sequentially generates the peptide by docking its residues pair by pair along a chosen path on a protein. The prior method needed for the Viterbi algorithm to run properly is given in Fig. 1.

3.1 Prediction of the Active Site Residues of the Protein

In this step, X-ray crystallographic coordinates of CDK2 from Protein Data Bank (PDB) [8] may be given as input file in web server Hotpoint (http://prism.ccbb.ku.edu.tr/hotpoint). Gaussian Network model (GNM) (*see* **Note 1**) can be used to find out the binding site residues of protein by two ways: (1) if the protein exists in complex with other proteins, and (2) if the site determined by the GNM lies in an interface in the complex, then the complex is used to determine sequence of residues on the binding site surface. The regions of hot spot residues present in the CDK2/Cyclin A complex are given in Fig. 2.

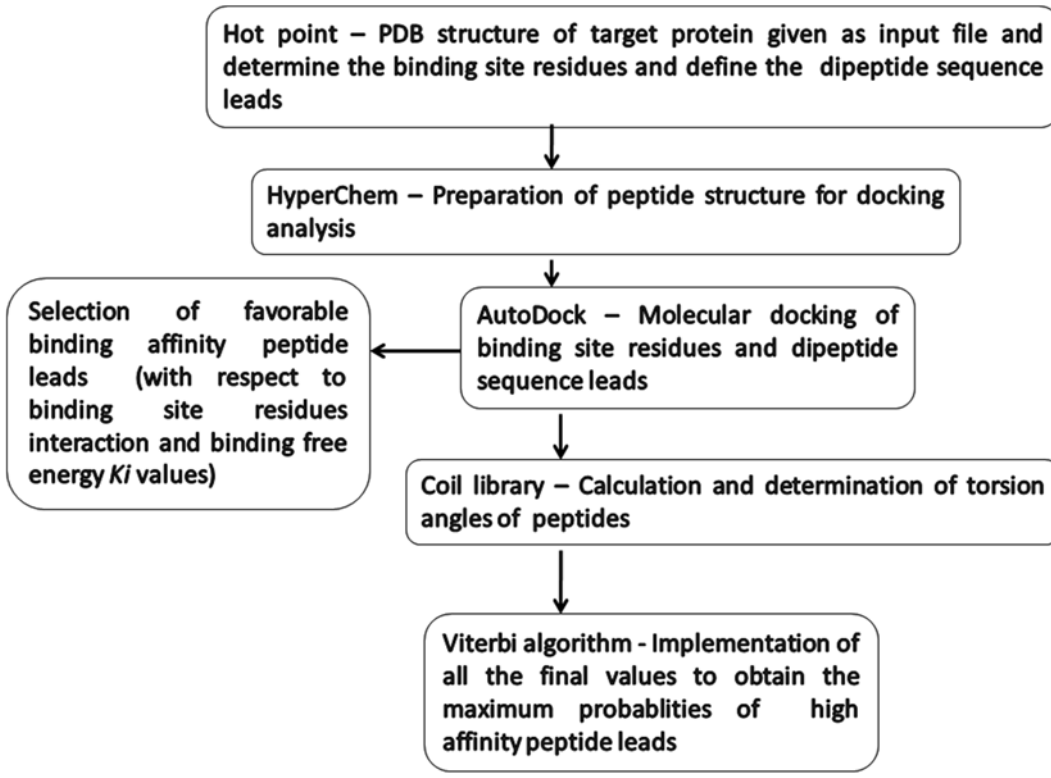

Fig. 1 The representation of steps involved in the Viterbi algorithm based de novo peptide design

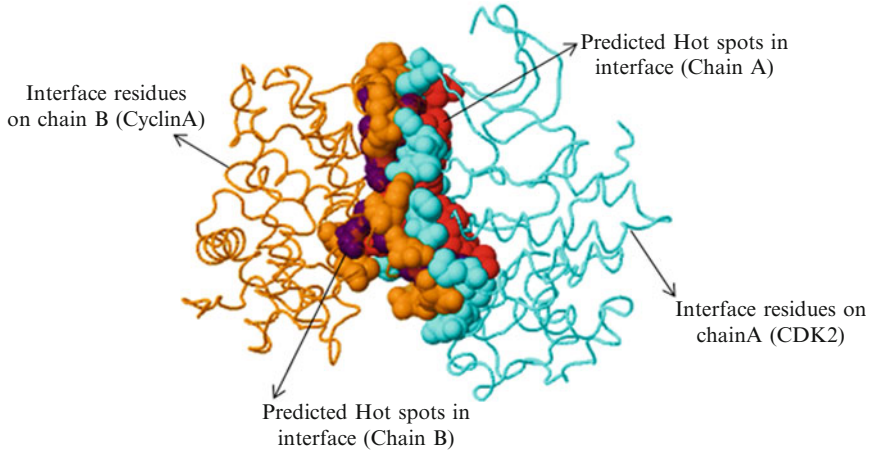

Fig. 2 Hot spot server aid to predict the CDK2/Cyclin A complex (PDB ID: 1FIN) binding site residues. The space fill model denotes the active site amino acids of CDK2 and Cyclin A (predicted hot spots in interface of CDK2 in chain A are shown as *red* and predicted hot spots in interface of Cyclin A in chain B are shown as *purple*)

3.2 Determination of "n" Amino Acid in the Grid Box

To accomplish this step, the grid box is generated based on the binding site residue prediction (probe peptide or the interacting protein portion) in CDK2 protein. The first and the second grids along the path contain the first and the second amino acids. The tth and $t+1$st grids contain the tth and $t+1$st residues. The "n" chiral carbon atoms of the path define the centers of the "n" grid boxes. Grid box is determined (possible region of interaction between ligand and receptor molecule) by AutoDock software tool [7]. The GOLD and GLIDE module can also be used for grid generation and docking process [9].

3.3 Amino Acid and Dipeptide Preparation

HyperChem tool has to be used to prepare the structure of amino acids and dipeptides for molecular docking (*see* **Note 2**) [6]. At the N-terminal end of dipeptide, acetyl group has to be added for their stability.

3.4 Docking and Binding Energy Quantification

The AutoDock program has to be used as the docking tool to quantify the binding affinity between the dipeptides and the selected protein surface. In the initial part of docking, first grid box path docked with 20 amino acids, then 400 possible dipeptides (20×20) are docked with first and second grid box, thus their chiral carbon atoms forced to overlap with first grid center with the successive chiral carbons, located at the grid centers. The pair wise docking of the dipeptides is continued in this way up to the last dipeptide along the path. AutoDock program gives the bound conformation of protein-peptide, the binding energy and Ki value.

3.5 Principle to Find the Probabilities of Dipeptide Binding

Rotational Isomeric States (RIS) approach (*see* **Note 3**) has to be used to determine the type and length of the amino acid. Statistical analysis of the binding energies of dipeptides determines the significant and possible interaction and transition probabilities, and derivation of equation elaborately given by Unal et al. [5].

3.6 Selection of Favorable Dipeptide Probability by Coil Library

1. Energetically favorable φ, ψ torsion angle peptides used and other conformations are excluded. Two sets of probabilities are needed for specifying the conformation of the peptide. $\Phi t - \psi t$ (grid box 1) and $\Phi t - \psi t_{+1}$ (grid box 2) set of torsion angles selected for the probability analysis.
2. Depends on the chemical nature of the amino acids the repulsive, attraction, steric hindrances effects are formed. Hydrogen bond formation is consider as most favorable interaction between protein-peptide (*see* **Note 4**).
3. Web server, coil library (http://www.roselab.jhu.edu/coil) that contains the precalculated torsion angle for the fragments as well as crystal structure of the peptides available in the PDB [8]. Number of peptide sequence structure is retrieved from the coil library data and selected by various criteria (*see* **Note 5**).

Table 2
Backbone torsion angle calculation of known CDK2 complex inhibitor p27 derived peptide sequence (PDB ID: 1H27) using coil library tool

Amino acid	φ	Ψ	ω	Secondary structure
LEU	−103.16	151.07	−170.20	E
ILE	−129.93	144.76	179.59	E
ASN	−112.51	−178.10	178.73	C
THR	−76.15	−11.78	−173.20	T
GLU	−98.21	9.80	−175.27	T
GLY	88.18	3.65	176.72	C
ALA	−77.99	146.21	173.54	E
ILE	−125.12	150.21	165.44	E

T—β-turn; C—Coil; E—β-strand, secondary structure conformation formed by the amino acids (http://www.roselab.jhu.edu/coil)

The p27 peptide sequence (PDB ID: 1H27) taken as example and their torsion angles are given in Table 2.

4. Description of variables and equations to obtain the possible peptide conformation was given by Unal et al. [5].

3.7 Accuracy of the Protein-Peptide Interaction

After the prediction of possible and reliable peptide structure can be docked with receptor CDK2 or CDK2/Cyclin complexes. In case of CDK2, some previously reported peptide inhibitors structure and information are available [3, 10] so the binding energy and interactions of the newly designed peptide inhibitors can be compared with the parent inhibitors.

3.8 Implementation of Viterbi Algorithm

All the previous steps final values are employed in Viterbi algorithm equations. This process is divided into two steps, namely forward tracking and backward tracking method. Both of the steps are elaborated by Unal et al. [5]. Each step leads to increase the probability of the peptide sequence and to determine a peptide sequence with possible affinity to protein binding site.

Different algorithms are available for successful design of peptide inhibitors. The predicted peptide inhibitors should go for experimental validation to examine the potential against applicable target. Thus, in terms of accuracy the prediction must be accurate and reliable for such novel and potent peptide inhibitors. In addition to VitAL-Viterbi, Rosetta is one of the important algorithm based tool (http://www.rosettacommons.org/) which gives the accurate and reliable results for such potent inhibitors [11, 12]. CDKs have

high sequence similarity and many natural inhibitors for regulation of their mechanism. It will improve the search of inhibitors based on the binding pocket of protein to find out the potent and reliable specific inhibitors against CDKs. Development of more computational algorithms evokes the emerging of novel peptide inhibitors for CDKs. In general, the algorithm should be simple and give the accurate output form of peptide antagonist or ligand.

4 Notes

1. Based on the statistical thermodynamic model, GNM has been proposed the potential of residue-residue interactions. Thus offers a model for determining structurally and functionally important residues in relation to ligand-protein interactions. Although, provides the protein transferring information from one point to the other [13].
2. HyperChem tool has been used to get the amino acid structure, and other tools like Chimera, Sybyl, and Schrodinger can also be used to get the amino acid structure [9].
3. The α-helical and β-strand amino acid shows significant energy differences. RIS polymer physics facilitates to determine that energy difference either due to favorable or unfavorable interactions with the peptide sequence. Torsion angles adjacent to the peptide bond (Ramachandran map) should be considered to check the reliable conformation of the protein. Higher order interdependences between bond dihedral angles can be ignored [14].
4. Different levels of correlations among the φ ψ angles are already identified and studied for native as well as denatured proteins. Ramachandran map gives the correlations among the φ and ψ and angles of a residue resulting from exclusion of steric overlaps that hold both for denatured and native proteins.
5. The selection criteria may be chosen by the user. For example, less than 20 % sequence identity, 1.6 Å resolution, and 0.25 refinement factor was followed to select the peptides derived from CDK2/p27 complex.

Acknowledgments

The authors thank the DST New Delhi (SR/FT/CS-66/2010) for financial support. AK and SKT gratefully acknowledge DST (New Delhi) for JRF and CSIR (New Delhi) for SRF respectively. One of the authors thanks CSIR-CDRI for support.

References

1. Gadek JW, Maurer M, Zulehner N et al (2011) Whether to target single or multiple CDKs for therapy? That is the question. J Cell Physiol 226:341–349
2. Senderowicz AM (2000) Small molecule modulators of cyclin-dependent kinases for cancer therapy. Oncogene 19:6600–6606
3. Andrews MJI, McInnes C, Kontopidis G et al (2004) Design, synthesis, biological activity and structural analysis of cyclic peptide inhibitors targeting the substrate recruitment site of cyclin dependent kinase complexes. Org Biomol Chem 2:2735–2741
4. Mutoh M, Lung FDT, Long YQ et al (1999) $p21^{Waf/cip1}$ carboxyl-terminal peptide exhibited cyclin-dependent kinase inhibitory activity and cytotoxicity when introduced into human cells. Cancer Res 59:3480–3488
5. Unal EB, Gursoy A, Erman B (2010) VitAL: Viterbi algorithm for *de novo* peptide design. PLoS One 5(6), e10926
6. HyperChem (TM) Professional 7.51, Hypercube, Inc., 1115 NW 4th Street, Gainesville, Florida 32601, USA
7. Morris GM, Goodsell DS, Halliday RS et al (1998) Automated docking using a Lamarckian genetic algorithm and empirical binding free energy function. J Comput Chem 19:1639–1662
8. Berman HM, Westbrook J, Feng Z et al (2000) The Protein Data Bank. Nucleic Acids Res 28(1):235–242
9. Liao C, Sitzmann M, Pugliese A et al (2011) Software and resources for computational medicinal chemistry. Future Med Chem 3(8): 1057–1085
10. Lowe ED, Tews I, Cheng KY et al (2002) Specificity determinants of recruitment peptides bound to phospho-CDK2/cyclin A. Biochemistry 41:5625
11. Kuhlman B, Dantas G, Ireton GC et al (2003) Design of a novel globular protein fold with atomic-level accuracy. Science 302: 1364–1368
12. Sievers SN, Karanicolas J, Chang HW et al (2011) Structure-based design of non-natural amino-acid inhibitors of amyloid fibril formation. Nature 475:96–100
13. Tuncbag N, Kar G, Gursoy A et al (2009) Towards inferring time dimensionality in protein-protein interaction networks by integrating structures: the p53 example. Mol Biosyst 5:1770–1778
14. Keskin O, Yuret D, Gursoy A et al (2004) Relationships between amino acid sequence and backbone torsion angle preferences in proteins. Proteins 55:992–998

Chapter 7

Identification of Cyclin A Binders with a Fluorescent Peptide Sensor

Elena Pazos, José L. Mascareñas, and M. Eugenio Vázquez

Abstract

A peptide sensor that integrates the 4-dimethylaminophthalimide (4-DMAP) fluorophore in a short cyclin A binding sequence displays a large fluorescence emission increase upon interacting with the cyclin A Binding Groove (CBG). Competitive displacement assays of this probe allow the straightforward identification of peptides that interact with the CBG, which could potentially block the recognition of CDK/cyclin A kinase substrates.

Key words Competition titration, Cyclin A, Fluorescence, Inhibitors, Peptides, Sensors

1 Introduction

Fluorescence techniques, allowing us to visualize biomolecular events with extraordinary sensitivity and selectivity, have transformed the study of biological systems [1–3]. Smart chemical sensors, specifically designed to change their spectroscopic properties in response to a particular external stimuli, are especially interesting, as they provide a simple and powerful means to monitor many physicochemical variables [4–9]. Environment-sensitive sensors represent a powerful approach for monitoring interactions between biomacromolecules because they are often accompanied by large changes in the solvation of the interacting molecular surfaces [10–13]. In this context, solvatochromic fluorophores, such as 2-propionyl-6-dimethylaminonaphthalene (PRODAN) [14], 6-dimethylaminonaphthalimide (6-DMN) [15], or 4-dimethylaminophthalimide (4-DMAP) [16], are a particularly interesting type of environment-sensitive fluorophores, owing to their change in emissive properties in response to variations in the polarity of their microenvironment [17]. These species generally display low quantum yields in aqueous solution, but are highly fluorescent in nonpolar solvents, or when bound to hydrophobic

Mar Orzáez et al. (eds.), *Cyclin-Dependent Kinase (CDK) Inhibitors: Methods and Protocols*, Methods in Molecular Biology, vol. 1336, DOI 10.1007/978-1-4939-2926-9_7,

sites in proteins; this sensitivity to the changes in their surroundings has been exploited for the development of specific peptide probes for a number of biomolecules [6].

It is known that alterations in the regulation of CDK kinases can lead to aberrant cell proliferation [18], and therefore there is a growing interest in the development of CDK inhibitors, including those that target the cyclin A binding groove (CBG) that mediates substrate recognition [19, 20]. Earlier efforts in our group have been focused on the development of lanthanide-based sensors directed towards the CBG [21], and in this chapter we show how a fluorescent peptide sensor incorporating the 4-DMAP fluorophore can be used in competition titrations for the straightforward identification of potential inhibitors targeting the CBG [22].

Preliminary molecular modeling studies, based on the X-ray structures of cyclin A bound to small peptides [23], followed by a screening in which we introduced the sensing fluorophore into slightly different sequence contexts, allowed us to identify the short fluorescent octapeptide AKRRLIϕE (where ϕ = Dap(4-DMAP) residue) that displayed a large emission increase as well as blue shifted emission upon incubation with cyclin A. Moreover, addition of increasing amounts of competitive binders over the preformed cyclin A/sensor complex results in a progressive reduction of the fluorescence emission, as the probe is being displaced from the CBG into the aqueous solution by the peptide inhibitors. Analysis of the resulting competition curves allows the quantitative study of the affinity of the unknown binders for the CBG. Herein we describe in detail how to synthesize the fluorescent peptide probe, characterize its interaction with cyclin A, and exploit its changes in fluorescence emission for the identification of new CBG targeting molecules using fluorescence competitive assays.

1.1 Synthesis of the Fluorescent Peptide Sensor

The synthesis of the fluorescent octapeptide sensor is outlined below (*see* Fig. 1). In short, the peptide sequence is assembled in the solid phase containing the orthogonally protected Dap(Alloc) residue, which is selectively deprotected while still attached to the solid phase by Pd catalysis. The 4-DMAP anhydride is then coupled to the amine at the deprotected Dap side chain and finally, the modified peptide is Fmoc-deprotected by standard treatment with 4-methylpiperidine and cleaved from the solid support with an acidic TFA cocktail. The crude mixture from the cleavage is added over ice-cold ether to precipitate the peptide product, which is finally purified by HPLC to give the desired fluorescent peptide sensor.

1.2 Determination of the Binding Constant of the Peptide Probe

Knowing the dissociation constant of the peptide probe/cyclin A complex is necessary for the quantitative analysis of the competitive titrations with unknown binders. In order to characterize the interaction of the fluorescent peptide with cyclin A, a simple titration of the probe with increasing concentrations of cyclin A is performed.

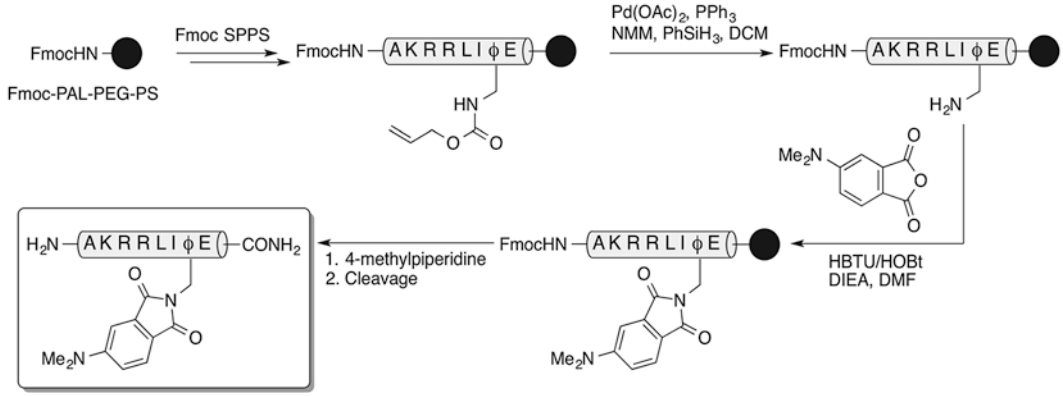

Fig. 1 Solid phase peptide synthesis of the environment-sensitive fluorescent sensor outlining the reagents (*see* text for details on the reaction conditions)

The fluorescence spectra after each addition of the protein are recorded, and the emission at 512 nm is plotted against the total concentration of the protein. A nonlinear regression fit of the resulting titration isotherm to a standard one-site binding model allows the determination of the binding constant of the probe [24, 25].

1.3 Competitive Titrations with Unknown CBG Binders

The dissociation constant for the binding of the nonfluorescent cyclin A binders was determined in the competition titrations by the decrease in the emission from the fluorescent sensor. In these experiments increasing concentrations of the unknown binder are added over a solution containing known concentrations of cyclin A and peptide probe and the emission spectra are recorded after each addition of binder. The emission intensity at 512 nm is plotted against the total binder concentration, and the resulting experimental data are fitted to a mathematical expression that describes the competitive binding of two different ligands to a protein in terms of the total concentrations of the species. This fit allows us to obtain the dissociation constant of the unknown binder, given that the binding constant of the probe is already known [26, 27].

2 Materials

2.1 Peptide Synthesis

Amino acids were purchased as protected Fmoc amino acids with the standard side chain protecting scheme: Fmoc–Ala–OH, Fmoc–Arg(Pbf)–OH, Fmoc–Glu(O*t*Bu)–OH, Fmoc–Ile–OH, Fmoc–Leu–OH, Fmoc–Lys(Boc)–OH, except for the orthogonally protected Fmoc–Dap(Alloc)–OH, which was purchased from *Bachem*. PAL-PEG-PS resin (0.21 mmol/g loading) was purchased from Applied Biosystems.

1. 0.195 M DIEA (*N,N′*-Diisopropylethylamine) in DMF (dimethylformamide): 3 mL of DIEA in 90 mL of DMF. Store at 4 °C.
2. 0.2 M HBTU/HOBt in DMF: Mix 3.8 g of HBTU (*O*-benzotriazole-*N,N,N′,N′*-tetramethyl-uroniumhexafluorophosphate) and 1.35 g of HOBt (*N*-hydroxybenzotriazole) in 50 mL of DMF and store it at 4 °C. Prepare a fresh solution before starting a new synthesis. The stock can be kept in the refrigerator for about 1 week with good coupling results.
3. 20 % (v/v) 4-methylpiperidine in DMF.
4. TNBS test: A solution of 1 % (v/v) TNBS (picrylsulfonic acid) in DMF (to prepare the working solution dilute the commercial solution, 5 % in water (v/v), 1:4 in DMF) and a solution of 10 % DIEA in DMF are required to test the presence or the absence of free primary amino groups. Both solutions should be stored at 4 °C. The test is performed on a few resin beads suspended in a drop of each solution. Beads turning red after a couple of minutes indicate the presence of free amino groups [28] and thus incomplete couplings.
5. Cocktail for peptide cleavage: Prepare a fresh solution of TIS (triisopropylsilane)/H_2O/CH_2Cl_2/TFA(trifluoroacetic acid) (2.5:2.5:5:90). Use 1 mL of the cleavage cocktail per 30 mg of resin. CAUTION: TFA is highly corrosive, wear protective clothing, and work in a fume hood.
6. HPLC solvents: Milli-Q water, 0.1 % TFA (v/v) and acetonitrile, 0.1 % TFA (v/v).
7. HEPES buffer: 10 mM HEPES (4-(2-hydroxyethyl) piperazine-1-ethanesulfonic acid), 100 mM NaCl, pH 7.6.

2.2 Laboratory Equipment

2.2.1 Labware

Standard synthetic equipment and glassware including round-bottom flasks, stir bars, oil bath, hotplate, silica gel thin-layer chromatography plates (TLC), Büchner funnel, rotary evaporator, and sublimation apparatus.

Manual peptide synthesis is performed on a pressure filter funnel attached to a 250 mL round-bottom flask for residue collection. Other setups that allow gentle mixing of the resin beads with the reactive mixtures and washing solvents are also possible.

2.2.2 Small Equipment

1. Micropipettes.
2. Shakers.
3. Centrifuge.
4. Spectrophotometer. Concentrations are measured using 6480 M^{-1} cm^{-1} as the extinction coefficient for 4-DMAP at 421 nm.

2.2.3 Instruments

1. *Peptide Synthesizer (optional)*: *PS3 automatic peptide synthesizer* from *Protein Technologies*. The amino acids are coupled in fourfold excess using HBTU as activating agent. Each amino acid is activated for 30 s in DMF before being added onto the resin. Peptide bond-forming couplings are conducted for 30 min to 45 min. The deprotection of the temporal Fmoc protecting group is performed by treating the resin with 20 % 4-methylpiperidine in DMF solution for 10 min following the standard operation instruction from the instrument.
2. *High-Performance Liquid Chromatography (HPLC)* is performed using an *Agilent 1100 series* Liquid Chromatograph Mass Spectrometer system. Analytical HPLC is run using a *Zorbax Eclipse XDB-C8* (5 μm) 4.6×150 mm analytical column from *Agilent*. The purification of the peptide is performed on a *Jupiter Proteo 90A* (4 μm) 10×250 mm reverse-phase column from *Phenomenex*. The standard gradient used for analytical and preparative HPLC was 15→95 % CH_3CN, 0.1 % TFA/H_2O, 0.1 % TFA over 30 min. Electrospray Ionization Mass Spectrometry (ESI/MS) is performed with an *Agilent LC/MSD*, *VL G1956A* model in positive scan mode using direct injection of the purified peptide solution.
3. *Lyophilizer*.
4. *Fluorescence spectroscopy:* measurements are made with a *Jobin-Yvon Fluoromax-3*, (DataMax 2.20), coupled to a temperature controller. All measurements are made at 20 °C, using the following settings: excitation wavelength 395 nm; excitation slit width 5.0 nm, emission slit width 10.0 nm; increment 1.0 nm; integration time 0.20 s. The emission spectra are recorded from 430 to 700 nm.

3 Methods

3.1 Synthesis of 4-N,N-Dimethylaminophthalic Anhydride (See Fig. 2)

1. Weigh 500 mg of 4-aminophthalic acid into a 500 mL round-bottom flask equipped with a stir bar.
2. Add 150 mL of MeOH (methanol), 15 mL of formalin and purge the flask with argon for 15 min.
3. Add 200 mg of Pd/C 10 % and purge the flask with hydrogen.
4. Stir the resulting solution at room temperature under hydrogen (balloon pressure) for 3 h.
5. Run a TLC with 1 % AcOH (acetic acid) and 10 % MeOH in CH_2Cl_2 to check the reaction (*see* **Note 1**).
6. Filter the solution through celite.

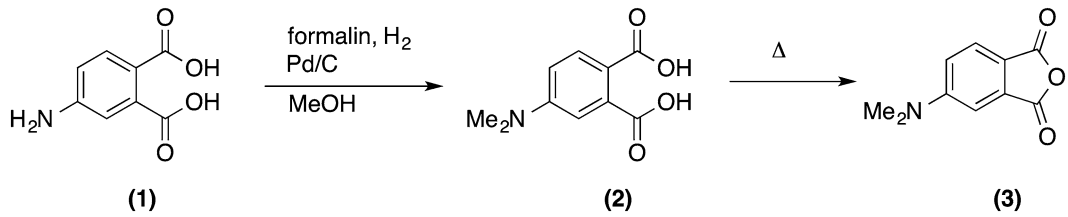

Fig. 2 Synthesis of the environment-sensitive 4-DMAP anhydride

7. Concentrate the solution in a rotary evaporator at 30 °C.
8. Dry the resulting solid under vacuum.
9. Place the solid in a sublimator and heat it at 140–160 °C under vacuum for 10 h (*see* **Note 2**).
10. A bright yellow solid should be obtained in an approximately 80 % yield (*see* **Note 3**).

3.2 Manual Peptide Synthesis

1. Synthesize the full-length peptide using standard Fmoc-based SPPS (solid phase peptide synthesis) procedures as described elsewhere [29]. The peptide sequence will incorporate the Dap(Alloc) residue at the desired position in the peptide; this residue is introduced following the same conditions used for any other standard Fmoc-protected amino acid as explained below.
2. Take 0.05 mmol of Fmoc-PAL-PEG-PS (≈ 240 mg) and place it in a pressure filter funnel (*see* **Note 4**).
3. Wash the resin with DMF (2 × 5 mL × 10 min) passing N_2 through the funnel (*see* Fig. 5, **Note 5**).
4. Filter the resin.
5. Deprotect the amine group of the resin by treating it with 20 % 4-methylpiperidine in DMF (2 × 5 mL × 10 min). Subsequent Fmoc deprotections in the synthesis are performed by a single 5 mL × 15 min treatment.
6. Wash the resin with DMF (3 × 5 mL × 3 min).
7. Run a TNBS test to check that the amino group is deprotected. The resin beads should turn bright red-orange.
8. Activate 0.2 mmol (4 eq.) of the Fmoc-protected glutamic acid (Fmoc–Glu(O*t*Bu)–OH) by mixing it, in a 50 mL falcon tube, with 1.0 mL (4 eq.) of a 0.2 M mixture of HBTU/HOBt in DMF and 1.5 mL (6 eq.) of 0.195 M DIEA/DMF.
9. After 1.5–2 min, add the resulting mixture onto the deprotected amine attached to the solid support and react for 30–45 min.
10. Wash the resin with DMF (2 × 5 mL × 3 min).

11. Run a TNBS test to check that the amino acid is coupled to the solid support. The resin beads should not change their color if the coupling was successful. If any bead turns red, then repeat the coupling procedure with half the amount of reagents (0.1 mmol of Fmoc-amino acid and the corresponding equivalents of each reagent).
12. To assemble the rest of the peptide sequence, repeat **steps 5–11** for all the remaining amino acids in the following order: Fmoc–Dap(Alloc)–OH; Fmoc–Ile–OH; Fmoc–Leu–OH;

    Fmoc–Arg(Pbf)–OH; Fmoc–Arg(Pbf)–OH;
    Fmoc–Lys(Boc)–OH; Fmoc–Ala–OH (*see* **Note 6**).
13. At this point an HPLC analysis of a small amount of the resin can be done to check the synthesis of the peptide. In order to do that, follow this procedure:
    (a) Place ≈ 4 mg of the resin in a 1.5 mL tube, add 150 μL of the cleavage cocktail over it, and shake for 2 h at 600 rpm.
    (b) Take the solution and precipitate the peptide by adding the TFA solution over 1.5 mL of ice-cold Et_2O (optional, *see* **Note 7**).
    (c) Centrifuge the suspension at 16,000 rcf for 5 min.
    (d) Remove the supernatant and dissolve the precipitate in 300 μL of CH_3CN/H_2O (1:1) and inject 50 μL in the HPLC (*see* **Note 8**).
14. *Alloc deprotection*: Once the full peptide is synthesized and the N-terminal end is still protected with the Fmoc protecting group, proceed with the deprotection of the Dap side chain. Start by suspending the resin in 2.5 mL of CH_2Cl_2 and bubble N_2.
15. Over this suspension add 19.7 mg of PPh_3 (0.075 mmol), 55 μL of NMM (*N*-methylmorpholine, 0.5 mmol), and 62 μL of $PhSiH_3$ (0.5 mmol) and mix with N_2 stream for 5 min.
16. Add 3.4 mg of $Pd(OAc)_2$ (0.015 mmol) and react for 12 h (*see* **Note 9**).
17. Filter the resin and wash it with DMF (2×5 mL×2 min), DEDTC (diethyldithiocarbamate, 25 mg in 5 mL of DMF, 2×5 min), DMF (2×5 mL×2 min), and CH_2Cl_2 (2×5 mL×2 min).
18. At this point an HPLC analysis of a small amount of the resin should be done to check the deprotection step. For this purpose follow **step 13** (*see* **Note 10**).
19. *4-DMAP coupling*: Dissolve 40 mg of 4-*N,N*-dimethylaminophthalic anhydride (0.2 mmol) in 2 mL of the 0.195 M DIEA solution in DMF.
20. Add the resulting mixture over the Alloc-deprotected peptide, attached to the resin (0.05 mmol), and shake the suspension for 1 h.

21. Add 250 μL of the 0.2 M HBTU/HOBt mixture in DMF (0.05 mmol) and shake it overnight.
22. Wash the resin with DMF (3 × 5 mL × 3 min).
23. At this point an HPLC analysis of a small amount of the resin should be done to check the efficiency of the coupling reaction. Follow the procedure detailed in **step 13** (*see* **Note 11**).
24. If the fluorophore is efficiently coupled to the peptide, remove the *N*-terminal Fmoc using the standard SPPS conditions detailed in **steps 5**–**7**.
25. *Cleave the final peptide from the resin:* Place ≈ 0.025 mmol of the resin-bound peptide in a 50 mL falcon tube. Add 3 mL of the cleavage cocktail—150 μL of CH_2Cl_2, 75 μL of water, 75 μL of TIS and TFA to 3 mL—and shake the resulting suspension at ≈ 500 osc/min in a flask shaker for 2 h.
26. Filter the resin and concentrate the TFA solution under an argon current to a volume of approximately 2 mL. Add the residue over 40 mL of ice-cold Et_2O.
27. Centrifuge the suspension at 6600 rcf for 10 min and remove the supernatant.
28. Wash the precipitate with 20 mL of ice-cold ether and repeat **step 27**.
29. Dry the solid residue under argon and dissolve it in acetonitrile/water 1:1 (1 mL) for HPLC purification (*see* details under Subheading 2).
30. Collect the major peak in the chromatogram. Check the identity of the product by mass spectrometry (*see* **Note 12**).
31. Lyophilize the collected fractions containing the product.

3.3 Peptide and Cyclin Quantification by UV Spectroscopy

Cyclin A was expressed, purified and quantified following reported procedures [30].

3.3.1 Peptide Quantification

1. Dissolve a small amount of the peptide (≈ 1 mg) in 50–100 μL of HEPES buffer.
2. Set the UV Spectrophotometer to read the absorbance at 421 nm.
3. Place in a UV cuvette 100 μL of HEPES solution and run a blank reading (*see* **Note 13**).
4. Add 1 μL of your peptide stock solution to the cuvette and mix it carefully by using a micropipette.
5. Read the absorbance of the mixture and take the value.
6. Add another microliter of your peptide stock solution to the cuvette, mix it carefully, and read the absorbance of the mixture and take the obtained value.

7. Repeat **step 6** twice more.
8. Replace every absorbance value obtained in the next equation:

$$C_m = A \times \frac{100 + v}{6480 \times v \times \ell}$$

where A is the absorbance measured, v is the total volume of the peptide stock solution added to the cuvette for every read (in μL), l is the path length (in cm).

9. Make the arithmetic mean between all the C_m values obtained to get the concentration of your peptide stock solution.

3.4 Peptide-Cyclin Binding Assays

The mathematical treatment of the competition titration data relies on the accurate knowledge of the dissociation constant of the fluorescent probe in the particular conditions of the assay (pH, buffer, temperature, etc.). In order to calculate it, perform a simple titration of the peptide with increasing amounts of cyclin A as explained below:

1. Place in a fluorescence cuvette 150 μL of a 1.5 μM solution of the peptide, prepared by dilution of the peptide stock solution with HEPES buffer, and record the fluorescence spectrum.
2. Add 1 μL of a solution of cyclin A (≈ 100 μM), mix it carefully by using a micropipette, and record the fluorescence spectrum of the mixture.
3. Repeat **step 2** from 15 to 20 times (*see* **Note 14**).
4. Represent the fluorescence emission at the maximum emission wavelength (512 nm) against the concentration of cyclin A in the solution (in μM) for each point of the titration (*see* Fig. 3).

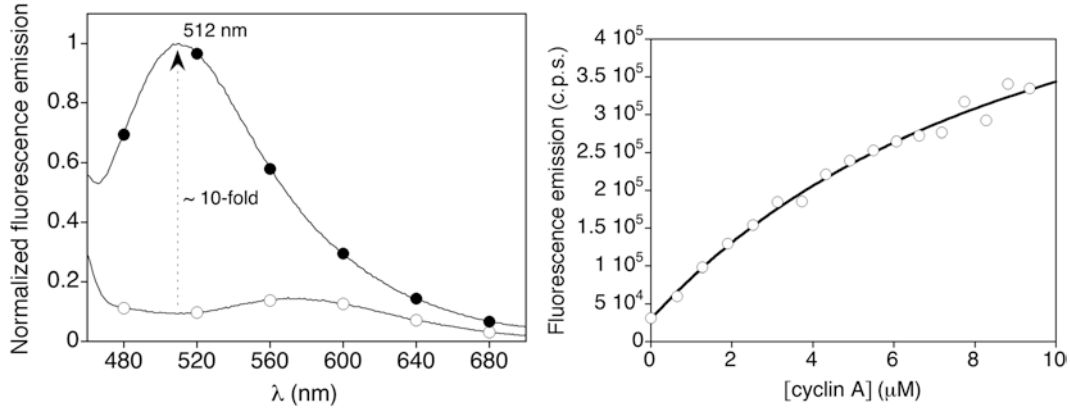

Fig. 3 *Left*: Fluorescence emission spectra of a 1.5 μM solution of the fluorescent peptide sensor in 10 mM HEPES, 100 mM NaCl pH 7.6 buffer (*white circles*), and in the presence of 6 eq. of cyclin A (*black circles*). *Right*: Fluorescence emission of the fluorescent peptide sensor at 512 nm with increasing amounts of cyclin A, and best fit to a 1:1 binding model used to calculate the binding constant

5. Repeat the full titration (**steps 1–4**) twice more to calculate an arithmetical average of the dissociation constant.

Considering F the total measured fluorescence, F_0 an adjustable parameter accounting for the background fluorescence, F_{SC} an adjustable parameter for the fluorescent sensor-cyclin complex molar fluorescence, K_S the dissociation constant of the interaction between the fluorescent sensor and the cyclin A, $[S]_T$ and $[\text{cyclin}]_T$ the total concentrations of sensor and cyclin A, $[S]$ and $[\text{cyclin}]$ the concentration of the free sensor and cyclin A in the equilibrium, and $[\text{S-cyclin}]$ the concentration of fluorescent sensor-cyclin complex [25, 31–33] then:

$$F = \frac{1}{2}\left(2F_0 + F_{SC} \times \left[K_S + [S]_T + [\text{cyclin}]_T - \sqrt{\left(K_S + [S]_T + [\text{cyclin}]_T\right)^2 - 4[S]_T[\text{cyclin}]_T}\right]\right) \quad (1)$$

where:

$$K_S = \frac{[\text{cyclin}] \times [S]}{[S - \text{cyclin}]} \quad (2)$$

$$[\text{cyclin}]_T = [\text{cyclin}] + [S - \text{cyclin}] \quad (3)$$

$$[S]_T = [S] + [S - \text{cyclin}] \quad (4)$$

$$F = F_0 + F_{SC} \times [S - \text{cyclin}] \quad (5)$$

The fluorescence emission experimental data can be fit to Eq. 1 by nonlinear regression to obtain optimized values for K_S, F_0, and F_{SC} (*see* **Note 15**).

3.5 Competition Titrations

The fluorescent sensor can be used as a tool to identify new cyclin A inhibitors and characterize their binding to the protein by performing competition titrations. Here is presented the competition assay with a short peptide, HAKRRLFG, that has known CDK2/cyclin A inhibitory properties (inhibitor **I1**) [34]. In order to calculate the dissociation constant of the new inhibitor, perform a simple titration of the complex fluorescent sensor-cyclin A with increasing amounts of the inhibitor as explained below:

1. Place in a fluorescence cuvette 150 μL of an equimolar 1.5 μM solution of cyclin A and the peptide sensor in HEPES buffer and record the fluorescence spectrum.
2. Add 1 μL of a solution of the inhibitor (≈ 30 μM), mix it carefully by using a micropipette, and record the fluorescence spectrum of the mixture.
3. Repeat **step 2** from 15 to 20 times (*see* **Note 16**).
4. Represent the normalized fluorescence emission at the maximum emission wavelength (in this case 512 nm) against the concentration of inhibitor in the solution (in μM) for each point of the titration (*see* Fig. 4).

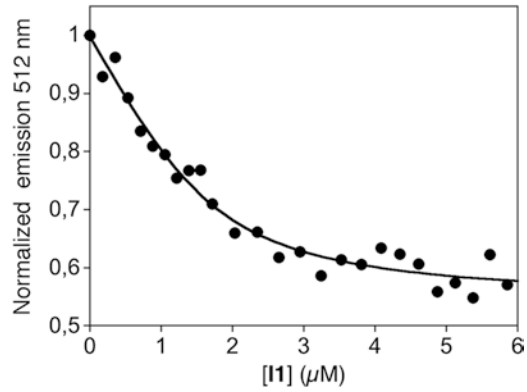

Fig. 4 Competition titration of cyclin A (1.5 μM) and the environment-sensitive probe (1.5 μM in 10 mM HEPES, 100 mM NaCl pH 7.6 buffer) with increasing concentrations of the peptide inhibitor **I1**. The curve represents the best fit to a 1:1 competition model

5. Repeat the full titration (**steps 1**–**4**) twice more to calculate an arithmetical average of the dissociation constant.

Considering F the total measured fluorescence, F_0 the initial fluorescence emission in absence of inhibitor, F_{max} the fluorescence once the sensor has been fully displaced at the end of the titration, K_S the dissociation constant measured for the fluorescent sensor for cyclin A, K_I the inhibitor dissociation constant, and $[S]_T$, $[I]_T$, $[\text{cyclin}]_T$ the total concentrations of sensor, inhibitor, and cyclin A respectively, then:

$$F = F_0 + \left(F_{max} - F_0\right)\frac{2\sqrt{\left(a^2 - 3b\right)}\cos\left(\theta/3\right) - a}{3K_S + 2\sqrt{\left(a^2 - 3b\right)}\cos\left(\theta/3\right) - a} \tag{6}$$

where:

$$\theta = \arccos\left[\frac{-2a^3 + 9ab - 27c}{2\sqrt{\left(a^2 - 3b\right)^3}}\right] \tag{7}$$

$$a = K_S + K_I + [S]_T + [I]_T - [\text{cyclin}]_T \tag{8}$$

$$b = \left([S]_T - [\text{cyclin}]_T\right)K_I + \left([I]_T - [\text{cyclin}]_T\right)K_S + K_S K_I \tag{9}$$

$$c = -K_S K_I [\text{cyclin}]_T \tag{10}$$

The fluorescence emission experimental data can be fit to Eq. (6) by nonlinear regression to obtain optimized values for K_I, F_0, and F_{max} (*see* **Note 17**).

4 Notes

1. The TLC plate could show the starting material, as well as the mono- and the desired dimethylated product. If the monomethylated product were still present in the reaction mixture, allow the reaction to stir for an extra hour.
2. The exact time for sublimation will greatly depend on the vacuum reached inside the sublimator chamber. The anhydride is collected as a bright yellow solid. If too much product is sublimated, it could be difficult to open the sublimator without part of the product falling back to the chamber; this could be avoided by collecting the sublimated product periodically.
3. ^{1}H-RMN (300 MHz, $CDCl_3$) δ: 3.16 (s, 6H), 6.95 (dd, 1H, J_1 = 2.4 Hz, J_2 = 8.7 Hz), 7.08 (d, 1H, J = 2.4 Hz), 7.75 (d, 1H, J = 8.6 Hz).

   ^{13}C-NMR (75.5 MHz, $CDCl_3$) δ: 40.8 (CH_3), 106.6 (CH), 116.0 (C), 117.4 (CH), 127.2 (CH), 134.4 (C), 155.5 (C), 163.4 (CO), 164.7 (CO).

   HRMS-ESI (m/z): $[MH]^+$ calcd for $C_{10}H_{10}NO_3$ 192.0655, found 192.0658.
4. Any standard SPPS amide resin with medium-low loading could also be used with equivalent results. Alternatively, an automatic peptide synthesizer can be used to assemble the peptide.
5. Schematic representation of the experimental setup for manual peptide synthesis (*see* Fig. 5).
   (a) Represents the system during the coupling, deprotection, and wash steps. Connect the flow of N_2 directly to the reaction vessel before adding any solution to avoid any loss of the reagents; the N_2 flow will gently mix the resin beads with the reactants in solution. It is advisable to check the N_2 flow rate before attaching the tubing to the reaction vessel. Avoid excessive flow that could cause ejection of the reaction mixture through the upper opening of the vessel, which must be *always open*.
   (b) Represents the system during the filtration step. Connect directly the reaction vessel to the vacuum pump to remove the solutions. Vacuum from a small pump or in-house vacuum found in many laboratories should be enough for filtering the reaction mixture.
6. Solid Phase Peptide Synthesis is very simple to perform and does not require any advance training in synthetic chemistry. However, we have found that it is very easy to forget and/or mix-up the particular step of the synthesis that is being carried out; the best way to avoid this is to prepare a simple

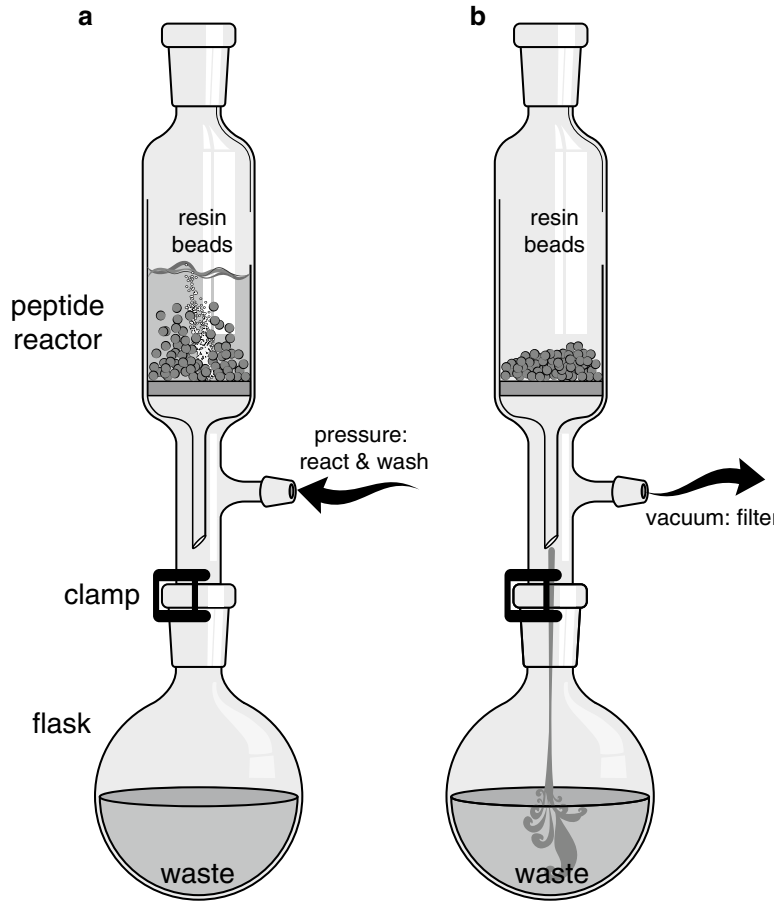

Fig. 5 Schematic representation of the experimental setup for the manual solid phase synthesis of the peptide sensor

checkbox-style table including every step of the synthesis and stick it to the fume hood next to the reaction vessel (*see* Table 1). Tick each box when starting the corresponding step for maintaining a clear record of the synthetic procedure. Other relevant data can be also included in the table, i.e., if the coupling had to be repeated, the TNBS test was inconclusive or the specific start and end times of each step.

7. TFA can be stored at 4 °C in the refrigerator to minimize the released vapors.
8. The identity of the desired Fmoc-protected peptide is confirmed by ESI-MS (Fmoc–AKRRLIϕE–NH_2, where ϕ = Dap(Alloc)), $C_{60}H_{93}N_{17}O_{14}$, $[MH]^+$ calcd. 1276.71.
9. Alternatively, the mixture can be bubbled with N_2 for 15 min and then close the reaction vessel and leave it under agitation (≈ 500 osc/min) in a flask shaker.

Table 1
Solid phase peptide synthesis checklist

	Coupling (recouple)	DMF wash	TNBS test	Fmoc deprotection	DMF wash	TNBS test (optional)
Resin preparation 0.05 mmol resin		☐☐		☐☐	☐☐☐	☐
Fmoc–Glu(O*t*Bu)–OH FW: 425.5; 0.2 mmol: **85 mg**	☐(☐)	☐☐	☐	☐	☐☐☐	☐
Fmoc–Dap(Alloc)–OH FW:410.4; 0.2 mmol: **82 mg**	☐(☐)	☐☐	☐	☐	☐☐☐	☐
Fmoc–Ile–OH FW:353.4; 0.2 mmol: **71 mg**	☐(☐)	☐☐	☐	☐	☐☐☐	☐
Fmoc–Leu–OH FW:353.4; 0.2 mmol: **71 mg**	☐(☐)	☐☐	☐	☐	☐☐☐	☐
Fmoc–Arg(Pbf)–OH FW:648.8; 0.2 mmol: **130 mg**	☐(☐)	☐☐	☐	☐	☐☐☐	☐
Fmoc–Arg(Pbf)–OH FW:648.8; 0.2 mmol: **130 mg**	☐(☐)	☐☐	☐	☐	☐☐☐	☐
Fmoc–Lys(Boc)–OH FW:468.5; 0.2 mmol: **94 mg**	☐(☐)	☐☐	☐	☐	☐☐☐	☐
Fmoc–Ala–OH FW: 311.3; 0.2 mmol: **62 mg**	☐(☐)	☐☐	☐			

10. The identity of the desired Fmoc-protected/Alloc-deprotected peptide is confirmed by ESI-MS (Fmoc–AKRRLIϕE–NH_2, where ϕ = Dap(NH_2)), $C_{56}H_{89}N_{17}O_{12}$, $[MH]^+$ calcd. 1192.69.
11. The identity of the desired Fmoc-protected peptide is confirmed by ESI-MS (Fmoc–AKRRLIϕE–NH_2, where ϕ = Dap(4-DMAP)), $C_{66}H_{96}N_{18}O_{14}$, $[MH]^+$ calcd. 1365.74. If you observe a peak at 1383.75 (mass of the semi-coupled fluorophore), add 2 mL of DMF and 250 μL of the 0.2 M HBTU/HOBt mixture in DMF (0.05 mmol) and shake it overnight to complete the cyclization of the fluorophore.
12. The identity of the desired peptide product is confirmed by ESI-MS (H–AKRRLIϕE–NH_2, where ϕ = Dap(4-DMAP)), $C_{51}H_{86}N_{18}O_{12}$, $[MH]^+$ calcd. 1143.67.
13. The *SmartSpec Plus* Spectrophotometer from *Bio-Rad* allows subtracting automatically the background reading to the sample. If this is not possible in the configuration of your spectrophotometer, subtract manually this read to your sample reads.
14. To get a good fit of the collected data, run experiments until the signal reaches the saturation plateau. You will need a data set with

about 15–20 points for a good fitting curve. The fluorescence increase upon addition of the protein is immediate; therefore it is not necessary to have an incubation time between readings.

15. Data fitting was made with *Mathematica*® 8.0.0.0 program for *Mac OS* X (*Wolfram Research*). Our calculations resulted in a dissociation constant (K_s) of 8.4 μM.
16. To get a good fit of the collected data, run experiments until reaching the titration plateau when the decrease in emission upon each addition is small. Again you will need 15–20 points for a good fitting. These titrations can also be easily adapted for a more high-throughput screening of inhibitors using a 96-well plate by scaling the volumes used in the experiments.
17. Our competition experiments resulted in a $K_I \approx 0.31$ μM for **I1**. Data fitting was made with *Mathematica*® 8.0.0.0 program for *Mac OS* X (*Wolfram Research*). Alternatively there are a number of specialized software packages (e.g., *DynaFit* from *BioKin*, Ltd., which provides free academic licenses) that can be used to fit both simple one-site and competitive titrations. Some of these software packages also allow a global fit of all the titrations simultaneously to obtain the best values that reproduce all the experimental data.

Acknowledgments

We thank the support given by the Spanish grants SAF2010-20822-C02, CTQ2009-14431/BQU, *Consolider Ingenio* 2010 and the *Xunta de Galicia* INCITE09 209084PR, GRC2010/12, PGIDIT08CSA-047209PR. We also thank Prof. Anxo Vidal, from the Universidade de Santiago de Compostela, and Mar Orzáez and Enrique Pérez-Payá from *Príncipe Felipe Research Centre* in Valencia for their help with cyclin A expression. E. P. thanks the Xunta de Galicia for her postdoctoral contract.

References

1. Zhang J, Campbell RE, Ting AY, Tsien RY (2002) Creating new fluorescent probes for cell biology. Nat Rev Mol Cell Biol 3:906–918
2. Lavis LD, Raines RT (2008) Bright ideas for chemical biology. ACS Chem Biol 3:142–155
3. Giepmans BNG, Adams SR, Ellisman MH, Tsien RY (2006) The fluorescent toolbox for assessing protein location and function. Science 312:217–224
4. Schäferling M (2012) The art of fluorescence imaging with chemical sensors. Angew Chem Int Ed 51:3532–3554
5. Lemke EA, Schultz C (2011) Principles for designing fluorescent sensors and reporters. Nat Chem Biol 7:480–483
6. Pazos E, Vazquez O, Mascareñas JL, Vazquez ME (2009) Peptide-based fluorescent biosensors. Chem Soc Rev 38:3348–3359
7. VanEngelenburg SB, Palmer AE (2008) Fluorescent biosensors of protein function. Curr Opin Chem Biol 12:60–65
8. Johnsson N, Johnsson K (2007) Chemical tools for biomolecular imaging. ACS Chem Biol 2:31–38

9. de Silva AP, Gunaratne H, Gunnlaugsson T, Huxley A, McCoy C, Rademacher J, Rice T (1997) Signaling recognition events with fluorescent sensors and switches. Chem Rev 97:1515–1566
10. Kossiakoff AA, Koide S (2008) Understanding mechanisms governing protein-protein interactions from synthetic binding interfaces. Curr Opin Struct Biol 18:499–506
11. Keskin O, Gursoy A, Ma B, Nussinov R (2008) Principles of protein-protein interactions: what are the preferred ways for proteins to interact? Chem Rev 108:1225–1244
12. Choulier L, Enander K (2010) Environmentally sensitive fluorescent sensors based on synthetic peptides. Sensors 10:3126–3144
13. Duke RM, Veale EB, Pfeffer FM, Kruger PE, Gunnlaugsson T (2010) Colorimetric and fluorescent anion sensors: an overview of recent developments in the use of 1,8-naphthalimide-based chemosensors. Chem Soc Rev 39: 3936–3953
14. Cohen BE, McAnaney TB, Park ES, Jan YN, Boxer SG, Jan LY (2002) Probing protein electrostatics with a synthetic fluorescent amino acid. Science 296:1700–1703
15. Vazquez ME, Blanco-Canosa JB, Imperiali B (2005) Photophysics and biological applications of the environment-sensitive fluorophore 6-N,N-dimethylamino-2,3-naphthalimide. J Am Chem Soc 127:1300–1306
16. Vazquez ME, Rothman DM, Imperiali B (2004) A new environment-sensitive fluorescent amino acid for Fmoc-based solid phase peptide synthesis. Org Biomol Chem 2: 1965–1966
17. Valeur B (2002) Molecular fluorescence: principles and applications. Wiley-VCH, Weinheim
18. Malumbres M, Carnero A (2003) Cell cycle deregulation: a common motif in cancer. Prog Cell Cycle Res 5:5–18
19. Ball KL, Lain S, Fåhraeus R, Smythe C, Lane DP (1996) Cell-cycle arrest and inhibition of Cdk4 activity by small peptides based on the carboxy-terminal domain of p21WAF1. Curr Biol 7:71–80
20. Mendoza N, Fong S, Marsters J, Koeppen H, Schwall R, Wickramasinghe D (2003) Selective cyclin-dependent kinase 2/cyclin A antagonists that differ from ATP site inhibitors block tumor growth. Cancer Res 63:1020–1024
21. Pazos E, Torrecilla D, Vázquez LM, Castedo L, Mascareñas JL, Vidal A, Vazquez ME (2008) Cyclin A probes by means of intermolecular sensitization of terbium-chelating peptides. J Am Chem Soc 130:9652–9653
22. Pazos E, Pérez M, Gutiérrez-de-Terán H, Orzáez M, Guevara T, Mascareñas JL, Vazquez ME (2011) Rational design of a cyclin A fluorescent peptide sensor. Org Biomol Chem 9:7629–7632
23. Kontopidis G, Andrews MJI, McInnes C, Cowan A, Powers H, Innes L, Plater A, Griffiths G, Paterson D, Zheleva DI, Lane DP, Green S, Walkinshaw MD, Fischer PM (2003) Insights into cyclin groove recognition: complex crystal structures and inhibitor design through ligand exchange. Structure 11:1537–1546
24. Chanvorachote B, Nimmannit U, Muangsiri W, Kirsch L (2009) An evaluation of a fluorometric method for determining binding parameters of drug–carrier complexes using mathematical models based on total drug concentration. J Fluoresc 19:747–753
25. Thordarson P (2011) Determining association constants from titration experiments in supramolecular chemistry. Chem Soc Rev 40: 1305–1323
26. Wang ZX (1995) An exact mathematical expression for describing competitive binding of two different ligands to a protein molecule. FEBS Lett 360:111–114
27. Wang ZX, Jiang RF (1996) A novel two-site binding equation presented in terms of the total ligand concentration. FEBS Lett 392: 245–249
28. Hancock WS, Battersby JE (1976) A new micro-test for detection of incomplete coupling reactions in solid-phase peptide-synthesis using 2,4,6-trinitrobenzenesulphonic acid. Anal Biochem 71:260–264
29. Hancock WS (2000) Fmoc solid phase peptide synthesis: a practical approach. Oxford University Press, Oxford
30. Wang X, Fu M, Ren J, Qu X (2007) Evaluation of different culture conditions for high-level soluble expression of human cyclin A2 with pET vector in BL21 (DE3) and spectroscopic characterization of its inclusion body structure. Protein Expr Purif 56:27–34
31. Roehrl MHA, Wang JY, Wagner G (2004) A general framework for development and data analysis of competitive high-throughput screens for small-molecule inhibitors of protein-protein interactions by fluorescence polarization. Biochemistry 43:16056–16066
32. Eftink MR (1997) Fluorescence methods for studying equilibrium macromolecule-ligand interactions. Methods Enzymol 278:221–257
33. Shi G, Gong Y, Savchenko A, Zeikus JG, Xiao B, Ji X, Yan H (2000) Dissecting the

nucleotide binding properties of *Escherichia coli* 6-hydroxymethyl-7,8-dihydropterin pyrophosphokinase with fluorescent 3'(2)' -*o*-anthraniloyladenosine 5'-triphosphate. Biochim Biophys Acta 1478:289–299

34. Zheleva DI, Mcinnes C, Gavine A-L, Zhelev NZ, Fischer PM, Lane DP (2002) Highly potent p21(WAF1)-derived peptide inhibitors of CDK-mediated pRb phosphorylation: delineation and structural insight into their interactions with cyclin A. J Pept Res 60:257–270

Chapter 8

Cell Synchronization Techniques to Study the Action of CDK Inhibitors

Beatriz Pérez-Benavente and Rosa Farràs

Abstract

Cell synchronization techniques have been used for the studies of mechanisms involved in cell cycle regulation. Synchronization involves the enrichment of subpopulations of cells in specific stages of the cell cycle. These subpopulations are then used to study regulatory mechanisms of the cell cycle such as DNA synthesis, gene expression, protein synthesis, protein phosphorylation, protein degradation, and development of new drugs (e.g., CDK inhibitors). Here, we describe several protocols for synchronization of cells from different phases of the cell cycle. We also describe protocols for determining cell viability and mitotic index and for validating the synchrony of the cells by flow cytometry.

Key words Cell cycle, DNA content, Flow cytometry, Mitotic index, Synchronization

1 Introduction

A precise control of all stages of the cell cycle is essential for normal cell division. Two major processes characterize the cell cycle: DNA replication and segregation of duplicated chromosomes in two daughter cells [1]. It consists of two main periods: the interphase and mitosis. The interphase comprises (1) the G1 phase, which extends from previous mitosis until the S phase, (2) the S phase during which the cell duplicates its DNA, and (3) the G2 phase during which the cell prepares for mitosis. Mitosis (M) is the cycle period during which take place (1) the segregation of duplicated chromosomes and (2) cytokinesis resulting in two daughter cells. The transitions from one phase to another take place in an orderly and sequential manner and are controlled by various kinases called cyclin-dependent kinases (CDK). The activity of these kinases is regulated by mechanisms such as phosphorylation/dephosphorylation, but also by the spatiotemporally regulated expression of cyclins (Cyc) and cyclin kinase inhibitors or CKIs.

Mar Orzáez et al. (eds.), *Cyclin-Dependent Kinase (CDK) Inhibitors: Methods and Protocols*, Methods in Molecular Biology, vol. 1336, DOI 10.1007/978-1-4939-2926-9_8,

The periodic variation in the abundance of cyclins and CKI_S depends on their synthesis and degradation by the ubiquitin-proteasome system (UPS).

Synchronization involves the enrichment of subpopulations of cells in specific stages of the cell cycle. Protocols for synchronizing cells are based on (1) physical properties of the cells and include physical fractionation (mitotic shake-off, flow cytometry, dielectrophoresis, cytofluorometric purification), (2) selective nutrient depletion, and (3) chemical blockade by the addition of pharmacological agents [2, 3]. Methods based on physical characteristics have the advantage that the cells are not exposed to pharmacological agents; however many of these methods require specific equipment. Several chemicals may reversibly block cells from cycling resulting in a homogeneous population of cells at a particular stage of the cell cycle. Cells that are synchronized are artificially induced to cycle in a homogeneous manner. However, the chemicals may alter gene expression and posttranslational modifications after the blockade. Synchronization using chemicals is achieved immediately after release of the drugs but it is gradually lost after cells divide. Synchronized cells can be used to study the activity of new drugs that target the cell cycle checkpoints responsible for the control of cell cycle progression. These drugs may either increase or decrease the degree of checkpoint arrest and may slow growth and induce cell death.

The protocols presented here describe procedures used to synchronize NIH 3T3, HeLa or U2OS cells [4–6], in various stages of the cell cycle (*see* Fig. 1). Protocols will be presented for synchronizing cells in the G1 by serum withdrawal [4], G1/S by feedback control through addition of excess nutrients (e.g., thymidine, [7, 8]) or by the use of chemical agents (e.g., aphidicolin, [9]), and in M by morphological differences (mitotic shake-off, [10]) or by the addition of chemical agents (e.g., nocodazole [11, 12]) (*see* Fig. 2).

For some cell types, serum starvation is not a viable method of synchronization either because cells arrest permanently in G_0, do not arrest (e.g., HeLa) or undergo apoptosis. To block cells in G1/S a double-blockade (thymidine/thymidine or thymidine/aphidicolin) procedure is generally used to block DNA synthesis. The addition of thymidine induces feedback inhibition of DNA replication and arrests cells throughout S phase [8]. After releasing cells from the thymidine blockade they cycle throughout S phase and mitosis and then are trapped in G1/S by a second block with thymidine or aphidicolin. Aphidicolin is an inhibitor of DNA polymerase-α and DNA polymerase-δ. This method is used to monitor S- and G2/M-phase progression [6, 8]. The procedures described below are for the synchronization of cells with a doubling time of 24 h (e.g., HeLa and U2OS). Synchronization of cells by mitotic shake-off or nocodazole (which prevents microtubule assembly [13]) is useful to study M-G1-S-phase

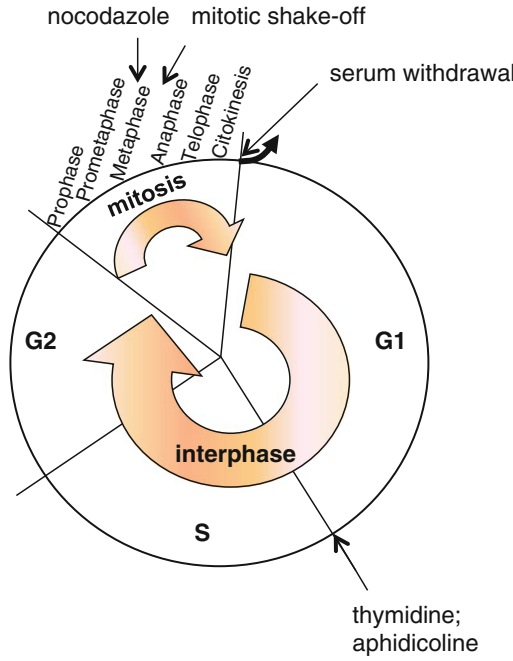

Fig. 1 Common methods for mammalian cell cycle synchronization. *Arrows* indicate the phase of the cell cycle at which cells are arrested

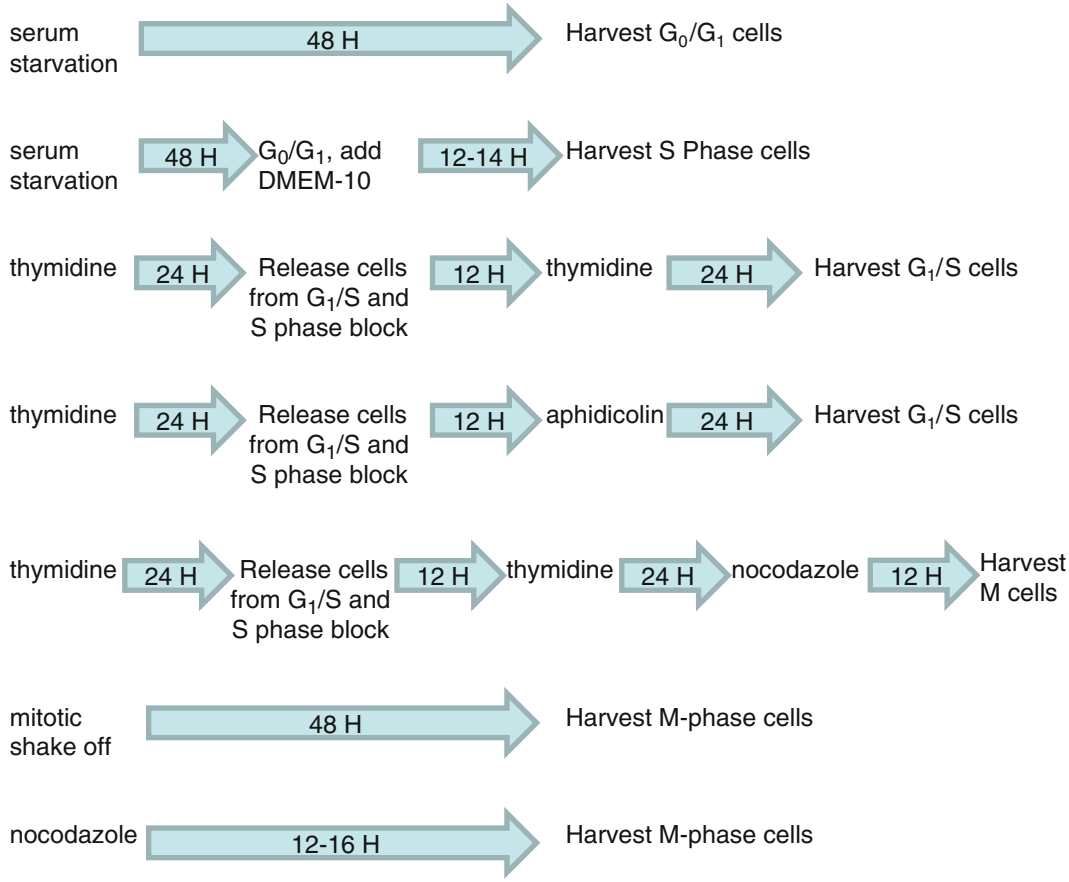

Fig. 2 Outline of the different synchronization methods described in this chapter

transition. Synchronization is achieved immediately after release of the drugs but after division cells lose synchrony rapidly. Methods are provided for determining cell viability and for measuring DNA content and mitotic index by flow cytometry.

2 Materials

1. NIH 3T3 cells, HeLa cells, U2OS cells.
2. DMEM prewarmed to 37 °C.
3. DMEM-1 supplemented with 1 % (v/v) fetal bovine serum (FBS) prewarmed to 37 °C.
4. DMEM-10 supplemented with 10 % (v/v) FBS prewarmed to 37 °C.
5. PBS.
6. 1× Trypsin.
7. CO_2 cell culture incubator.
8. Centrifuge.
9. 15 mL polypropylene V-bottomed tubes.
10. 50 mL polypropylene V-bottomed tubes.
11. Nocodazole.
12. Thymidine.
13. Aphidicolin.
14. Hemocytometer for cell counting.
15. Trypan blue 0.4 %.
16. Propidium iodide.
17. RNase A.
18. Ethanol 70 %.
19. 1 % BSA in PBS.
20. pS10-Histone H3 antibody.
21. FITC-conjugated secondary antibody.
22. 0.25 % Triton X-100 in PBS.

3 Methods

3.1 Method Enrichment of Cells at G0/G1 by Serum Starvation

1. Trypsinize exponentially growing NIH-3T3 cells and plate in prewarmed DMEM-1 at 30–40 % of their confluent density in a 100 mm tissue culture plate (*see* **Note 1**).
2. Incubate the cells for 48 h at 37 °C.

3. Remove DMEM-1 and add 10 mL DMEM-10 prewarmed at 37 °C (*see* **Note 2**). Incubate at 37 °C.
4. Approximately 12–14 h after stimulation cells progress into S phase.

3.2 Cell Synchronization at the Onset of S Phase by Double-Thymidine Block (See Note 3)

1. Trypsinize exponentially growing U2OS cells and plate in prewarmed DMEM-10 at 3×10^5 per 60 mm, 6×10^5 per 100 mm, or 1.5×10^6 cells per 150 mm tissue culture plates (*see* **Note 1**).
2. After 24 h, replace medium with new DMEM-10 prewarmed to 37 °C, add 1/40 volume of 100 mM thymidine in DMEM (*see* **Note 4**), and incubate cells for 25 h at 37 °C (*see* **Note 2**).
3. Release thymidine block by removing the thymidine-containing medium, and rinse the dishes twice with 5 mL prewarmed DMEM.
4. Add 10 mL prewarmed DMEM-10.
5. After 12–14 h add 1/40 volume of 100 mM thymidine in DMEM and incubate cells for 24 h at 37 °C.
6. Release thymidine block as above and add 10 mL prewarmed DMEM-10.
7. Monitor the progression of cells into S, G2/M, and M/G1 phase by flow cytometry (*see* Subheadings 3.8 and 3.9).

3.3 Cell Synchronization at the Onset of S Phase by Thymidine-Aphidicolin Block (See Note 3)

1. Trypsinize exponentially growing HeLa cells and plate in prewarmed DMEM-10 at 3×10^5 per 60 mm, 6×10^5 per 100 mm, or 1.5×10^6 cells per 150 mm tissue culture plates (*see* **Note 1**).
2. After 24 h, replace medium with new DMEM-10 prewarmed to 37 °C and add 1/40 volume of 100 mM thymidine in DMEM (*see* **Note 4**) and incubate cells for 25 h at 37 °C (*see* **Note 2**).
3. Release thymidine block by removing the thymidine-containing medium, and rinse the dishes twice with 10 mL fresh prewarmed DMEM.
4. Add 10 mL prewarmed DMEM-10.
5. After 12–14 h add 1/1000 volume of 5 mg/mL aphidicolin in DMSO (*see* **Note 5**) and incubate cells for 24 h at 37 °C.
6. Release as above and add 10 mL prewarmed DMEM-10.
7. Monitor the progression of cells into S, G2/M, and M/G1 phase by flow cytometry (*see* Subheadings 3.8 and 3.9).
8. If enrichment of M-phase cells is needed, add 1/1000 volume of 40 μg/mL nocodazole (*see* **Note 6**) 4 h after aphidicolin release. Cells will reach mitosis after 10–12 h. Harvest mitotic cells by gently pipetting off dish.

3.4 Cell Synchronization at M by Thymidine-Nocodazole Block

1. Plate log-phase cells, 2×10^6 per 150 mm tissue culture plates.
2. After 24 h add 1/40 volume of 100 mM thymidine.
3. Block cells for 25 h.
4. Release block by washing cells with prewarmed serum-free DMEM, and replace with complete medium (*see* **Note 2**).
5. After 4 h add 1/1000 volume of 40 μg/mL nocodazole in DMSO (*see* **Note 6**).
6. Block for 12 h and harvest mitotic cells by gently pipetting off dish (*see* **Note 7**).
7. Release cells by centrifugation for 5 min at $400 \times g$ and wash twice with 10 mL DMEM prewarmed at 37 °C.
8. Resuspend cells in 10 mL prewarmed DMEM-10 and replate cells in a 100 mm tissue culture plate; cells take 1–2 h to reattach.
9. Measure the cell cycle-related events during the M/G1/S-phase transitions.

3.5 Enrichment of Mitotic Cells by Mitotic Shake-Off

1. Trypsinize exponentially growing HeLa cells and plate in prewarmed DMEM-10 at 2.5×10^6 cells per 150 mm tissue culture plate.
2. After 24 h replace medium with new prewarmed DMEM-10 (*see* **Note 2**).
3. After 24 h harvest round mitotic cells by gently tapping the flask on the bench to shake off any loosely rounded cells and then collect mitotic cells by gently pipetting off the medium contained in the dish (*see* **Note 7**).
4. Transfer cell suspension to 50 mL centrifuge tubes and centrifuge for 5 min at $400 \times g$ at room temperature.
5. Discard supernatant, resuspend pellet in 20 mL DMEM-10 prewarmed at 37 °C, and replate in a 150 mm tissue culture plate.
6. Cells take 1–2 h to attach.
7. Measure the cell cycle-related events during the M/G1/S-phase transitions.

3.6 Enrichment of Mitotic Cells by Nocodazole Arrest

1. Trypsinize exponentially growing HeLa cells and replate in prewarmed DMEM-10 at 2.5×10^6 cells per 150 mm tissue culture plate.
2. After 24 h replace medium with new DMEM-10 prewarmed to 37 °C and add 1/1000 volume of 40 μg/mL nocodazole in DMSO (*see* **Note 2**).
3. Block for 12–18 h and harvest mitotic cells by gently pipetting off dish (*see* **Note 7**).

4. Transfer cell suspension to 50 mL centrifuge tubes and centrifuge for 5 min at 400 × *g* at room temperature.
5. Discard supernatant, and resuspend pellet in 20 mL fresh, prewarmed DMEM. Repeat centrifugation and addition of 20 mL prewarmed DMEM. Repeat centrifugation.
6. Resuspend cells in 20 mL prewarmed DMEM-10 and replate cells in a 150 mm tissue culture plate.
7. Cells take 1–2 h to reattach, and 2 h approximately to exit mitosis.
8. Measure the cell cycle-related events during the M/G1/S-phase transitions.

3.7 Cell Counting and Viability Measurement Using Trypan Blue

Trypan blue is a vital dye used to selectively stain dead cells. Reactivity of trypan blue is based on the fact that the chromophore is negatively charged and does not interact with the cell unless the membrane is damaged. Therefore, all the cells which exclude the dye are viable.

1. Add 50 µL of 0.4 % trypan blue solution to 350 µL of media.
2. Add 100 µL of the cell suspension and mix well. This makes a final 1:5 cell suspension dilution. This will be referred to as the "dilution factor" in the formula below.
3. Fill a hemocytometer as for cell counting.
4. Under a microscope, observe if nonviable cells are stained and viable cells excluded the stain.
5. Determine cell viability using the formula below:

   Viable cell count/quadrants counted × dilution factor* × hemocytometer factor* = viable cells/mL.

   *Dilution factor in this protocol is 5

   *Hemocytometer factor is 10,000.

3.8 Quantification of DNA Content by Flow Cytometry

1. Harvest cells by trypsinizing and prepare single-cell suspension in PBS.
2. Wash cells and resuspend at 1–2 × 10^6 cells/mL.
3. Aliquot 1 mL cells in a 15 mL polypropylene V-bottomed tube, centrifuge, and resuspend in 200 µL PBS.
4. Add 1 mL cold 70 % ethanol, dropwise, while vortexing to prevent cell clumping.
5. Fix cells for at least 2 h at –20 °C. (*see* **Note 8**).
6. Wash cells in PBS.
7. Add 1 mL of propidium iodide/RNase A staining solution (*see* **Note 5**) to cell pellet, mix well, and incubate for 30 min at 37 °C.
8. Store samples at 4 °C until analyzed by flow cytometry.

3.9 Determination of Mitotic Index by Flow Cytometry

Mitotic cells are indistinguishable from G2 cells when quantifying DNA content by flow cytometry. Since histone H3 is phosphorylated exclusively during mitosis the specific detection of this modification can be used to identify mitotic cells [14].

1. Harvest cells by trypsinizing and prepare single-cell suspension in PBS.
2. Wash cells with PBS and resuspend at $1–2 \times 10^6$ cells/mL.
3. Aliquot 1 mL cells in a 15 mL polypropylene V-bottomed tube, centrifuge, and resuspend in 200 μL PBS.
4. Add 1 mL cold 70 % ethanol, dropwise, while vortexing to prevent cell clumping.
5. Fix cells for at least 2 h at −20 °C (*see* **Note 8**).
6. Wash cells in cold PBS.
7. Add 1 mL 0.25 % Triton X-100 in PBS and incubate for 15 min on ice.
8. Wash cells in cold PBS.
9. Resuspend cells in 100 μL of 1 % solution of BSA in PBS containing an antibody that specifically recognizes the phosphorylated form of histone 3 at serine 10. Incubate for 1–3 h at room temperature.
10. Wash cells twice with 1 % BSA in PBS.
11. Resuspend cells in 100 μL of 1 % solution of BSA in PBS containing the appropriate FITC-conjugated secondary antibody. Incubate for 1 h at room temperature in the dark.
12. Wash cells twice with 1 % BSA in PBS.
13. Add 500 μL of propidium iodide/RNase A staining solution (*see* **Note 9**) to cell pellet, mix well, and incubate for 30 min at 37 °C.
14. Analyze samples by flow cytometry.

4 Notes

1. Density of cells is important to ensure cell cycle progression and to avoid reaching confluency during the assay.
2. To prevent losing synchronization is important to use cell culture media prewarmed at 37 °C.
3. The protocols for synchronization of cells at the onset of S phase indicated here are only convenient for cells with up to 24 h doubling time.
4. Prepare a 100 mM stock solution of thymidine in DMEM and store at −20 °C.
5. Prepare a 5 mg/mL stock solution of aphidicolin in DMSO and store at −20 °C.

6. Dissolve nocodazole in DMSO to a concentration of 4 mg/mL and store at −20 °C. Dilute this solution to 40 μg/mL nocodazole in DMSO and store at −20 °C.
7. Mitotic shake-off method is based on the observation that as cells progress into metaphase during mitosis they become rounded and have fewer points of attachment with the culture vessel [15].
8. Cells may be stored at −20 °C for 2–3 weeks prior to propidium iodide staining and flow cytometric analysis.
9. Propidium iodide/RNase solution working concentration contains propidium iodide 50 μg/mL in PBS and RNase A 0.1 mg/mL. This solution should be stored at 4 °C in the dark.

References

1. Morgan DO (2007) The cell cycle: principles of control, Primers in biology. New Science Press Ltd in association with Oxford University Press, London
2. Banfalvi G (2011) Overview of cell synchronization. Methods Mol Biol 761:1–23
3. Rosner M, Schipany K, Hengstschlager M (2013) Merging high-quality biochemical fractionation with a refined flow cytometry approach to monitor nucleocytoplasmic protein expression throughout the unperturbed mammalian cell cycle. Nat Protoc 8(3):602–626
4. Campisi J, Morreo G, Pardee AB (1984) Kinetics of G1 transit following brief starvation for serum factors. Exp Cell Res 152(2):459–466
5. Masters JR (2002) HeLa cells 50 years on: the good, the bad and the ugly. Nat Rev Cancer 2(4):315–319
6. Farras R, Baldin V, Gallach S, Acquaviva C, Bossis G, Jariel-Encontre I, Piechaczyk M (2008) JunB breakdown in mid-/late G2 is required for down-regulation of cyclin A2 levels and proper mitosis. Mol Cell Biol 28(12):4173–4187. MCB.01620-07 [pii]
7. Stein GS, Borun TW (1972) The synthesis of acidic chromosomal proteins during the cell cycle of HeLa S-3 cells. I. The accelerated accumulation of acidic residual nuclear protein before the initiation of DNA replication. J Cell Biol 52(2):292–307
8. Harper JV (2005) Synchronization of cell populations in G1/S and G2/M phases of the cell cycle. Methods Mol Biol 296:157–166
9. Heintz N, Sive HL, Roeder RG (1983) Regulation of human histone gene expression: kinetics of accumulation and changes in the rate of synthesis and in the half-lives of individual histone mRNAs during the HeLa cell cycle. Mol Cell Biol 3(4):539–550
10. Pines J, Hunter T (1989) Isolation of a human cyclin cDNA: evidence for cyclin mRNA and protein regulation in the cell cycle and for interaction with p34cdc2. Cell 58(5):833–846, 0092-8674(89)90936-7 [pii]
11. Kohn KW, Jackman J, O'Connor PM (1994) Cell cycle control and cancer chemotherapy. J Cell Biochem 54(4):440–452
12. Perez-Benavente B, Garcia JL, Rodriguez MS, Pineda-Lucena A, Piechaczyk M, Font de Mora J, Farras R (2013) GSK3-SCF(FBXW7) targets JunB for degradation in G2 to preserve chromatid cohesion before anaphase. Oncogene 32(17):2189–2199
13. Ferrero M, Ferragud J, Orlando L, Valero L, Sanchez del Pino M, Farras R, Font de Mora J (2011) Phosphorylation of AIB1 at mitosis is regulated by CDK1/CYCLIN B. PLoS One 6(12), e28602
14. Xu B, Kim S, Kastan MB (2001) Involvement of Brca1 in S-phase and G(2)-phase checkpoints after ionizing irradiation. Mol Cell Biol 21(10):3445–3450
15. Elvin P, Evans CW (1983) Cell adhesiveness and the cell cycle: correlation in synchronized Balb/c 3T3 cells. Biol Cell 48(1):1–9

Chapter 9

Analysis of CDK Inhibitor Action on Mitochondria-Mediated Apoptosis

Anna Gortat

Abstract

The role of cyclin-dependent kinase inhibitors (CDKIs) is to negatively regulate cyclin-dependent kinases as a mechanism of control of cell proliferation. As such, CDKIs are being used to induce apoptosis in cancer cells to prevent their excessive reproduction. This chapter describes procedures to study apoptosis induction upon treatment with any CDKI through the evaluation of morphological and functional mitochondrial alterations, in particular, how to measure the mitochondrial membrane potential ($\Delta\Psi m$) using TMRE dye, determine the content of intracellular ATP, observe mitochondrial network morphology using HeLa cells stably expressing fluorescent reporter DsRed targeting mitochondrial matrix, observe ultrastructure of the organelle using transmission electron microscopy, and, finally, assure that mitochondrial outer membrane permeabilization takes place by assessing the subcellular localization of cyt C in HeLa cells stably expressing fluorescent cyt C-GFP.

Key words Apoptosis, ATP, CDKIs, Mitochondrial membrane potential disruption, Mitochondrial network, MOMP

1 Introduction

Cyclin-dependent kinases (CDKs) are a family of serine/threonine kinases which are essential for driving cell cycle phases in eukaryotic cells and as such are considered a potential target for anticancer treatment [1]. Cancer cells proliferate outside their normal growth restraints. Selective interruption of the cell cycle in cancer cells by interfering with CDK action triggers apoptotic cell death. Therefore, development of molecules that can specifically inhibit CDKs is a pharmacological challenge and some of them are currently undergoing clinical trials [2–4].

Apoptosis is a mechanism by which eukaryotic cells commit suicide. It permits to eliminate unwanted and defective cells through an ordered process that excludes inflammatory response induction [5]. Mitochondria play a central role in apoptosis. They control the intrinsic pathway of apoptosis [6], participate in the

Mar Orzáez et al. (eds.), *Cyclin-Dependent Kinase (CDK) Inhibitors: Methods and Protocols*, Methods in Molecular Biology, vol. 1336, DOI 10.1007/978-1-4939-2926-9_9,

extrinsic pathway [7, 8], and additionally are implicated in nonapoptotic cell death [9–13]. When a cell starts to die, the mitochondrial outer membrane permeabilization (MOMP) occurs, and the proteins residing in the intermembrane space (IMS) are being released into the cytosol until, finally, dissipation of the mitochondrial membrane potential ($\Delta\Psi m$), shutdown of ATP synthesis, and structural collapse of mitochondria take place. This triggers caspase-dependent [14] as well as caspase-independent executionary cascade [15–17] resulting in the final dismantling of the cell.

In this section, the materials and methods used to determine the state of mitochondria are presented. We describe in detail how to measure the mitochondrial membrane potential ($\Delta\Psi m$) using TMRE dye, how to determine the content of intracellular ATP, how to observe mitochondrial network morphology using HeLa cells stably expressing fluorescent reporter DsRed targeting mitochondrial matrix, how to observe ultrastructure of the organelle using transmission electron microscopy, and, finally, how to assure that MOMP takes place by assessing the subcellular localization of cyt C in HeLa cells stably expressing fluorescent cyt C-GFP.

2 Materials

1. Culture medium adequate for the cell line of your choice complemented or not with fetal bovine serum (FBS): Here, we use high-glucose (4.5 g/l) DMEM complemented with 10 % FBS to grow HeLa cells and their derivatives.
2. Petri dishes.
3. Serological pipettes, sterile.
4. Plates 6-well, 96-well.
5. Laminar flow chamber.
6. Cell culture incubator at 37 °C and 5 % CO_2.
7. Centrifuge.
8. Conical tubes (15 and 50 ml).
9. Cover slips.
10. Hemocytometer.
11. Light microscope, e.g., Olympus.
12. Fluorescence microscope, e.g., Leica.
13. Phosphate-buffered saline (PBS) (137 mM NaCl, 2.7 mM KCl, 10 mM Na_2HPO_4, 1.8 mM KH_2PO_4 pH 7.4).
14. Distilled water.
15. Dimethylsulfoxide (DMSO).
16. Ethanol absolute.

2.1 Staining with TMRE

1. Tetramethylrhodamine ethyl ester perchlorate (TMRE) stock solution: For 10 ml of stock solution, add 2.5 mg of TMRE to 10 ml of 95 % ethanol and store frozen at –20 °C. Take 20 µl of the 0.5 mM stock solution and dilute in 100 µl normal buffer (NB: 130 mM NaCl, 5.5 mM KCl, 1.8 mM $CaCl_2$, 1 mM $MgCl_2 \cdot 7H_2O$, 25 mM glucose, 20 mM HEPES pH 7.4) to prepare the working solution.
2. Carbonyl cyanide 4-(trifluoromethoxy)phenylhydrazone (FCCP) stock solution at 1 mM should be prepared in 99.9 % ethanol and stored at –20 °C.

2.2 Intracellular ATP Content

1. White-walled 96-well luminometer plates for cell culture.
2. Plate shaker, for mixing multiple plate.
3. Luminometer capable of reading multiwell plates, e.g., Wallac Victor 2.

2.3 Mitochondrial Network Morphology Using HeLa Cells Stably Expressing mt-DsRED

1. Paraformaldehyde (PFA).
2. Gelatin.
3. Kimwipes.

2.4 Ultrastructure of the Mitochondria Using Transmission Electron Microscopy

1. Lab-Tek chamber slides.
2. Uranyl acetate.
3. Glutaraldehyde.
4. OsO_4.
5. Glue.
6. Araldite blocks.
7. Toluidine blue.
8. Lead citrate.
9. Liquid nitrogen.
10. Ultra Cut UC-6.
11. Transmission electron microscope.
12. Triton X-100.
13. Trypsin-EDTA solution.

2.5 Observation of the cyt C Translocation Using HeLa Cells Stably Expressing cyt C-GFP

1. PFA.
2. Gelatin.
3. Kimwipes.

3 Methods

We describe here general protocols for mitochondrial network visualization using HeLa cell line or its derivatives, upon apoptosis induction by CDK inhibitors. You should adapt these protocols to a cell line and the CDK inhibitors of your choice.

3.1 Mitochondrial Transmembrane Potential ($\Delta\psi m$) Measurement by Flow Cytometry Using TMRE Dye

The majority of energy required by the cells is produced by mitochondria in the form of adenosine 5′-triphosphate (ATP). This process requires that the electron transport chain (ETC) generates an electrical potential across the mitochondrial inner membrane ($\Delta\psi m$) which is used by ATP synthase (Complex V) to fuse free phosphate with adenosine diphosphate (ADP). $\Delta\psi m$ can be detected by a series of positively charged dyes that can penetrate the mitochondrial membrane such as TMRE, TMRM, and mitotracker. TMRE (tetramethylrhodamine, ethyl ester) is a cell-permeant, positively charged, red-orange dye that accumulates promptly in active mitochondria due to their relative negative charge [18]. The lipophilic structure of this dye allows it to penetrate cell and mitochondrial lipid bilayer membrane barriers within few minutes and thus TMRE is widely used for detection of the mitochondrial permeability transition in whole cells via fluorescence analysis methods. Depolarized or inactive mitochondria with affected membrane potential fail to accumulate TMRE and thus remain unstained. Then, the dye accumulation in mitochondria may be optically detected by flow cytometry allowing for at least qualitative assessment of $\Delta\psi m$ among experimental conditions (*see* **Note 1**).

3.1.1 Staining with TMRE

1. Culture HeLa cells for a non-induced negative control as well as a positive control at 1×10^5 cells per well (2 ml/well in 6-well plate) in high-glucose (4.5 g/L) DMEM complemented with 10 % fetal bovine serum (FBS) and grow overnight at 37 °C under 5 % CO_2.
2. For the first-time flow cytometry measurement, additional two controls of untreated cell population have to be prepared to calibrate the cytometer.
3. Induce $\Delta\psi m$ depolarization by treating the cells (except the untreated controls) with 250 nM FCCP for 10 min at 37 °C (*see* **Note 2**).
4. Remove medium from cells, replace with fresh complete medium containing TMRE, and incubate for 15 min at 37 °C 5 % CO_2. One of the additional controls of untreated cells is stained with TMRE and the other one is left unstained (*see* **Notes 3** and **4**).
5. Remove the medium and detach the cells gently from the culture dish using trypsin.

6. Resuspend cells in fresh complete medium to a density required for flow cytometry (0.5×10^6 cells/ml) so that their final volume should be close to 0.5 ml.
7. Transfer cell suspension into a clean polypropylene tube and submit to flow cytometry measurements using settings as described below (*see* **Note 5**).

3.1.2 Flow Cytometer Settings

1. The excitation peak of TMRE is at 549 nm but using the common Argon blue line (488 nm) laser most flow cytometers yield excellent results. The emission peak of TMRE is at 574 nm and lies within the FL2 emission region.
2. A log FL2 (X-axis) versus relative cell number (Y-axis) histogram has to be created.
3. First, the untreated control cell population stained with TMRE (max $\Delta\psi m$) has to be run and the FL2 PMT voltage adjusted to allow the peak to fall within the third log decade.
4. Second, the untreated control cell population without TMRE staining (no $\Delta\psi m$) has to be run and the peak adjusted to fall within the first log decade.
5. For the final calibration step, the FCCP-depolarized positive sample stained with TMRE has to be run using the same voltage settings as above to assure that the histogram peak is visible on the X-axis. If this is not the case, PMT voltage has to be increased slightly to achieve positive control staining within the first decade of the log scale similar to the untreated control cell population without TMRE staining (*see* **Note 3**).
6. Finally, samples have to be run using the established conditions. Data can be analyzed by several software such as WinMDI FlowJo, ModFit, and Cell Quest.

3.2 Intracellular ATP Content

Apoptosis is an energy-consuming process and thus requires ATP to occur [19, 20]. For a short period of time after apoptosis induction a brief burst of ATP production can be observed [21]. However, due to inevitable shutdown of the mitochondria, intracellular concentration of ATP drops below the steady-state levels. Therefore, measurements of the intracellular ATP concentration may be considered as additional informative parameter related to mitochondrial function and metabolism [22, 23]. Here, we use ATPLite, the commercially available luminescence ATP detection assay system from Perkin Elmer. It is an ATP monitoring system based on firefly luciferase which is highly sensitive and produces a long-lived luminescence signal (half-life above 5 h). The ATPLite system permits measurement of the amount of light produced by the reaction of ATP with luciferase and d-luciferin in which, within certain limits, the emitted amount of light is proportional to the ATP concentration.

3.2.1 Determining Intracellular ATP Content

1. Culture HeLa cells at 5×10^4 per well (100 µl/well in 96-well plate) overnight. Prepare at least two wells for each predicted condition (*see* **Note 6**).
2. Series of seven 100 µl complete culture media without cells in duplicates has to be pipetted into the wells on the plate to be used for determining the ATP standard curve.
3. Treat the cells with your CDK inhibitor of choice for different times (3, 6, and 12 h) at 37 °C under 5 % CO_2. Include untreated and vehicle controls for each experiment.
4. Equilibrate reagents of the ATPLite system to room temperature for at least half an hour.
5. Prepare the ATP standard curve recommended in the manufacturer's protocol (*see* **Note 7**).
6. Reconstitute lyophilized substrate according to the manufacturer's instructions.
7. Lyse cells by adding 50 µl of mammalian cell lysis solution to 100 µl of cell suspension per well. It permits to lyse the cells and inactivate the endogenous ATPases in order to maintain the original intracellular levels of ATP. Lysis will be completed after 5 min of shaking at 700 rpm. Also, 50 µl of mammalian cell lysis solution will be added to 100 µl cell-free wells to determine the ATP standard curve.
8. Add 10 µl of each ATP standard dilution to the corresponding wells (in duplicates) and shake the plate for 5 min at 700 rpm.
9. Add 50 µl of substrate solution and let the reaction to run for 5 min in an orbital shaker at 700 rpm.
10. Incubate the plate on dark for 10 min and measure luminescence in a luminometer microplate reader (*see* **Note 8**).

3.3 Mitochondrial Network Morphology Using HeLa Cells Stably Expressing mt-DsRED

In healthy cells mitochondria form a network that undergoes constant rearrangements controlled by the balance between fusion and fission events mediated by specific proteins [24–26]. Mitochondrial fusion/fission events within the network are precisely controlled and respond to physiological and pathological conditions. It is an efficient, dynamic system to deliver energy, lipids, proteins, calcium, and metabolites between different areas of the cell [27, 28]. Also, mitochondrial DNA showed to be efficiently transferred throughout the network by matrix mixing during fusion events [29]. Mitochondria play a crucial role in apoptosis. A clear functional link of mitochondrial morphology and apoptosis exists. The rate of fission increases rapidly at the early stages of apoptosis [26] which is accompanied by cristae disorganization (*see* Fig. 1) and, in consequence, MOMP. Therefore, monitoring the mitochondrial network morphology may be an adequate determinant to establish changes in mitochondrial functioning upon CDK inhibitor treatment.

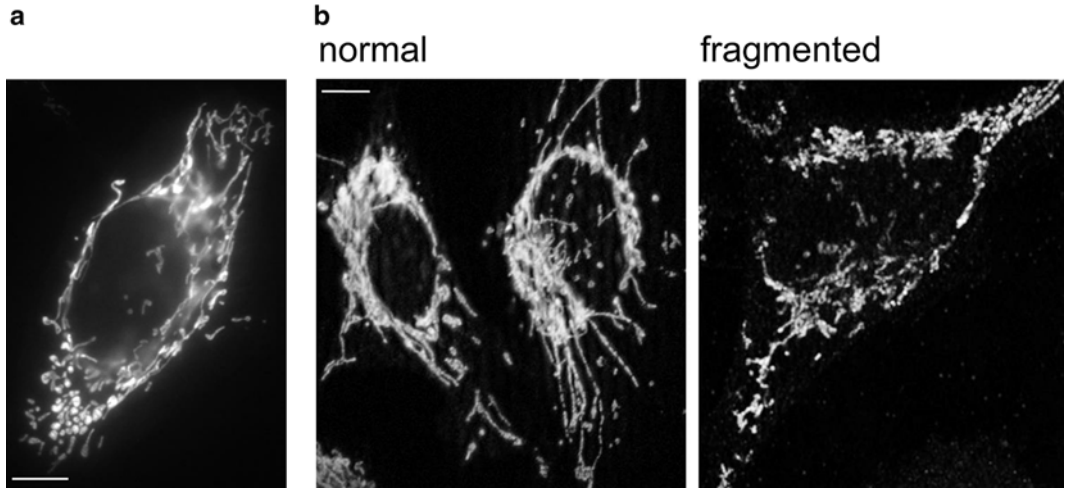

Fig. 1 Mitochondrial network is heterogenous within a cell. (**a**). Mitochondria in HeLa cells stably expressing mtDsRED form a dynamic, tubular network under physiological conditions. Mitochondrial morphology within a cell, although highly organized, appears heterogenous varying in density of clumps and tubules. (**b**). HeLa-mtDsRED were submitted (fragmented) or not (normal) to an apoptotic stimuli using 0.5 μM staurosporine (ST) for 6 h. Fragmented mitochondrial network is clearly visible upon apoptosis induction. Scale bars: 5 μm

3.3.1 Preparation of HeLa-DsRED Cells for Fluorescence

1. Place clean and sterile cover slips in a 6-well plate (you can place up to four cover slips per well).
2. Plate HeLa-DsRED cells at 1×10^5 cells (*see* **Note 9**) per well and let to attach overnight (*see* **Note 10**).
3. Treat the cells with the CDK inhibitor of your choice at different times to induce apoptosis.
4. A non-induced control as well as a positive control to fragment the mitochondrial network have to be introduced. Treat the cells with 250 nM FCCP for 10 min to depolarize mitochondria and obtain the mitochondrial network fragmentation (*see* **Note 2**).
5. Remove the medium and wash gently with PBS.
6. Fix the cover slips with 3 % PFA in PBS, incubate for 20 min at room temperature, and then wash twice with PBS to remove any remaining PFA (*see* **Note 11**).
7. Permeabilize the cells with 0.1 % Triton X-100 (in PBS) for 10 min and wash twice for 5 min with PBS to remove all the detergent.
8. Wash the cells once with PBS-gelatin 0.2 % and block with PBS-gelatin 0.2 % for 30 min at room temperature. Then, wash the cells with PBS for 5 min.
9. Drop cover slips water one by one, dry immediately using Kimwipes, and mount on 2 μl Mowiol 4-88 facing the slide.

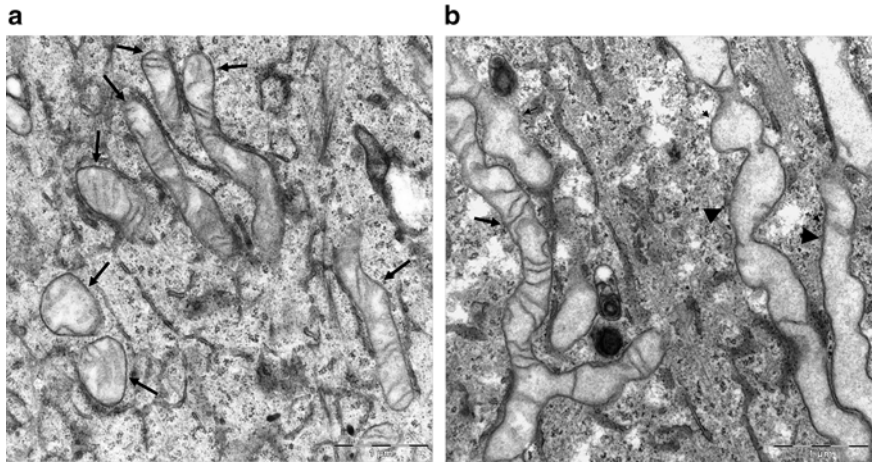

Fig. 2 Remodeling of mitochondrial ultrastructure upon apoptosis. HeLa cells were induced to apoptosis with 2 μM doxorubicin for 24 h (**b**) and submitted to transmission electron microscopy (TEM) as described. As a control, vehicle-treated cells were used (**a**). *Black arrows* in (**a**) show normal cristae organization. *Black arrow* in (**b**) shows mitochondria with partially affected, still visible cristae structure upon apoptosis induction. The cristae are not as well organized as in (**a**). *Black arrowheads* in (**b**) show mitochondria with heavily affected ultrastructure upon apoptosis induction. There are only few, very short and unorganized cristae visible. Scale bars: 1 μm

10. Dry slides overnight at room temperature, well covered from light.
11. Mitochondrial network is observed under fluorescence microscope using standard Cy3 filter.

3.4 Ultrastructure of the Mitochondria Using Transmission Electron Microscopy

Electron microscopy is a very powerful tool for the examination of mitochondrial ultrastructure in nanometer scale. It reveals that mitochondria vary in their shape; they can exist as spheres, rods, and a sausage-like structure with diameter ranging from 0.5 to 1 μm (*see* Fig. 2). During apoptosis, the ultrastructure of mitochondria undergoes a profound remodeling (*see* Fig. 2). The change in morphology is progressive and consists of losing the packed and folded appearance of the cristae. Individual crista fuses, cristae junctions open, the matrix and the intermembrane space expand, and, finally, the whole mitochondrial morphology appears vesiculated or even swollen without any cristae possible to identify [30–32] (*see* Fig. 2b).

3.4.1 Preparation of Cells for Transmission Electron Microscopy

1. Plate 3×10^4 HeLa cells per chamber in a Lab-Tek chamber slide containing four wells and treat or not with 2 μM doxorubicin or your CDK inhibitor of choice to induce apoptosis.
2. Remove the medium and fix the cells for 1 h in 3.5 % glutaraldehyde at 37 °C and then post-fix for 1 h in 2 % OsO_4 at room temperature.

3. Stain the cells in the dark at 4 °C for 2 h with 2 % uranyl acetate.
4. Rinse the cells in sodium phosphate buffer (0.1 M pH 7.2), dehydrate in ethanol, and infiltrate overnight in araldite base embedding agent.
5. After polymerization, detach the embedded cultures from the chamber slide and glue to araldite blocks.
6. Cut serial semi-thin sections (1.5 μm) with an Ultracut UC-6-, mount onto slides, and stain with 1 % toluidine blue.
7. Select semi-thin sections containing cells and glue to araldite blocks.
8. Detach semi-thin sections from the glass slide by repeated freezing and thawing in liquid nitrogen.
9. Prepare ultrathin sections (0.07 μm) with the Ultracut and stain with lead citrate.
10. Submit the samples to a transmission electron microscope and obtain photomicrographs of the mitochondria.

3.5 Observation of the cyt C Translocation Using HeLa Cells Stably Expressing cyt C-GFP

Mitochondria lie at the center of the intrinsic apoptotic pathway. It is not only the bioenergetic center of the cell, but it also contains pro-death factor such as cytochrome C (cyt C) which resides in the mitochondrial intermembrane space (IMS). Release of cyt C from the IMS induces a signaling cascade that leads to demise of the cell. Thus, MOMP is the critical event that permits the release of pro-apoptotic molecules from the IMS and disrupts mitochondrial bioenergetics (*see* **Note 12**). Here, we describe how to follow translocation of the mitochondria-targeted fluorescent protein cyt C-GFP stably expressed in HeLa cells (HeLa-GFP; kind gift from C. Muñoz-Pinedo).

3.5.1 Establishing Homogeneous HeLa-GFP Stable Cell Line

First, we need to assure that the level of fluorescence intensity provided by the expression of cyt C-GFP within HeLa cells is relatively homogeneous throughout the whole population to facilitate the posterior analysis.

1. Plate 6×10^6 HeLa-GFP cells in 150 mm petri dish. 20 ml high-glucose (4.5 g/L) Dulbecco's modified Eagle medium (DMEM) complemented with 10 % fetal bovine serum (FBS) and penicillin/streptomycin mixture of antibiotics to avoid cell culture contamination is used. 1×10^6 of regular HeLa cells that do not express fluorescent reporter have to be plated in a 100 mm petri dish with 10 ml high-glucose complete DMEM. Grow the cells overnight at 37 °C under 5 % CO_2.
2. Trypsinize cells and count using hemocytometer.

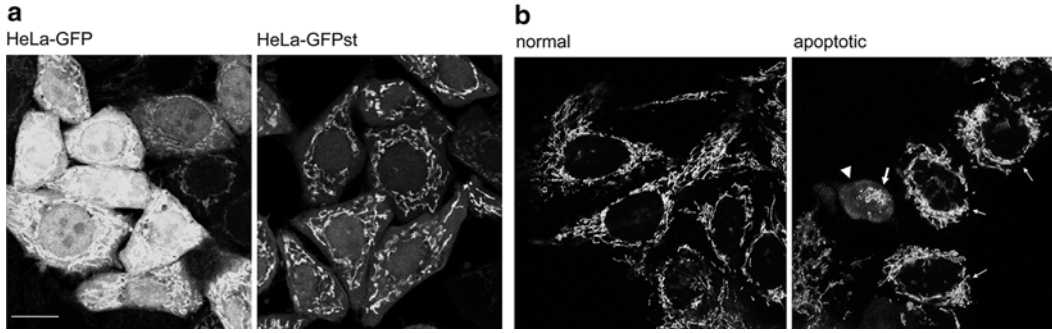

Fig. 3 Translocation of cyt C upon apoptosis induction. (**a**). HeLa-GFP cells stably expressing cyt C-GFP show heterogenous fluorescence intensity. After FACS, a homogeneous population of HeLa-GFP cells with an intermediate fluorescence intensity was selected and called HeLa-GFPst. (**b**). HeLa-GFPst were induced to apoptosis (apoptotic) or not (normal) with 2 μM doxorubicin for 24 h. *White arrowhead* shows a cell with cytosolic staining that appears upon cyt C-GFP translocation. Fragmented, collapsed mitochondria within the apoptotic cell are indicated by a *bold arrow. Thin arrows* show cells where cyt C-GFP translocation did not yet occurred. However, the cells were already affected by the apoptotic treatment as assessed by fragmentation of the mitochondrial network (compared to (**b**) normal and with ST-treated HeLa-mtDsRED cells in Fig. 1). Scale bar: 20 μm

3. Centrifuge the cells for 5 min at $700 \times g$ at room temperature and resuspend the pellets in room temperature PBS to a density of 1×10^6 cells per ml.
4. Submit the cells to fluorescence-activated cell sorter (FACS) using blue Argon series laser for emission and the FL1 detector (*see* **Note 13**).
5. Calibrate FACS using as a negative control regular HeLa cells that do not express fluorescent reporter, and then run a small sample of HeLa-GFP cells to adjust the FL1 PMT voltage by allowing the peak of GFP fluorescence to fall within the third log decade.
6. Then, recover HeLa-GFP cells with an intermediate fluorescence intensity of cyt C-GFP (between the second and the third log decades) (*see* **Note 14**).
7. Plate 1×10^5 of the recovered cells per well in 6-well plate and grow overnight.
8. Inverted fluorescence microscope can be used to confirm that the cells within the wells show a homogeneous intensity of fluorescence.
9. After this procedure we refer to these cells as HeLa-GFPst (*see* Fig. 3a).

3.5.2 Observation of cyt C Translocation Using Fluorescence Microscopy

1. Place clean and sterile cover slips in a 6-well plate. Plate 1×10^5 of Hela-GFPst cells per well and left to attach overnight.
2. Treat the cells with 2 μM doxorubicin for 24 h or the CDK inhibitor of interest to induce apoptosis. Include a non-induced control.

3. Remove medium from wells and wash them gently with PBS.
4. Fix cover slips with 3 % PFA, incubate for 20 min at room temperature, and then wash twice with PBS to remove any remaining PFA (*see* **Note 15**).
5. Permeabilize cells with 0.1 % Triton X-100 (in PBS) for 10 min and then wash twice with PBS to remove all the remaining detergent.
6. Wash cells with PBS-gelatin 0.2 % and block with PBS-gelatin 0.2 % for 30 min at room temperature. Then, wash with PBS for 5 min.
7. Drop cover slips into water, dry immediately using Kimwipes, and mount on 2 μl Mowiol 4-88 facing the slide.
8. Dry slides overnight at room temperature, well covered from light.
9. Observe the samples under fluorescence microscope using standard FITC filter.

4 Notes

1. We strongly recommend to use TMRE at concentrations below 50 nM. At low concentrations, it does not form aggregates (nonquenching conditions) in cell membranes and interacts with membrane proteins minimally; thus the transmembrane distribution of TMRE is directly related to the membrane potential in accordance to the Nernst equation [18, 33]. To avoid dye aggregation, TMRE concentrations ranging between 0.5 and 30 nM are used in our setups. We recommend to determine empirically the best concentration of TMRE to be used for each cell line and treatment conditions. It is always desirable to use the lowest possible dye concentration to avoid any variation in its degree of binding to mitochondria which may result in greater dye accumulation than predicted. In practice, at nonquenching concentrations TMRE does not inhibit the electron transport chain (ETC) [34] which makes it a reliable dye for $\Delta\psi m$ studies. Also, at high concentrations TMRE may stain endoplasmic reticulum in addition to mitochondria and that would interfere with the interpretation of results.
2. We recommend to use mitochondrial oxidative phosphorylation (OxPhos) inhibitor FCCP to depolarize $\Delta\psi m$. FCCP is a protonophore which uncouples the ETC from OxPhos system by inducing reversal of the ATPase and thus depolarizes mitochondria by increasing their permeability to protons. Collapse of $\Delta\psi m$ can be achieved by addition of 250 nM FCCP 10 min prior to measurement. However, in the absence of FCCP any inducer of apoptosis may be used, e.g., 0.5 μM staurosporine (ST), for 6 h to collapse $\Delta\psi m$.

3. Working solution (100 nM) of TMRE from a stock solution (0.5 mM) is prepared. It is used only on the day of preparation.
4. TMRE working solution is diluted to a final concentration of 30 nM directly in the fresh complete medium.
5. After staining with TMRE, samples should be stored protected from light until they can be analyzed on the flow cytometer. However, we strongly recommend to perform the measurements as soon as possible and as late as within 30 min after TMRE equilibration. Temperature can affect TMRE staining; therefore we recommend to avoid storing the samples on ice prior to analysis.
6. For plating the cells we use white opaque 96-well plates. White plates, in contrast to the black ones, reflect light and will maximize light output signal; therefore we strongly recommend their use.
7. For ATP standard curve we recommend to prepare standards of 1×10^{-5} M, 1×10^{-6} M, 1×10^{-7} M, 1×10^{-8} M, 1×10^{-9} M, 1×10^{-10} M, and blank. Values of intracellular ATP concentrations should fall within this range of ATP concentrations.
8. It is very important to handle the plate in reduced illumination conditions prior to measurement for avoiding the plate phosphorescence which may result in higher background levels.
9. The major advantage of using stable cell line expressing a fluorescent reporter is that changes in mitochondrial network morphology can be visualized in living cells. Also, if required, DsRED fluorescence is stable under fixation conditions, thus enabling a wide range of flexibility for a variety of applications.
10. For tracking the mitochondrial network morphology, we use HeLa cells stably expressing an mtDsRED fluorescent reporter (kind gift from M. Rojo). mtDsRED bears mitochondrial targeting sequence fused to 5′ end of the DsRED molecule, thus targeting the DsRED fluorescent reporter to the mitochondrial matrix. This permits to observe morphology of the mitochondrial network in extreme conditions such as apoptosis without diffusion of the fluorescent signal as occurs when using proteins residing in the mitochondrial IMS, e.g., cyt C and SMAC. Proteins residing in the IMS get translocated to the cytosol upon apoptosis induction whereas mtDsRED staining remains in the mitochondrial matrix, thus making the fragmentation processes observable (*see* Fig. 1b, normal and fragmented).
11. PFA fixation is a method of choice for membrane-bound and cytoskeletal structure observation and for that reason we use it here to visualize mitochondrial network. Prepare a 12 % PFA stock solution in PBS. It is difficult to dissolve. Weight the exact amount of PFA and add it to warm PBS. Stir for a couple

of hours in a water bath. Do not exceed 60 °C. You can add a few drops of 10 N NaOH to facilitate the dissolution. Once prepared, store frozen at −20 °C for up to 1 year. Prepare a 3 % working solution by diluting with PBS just before use and throw away the excess. Check each batch of PFA before use.

12. Until now, we were determining apoptosis by measuring mitochondrial membrane depolarization and cellular ATP concentration and observing mitochondrial network morphology. In most cases, all these can be used as surrogate for measuring MOMP which is the determinant of commitment to apoptosis but additional techniques must be used to assure that MOMP actually took place. One has to keep in mind the restriction of each of the methods described previously. The drop in $\Delta\psi m$ is not always equivalent to MOMP. Some protonophores, i.e., FCCP used as a positive control in our measurements, depolarize mitochondria in the absence of MOMP. The same is true for the mitochondrial network fragmentation. Although mitochondrial fragmentation is indeed associated with apoptosis, excessive mitochondrial fragmentation can occur in a variety of conditions independently of apoptosis processes, such as that occurring upon exposure to carbonyl cyanide m-chlorophenyl hydrazone (CCCP), uncoupling agent that disrupts the electrochemical potential of the mitochondrial inner membrane. To unambiguously establish the occurrence of MOMP a translocation of the IMS residing factors such as cyt C must be assessed (*see* Fig. 3b).
13. The green fluorescent protein (GFP) absorbs light with an excitation maximum of 395 nm and fluoresces with an emission maxima of 510 nm. However, it may be excited at 488 nm by a standard blue Argon series laser and the emission peak can be detected in the FL1 detector.
14. The key for an efficient recovery of cells during FACS is the optimal number of cells and their density. We recommend to prepare 5 ml of cell suspension at the density of 1×10^6 cells per ml.
15. PFA fixation will affect the GFP fluorescence only slightly, in contrast to methanol or ethanol fixation which can completely abolish the GFP signal.

References

1. Malumbres M, Harlow E, Hunt T et al (2009) Cyclin-dependent kinases: a family portrait. Nat Cell Biol 11:1275–1276
2. Guha M (2012) Cyclin-dependent kinase inhibitors move into Phase III. Nat Rev Drug Discov 11:892–894
3. Krystof V, Uldrijan S (2010) Cyclin-dependent kinase inhibitors as anticancer drugs. Curr Drug Targets 11:291–302
4. Lapenna S, Giordano A (2009) Cell cycle kinases as therapeutic targets for cancer. Nat Rev Drug Discov 8:547–566

5. Jacobson MD, Weil M, Raff MC (1997) Programmed cell death in animal development. Cell 88:347–354
6. Kroemer G, Reed JC (2000) Mitochondrial control of cell death. Nat Med 6:513–519
7. Kantari C, Walczak H (2011) Caspase-8 and bid: caught in the act between death receptors and mitochondria. Biochim Biophys Acta 1813:558–563
8. Li H, Zhu H, Xu CJ et al (1998) Cleavage of BID by caspase 8 mediates the mitochondrial damage in the Fas pathway of apoptosis. Cell 94:491–501
9. Baines CP, Kaiser RA, Purcell NH et al (2005) Loss of cyclophilin D reveals a critical role for mitochondrial permeability transition in cell death. Nature 434:658–662
10. Ikegami K, Koike T (2003) Non-apoptotic neurite degeneration in apoptotic neuronal death: pivotal role of mitochondrial function in neurites. Neuroscience 122:617–626
11. Nakagawa T, Shimizu S, Watanabe T et al (2005) Cyclophilin D-dependent mitochondrial permeability transition regulates some necrotic but not apoptotic cell death. Nature 434:652–658
12. Schulze-Osthoff K, Bakker AC, Vanhaesebroeck B et al (1992) Cytotoxic activity of tumor necrosis factor is mediated by early damage of mitochondrial functions. Evidence for the involvement of mitochondrial radical generation. J Biol Chem 267:5317–5323
13. Zhang D-W, Shao J, Lin J et al (2009) RIP3, an energy metabolism regulator that switches TNF-induced cell death from apoptosis to necrosis. Science 325:332–336
14. Tait SWG, Green DR (2010) Mitochondria and cell death: outer membrane permeabilization and beyond. Nat Rev Mol Cell Biol 11:621–632
15. Belmokhtar CA, Hillion J, Ségal-Bendirdjian E (2001) Staurosporine induces apoptosis through both caspase-dependent and caspase-independent mechanisms. Oncogene 20: 3354–3362
16. Pradelli LA, Bénéteau M, Ricci J-E (2010) Mitochondrial control of caspase-dependent and -independent cell death. Cell Mol Life Sci 67:1589–1597
17. Tait SWG, Green DR (2008) Caspase-independent cell death: leaving the set without the final cut. Oncogene 27:6452–6461
18. Ehrenberg B, Montana V, Wei MD et al (1988) Membrane potential can be determined in individual cells from the Nernstian distribution of cationic dyes. Biophys J 53:785–794
19. Eguchi Y, Shimizu S, Tsujimoto Y (1997) Intracellular ATP levels determine cell death fate by apoptosis or necrosis. Cancer Res 57:1835–1840
20. Leist M, Single B, Castoldi AF et al (1997) Intracellular adenosine triphosphate (ATP) concentration: a switch in the decision between apoptosis and necrosis. J Exp Med 185: 1481–1486
21. Zamaraeva MV, Sabirov RZ, Maeno E et al (2005) Cells die with increased cytosolic ATP during apoptosis: a bioluminescence study with intracellular luciferase. Cell Death Differ 12:1390–1397
22. Perry SW, Norman JP, Litzburg A et al (2005) HIV-1 transactivator of transcription protein induces mitochondrial hyperpolarization and synaptic stress leading to apoptosis. J Immunol 174:4333–4344
23. Zhou Y, Tozzi F, Chen J et al (2012) Intracellular ATP levels are a pivotal determinant of chemoresistance in colon cancer cells. Cancer Res 72:304–314
24. Karbowski M, Youle RJ (2003) Dynamics of mitochondrial morphology in healthy cells and during apoptosis. Cell Death Differ 10:870–880
25. Suen D-F, Norris KL, Youle RJ (2008) Mitochondrial dynamics and apoptosis. Genes Dev 22:1577–1590
26. Youle RJ, Karbowski M (2005) Mitochondrial fission in apoptosis. Nat Rev Mol Cell Biol 6:657–663
27. Giorgi FD, Lartigue L, Ichas F (2000) Electrical coupling and plasticity of the mitochondrial network. Cell Calcium 28:365–370
28. Skulachev VP (2001) Mitochondrial filaments and clusters as intracellular power-transmitting cables. Trends Biochem Sci 26:23–29
29. Nakada K, Inoue K, Ono T et al (2001) Inter-mitochondrial complementation: mitochondria-specific system preventing mice from expression of disease phenotypes by mutant mtDNA. Nat Med 7:934–940
30. Frank S, Gaume B, Bergmann-Leitner ES et al (2001) The role of dynamin-related protein 1, a mediator of mitochondrial fission, in apoptosis. Dev Cell 1:515–525
31. Scorrano L, Ashiya M, Buttle K et al (2002) A distinct pathway remodels mitochondrial cristae and mobilizes cytochrome c during apoptosis. Dev Cell 2:55–67
32. Sun MG, Williams J, Munoz-Pinedo C et al (2007) Correlated three-dimensional light and electron microscopy reveals transformation of mitochondria during apoptosis. Nat Cell Biol 9:1057–1065

33. Ward MW, Huber HJ, Weisová P et al (2007) Mitochondrial and plasma membrane potential of cultured cerebellar neurons during glutamate-induced necrosis, apoptosis, and tolerance. J Neurosci 27:8238–8249

34. Scaduto RC, Grotyohann LW (1999) Measurement of mitochondrial membrane potential using fluorescent rhodamine derivatives. Biophys J 76:469–477

Chapter 10

Evaluating the Effects of CDK Inhibitors in Ischemia–Reperfusion Injury Models

Tatiana Guevara

Abstract

CDK inhibitors have been used to induce protection in various experimental models. Kidney ischemia–reperfusion (I/R) is a form of acute kidney injury resulting in a cascade of cellular events prompting rapid cellular damage and suppression of kidney function. I/R injury, an inevitable impairment during renal transplant surgery, remains one of the major causes of acute kidney injury and represents the most prominent factor leading to delayed graft function after transplantation. Understanding the molecular events responsible for tubule damage and recovery would help to develop new strategies for organ preservation. This chapter describes procedures to study the effect of CDK inhibitors in the cellular I/R model developed from an epithelial cell line deriving from pig kidney proximal tubule cells (LLC–PK1). We briefly describe methods for determining the protective effect of CDK inhibitors such as activation of caspase 3/7, western blot analysis, gene silencing, and immunoprecipitation.

Key words CDK inhibitors, Kidney injury, Ischemia–reperfusion, Renal preservation

1 Introduction

1.1 Pharmacological Inhibitors of CDK/Cyclin Complexes

Alterations in the activity of the CDKs are related to the proliferation of tumor cells and it is well established that their inhibition contributes to loss of proliferation and induction of apoptosis [1]. However, under certain physiological conditions, the cell cycle arrest during the use of CDK inhibitors can permit the initiation of cell repair mechanisms. In this sense, new research into inhibitors of CDK as potential therapeutic agents in the treatment of neurological damage has been developed. The administration of inhibitors of CDK that induce the inhibition of apoptosis with neuroprotective, anti-excitotoxicity and anti-inflammatory effects in models of cerebral and renal ischemia, and also neurodegenerative diseases, has been already described [2–5].

Chronic kidney disease (CKD) is an inflammatory disease that causes a progressive and irreversible loss of the kidney function characterized by a lower glomerular filtration rate below 50 % [6].

Mar Orzáez et al. (eds.), *Cyclin-Dependent Kinase (CDK) Inhibitors: Methods and Protocols*, Methods in Molecular Biology, vol. 1336, DOI 10.1007/978-1-4939-2926-9_10,

There are two types of treatment available for patients with CKD: dialysis (hemodialysis or peritoneal dialysis) and renal transplantation. When transplantation is possible, the patients' half-life and quality of life is increased [6]. However, 25 % of all available kidneys are discarded as they are not suitable for transplantation. It is known that short periods of ischemia are sufficient to induce pathophysiological events in renal tubules that could compromise transplant viability. A kidney for transplantation will be subjected to a deprivation of oxygen, resulting in cellular hypoxia. The reperfusion process is also critical for the organ, mainly due to two processes. Firstly, there is oxidative damage caused from the increase in reactive oxygen species (ROS) during the reintroduction of oxygen to previously ischemic tissue. Secondly, there is an inflammatory response that initiates the infiltration of polymorphonuclear (PMN) cells that amplify cell damage. The reintroduction of oxygen reestablishes normal metabolic activity. This coincides with a peak in cell death caused by necrosis or apoptosis [7]. There are evidences showing that damage produced by PMN can be reduced by the use of immunosuppressants, for example cyclosporine [8], or fingolimod [9]. Similarly, compounds that inhibit CDK, for example flavopiridol or roscovitine [10] have been used as immunosuppressants and have shown to be protective against damages caused by the processes of I/R [11].

We have reported that the CDK inhibitors (roscovitine and TAT–NBI1) [5, 12] provide protection against cell death in a well established ischemia/reperfusion (I/R) model in porcine renal tubular cells (LLC–PK1) [13].

In this section, we describe the materials and methods used to evaluate the use of the CDK inhibitors for the prevention and treatment of damage produced in kidneys as a result of renal I/R injury.

2 Materials

2.1 Model for Renal Ischemia–Reperfusion (I/R) Injury in LLC-PK1

1. LLC-PK-1 Proximal tubular porcine LLC-PK-1 cells were obtained from ATCC (Rockville, MD). Cells were grown in M199 supplemented with 3 % FBS and were maintained at 37 °C in a 5 % carbon dioxide atmosphere in 20-cm tissue culture plates or T150 culture flasks. Cells were transferred two times per week.
2. M199 supplemented with 3 % (w/v) FBS.
3. 0.25 % trypsin–1 mM EDTA.
4. 20-cm tissue culture plates or T150 culture flasks.
5. 6-well tissue culture plates.
6. 40-μm cell strainers.

7. 37 °C tissue culture incubator, 5 % CO_2.
8. 37 °C tissue culture incubator, 18 % CO, 1.5 % O_2
9. Additional equipment and reagents for culturing cells, determining cell concentration with a hemacytometer.

2.2 Caspase 3/7 Activity Assays

1. 5 mM EDTA in PBS.
2. Extraction Buffer: 50 mM PIPES, 50 mM KCl, 5 mM EDTA, 2 mM $MgCl_2$, 2 mM DTT, supplemented with protease inhibitors.
3. Caspase assay buffer: PBS, 10 %, glycerol, 0.1 mM EDTA, 2 mM DTT, and 20 μM of Ac-DEVD-AFC (caspase-3 substrate).
4. 96-well microplates: Tissue culture microplate with black wall is recommended.
5. Liquid nitrogen.
6. A fluorescence microplate reader: Capable of monitoring fluorescence intensity at Ex/Em = 390/510 nm.
7. Kit for quantification of protein: Pierce BCA Protein Assay Kit (Pierce) is recommended.

2.3 Western Blot Analysis

1. Equipment for SDS-PAGE and Immunoblotting (Vertical acrylamide electrophoresis unit and Electroblotting unit-fully submerged, Bio-Rad Mini-PROTEAN series recommended).
2. Kit for quantification of protein: Pierce BCA Protein Assay Kit (Pierce) is recommended.
3. Nitrocellulose and chromatography paper.
4. Buffer lysis: 25 mM Tris–HCl pH 7.4, 1 mM EDTA, 1 mM EGTA, 1 % SDS, plus protease and phosphatase inhibitors.
5. TBS solution: 10 mM Tris–HCl, pH 8.0, 150 mM NaCl.
6. Buffer transfer: 25 mM Tris–HCl pH 7.5, 192 mM glycine, and 20 % methanol.
7. Nonfat milk powder.
8. Primary antibody.
9. Antibody-HRP.
10. Substrate for detection (ECL system).

2.4 Gene Silencing with Small Interfering RNA

1. siRNA of interest. The siRNA for CDK5 mRNA (#6216) and the negative control siRNA (#6568) are from Cell Signaling. The siRNAs for p35 and Cyclin I are from Santa Cruz Biotechnology (sc-36153 and sc-35141, respectively).
2. Lipofectamine 2000 (store at +4 °C until use).
3. Opti-MEM I Reduced Serum Medium (prewarmed).
4. 6-well tissue culture plates.

5. Equipment for culturing cells.
6. Solution A: Dilute 50–100 nM of siRNA transfection into 100 µl of Opti-MEM® I Reduced Serum Medium without serum.
7. Solution B: Mix Lipofectamine™ 2000 gently before use, then dilute the appropriate amount (50 pmol) in 100 µl of Opti-MEM® I Medium without serum.
8. SDS-PAGE and Immunoblotting equipment and reagents.

2.5 Immunoprecipitation Assay

1. The Co-IP kit Pierce Direct IP Kit #26148 is recommended and is used with the following solutions:
   - Coupling Buffer: 0.01 M sodium phosphate, 0.15 M sodium chloride; pH 7.2
   - IP Lysis/Wash Buffer: 0.025 M Tris–HCl, 0.15 M NaCl, 0.001 M EDTA, 1 % NP-40, 5 % glycerol, pH 7.4
   - 100× Conditioning Buffer: neutral pH buffer and Elution Buffer: pH 2.8, containing primary amine.
   - Lane Marker Sample Buffer 5×, 0.3 M Tris–HCl, 5 % SDS, 50 % glycerol, 100 mM DTT, pH 6.8.
2. Kit for quantification of protein: Pierce BCA Protein Assay Kit (Pierce) is recommended.
3. The antibodies Cyclin I (sc-5547) and p35/p35 (sc-820) are obtained from Santa Cruz Biotechnology and Tubulin (T8203) are from Sigma Aldrich.
4. Rocking platform or rotator.
5. SDS-PAGE and Immunoblotting equipment and reagents.

3 Methods

These methods describe some techniques which allow the study of the effect of CDKI in the cellular I/R model developed from an epithelial cell line deriving from pig kidney proximal tubule cells (LLC–PK1). LLC–PK1 cells are subjected to Hx–Hp/Nx conditions in the presence and absence of the CDK/cyclin inhibitors (*see* Subheading 3.1). In the vehicle control-treated cells, Hx–Hp/Nx conditions induce cell death, which is characterized by increased caspase-3/-7 activity (*see* Subheading 3.2). Also, comparison between the expression levels of different proteins under normoxic and Hx–Hp/Nx conditions are characterized by Western blot analysis (*see* Subheading 3.3). The molecular mechanism of cell death protection provided by treatment with CDK/cyclin inhibitors is obtained from gene silencing (*see* Subheading 3.4) and immunoprecipitation studies (*see* Subheading 3.5).

3.1 Model Renal Ischemia–Reperfusion (I/R) Injury in LLC-PK1

1. Culture the cells until they are 60–80 % confluent (*see* **Note 1**).
2. Aspirate the cell culture medium and wash the cells twice with PBS, then add 5 ml of 0.05 % Trypsin–EDTA.
3. Incubate at 37 °C for 8–10 min.
4. Add 10 ml of cell culture medium containing FBS per flask.
5. Using a 1000 μl tip, pipette the medium across the wells to detach the colonies. Pipette up and down five times to break up cell colonies into a single cell suspension.
6. Transfer the cell suspension to a 15 or 50 ml conical tube and centrifuge at $300 \times g$ for 5 min at room temperature.
7. Aspirate the supernatant and loosen the cell pellet by tapping the bottom of the tube.
8. Resuspend with 2–5 ml of cell culture medium.
9. Place a 40 μm cell strainer into a 50 ml conical tube and add the cell suspension to the cell strainer (Clumps of cells will be retained while single cells and medium will pass into the conical tube). When all of the suspension has passed through, remove the cell strainer and discard.
10. Remove a sample of the single cell suspension to perform a cell count, determine the cell number and calculate the amount of the medium needed to achieve the desired cell density. Grow the cells to form a confluent monolayer in a 6-well plate format at a cellular density of 4×10^5 cells/well. Prepare two identical experiments (Nx group and Hx-Hp/Hx group).
11. Incubate both groups at 37 °C, 21 % O_2; 5 % CO_2 overnight.
12. The next day, change the Hx-Hp/Hx group to hypoxia-hypercapnia conditions (Hx-Hp). Incubate the cells at 37 °C and 1.5 % O_2; 18 % CO_2 overnight (*see* **Note 2**).
13. Maintain the Nx group at 37 °C, 21 % O_2; 5 % CO_2 overnight.
14. Treat the cells with the CDK inhibitors and incubate both groups at 37 °C, 21 % O_2; 5 % CO_2 for an additional 24-h period (*see* **Note 3**).
15. Evaluate the hypoxic induction through caspase 3/7 activity.

3.2 Evaluation of Hypoxia: Caspase 3/7 Activity Measurements

Subjecting the cells to hypoxia and hypercapnia and afterwards reoxygenating will cause cellular damage and cell loss attributable to apoptosis (*see* **Note 4**). The method to measure the induction of Hx-Hp/Nx is through the activation of caspase 3/7 (*see* **Note 5**).

1. Carefully remove the culture medium and cells in suspension into a labeled 15 ml conical centrifuge tube for the appropriate condition. Keep on ice throughout the remainder of the protocol.
2. Wash the well two times in cold PBS for 5 min at room temperature and keep the washings.

3. Harvest cells by adding a solution of 5 mM EDTA in PBS and incubate at 37 °C for 10–15 min (This procedure may take longer than normal trypsinization).
4. Collect the cells and centrifuge the cell suspension at 300 × *g* for 5 min to pellet the cells. Discard the supernatant.
5. Add cold extraction buffer to the cell pellet, use 30 μl of extraction buffer per 2 wells of a 6-well plate and incubate the cells on ice for 5 min. This hypotonic buffer allows the liberation of the cell contents without completely breaking the cells.
6. Transfer the cell lysate into new microcentrifuge tube. Make sure the tubes are closed. Drop the tube into liquid nitrogen to freeze. Thaw sample on cold water (thawing takes a few minutes). Vortex briefly.
7. Repeat freeze-thaw cycle two more times.
8. Thaw the cell lysate. Collect the supernatant by centrifugation at 16000 × *g* for 7 min at 4 °C.
9. Measure the protein concentration.
10. For 50 μg of cellular lysate (*see* **Note 6**), add 200 μl of caspase assay buffer.
11. The DVDase activity is continuously monitored following the release of fluorescent AFC at 37 °C with a spectrofluorometer such as Wallac 1420 Workstation (λexc 390 nm; λem 510 nm).
12. The DEVDase activity is expressed with an increase in caspase-3 activity compared to a positive control (cells under Hx–Hp/Nx conditions without treatment) and measured by the relative fluorescence or as percentage of the initial fluorescence signal value.

3.3 Western Blot Analysis

We studied the molecular mechanism and found that the CDK5 was responsible for the protective effect in the I/R model [14–16]. In order to analyze the role of CDK5 in cell survival it is necessary to evaluate the protein expression levels of CDK5, the regulatory proteins and their substrates in LLC–PK1 renal tubular cells under normoxic and Hx–Hp/Nx conditions. This is measured in the absence or presence of CDK/cyclin inhibitors using western blot analysis (*see* **Note 7**).

1. Obtain whole cell extracts by lysing the cells in a buffer lysis. Determine the protein concentration by the BCA protein assay.
2. Load the cell extracts and separate in 10–12 % SDS-PAGE and then transfer to a nitrocellulose membrane.
3. Block the membrane with 5 % nonfat dried milk in TBS containing 0.1 % Tween 20 at room temperature with shaking for 1 h.
4. Incubate the membrane with primary antibody in the blocking solution at 4 °C overnight by shaking.

5. Wash the membranes in TBS containing 0.1 % Tween 20 four times for at least 10 min each time with extensive agitation.
6. Incubate with appropriate horseradish peroxidase secondary antibodies with 5 % nonfat dried milk in TBS containing 0.1 % Tween 20 at room temperature for 90 min with shaking. Visualize the proteins using enhanced chemiluminescence technology.

3.4 Gene Silencing with Small Interfering RNA

CDK5 plays a key regulatory role in cell death and survival in the cellular pathways related to I/R-induced damage. Silencing of CDK5 and their regulatory proteins is needed to demonstrate the involvement of these proteins in the recovery process (*see* **Note 8**).

1. Grow the LLC-PK1 cells to form a confluent monolayer in a 6-well plate format at a cellular density of 3×10^5 cells/well. Prepare two identical experiments (Random group and siRNA group). Incubate both groups at 37 °C, 21 % O_2; 5 % CO_2 overnight.
2. The next day, the cells will be 30–50 % confluent at the time of transfection (*see* **Note 9**). Transfect the siRNA oligonucleotides in Opti-MEM at the recommended concentrations using Lipofectamine 2000 according to the manufacturer's instructions (*see* **Note 10**).
3. Remove the growth medium by aspiration and wash the cells with PBS. Add 800 μl of Opti-MEM to the plate and incubate at 37 °C in a CO_2 incubator whilst preparing the solutions.
4. Prepare the solutions A and B (*see* **Note 11**), mix gently and incubate for 5 min at room temperature.
5. After the 5 min incubation period at room temperature, combine solution A with solution B. Mix gently and incubate for 20 min at room temperature.
6. Add 200 μl of the solution to each well containing cells and medium. Mix gently by rocking the plate back and forth.
7. Incubate the transfected cells for 4 h at 37 °C in a CO_2 incubator (*see* **Note 12**)
8. Remove the transfection mixture and replace with normal growth medium and incubate the cells for an additional 24 h at 37 °C, 21 % O_2; 5 % CO_2.
9. At 24 h post-transfection, incubate the cells under Hx–Hp conditions (37 °C and 1.5 % O_2; 18 % CO_2) for 24 h. Treat with the CDK inhibitors and maintain under Nx conditions for a further 24 h.
10. Check the efficacy of the silencing by Western blot.

3.5 Immunoprecipitation Studies

Evaluation of the influence of CDK inhibitors on the regulation of CDK5 and its regulatory subunits by co-immunoprecipitation experiments is described (*see* **Note 13**).

1. Prepare cellular extracts from the LLC–PK1 control cells or from those cells subjected to Hx–Hp/Nx conditions in the presence or absence of the CDK/cyclin inhibitor.
2. Use the Co-IP kit for the immunoprecipitation studies according to the manufacturer's instructions (*see* **Note 14**).
3. Obtain 1 mg of protein, seed and treat 2 plates for the treatment (100 × 100 mm).
4. Aspirate media and rinse cells once with Coupling Buffer.
5. Remove PBS and add 1 ml of ice-cold IP Lysis/Wash Buffer to each plate and incubate the plates on ice for 5 min with periodic mixing.
6. Transfer the lysate to a microcentrifuge tube and centrifuge at ~13,000 × *g* for 10 min to pellet the cell debris.
7. Transfer supernatant to a new tube for protein concentration determination. Measure the protein concentration in the cell lysates using a BCA protein assay, according to the manufacturer's protocol. Use bovine serum albumin (BSA) as a standard.
8. Dilute the cell extract in 400 μl of IP Lysis/Wash Buffer.
9. Add the sample to the 10 μg of antibody-coupled resin in the spin column and incubate the column with gentle end-over-end mixing or shaking for 1 h to overnight at 4 °C (*see* **Note 15**).
10. Remove the bottom plug, loosen the screw cap and place the column in a collection tube. Centrifuge the column and save the flow-through. Do not discard the flow-through until confirming that the IP was successful.
11. Place the column into a new collection tube, add 200 μl of IP Lysis/Wash Buffer and centrifuge. Wash the sample three times.
12. Wash the sample once with 100 μl of 1× Conditioning Buffer.
13. Place the spin column into a new collection tube, add 25 μl of Elution Buffer and centrifuge.
14. Keep the column in the tube and add 75 μl of Elution Buffer. Incubate for 10 min at room temperature.
15. Centrifuge the tube and collect the flow-through. Perform additional elutions as needed.
16. Add 5× Sample Buffer to the sample to make a 1× final solution (i.e., add 5 μl of 5× Sample Buffer to 20 μl of sample).
17. Heat the sample at 95–100 °C for ~5 min. Analyze the eluate to ensure that the antigen has completely eluted.
18. Analyze by western blot to reveal that the immunoprecipitation of CDK5 and cyclin I has been effective. Separate the co-immunoprecipitation by SDS-PAGE and transfer to a nitrocellulose membrane. Incubate the membrane in 5 % nonfat milk powder overnight at 4 °C with primary antibodies, fol-

lowed by incubation with appropriate horseradish peroxidase secondary antibodies. Visualize the signals with the ECL system.

4 Notes

1. All solutions and equipment must be sterile, and aseptic technique should be used accordingly.
2. The door of the hypoxia incubator should remain closed for the incubation period of 24 h.
3. It is important to leave some wells without treatment as a control for hypoxia or normoxia.
4. LLC–PK1 cells were subjected to Hx–Hp/Nx conditions in the presence and absence of the CDK/cyclin inhibitors. In the vehicle control treated cells, Hx–Hp/Nx conditions induced cell death, which was characterized by increased caspase-3/-7 activity. The presence of CDK/cyclin inhibitors enhanced cell viability under Hx–Hp/Nx conditions, together with diminished caspase-3/7 activity.
5. For the determination of the caspase-3/7 activity a fluorescence assay was used [17]. The caspases are cysteine-proteases characterized by the presence of a cysteine residue that breaks other proteins on an aspartic residue. In this assay, the caspase-3/7 from the cell lysate hydrolyses the substrate: Acetyl-Asp-Glu-Val-Asp-7-amino-trifluoromethyl-coumarin (Ac-DEVD-AFC), liberating the AFC, which is a fluorescent marker. The liberation of AFC as a function of time allows for the evaluation of the activity of caspase-3/7 in each sample.
6. For the protocol for caspase-3/7 activity determination it is necessary to have 2 wells per treatment to obtain a sufficient quantity of protein.
7. The expression of CDK5, p35/p25, cyclin I as well as phosphorylation levels of ERK1/2, H2A.x, and Chk1 in total cell extracts was analyzed by western blot in the presence of CDK inhibitors (TAT-NBI1 or roscovitine). The results showed that the treatment with CDK inhibitors restores the normoxic phenotype in the LLC–PK1 Hx–Hp/Nx model [5].
8. The silencing of CDK5 and cyclin I hinders the protective action of CDK inhibitors, but, in contrast, p35 silencing had a protective effect itself in Hx–Hp/Nx renal tubular cell.
9. Subconfluent cells are healthy and are required for successful transfection experiments. It is recommended to ensure cell viability 1 day prior to transfection.
10. Do not add antibiotics to media during transfection as this will cause cell death.

11. The siRNA and Lipofectamine calculations are made to have a final volume of 1 ml per well.
12. Prolonged serum starvation may result in unwanted cell detachment or death.
13. Under Nx conditions, CDK5 maintains a binding equilibrium between both partners p35/p25 and cyclin I signaling to cell survival. Hx–Hp/Nx conditions would produce an increase in the p35 protein levels promoting cell death and under Hx–p/Nx conditions, treatment with the CDK5 inhibitors would affect the CDK5/p35 complex without affecting the activity of the pro-survival CDK5/cyclin I complex. This differential inhibition would promote the degradation of p35, the stabilization of the CDK5/cyclin I complex, and the engagement of a cell survival program that would protect cells from Hx–Hp/Nx-induced damage.
14. The Co-IP kit (Pierce Direct IP Kit #26148) is useful for the immunoprecipitation of a target protein whose molecular weight is similar to the heavy or light chain antibody fragment.
15. Immunoprecipitation is achieved using less than 10 μg of antibody. After the antibody is coupled to the AminoLink Resin, the antigen sample is incubated with the immobilized antibody to form the immune complex. The complex is washed to remove non-bound material, and a low pH elution buffer is used to dissociate the bound antigen from the antibody.

References

1. Orzaez M, Guevara T, Sancho M, Perez-Paya E (2012) Intrinsic caspase-8 activation mediates sensitization of erlotinib-resistant tumor cells to erlotinib/cell-cycle inhibitors combination treatment. Cell Death Dis 3:e415
2. Iyirhiaro GO, Brust TB, Rashidian J, Galehdar Z, Osman A, Phillips M, Slack RS, Macvicar BA, Park DS (2008) Delayed combinatorial treatment with flavopiridol and minocycline provides longer term protection for neuronal soma but not dendrites following global ischemia. J Neurochem 105(3):703–713
3. Hilton GD, Stoica BA, Byrnes KR, Faden AI (2008) Roscovitine reduces neuronal loss, glial activation, and neurologic deficits after brain trauma. J Cereb Blood Flow Metab 28(11): 1845–1859
4. Menn B, Bach S, Blevins TL, Campbell M, Meijer L, Timsit S (2010) Delayed treatment with systemic (S)-roscovitine provides neuroprotection and inhibits in vivo CDK5 activity increase in animal stroke models. PLoS One 5(8):e12117
5. Guevara T, Sancho M, Perez-Paya E, Orzaez M (2014) Role of CDK5/cyclin complexes in ischemia-induced death and survival of renal tubular cells. Cell Cycle 13(10):1617–1626
6. Bagshaw SM, Mortis G, Godinez-Luna T, Doig CJ, Laupland KB (2006) Renal recovery after severe acute renal failure. Int J Artif Organs 29(11):1023–1030
7. Kosieradzki M, Rowinski W (2008) Ischemia/reperfusion injury in kidney transplantation: mechanisms and prevention. Transplant Proc 40(10):3279–3288
8. Singh D, Chander V, Chopra K (2005) Cyclosporine protects against ischemia/reperfusion injury in rat kidneys. Toxicology 207(3): 339–347
9. Delbridge MS, Shrestha BM, Raftery AT, El Nahas AM, Haylor JL (2007) Reduction of ischemia-reperfusion injury in the rat kidney by FTY720, a synthetic derivative of sphingosine. Transplantation 84(2):187–195
10. Aydemir A, Abbasoglu O, Topaloglu S, Ertoy D, Ayhan A, Kilinc K, Karabulut E, Sayek I

(2002) Protective effect of roscovitine on renal ischemia-reperfusion injury. Transplant Proc 34(6):2027–2028

11. Osuga H, Osuga S, Wang F, Fetni R, Hogan MJ, Slack RS, Hakim AM, Ikeda JE, Park DS (2000) Cyclin-dependent kinases as a therapeutic target for stroke. Proc Natl Acad Sci U S A 97(18):10254–10259
12. Canela N, Orzaez M, Fucho R, Mateo F, Gutierrez R, Pineda-Lucena A, Bachs O, Perez-Paya E (2006) Identification of an hexapeptide that binds to a surface pocket in cyclin A and inhibits the catalytic activity of the complex cyclin-dependent kinase 2-cyclin A. J Biol Chem 281(47):35942–35953
13. Hotter G, Palacios L, Sola A (2004) Low O2 and high CO2 in LLC-PK1 cells culture mimics renal ischemia-induced apoptosis. Lab Invest 84(2):213–220
14. Taniguchi Y, Pippin JW, Hagmann H, Krofft RD, Chang AM, Zhang J, Terada Y, Brinkkoetter P, Shankland SJ (2012) Both cyclin I and p35 are required for maximal survival benefit of cyclin-dependent kinase 5 in kidney podocytes. Am J Physiol Renal Physiol 302(9):F1161–F1171
15. Brinkkoetter PT, Olivier P, Wu JS, Henderson S, Krofft RD, Pippin JW, Hockenbery D, Roberts JM, Shankland SJ (2009) Cyclin I activates Cdk5 and regulates expression of Bcl-2 and Bcl-XL in postmitotic mouse cells. J Clin Invest 119:3089
16. Brinkkoetter PT, Pippin JW, Shankland SJ (2010) Cyclin I-Cdk5 governs survival in postmitotic cells. Cell Cycle 9(9):1729–1731
17. Fearnhead HO (2001) Cell-free systems to study apoptosis. Methods Cell Biol 66: 167–185

Chapter 11

Assessing Cell Cycle Independent Function of the CDK Inhibitor p21^{CDKN1A} in DNA Repair

Ilaria Dutto, Micol Tillhon, and Ennio Prosperi

Abstract

The cyclin-dependent kinase (CDK) inhibitor p21^{CDKN1A} is a small protein that is able to regulate many important cell functions, often independently of its activity of CDK inhibitor. In addition to cell cycle, this protein regulates cell transcription, apoptosis, cell motility, and DNA repair. In particular, p21 may participate in different DNA repair processes, like the nucleotide excision repair (NER), base excision repair (BER), and double-strand breaks (DSB) repair, because of its ability to interact with DNA repair proteins, such as proliferating cell nuclear antigen (PCNA), a master regulator of many DNA transactions. Although this role has been debated for a long time, the influence of p21 in DNA repair has been now established. However, it remain to be clarified how this role is coupled to proteasomal degradation that has been shown to occur after DNA damage. This chapter describes procedures to study p21 protein recruitment to localized DNA damage sites in the cell nucleus. In particular, we describe a technique based on local irradiation with UV light through a polycarbonate filter with micropores; an in situ lysis procedure to detect chromatin-bound proteins by immunofluorescence; a cell fractionation procedure to study chromatin association of p21 by Western blot analysis, and p21 protein–protein interactions by an immunoprecipitation assay.

Key words DNA repair, Localized DNA damage, p21^{CDKN1A}, p21 degradation, p21 recruitment, PCNA

1 Introduction

The cyclin-dependent kinase (CDK) inhibitor p21$^{waf1/cip1}$ plays important roles in several cellular pathways in response to intracellular and extracellular stimuli. In particular, p21 was identified as a target of p53 tumor-suppressor gene in response to DNA damage [1, 2]. However, it was afterwards recognized that p21 exerts also its functions in physiological conditions, such as in cellular quiescence and senescence, and in the control of cell differentiation of different cell types [3–5]. In addition to cell cycle control, p21 is involved, independently of CDK inhibition, in the regulation of: (1) transcription, (2) apoptosis and possibly autophagy, (3) cell motility, and (4) DNA repair processes [5–9].

Mar Orzáez et al. (eds.), *Cyclin-Dependent Kinase (CDK) Inhibitors: Methods and Protocols*, Methods in Molecular Biology, vol. 1336, DOI 10.1007/978-1-4939-2926-9_11, © Springer Science+Business Media, LLC 2016

p21 is the main intermediary of cell cycle arrest in response to DNA damage, not only by inactivating the G_1-phase CDK/cyclin complexes but also through the direct interaction with proliferating cell nuclear antigen (PCNA), a master regulator of important DNA transactions [10–12]. This activity occurs thanks to the high affinity binding to PCNA, through which p21 may displace relevant PCNA partner proteins involved in DNA replication [13, 14]. However, this mechanism has been demonstrated in vitro, and in overexpression systems, while its occurrence in normal cells has never been demonstrated, likely because p21 is degraded in S phase [9, 15].

As a transcription regulator, p21 may act not only through the inhibition of CDK [6, 7] but also with a CDK-independent mechanism, by direct binding to transcription factors, or transcriptional co-activators [7, 16]. An active role of p21 is also found in the regulation (mainly inhibition) of the apoptotic process, through the interaction with procaspase 3, with the apoptosis signal-regulating kinase-1 (ASK-1), and with stress-activated MAP kinases [5, 17].

More recent is the discovery of the involvement of p21 in cell motility regulation through the inhibition of Rho kinase, and by interfering with substrate adhesion, as reviewed in ref. [5].

Another important function of p21 is the participation in DNA repair, due to its ability to interact with PCNA. However, this matter has been debated for a long time, since both negative and absent effects have been reported in contrast with findings supporting a positive role of p21 in the process [5, 9, 18]. Furthermore, it was suggested that p21 proteasomal degradation is necessary for DNA repair [19]. In contrast, the findings for a positive role for p21 in nucleotide excision repair (NER) are based on the evidence that p21-null fibroblasts showed a reduced DNA repair efficiency [20], that endogenous p21 protein co-localized with NER factors interacting with PCNA (like XPG, DNA polymerase δ, and CAF-1), and that p21 was present in complexes with these proteins without inhibiting DNA repair [21, 22]. Finally, p21 has been shown to play a role in NER by restoring the acetyltransferase activity of p300 [23], which is required for DNA repair [24], but is inhibited by PCNA [25].

The interaction of p21 with PCNA has been also reported to be important in the Translesion DNA Synthesis (TLS), in order to limit a mutagenic load effect [22, 26]. In addition, p21 has been suggested to play a role in the base excision repair (BER) process by associating with poly(ADP-ribose) polymerase-1 (PARP-1) to regulate its interaction with BER factors [27, 28]. More recently, a PCNA-dependent accumulation of p21 into foci after ionizing irradiation inducing double-strand breaks (DSB), has been also reported [29, 30], further indicating that p21 function in DNA repair is strictly related to PCNA [9, 18]. However, a CDK-dependent function of p21 in DSB repair, has been also described [31, 32].

In the S phase of the cell cycle and after UV irradiation, an ubiquitin-dependent degradation of p21 occurs when it is bound

to chromatin-associated PCNA [33]; this process is mediated by the interaction with E3 complex Cul4-DDB1^{Cdt2} [34, 35]. Degradation of p21 in S phase and after DNA damage has been explained with the need to avoid inhibition of the PCNA-mediated DNA synthesis step of the repair process. However, p21 degradation does not appear to be strictly required for efficient DNA repair in normal cells [9]. Interestingly, in vivo kinetic analysis has shown that p21 recruitment to DNA damage sites follows that of PCNA after a short delay [21, 30]. This behavior suggests that p21 degradation might occur after regulation of the interaction between PCNA with relevant partners participating in DNA repair [36].

Analysis of protein recruitment to DNA damage sites has provided useful information on the orchestration of the DNA damage response [37]. Although expensive instrumentation is required to follow this process in vivo, more cheap techniques are also available to perform similar studies in fixed cells or in cell extracts.

In this chapter we describe some techniques which allow to investigate the behavior of p21 in the DNA repair process, by analyzing its recruitment and localization at DNA repair sites, and its interaction with relevant proteins (e.g., PCNA) participating in the process. The micropore irradiation technique [38, 39] allows DNA damage to be localized within restricted regions of the cell nucleus, thus enabling the recruitment process to be precisely analyzed. This approach may be coupled with an in situ extraction procedure necessary for analyzing chromatin-bound proteins by immunofluorescence (or autofluorescence) detection [21, 40]. Biochemical techniques of chromatin release may be also used to investigate the process of protein recruitment by western blot, and also to perform immunoprecipitation assays. Experimental conditions for using inhibitors of proteasomal activity (such as MG132), in order to study the effect of p21 protein accumulation at sites of DNA damage, are also described.

2 Materials

1. UV-C germicidal lamp T-UV9 (Philips, emission peak at ~254 nm).
2. UV-C radiometer (e.g., DRC-100X, Spectronics).
3. Isopore polycarbonate filters (Millipore) with 3 μm pores of diameter.
4. Fluorescence microscope (e.g., Olympus BX51).
5. Standard polyacrylamide gel electrophoresis (PAGE) and protein transfer equipments.
6. Culture media for untransformed human cells (e.g., fibroblasts), or transformed cells (e.g., HeLa).

7. Carbobenzoxy-l-leucyl-l-leucyl-l-leucinal (MG132), proteasome inhibitor (Sigma or Calbiochem). Prepare a 25 mM stock solution in DMSO.
8. Protease inhibitor cocktail solution in DMSO without EDTA (Sigma). Store in aliquots at −20 °C.
9. Formaldehyde (supplied as 37 % solution stabilized with methanol).
10. p21 monoclonal antibodies: DCS 60.2 (NeoMarkers); CP-74 (Sigma); p21 polyclonal antibodies C-19, or N-20 (Santa Cruz Biotech.).
11. Goat anti-mouse and anti-rabbit secondary antibodies conjugated with Alexa 488 or 594 fluorochromes (Life Technologies), or antibodies conjugated with DyLight 488 or 594 (KPL).
12. Goat anti-mouse or anti-rabbit antibodies conjugated with horseradish peroxidase (HRP).
13. Protein G-agarose magnetic beads and magnet (Dynal, Life Technologies).
14. Citrate-Phosphate buffer: 24.5 mM citric acid, 5.2 mM Na_2HPO_4, pH 5.0.
15. Bovine serum albumin (BSA).
16. Peroxidase substrates for enhanced chemiluminescence (ECL) detection (Cyanagen)
17. Phosphate buffered saline (PBS): 137 mM NaCl, 2.7 mM KCl, 10.6 mM Na_2HPO_4, 1.4 mM KH_2PO_4, pH 7.4.
18. Physiological saline: 154 mM NaCl.
19. Hypotonic lysis buffer: 10 mM Tris–HCl, pH 7.4, 2.5 mM $MgCl_2$, 0.5 % Igepal. Use freshly prepared solution, and immediately before use add 1 mM DTT (dithiothreitol; stock is 1 M, store in aliquots at −20 °C), 1 mM PMSF (phenylmethylsulfonyl fluoride; stock is 200 mM in isopropanol or DMSO, store at 4 °C or r.t.), 0.2 mM sodium vanadate (Na_3VO_4; stock is 100 mM; store in aliquots at −20 °C), and 100 μL/10^7 cells of protease inhibitor cocktail. Keep supplemented buffer on ice.
20. Washing buffer: 10 mM Tris–HCl, pH 7.4, 150 mM NaCl, 1 mM PMSF, and 50 μL/10^7 cells of protease inhibitor cocktail.
21. DNA digestion buffer: 2× solution is 20 mM Tris–HCl, pH 7.4, 20 mM NaCl, 10 mM $MgCl_2$, 20 μL/10^7 cells of protease inhibitor cocktail. Prepare fresh solution each time.
22. DNase I solution: DNase I (Sigma, D-4527, or equivalent) dissolved in 20 mM NaCl and 0.1 mM PMSF just prior to use.

23. SDS-loading buffer: 65 mM Tris–HCl, pH 7.4, 100 mM DTT, 1 % SDS (sodium dodecyl sulfate), 10 % glycerol, 0.02 % bromophenol blue. Store at −20 °C.
24. PBS-Tween 20 solution: PBS containing 0.2 % Tween 20.
25. PBT solution: PBS containing 1 % BSA and 0.2 % Tween 20. Prepare fresh solution each time.
26. Ponceau S: 0.1 % in 5 % acetic acid solution. Store at room temperature.
27. Blocking solution: 5 % nonfat dry milk plus 0.2 % Tween 20 in PBS. Prepare fresh solution each time.
28. Bisbenzimide H 33258 (Hoechst 33258): stock solution is 1 mM in bidistilled H_2O. Store at 4 °C.
29. Mounting medium (e.g., Mowiol) containing 0.25 % antifading agent (1,4-diazabicycloctane).

3 Methods

The methods described here allow to study the recruitment of p21 protein to localized sites of cell nucleus where DNA damage is induced. To accomplish this step, a microirradiation technique, based on the use of filter with micropores, which is layered on top of cells so that the damaging radiation (in this case, UV light) will pass only through the filter pores. DNA repair is triggered in the nuclear regions exposed to the light and accumulation of DNA repair proteins will become detectable (*see* Fig. 1). To obtain reliable results, accurately determined conditions of exposure of the cells to UV light, are first described (*see* Subheading 3.1).

Recruitment of p21 protein to DNA damage sites may be detected as chromatin-bound protein by means of immunocytochemical techniques and fluorescence microscopy (*see* Subheading 3.2), which allow direct visualization of the protein associated with DNA repair sites.

The same process may be investigated with biochemical techniques by using cell fractionation procedures allowing to isolate p21 protein associated with chromatin in a detergent-resistant form (*see* Subheading 3.3). The extraction of the detergent-soluble protein is first obtained with a hypotonic solution in the presence of a non-ionic detergent [20, 21]. The subsequent release of chromatin-bound proteins is obtained by DNA digestion [20, 21]. Detection of p21 in each cell extract fraction is obtained by Western blot analysis. Immunoprecipitation studies using commercially available p21 antibodies can also be easily performed [21, 27].

3.1 Induction of DNA Damage with Irradiation

The pathway of DNA repair induced by DNA damage greatly depends on the type of lesion. In order to detect chromatin-bound p21 involved in DNA repair, one of the most suitable procedures

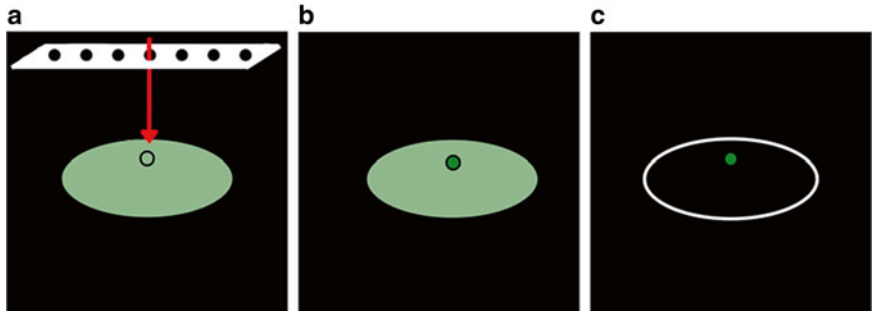

Fig. 1 Schematic representation of the protocol to obtain localized damage in specific regions of DNA: (**a**) the cells are irradiated with UV-C light (*arrow*) through a polycarbonate filter (*white*) with micropores. A localized damage is thus obtained in a nuclear region corresponding to the micropore (*small circle*). (**b**) The protein of interest, distributed across the whole nucleus, is then accumulated only in the region corresponding to the irradiated area (*darker circle*). (**c**) Accumulation of the protein at the site of DNA damage is better visualized after in situ hypotonic lysis allowing to detect only the protein bound to these sites (*small circle*)

is based on the cell exposure to UV-C light (*see* **Note 1**). Best results are obtained with quiescent cells (e.g., fibroblasts growth-arrested by serum starvation) since DNA synthesis proteins involved in DNA repair (e.g., PCNA) also participate in DNA replication, and cells in S phase may give confounding results. However, studies with proliferating cells may be also performed to obtain information otherwise not available on quiescent cells. Studies may also be undertaken with transformed cells, but their DNA repair capacity must be taken into account, depending particularly on the p53 status [1, 2].

To investigate the effect of p21 degradation on DNA repair, an inhibitor of the proteasome (e.g., MG132) may be used before UV-irradiation. This step is described below.

3.1.1 Exposure to Proteasomal Inhibitors

1. Cells grown in petri dishes (*see* below), are treated with proteasomal inhibitors (e.g., MG132, final concentration 25 μM in culture medium) for times ranging from 30 min to 5 h, depending on the type of the experiment. If cells must be grown for periods longer than 2–3 h after UV exposure, the cells should be previously incubated with MG132 for 30 min, and then re-incubated in the presence of the inhibitor also after irradiation.
2. When the effect of p21 on DNA repair is to be investigated, the cells may be treated for 5 h in the presence of MG132, in order to allow accumulation of p21 protein. Then, the cells are exposed to UV light and collected 30 min later.

3.1.2 UV Light Irradiation

UV-C irradiation (254 nm) is one of the most used methods to induce DNA damage and to induce DNA repair by the NER pathway: typical lesions produced are cyclobutane pyrimidine dimers, and 6–4 photoproducts. Since the emission spectrum of commonly

used UV lamps (often used are germicidal lamps) may be different, an accurate determination of the energy supplied to the cells, must be performed.

Particular care must be taken to avoid accidental exposure to the UV-C light of the lamp. Wear appropriate gloves and eye protection. As the optimal condition, the lamp is placed under a three-side closed wooden box, with the open side covered with a black sheet of paper or cloth, which can be lifted to introduce the petri dishes. If possible, perform all subsequent steps under a laminar flow hood to avoid contamination during exposure. The glass window of the hood will also protect from UV light reflected from the steel working level. To avoid reflection, a sheet of black paper may be used.

1. Monitor the energy of the lamp (e.g., T-UV9, Philips) in the UV-C region by using a radiometer (e.g., Spectronics, USA) equipped with a detector sensitive in the 200–280 nm range.
2. Set the distance of the UV source from the working level, so that the fluence of UV light will be 0.5–1 $J/m^2/s$. Check that the UV energy will be uniformly distributed throughout the surface to be exposed.
3. Use cells grown on petri dishes (e.g., 10 cm diameter). For immunofluorescence analysis, grow the cells attached on coverslips (24 × 24 mm) placed into 35-mm diameter dishes. Cells in suspension may be also used, but care must be taken to layer into a petri dish as a thin film in PBS, so that irradiation will be as much as possible uniform.
4. Remove the culture medium and wash the cells twice with warm sterile PBS. Aspirate almost all PBS, leaving just a thin liquid layer on top of the cells.
5. Remove the dish lid and expose the cells to UV light for the period of time required to supply the chosen dose (e.g., 10 J/m^2).
6. Add back the culture medium and re-incubate cells at 37 °C for the desired period of time (a suitable time course ranges from 30 min to 24 h).

3.1.3 Localized Micropore Irradiation

1. To obtain a damage localized to a limited portion of nuclear DNA, the cells on the slides are covered with polycarbonate filters. In this way only the regions corresponding to the pores will be exposed to the radiation, since polycarbonate will stop the majority of UV-C light [38, 39]. Filters are available with pores (randomly distributed) of 3, 5, or 8 μm in diameter. The choice may be based both on the nuclear size of the cells under investigation, or on the extent of the nuclear area that it is to be irradiated.

2. The filter is previously rinsed with PBS to ensure that all pores are open. This operation may be performed by placing the filter into an appropriate filter holder and flushing energetically the solution with a syringe.
3. Under a hood, remove the lid of the petri dish, as in previous section (**step 4**) and lay the filter on top of the cells on the coverslip, taking care to avoid exposure to the UV lamp.
4. Irradiated the cells, as described in the previous section (**step 5**) and expose the cells to a dose ranging from 10 to 30 J/m^2 (*see* **Note 2**).
5. Stop irradiation and add back the culture medium so that the filter will float. Remove the filter with a small clamp. If the cells must be kept alive from periods longer than a few hours, use all sterilized materials (including filters and clamp).
6. Re-incubated cells at 37 °C for the period required and then proceed to the extraction-fixation procedure (next section).

3.2 Detection of p21 Recruitment to DNA Repair Sites by Immunofluorescence Microscopy

To determine the recruitment of p21 protein to DNA damage sites by immunofluorescence microscopy, an in situ hypotonic extraction procedure is necessary to remove the soluble protein not associated with DNA repair sites [20, 21].

3.2.1 In Situ Extraction for Immunofluorescence Microscopy Analysis of Chromatin-Bound p21

1. Seed cells (about 5×10^4) on coverslips or microscope slides (previously cleaned with a 1:1 mixture ethanol/ether, and sterilized). Grow the cells to an 80 % density before use.
2. Rinse the coverslips with PBS, then dip into cold bi-distilled H_2O for about 4 s. For some cells dipping in cold physiological saline may be preferable (*see* **Note 3**).
3. Transfer the coverslips to a petri dish containing cold hypotonic lysis buffer (containing 0.1 mM PMSF), in which the detergent (Igepal) concentration has been reduced to 0.1 %, to avoid detachment of cells (*see* **Note 4**). Keep the petri dishes at 4 °C for about 10 min, with gentle agitation every 3–4 min.
4. Remove the lysis solution and wash the cells carefully with cold PBS or physiological saline, then aspirate and replace with fresh PBS (e.g., 2 mL for a 35-mm dish).
5. Add an equal volume of 2 % formaldehyde (*see* **Note 5**) to reach a final 1 % concentration in PBS, and fix the permeabilized cells for 5 min at r.t. under continuous agitation (*see* **Note 6**).
6. Wash the coverslips again with PBS and further post-fix in cold 70 % ethanol. The samples can be stored in this solution at −20 °C for 1–2 months before further processing for immunocytochemical staining.
7. Remove the fixative and wash the cells with PBS. All subsequent steps are done at r.t.

8. Block the unspecific staining sites by incubation for 15 min with PBT solution.
9. Incubate the coverslips for 1 h at r.t. with anti-p21 monoclonal (DCS 60.2) or polyclonal antibody (C-19 or N-20), diluted 1:100 in PBT solution. The coverslips are placed with cells facing upside-down, onto a drop (50 μL) of antibody on a flat Parafilm strip, so that a sandwich is formed (*see* **Note 7**).
10. Stop the incubation by returning the coverslips into petri dishes with the cells facing up, and wash three times (10 min each) with PBS-Tween 20.
11. The following steps are performed in the dark to avoid photobleaching of fluorochromes. Incubate the coverslips for 30 min with appropriate secondary antibody (diluted 1:200 in PBT solution) by placing again the cells upside-down onto a drop of antibody, as described above. Choose a secondary antibody conjugated with suitable fluorochromes (e.g., Alexa or DyLight 488 for green fluorescence, Alexa or DyLight 594 for red fluorescence), depending on the color emission required (*see* **Note 8**).
12. Remove the coverslips and wash them in petri dishes three times (10 min each) with PBS-Tween 20.
13. If the fluorescent signal is too weak, a third antibody against the secondary one (e.g., donkey anti-goat) labeled with same fluorochrome may be used. In this case, after the step with secondary antibody, incubate for 30 min with the third antibody (increase dilution to 1:300 dilution to avoid high background fluorescence), and then wash three times with PBS-Tween 20, as in **step 12**.
14. Counterstain DNA with Hoechst 33258 or DAPI (0.2 μM in PBS) for 2 min, then remove the dye and wash the coverslips twice (5 min each) with PBS.
15. Mount the coverslips in aqueous mounting medium (e.g., Mowiol) containing anti-fading.
16. After mounting, view slides with a fluorescence microscope (*see* Fig. 2) equipped with filter sets for UV, blue, and green excitation of fluorescence.
17. Seal the coverslips with transparent nail polish to prevent them from drying, and to allow storage of slides at –20 °C.

3.3 Biochemical Analysis of p21 Associated with DNA Repair Sites

The analysis of p21 associated with DNA repair sites by biochemical techniques includes: (1) extraction of the detergent-soluble protein; (2) release of chromatin-bound protein by DNA digestion with DNase I; when necessary, (3) immunoprecipitation of both detergent-soluble and DNase-released fractions with anti-p21 antibodies.

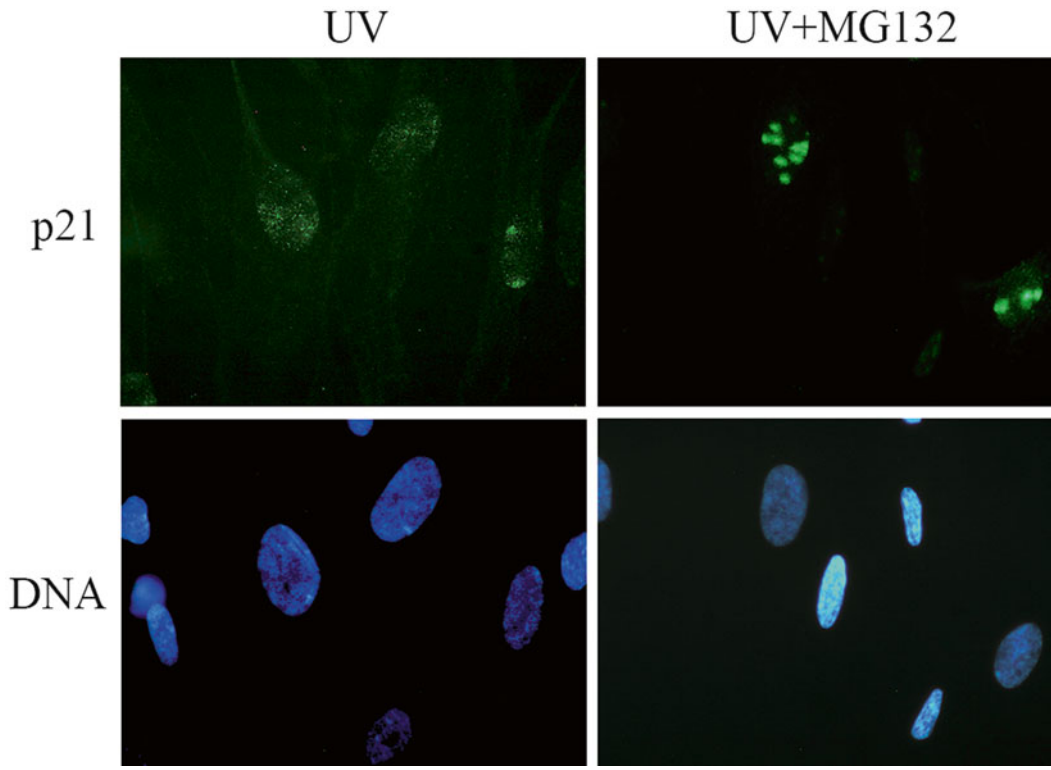

Fig. 2 Immunofluorescence analysis of p21 recruiment to localized sites of UV-induced DNA damage. Mock and MG132-treated human fibroblasts grown on coverslips were exposed to local UV-C irradiation (30 J/m^2) and then re-incubated in culture medium for 30 min. Cells were then treated with hypotonic lysis solution and fixed. Immunofluorescence staining with polyclonal p21 antibody (N-20) is shown in the *upper panels*, while the corresponding fields showing DNA staining with Hoechst dye is shown in the *lower panels*

3.3.1 Extraction of Detergent-Soluble p21 Protein

Both fresh cells and frozen pellets in 2 mL-Eppendorf tubes can be used with this extraction procedure.

1. Chill fresh cells, or thaw frozen samples to 0 °C on ice and resuspend in 1 mL of hypotonic lysis buffer. The volume of lysis buffer (1 mL) is given for extraction from a cell pellet of about 10^7 cells, but it can be scaled down for smaller samples (*see* **Note 9**). However, for an efficient extraction of soluble nuclear proteins, add about 10 volumes of lysis buffer to the cell pellet.
2. Gently resuspend the cell pellet by pipetting the sample about 3–4 times and allow lysis to occur for 10 min on ice (*see* **Note 10**).
3. Pellet the samples by low-speed centrifugation (300 × *g*, 1 min, 4 °C). Collect the supernatant containing the detergent-soluble protein fraction, and measure protein content with the

Bradford method. For normal human fibroblasts, about 2 mg/mL of soluble proteins are released from 10^7 cells. If this amount is lower, other soluble proteins may be released in the next washing step (*see* below), meaning that extraction has not been complete (*see* **Note 11**). Determine the protein concentration also in the fraction released in the washing buffer, and if necessary, add a further washing step. The detergent-soluble proteins may be analyzed by western blot, or used for subsequent immunoprecipitation studies, to be compared to the chromatin-bound protein fraction.

3.3.2 Extraction of Chromatin-Bound p21 by DNA Digestion with DNase I

After extraction of the detergent-soluble protein fraction, chromatin-bound proteins must be solubilized for Western blot analysis. The procedure described below, which is also suitable for immunoprecipitation studies [21, 27], allows the release of DNA-bound protein complexes, and it is based on DNA digestion with DNase I (*see* **Note 12**).

1. Resuspend pelleted permeabilized cells in washing buffer in order to remove as much as possible any trace of soluble proteins.
2. Centrifuge the samples (300×*g*, 1 min), and then resuspend the pellets in half-volume of DNase I solution (e.g., 250 μL for a final digestion volume of 500 μL) containing 100–200 DNase I units/10^7 cells. After thorough resuspension, add the second-half volume of 2× digestion buffer (*see* **Note 13**). The amount of DNase I (*see* **Note 14**) to be added is dependent on the cell type (e.g., cells with a DNA content higher than diploidy, require proportionally higher amounts of DNase I, as compared with normal diploid cells).
3. Carry out the digestion for 15–30 min at 4 °C, with constant agitation in order to avoid cell sedimentation and clumping (*see* **Note 15**).
4. Pellet the samples by high-speed centrifugation (13,000×*g*, 1 min) and collect the resulting supernatants, containing the DNase-released proteins, for subsequent use.
5. Load 40–60 μg of detergent-soluble proteins, and a similar, or higher volume (*see* **Note 16**) of the DNase-released fraction, on a 12 % polyacrylamide gel for standard Western blot analysis.

3.3.3 Immunoprecipitation of Detergent-Soluble and DNase-Released Proteins

If fractionated extracts will be used for immunoprecipitation studies, perform the following steps:

1. Take 100–200 μL of protein G-agarose magnetic beads with a wide-bore pipet from the 50 % suspension; choose the bead volume as a function of the amount of antibody to be used, according to the manufacturer instructions.

2. Resuspend the beads and wash (three times) in citrate-phosphate buffer (pH 5.0).
3. Incubate the p21 antibody with dried protein G-agarose beads in citrate-phosphate buffer (pH 5.0) for at least 1 h at r.t., in a total volume of 100–150 μL. Usually, 4 μg of antibody are sufficient to immunoprecipitate p21 protein from the soluble fraction. Since the amount of p21 protein in the DNase-fraction is generally lower, the amount of antibody to be added may be reduced (e.g., 2 μg).
4. Take a sample of soluble cell lysate containing 1–1.5 mg total protein, and use the whole sample of DNase-released proteins. Set apart a small volume (30–50 μL) of each fraction to check the amount of protein input.
5. Add a suitable amount of p21 antibody pre-bound to protein G-agarose magnetic beads to each cell extract. Incubate for 3 h at 4 °C on a rotating wheel.
6. Precipitate the beads by placing the tubes on a magnet for 2 min at 4 °C. Remove the supernatant by gentle aspiration with a Pasteur pipette, being careful not to touch the beads (if the beads are touched on, place the tube again on the magnet and repeat the step).
7. Wash the immune complexes bound to beads three times with washing buffer. Each time, add 0.5–1 mL of washing buffer and resuspend the beads by gentle vortexing. The final wash should be removed completely.
8. For SDS-PAGE, add 60 μL of SDS-loading buffer to each sample.
9. Denature the proteins in the sample by heating to 100 °C for 5 min. Centrifuge for 15 s at 10,000 × *g* and load half of the supernatant (30 μL) on the gel.

3.3.4 Immunoblot Analysis of Fractionated Cell Extracts, or Immunoprecipitated Proteins

1. After SDS-PAGE, transfer the proteins to a nitrocellulose (or PVDF) membrane with a conventional apparatus (semidry or immersion).
2. Check the protein transfer to the membrane by Ponceau S staining.
3. Remove excess stain with several washes in bi-distilled H_2O.
4. Block the membranes for 30 min at r.t. with blocking solution.
5. Incubate the membranes for 1 h at r.t. with monoclonal (CP-74) or polyclonal antibody to p21 (diluted 1:500 in PBS-Tween 20), then wash 4–6 times (10 min each) with PBS-Tween 20, under continuous agitation.

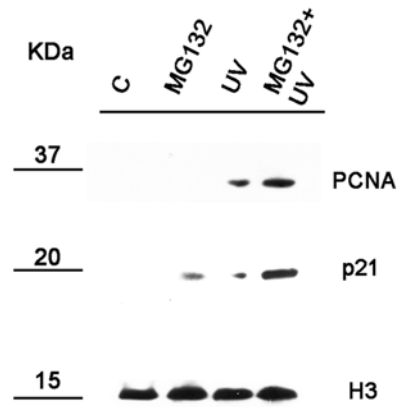

Fig. 3 Western blotting analysis of chromatin-bound proteins at the DNA damage sites. Mock and MG132-treated (5 h) human fibroblasts were exposed to UV-C irradiation (10 J/m^2), and then re-incubated in culture medium for 30 min. Cells were then detached and kept frozen at −80 °C until use. Hypotonic lysis and DNAse I digestion were performed to extract chromatin-bound proteins. Western blot analysis was performed with anti-p21, and anti-PCNA antibodies, to visualize association of these proteins to chromatin after DNA damage. Immunostaining with anti-histone H3 antibody was performed to check nuclear protein extraction and equal loading of samples

6. Incubate the membranes (30 min, r.t.) in a secondary HRP-conjugated antibody (diluted 1:2000 in PBS-Tween 20), then repeat washings as in the previous step.
7. Incubate the nitrocellulose (or PVDF) membranes with peroxidase substrates for ECL detection and expose to autoradiographic film (*see* Fig. 3).

4 Notes

1. In the case of UV light, the main DNA repair process which is initiated at these sites, is the NER process. However, if another source of focused radiation (e.g., a laser beam) is available, different DNA repair activities (e.g., DSB repair) may be investigated. In this case, the energy provided by the laser (whose emission must be properly chosen to induce DNA damage) is coupled with a photosensitizer to induce DNA lesions similar to those obtained with UV light, or to induce DSB [21, 40].
2. In the literature, local UV irradiation with doses as high as 100 J/m^2 may be found. However, we noticed that it is not necessary to use these conditions when studying recruitment of p21 and PCNA.

3. Dipping of the cover slips in cold ddH_2O is particularly useful with cells with large cytoplasm (e.g., fibroblasts) since this will favor the extraction of detergent-soluble proteins. However, when using cells with a small cytoplasm (e.g., some tumor cells, such as HEK 293 cells), the hypotonic stress is likely to result in a substantial detachment of the cells from the coverslip.
4. Avoid pipetting the hypotonic lysis solution directly onto the cells, since this will increase the risk of cell detachment from the coverslip.
5. Formaldehyde vapors are toxic. Solutions containing formaldehyde should be prepared in a chemical hood.
6. For some cell types (e.g., HeLa cells), the final formaldehyde concentration may be increased up to 4 % because it has been noticed that cells fixed with lower concentrations will lose their nuclear morphology after freezing–thawing of slides stored at −20 °C.
7. The antibody sandwich formed with the coverslip on the Parafilm strip will not dry under normal RT conditions, so that is not necessary to prepare a humid chamber. This has the advantage of reducing the incubation volume, thus saving antibody.
8. The choice of secondary antibody depends on the fluorescence emission to be detected under the microscope. In same case, it may be useful to perform a double staining with two primary antibodies (i.e., a monoclonal and a polyclonal). Choose secondary antibodies (e.g., anti-mouse and anti-rabbit) made in the same specie (goat), to avoid unwanted cross-reactions.
9. It is worth using not fewer than 5×10^6 cells to easily detect the chromatin-bound fraction of p21, and consider about 3.5×10^6 cells as the lower limit for detection.
10. Resuspension of the cell pellet by pipetting may produce foam due to the presence of detergent in the hypotonic lysis buffer. However, this will not compromise extraction of soluble p21 protein. Care must be taken if cells with small cytoplasm (e.g., lymphocytes) are used, since pipetting could result in nuclear damage and loss. In this case, pipette only two or three times.
11. When the extraction of detergent-soluble proteins is efficient, the amount of proteins released in the subsequent washing buffer should not be higher than 20 % of the initial release.
12. An alternative procedure to release chromatin-bound proteins is based on the production of DNA strand breaks by sonication. This procedure is equally effective for releasing chromatin-bound proteins in a form suitable for immunoprecipitation experiments. This would not be otherwise possible with protocols using SDS to release nuclear-bound proteins.

However, when using sonication, care must be taken to reduce protein degradation by using a "low" setting and short pulses, and by performing the entire procedure on ice.

13. Good resuspension of the cell pellet in the DNase solution is a requisite for efficient DNA digestion and consequent release of DNA-bound proteins. The addition of 2× digestion buffer after cell resuspension is performed because of the Mg^{2+} contained in the digestion buffer, which will favor cell clumping, thereby reducing the extent of DNA digestion.
14. The quality of DNase I is very important, since contaminants present in different preparations (e.g., chymotrypsin) may be responsible for proteolytic degradation. A chromatographically purified preparation (e.g., Sigma D-4527) is recommended.
15. Digestion conditions (e.g., time and temperature) should be determined depending on the experiment. For coimmunoprecipitation studies, possible degradation of proteins may be reduced by shortening both incubation time and temperature. If cell clumping occurs during DNA digestion, a very brief sonication will help to disrupt cellular aggregates and facilitate DNA breakage.
16. Given that p21 bound to chromatin constitutes only a minor fraction of the total cellular amount of the protein, loading of proportionally higher volumes of DNase extracts, as compared to the soluble fraction, may be required to improve detection by western blot. It is advisable to check the protein loading of different samples, by detecting another protein (e.g., actin or histone H3) as an internal standard.

References

1. El-Deiry WS, Tokino T, Velculescu VE et al (1993) WAF1, a potential mediator of p53 tumor suppression. Cell 75:817–825
2. Harper JW, Adami G, Wei N et al (1993) The p21 cdk-interacting protein Cip1 is a potent inhibitor of G1 cyclin dependent kinases. Cell 75:805–816
3. Herbig U, Sedivy JM (2006) Regulation of growth arrest in senescence: telomere damage is not the end of the story. Mech Ageing Dev 127:16–24
4. Perucca P, Cazzalini O, Madine M et al (2009) Loss of p21 CDKN1A impairs entry to quiescence and activates a DNA damage response in normal fibroblasts induced to quiescence. Cell Cycle 8:105–114
5. Stivala A, Cazzalini O, Prosperi E (2012) The cyclin-dependent kinase inhibitor p21CDKN1A as a target of anti-cancer drugs. Curr Cancer Drug Targets 12:85–96
6. Dotto GP (2000) p21(WAF1/Cip1): more than a break to cell cycle? Biochim Biophys Acta 1471:43–56
7. Coqueret O (2003) New roles for p21 and p27 cell-cycle inhibitors: a function for each cell compartment? Trends Cell Biol 13: 65–70
8. Abbas T, Dutta A (2009) p21 in cancer, intricate networks and multiple activities. Nat Rev Cancer 9:400–414
9. Cazzalini O, Scovassi AI, Savio M et al (2010) Multiple roles of the cell cycle inhibitor p21CDKN1A in the DNA damage response. Mutat Res Rev Mutat 704:12–20
10. Warbrick E (2000) The puzzle of PCNA's many partners. Bioessays 22:997–1006
11. Prosperi E (2006) The fellowship of the rings, distinct pools of proliferating cell nuclear antigen (PCNA) trimer at work. FASEB J 20: 833–837

12. Moldovan GL, Pfander B, Jentsch S (2007) PCNA, the maestro of replication fork. Cell 129:665–679
13. Oku T, Ikeda S, Sasaki H et al (1998) Functional sites of human PCNA which interact with p21(Cip1/Waf1), DNA polymerase delta and replication factor C. Genes Cells 3:357–369
14. Cazzalini O, Perucca P, Riva F et al (2003) p21CDKN1A does not interfere with loading of PCNA at DNA replication sites, but inhibits subsequent binding of DNA polymerase delta at the G1/S phase transition. Cell Cycle 2: 596–603
15. Soria G, Gottifredi V (2010) PCNA-coupled p21 degradation after DNA damage: the exception that confirms the rule? DNA Repair 9:358–364
16. Perkins ND (2002) Not just a Cdk inhibitor: regulation of transcription of $p21^{WAF1/CIP1/SDI1}$. Cell Cycle 1:39–41
17. Gartel AL (2005) The conflicting roles of the cdk inhibitor $p21^{CIP1/WAF1}$ in apoptosis. Leuk Res 29:1237–1238
18. Tillhon M, Cazzalini O, Stivala A et al (2010) Involvement of the cell cycle inhibitor p21CDKN1A in DNA repair processes. In: Thomas AE (ed) DNA damage repair, repair mechanisms and aging. Nova Science, Hauppauge, NY, pp 123–140
19. Bendjennat M, Boulaire J, Jascur T et al (2003) UV irradiation triggers ubiquitin-dependent degradation of $p21^{WAF1}$ to promote DNA repair. Cell 114:599–610
20. Stivala LA, Riva F, Cazzalini O et al (2001) p21(waf1/cip1)-null human fibroblasts are deficient in nucleotide excision repair downstream the recruitment of PCNA to DNA repair sites. Oncogene 20:563–570
21. Perucca P, Cazzalini O, Mortusewicz O et al (2006) Spatiotemporal dynamics of $p21^{CDKN1A}$ protein recruitment to DNA-damage sites and interaction with proliferating cellular nuclear antigen. J Cell Sci 119:1517–1527
22. Soria G, Speroni J, Podhajcer O et al (2008) p21 differentially regulates DNA replication and DNA repair associated processes after UV-irradiation. J Cell Sci 121:3271–3282
23. Cazzalini O, Perucca P, Savio M et al (2008) Interaction of p21(CDKN1A) with PCNA regulates the histon acetyltransferase activity of p300 in nucleotide excision repair. Nucleic Acids Res 36:1713–1722
24. Rubbi CP, Milner J (2003) p53 is a chromatin accessibility factor for nucleotide excision repair of DNA damage. EMBO J 22:975–986
25. Hong R, Chakravarti D (2003) The human proliferating cell nuclear antigen regulates transcriptional coactivator p300 activity and promotes transcriptional repression. J Biol Chem 278:44505–44513
26. Avkin S, Sevilya Z, Toube L et al (2006) p53 and p21 regulate error-prone DNA repair to yield a lower mutation load. Mol Cell 22: 407–413
27. Frouin I, Maga G, Denegri M et al (2003) Human proliferating cell nuclear antigen, poly(ADP-ribose) polymerase 1, and $p21^{Waf1/Cip1}$. A dynamic exchange of partners. J Biol Chem 278:39265–39268
28. Cazzalini O, Donà F, Savio M et al (2010) p21CDKN1A participates in base excision repair by regulating the activity of poly (ADP-ribose) polymerase-1. DNA Repair 9: 627–635
29. Koike M, Yutoku Y, Koike A (2011) Accumulation of p21 proteins at DNA damage sites independent of p53 and core NHEJ factors following irradiation. Biochem Biophys Res Commun 412:39–43
30. Wiese C, Rudolph JK, Jakob B et al (2012) PCNA-dependent accumulation of CDKN1A into nuclear foci after ionizing irradiation. DNA Repair 11:511–521
31. Mauro M, Rego MA, Boisvert RA, Esashi F, Cavallo F, Jasin M, Howlett NG (2012) p21 promotes error-free replication-coupled DNA double-strand break repair. Nucleic Acids Res 40:8348–8360
32. Dutto I, Tillhon M, Cazzalini O, Stivala LA, Prosperi E (2015) Biology of the cell cycle inhibitor p21CDKN1A: molecular mechanisms and relevance in chemical toxicology. Arch Toxicol 89:155–178
33. Havens CG, Walter JC (2009) Docking of a specialized PIP Box onto chromatin-bound PCNA creates a degron for the ubiquitin ligase CRL4Cdt2. Mol Cell 35:93–104
34. Abbas T, Sivaprasad U, Terai K et al (2008) PCNA-dependent regulation of p21 ubiquitylation and degradation via $CRL4^{Cdt2}$ ubiquitin ligase complex. Genes Dev 22:2496–2506
35. Nishitani H, Shiomi Y, Iida H et al (2008) CDK inhibitor p21 is degraded by a PCNA coupled Cul4-$DDB1^{CDT2}$ pathways during S phase and after UV irradiation. J Biol Chem 283:29045–29052
36. Tillhon M, Cazzalini O, Nardo T, Necchi D, Sommatis S, Stivala LA, Scovassi AI, Prosperi E (2012) p300/CBP acetyltransferases interact with and acetylate the nucleotide excision repair factor XPG. DNA Repair 11:844–852

37. Lukas J, Lukas C, Bartek J (2011) More than just a focus: the chromatin response to DNA damage and its role in genome integrity maintenance. Nat Cell Biol 13:1161–1169
38. Katsumi S, Kobayashi N, Imoto K et al (2001) *In situ* visualization of ultraviolet-light-induced DNA damage repair in locally irradiated human fibroblasts. J Invest Dermatol 117: 1156–1161
39. Volker M, Monè MJ, Karmakar P et al (2001) Sequential assembly of nucleotide excision repair factors in vivo. Mol Cell 8:213–224
40. Vermeulen W (2011) Dynamics of mammalian NER proteins. DNA Repair 10:760–771

Chapter 12

Drug Delivery Strategies of Chemical CDK Inhibitors

Daniel Alvira and Laura Mondragón

Abstract

The pharmacological use of new therapeutics is often limited by a safe and effective drug-delivery system. In this sense, new chemical CDK inhibitors are not an exception. Nanotechnology may be able to solve some of the main problems limiting cancer treatments such as more specific delivery of therapeutics and reduction of toxic secondary effects. It provides new delivery systems able to specifically target cancer cells and release the active molecules in a controlled fashion. Specifically, silica mesoporous supports (SMPS) have emerged as an alternative for more classical drug delivery systems based on polymers. In this chapter, we describe the synthesis of a SMPS containing the CDK inhibitor roscovitine as cargo molecule and the protocols for confirmation of the proper cargo release of the nanoparticles in cell culture employing cell viability, cellular internalization, and cell death induction studies.

Key words Cellular uptake, MCM-41, Silica mesoporous support, Specific cargo release, Roscovitine

1 Introduction

In the development of new cancer therapies, nanotechnology has been proved able to solve some of the main problems limiting cancer treatments such as more specific delivery of therapeutics and reduction of toxic secondary effects by providing new delivery systems able to specifically target cancer cells and release the active molecules in a controlled fashion. Initially, the delivery systems designed were based on the employ of organic polymers. Subsequent degradation of the polymeric matrix allows the release of the active molecule (cargo) once inside the cell, thus reaching its target. In the past few years, silica mesoporous supports (SMPS) have emerged as an alternative that complements the polymer-only release systems [1–4]. These materials have undergone an exponential growth thanks to its unique properties such as large loading capacity, low toxicity, and easy functionalization that allow its use as carriers for drug storage and delivery. One of the most interesting features of these materials is the possibility of including molecular or supramolecular caps onto its external surface of the

Mar Orzáez et al. (eds.), *Cyclin-Dependent Kinase (CDK) Inhibitors: Methods and Protocols*, Methods in Molecular Biology, vol. 1336, DOI 10.1007/978-1-4939-2926-9_12,

SMPS which has been previously loaded with a particular cargo. These caps will act as "gates" that will cover the pore of the material avoiding cargo release till the application of an external given stimulus.

Multiple examples employing different stimuli have been developed based on the use of changes in pH, light, redox properties, temperature, but we focus our attention on the use of enzymes as "biological-keys" to develop more biocompatible gated SMPS nanodevices [5]. This development is supported by the cellular internalization mechanism of nanoparticles: endocytosis. Due to its size 50–100 nm, SMPS are endocytosed and travel through the endosomal pathway till reaching lysosomes, where the existent lysosomal enzymes can degrade the capping molecules of the SMPS, thus allowing the release of the cargo. This cargo molecule will diffuse through the lysosomal membrane being able to reach its target in the cell and providing the desired therapeutic benefit.

In the present chapter, we depict the materials and methods employed to synthesize and chemically characterize the silica mesoporous support Mobile Companion Material 41 [6] (MCM-41) in order to include different chemical Cyclin-dependent kinases inhibitors (CDK) in their pores. Besides, we describe the most common methods to prove its biological activity once inside the cells.

2 Materials

2.1 Equipment

1. Stirring hotplate.
2. Muffle furnace.
3. X-ray diffractometer.
4. Automated sorption analyzer.
5. Transmission electron microscope.
6. Thermogravimetric analyzer.
7. Elemental microanalyzer.
8. UV spectrophotometer.
9. Fluorimeter Automated Peptide Synthesizer.
10. Confocal microscope Multilabel plate reader Flow Cytometer.
11. Centrifuge.
12. Steri-Cycle CO_2 incubator.

2.2 Reagents

1. Hexadecyltrimethylammonium bromide (CTAB).
2. Tetraethylorthosilicate (TEOS).

3. Sodium hydroxide (NaOH).
4. Ethanol.
5. Chlorhydric acid.
6. Glucidex®47.
7. 3-aminopropyltriethoxysilane.
8. Chloroform.
9. Roscovitine.
10. Dimethylsulfoxide (DMSO).
11. Digitonin.
12. zRR-7-amino-4-methylcoumarin (Z-RR-AMC).
13. Lipofectamine.
14. Fetal bovine serum.
15. Dulbecco's Modified Eagle's Medium (DMEM).
16. Opti-MEM.
17. Trypsin 0.05 %.
18. HeLa cell line.
19. Wheat Germ Agglutinin Alexa Fluor® 647.
20. Hoechst 33342.
21. Annexin V-FITC.
22. Propidium iodide solution 5 mg/mL.
23. 4-[3-(4-Iodophenyl)-2-(4-nitrophenyl)-2H-5-tetrazolio]-1,3-benzene disulfonate (WST-1).
24. RNAse A.

2.3 Buffers

1. Phosphate buffer saline (PBS): 137 mM NaCl, 2.7 mM KCl, 10.6 mM Na_2HPO_4, 1.4 mM KH_2PO_4 pH 7.4.
2. Cytosolic extraction buffer: 20 µg/mL digitonin, 250 mM sucrose, 20 mM Hepes, 10 mM KCl, 1.5 mM $MgCl_2$, 1 mM EDTA, 1 mM EGTA, 1 mM Pefabloc, pH 7.5.
3. Lysosomal extraction buffer: 200 µg/mL digitonin, 250 mM sucrose, 20 mM Hepes, 10 mM KCl, 1.5 mM $MgCl_2$, 1 mM EDTA, 1 mM EGTA, 1 mM Pefabloc, pH 7.5.
4. Cathepsin reaction buffer: 50 mM sodium acetate, 4 mM EDTA, 8 mM DTT, 1 mM Pefabloc, pH 6.0.
5. Annexin V binding buffer: 10 mM HEPES, 140 mM NaCl, 2.5 mM $CaCl_2$.
6. Kinetic release buffer: 50 mM AcNa, 1 mM EDTA, 8 mM DTT pH 5.4.

3 Methods

3.1 Synthesis of Solids Based on Mesoporous Material MCM-41

3.1.1 Synthesis of Mesoporous Material MCM-41

The preparation of ordered mesoporous materials is based on the use of structure-directing surfactants able to form micelles in aqueous media that will act as a template for the condensation of silica precursors around these micelles. Subsequent removal of the surfactant by extraction or calcination will give the final mesoporous material. In this chapter we propose as an example, the synthesis of MCM-41 nanoparticles employing hexadecyltrimethylammonium bromide (CTAB) as surfactant and tetraethylorthosilicate (TEOS) as inorganic nanoparticle precursor [7–9].

1. Dissolve the surfactant CTAB (1.00 g, 2.74 mmol) in 480 mL of deionized water by heating at 37 °C. When the turbidity is lost, add a solution of NaOH (3.5 mL, 2.00 M) to the CTAB solution to achieve a basic pH of approximately 8.00 units.
2. Once the basic pH is achieved, adjust the temperature of the solution to 95 °C prior to the dropwise addition of TEOS (5.00 mL, 2.57×10^{-2} mol) while stirring the solution at maximum speed. A few minutes later, the appearance of a white precipitate can be observed corresponding to the MCM-41 nanoparticles formation. Allow the mixture to stir for 2 h till the reaction is completed.
3. Centrifuge the precipitate obtained ($18{,}500 \times g$, 10 min) and wash with deionized water several times till the neutralization of the pH. Then, dry the solid at 60 °C overnight (MCM-41 as-synthesized).
4. Calcine the as-synthesized solid at 550 °C using oxidant atmosphere for 5 h in order to remove the template phase (*see* **Note 1**) and prepare the final porous material (MCM-41).

3.2 Loading and Surface Functionalization of MCM-41

Once synthesized the nanoparticle, the next step is to introduce the guest molecules into the pores. For that purpose, a selection of the solvents is done based on the maximum solubility of the cargo molecule. Once the nanoparticle is loaded, the chemical attachment of the molecular gate to the surface of MCM-41 is done. This step is based on the formation of a covalent bond between an organic alkoxysilane derivative and the siliceous surface of the former inorganic scaffolding employing nonaqueous solvents in order to avoid the hydrolysis of the alkoxysilane derivatives [10, 11] (*see* **Note 2**).

In the present chapter, we describe the synthesis of a MCM-41 solid containing the CDK2, 7 and 9 inhibitor roscovitine [12–14] as guest molecule (*see* Fig. 1).

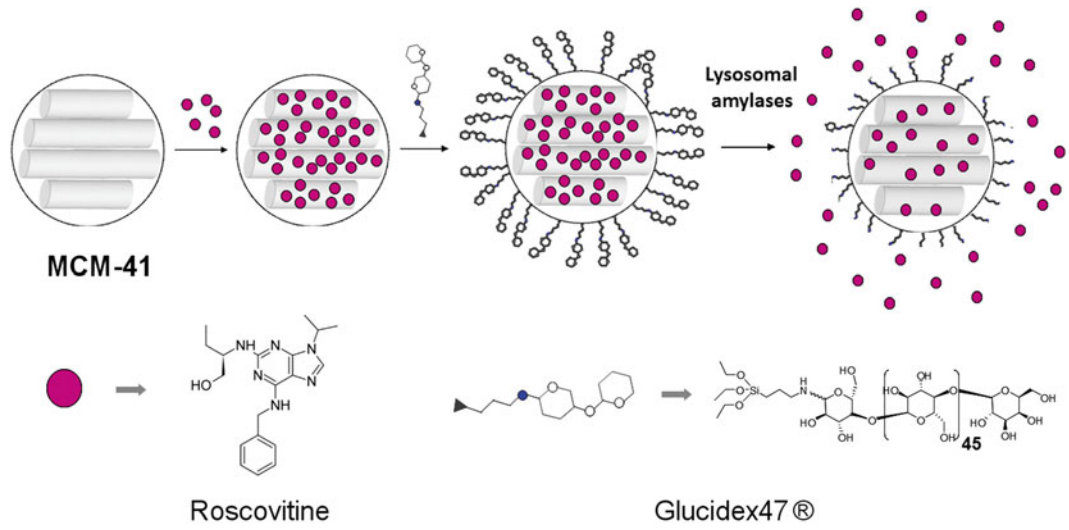

Fig. 1 Schematic representation of Glu47-RVT-S1 synthesis and degradation of its molecular gate

3.2.1 Synthesis of MCM-41 Containing a CDK Inhibitor as Cargo Molecule

As capping molecule, an L-glucose polysaccharide (Glucidex®47) is employed [15]. This polymer is easily hydrolyzed by the amylases present in the lysosomes, thus allowing the release of roscovitine once inside the lysosomes.

Synthesis of Glucidex®47 Molecular Gate [15]

1. Add a solution of 3-aminopropyltriethoxysilane (L) (2.35 mL, 10 mmol) in EtOH to a suspension of hydrolyzed starch Glucidex®47 (2 g) in EtOH (total volume 100 mL). Stir the reaction mixture for 24 h at room temperature and then heat at 60 °C for 30 min to complete the reaction.
2. The solvent is evaporated under reduced pressure to give a white solid (Glu47-L).

Synthesis of Glu47-Roscovitine-S1

1. In a typical synthesis, suspend 0.1 g of calcined MCM-41 and 0.06 g (proportion 1:0.6 g:g) of roscovitine (RVT) in 10 mL of chloroform, inside a round-bottom flask in an inert atmosphere. Stir the mixture for 24 h at room temperature with the aim of achieving maximum loading in the pores of the MCM-41 scaffolding (RVT-S1).
2. To 0.1 g of the RVT-S1 obtained, add 0.1 g of Glu47-L 10 mL of EtOH and stir the final mixture for 5.5 h at room temperature. Finally, filter off the solid RVT-S1 containing the molecular gate Glu47-L (Glu47-RVT-S1), wash with 40 mL of water, and dry at 37 °C for 12 h.
3. Once dried, suspend the solid in 40 mL of chloroform and stir to remove the dye remaining outside the pores. After 12 h, filter the solid again and dry at 37 °C for 24 h.

4. Finally, develop chemical characterization of the nanoparticle structure and determine the amount of cargo molecule and molecular gate (*see* **Note 3**).

3.3 Characterization of the Molecular Gate Aperture Mechanism

The solids synthesized consist of MCM-41 mesoporous containing roscovitine in the pores and a Glucidex®47 molecular gate. In order to check the proper functioning of the molecular gate of the solids, the aperture stimuli is applied in vitro and cargo release is measured as indicator of the aperture of the pore of the nanoparticle. In the example presented in this chapter (Glu47-RVT-S1), recombinant amylases or lysosomal extracts able to degrade the molecular gate are employed for this purpose [15–17] (*see* **Note 4**).

As a general example, we provide a kinetic release study of the cargo molecules employing lysosomal extracts that results valid for any nanoparticle before testing it in cell models.

3.3.1 Lysosomal Extracts Preparation

HeLa human cervix adenocarcinoma cell line is employed as an example, although other cell lines can be also used [18]. This cell line is cultured in DMEM supplemented with 10 % of fetal calf serum (FCS). Cells are maintained at 37 °C in an atmosphere of 5 % carbon dioxide and 95 % air and undergo passage twice a week.

1. Plate HeLa cells in three sterile 150 mm ϕ culture dish and keep in culture till they reach approximately 80 % of confluence.
2. Once the cells are ready, remove the medium, wash cells with PBS and add 10 mL of cytosolic extraction buffer per plate (*see* **Note 5**). Once the buffer is added, incubate cells for 10 min on ice and submit to continuous shaking.
3. After this initial incubation, remove buffer and add 8–10 mL of lysosomal extraction buffer with 200 μg/mL of digitonin to the plate. Incubate cells for 10 min on ice and submit to continuous shaking.
4. After 10 min, recover the lysosomal extraction buffer (this time containing the lysosomal extracts).
5. To determine the proper lysis of the lysosomes, determine cathepsin activity (a lysosomal enzyme) in the cytosolic and the lysosomal extracts. Mix one volume of the extracts with one volume of the cathepsin reaction buffer in the presence of a fluorogenic substrate of cathepsin B zRR-7-amino-4-methylcoumarin (Z-RR-AMC) (20 μM).
6. Kinetic release of the AMC ($\lambda exc = 380$ nm, $\lambda em = 442$ nm) is followed over 20 min at 37 °C with a fluorescence plate reader. Cathepsin B activity should only be detected in the lysosomal extracts but not in the cytosolic extracts.

3.3.2 Kinetic Release Experiment

1. In a typical experiment, suspend 0.5 mg of solid in 2.8 mL of kinetic release buffer at pH 5.4–6.0 (optimal conditions for enzyme activity as in the lysosomes) in the presence of 0.5 mL of lysosomal extract from HeLa cells (0.035 mg, 0.07 mg/mL protein content). As a control, suspend the same amount of solid but adding a mixture of non-lysosomal proteins at the same concentration than that measured for the lysosomal extract [17].
2. Stir the suspensions at 37 °C, take aliquots (0.3 mL) at different time points and centrifuge to eliminate the solid.
3. Cargo delivery is often determined by monitoring the fluorescence or UV-Visible absorbance spectra of the cargo molecules at different time points, as depicted in Fig. 2c. Alternatively, analysis through HPLC or mass spectroscopy can be developed to detect the cargo molecules released (*see* **Note 6**).

3.4 Internalization and Cargo Release of Silica Mesoporous Supports Containing CDKs Inhibitors in Cellular Models

For the study of cellular uptake of silica mesoporous supports, adherent cells are mostly used although any type of cell can be employed. Here, we exemplify the methods proposed employing HeLa cell line.

Our main objective is to determine the proper internalization of the nanoparticle by the cells and the arrival of the solids to lysosomes, where lysosomal enzymes will degrade the molecular gate allowing cargo release. For that purpose, confocal microscopy is used and the lysosomal-associated membrane protein 1 (LAMP1), a glycoprotein embedded in the lysosomal membrane, fused to the protein GFP is employed to prove the localization of the nanoparticles in the lysosomes. LAMP1-GFP presents a dotted pattern distribution related to its lysosomal membrane association; colocalization of the solids with the LAMP1-GFP dots will be pursued.

3.4.1 Cellular Uptake Studies

1. Seed HeLa cells at a final density of 2.5×10^4 cells/well in 24 mm ϕ cover-slips in 6-well plates and 24 h later substitute DMEM by Opti-MEM and transfect cells with Lipofectamine in the presence of the plasmid pLAMP1-GFP according to manufacturer instructions (*see* **Note 7**) [19].
2. 24 h later, substitute Opti-MEM by DMEM culture medium and treat cells for 20 min with 100 μg/mL of S1-P. Then, change the medium in order to remove nanoparticles and let the cells in culture for 24 h more.
3. Once the solids are incubated, stain cells with the nuclear marker Hoechst 33342 (10 nM) and the cell membrane marker Wheat Germ Agglutinin conjugated to Alexa Fluor 647® for 10 min (according to manufacturer instructions) prior its analysis by confocal microscopy (*see* **Note 8**) (*see* Fig. 3).

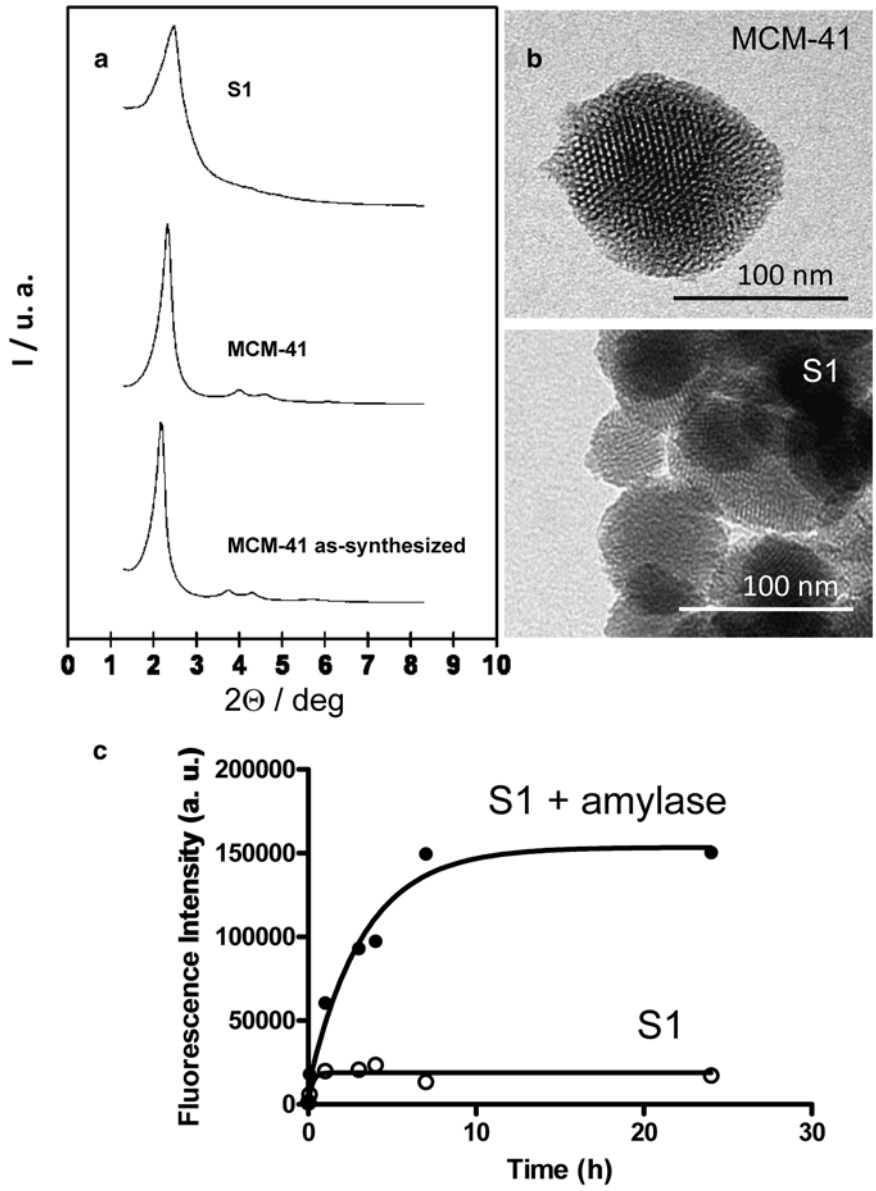

Fig. 2 Examples of (**a**) X-ray diffraction pattern, (**b**) TEM images and (**c**) release kinetics at 37 °C of MCM-41 nanoparticles (S1) loaded with Safranin O and containing a Glucidex47® molecular gate

3.4.2 Cellular Viability and Cell Cycle Studies

The final characterization assays aim at determining the effect of the molecules encapsulated in the nanoparticles or attached as molecular gates compared to the free drugs. The main objective is to demonstrate the advantage of the use of nanoparticles as drug delivery vehicles in terms of efficiency at equivalent dosis. In the examples presented in the chapter the main objective is to determine the anticancer activity at determined concentrations

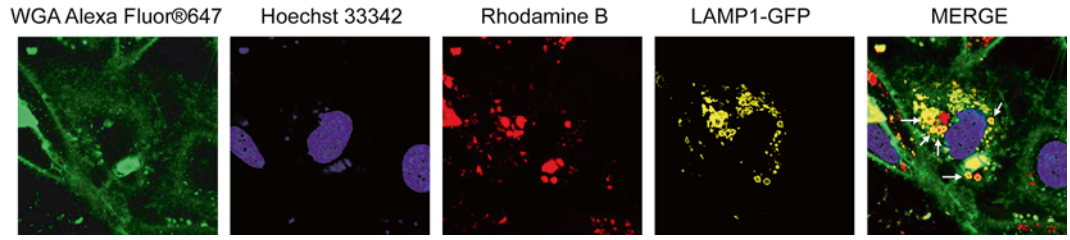

Fig. 3 Example of confocal images corresponding to HeLa cells treated with an MCM-41 nanoparticle loaded with Rhodamine B and containing a Glucidex39® molecular gate (S1). The *arrows* indicate colocalization among LAMP1-GFP vesicles and S1 proving the lysosomal localization of the nanoparticles

of the anticancer compounds introduced in the nanoparticle by cell viability measurements. Some of the most typical assays to achieve this objective are described.

Cell Viability Assay by WST-1

1. Plate HeLa cells in sterile 96-well microtiter plates at a seeding density of 2.5×10^3/well and allow to settle for 24 h.
2. Once the cells are attached, add the S1-P at concentrations of 50, 100, and 200 μg/mL.
3. After 23 and 47 h, add WST-1 (*see* **Note 9**) (10 μL, 5 mg/mL) to each well. Incubate cells for 1 h (a total of 24 or 48 h of incubation), and measure absorbance at 595 nm.

Annexin V and PI Stainings by Flow Cytometry

1. Plate HeLa cells at a final concentration of 2.5×10^4 cells/well in a 12-well plate.
2. 24 h later treat cells with 50, 100 and 200 μg/mL for 1 h and then change medium to eliminate the non-endocytosed nanoparticle.
3. After 24 and 48 h of incubation, trypsinize cells and centrifuge at $400 \times g$ for 5 min.
4. Resuspended the cells in 150 μL of Annexin V binding buffer containing Annexin V FITC (at a concentration according to manufacturer's indication) and incubate at 37 °C for 15 min.
5. Then, add 5 μL of PI (5 mg/mL) prior analysis through flow cytometry.

Cell Cycle Analysis by Flow Cytometry

1. Seed HeLa cells at a final concentration of 2.5×10^4 cells/well in a 12-well plate.
2. Once attached to the plate 24 h later, treat cells with 50, 100, and 200 μg/mL for 1 h and then change the medium to eliminate the nanoparticle.
3. After 24 and 48 h of incubation, trypsinize cells and centrifuge at $400 \times g$ for 5 min.

4. Fix the pellet obtained by adding 250 μL of a 80 % ice-cold EtOH solution drop by drop while stirring at medium speed. Place fixed cells at −20 °C 24 h to allow proper fixation.
5. Centrifuge cells at 400 × *g* for 5 min and wash once with PBS to remove the EtOH.
6. Resuspend in 200 μL of PBS containing RNAse (500 μg/μL) and propidium iodide (PI) (50 μg/mL) and incubate for 30 min at 37 °C.
7. Finally, analyze cells by flow cytometry.

4 Notes

1. Alternatively, removal of the surfactant can be achieved by refluxing the MCM-41 as-synthesized in a solution of EtOH/HCl 1 M for 48 h and subsequent centrifugation and washing of the solid obtained in deionized water till neutral pH (as described in Section 3.1.1, **step 3**) [9].
2. The functionalization of the surface of the nanoparticle can be achieved by: grafting (the one described above) and co-condensation, based on the functionalization of the nanoparticle after or during its synthesis, respectively. It is worthy to say that co-condensation allows a more homogeneous functionalization of the surface and inner side of the solid, but it does not permit the calcination of the material to remove the surfactant, as the organic molecules attached to the surface will also be destroyed [10, 11].
3. There are different strategies in order to determine the proper synthesis of silica mesoporous supports, the amount of cargo molecule in its pores and the degree of functionalization of its surface. For characterizing the structure of the MCM-41 material the techniques usually employed are:
   (a) *Powder X-ray diffraction*. For this characterization, 0.5 g of solid is smashed in an agate mortar and pestle in order to eliminate solid clods. The smashed solid is placed forming an homogeneus pill on the support that will be located in the X-ray diffractometer. MCM-41 material despite non presenting long length order structure as a crystalline material, it presents a series of unidirectional channels with a hexagonal disposition that give a series of peaks that can be indexed as (100), (110), (200) and (210). The detection of these peaks proves the maintenance of the structure of the material and it should be developed after each of the synthesis steps developed [20, 21]. In Fig. 2a an example of a typical X-ray pattern of MCM-41 material is depicted.

(b) *Transmission electron microscopy* (*TEM*). Complementing the X-ray diffraction technique, TEM employs an electron beam to visualize the nanoparticle [22]. The image is obtained from the electrons that go through the samples distributed in a metal grille in an ultrathin layer. Sample preparation is developed as follows:

- A few milligrams of MCM-41 material are resuspended in dichloromethane and sonicated for 5 min with the objective to eliminate nanoparticle aggregates.
- Suspension is added dropwise to a metal net that will act as support for the TEM analysis.
- Once the dichloromethane is evaporated, sample is introduced in the microscope. In Fig. 2b an example of TEM images corresponding to MCM-41 material is depicted.

(c) *N_2 adsorption–desorption isotherm*. For that purpose, 0.5 g of nanoparticles are needed. One key aspect for the success in this characterization process is the proper removal of the gas and vapors adsorbed onto the surface from the ambient air. Without changing the surface structure of the material, MCM-41 solid and the solid containing the cargo molecules and molecular gates are heated under conditions of dynamic vacuum or purging with an inert gassed to remove adsorbed or volatile compounds from the surface. These adsorption–desorption isotherms of N_2 are developed at the temperature of liquid N_2 and they allow us to calculate the specific area of the nanoparticle and the volume, the distribution and the size of the pores in the MCM-41 material [20, 22]. Equations of different mathematical models are employed to determine these values being the Brunauer–Emmet–Teller (BET) [23] one of the most commonly employed to determine the surface area and the Barrett–Joyner–Halenda (BJH) [24] the one commonly employed to calculate the pore size (*see* Fig. 2b).

The second part of the characterization of the nanoparticles synthesized is focused on determining the amount of cargo molecule and molecular gated present in the solid. In this case, the analysis developed are:

(d) *Thermogravimetry*. A known amount of solid ranging from 10 to 15 mg is introduced in crucibles and placed inside the thermogravimeter. Once introduced, sample will be submitted to an increase of temperature with time under a specific atmosphere and pressure. Changes in mass of the nanoparticle introduced during this process are monitored. This change in mass is due to the decomposition into gases of the water and organic molecules

contained in the material [25]. Three main peaks are found corresponding to the evaporation of the water contained in the material (approx. 100 °C), the decomposition of the organic material present in the molecular gate and cargo molecule (200–500 °C approx.) and the condensation of the silanol groups (1000 °C approx.) [15]. The remaining solid corresponds to SiO_2.

(e) *Elemental analysis.* A minimum amount of 3 mg of dried solid is employed per analysis. This technique is used to determine quantitatively the elements that constitute the material analyzed, particularly C, H, N and S. For that purpose, the material is burned in the presence of O_2 at 1000 °C and combustion products (CO_2, H_2O y N_2) are collected employing He as transporting gas, separated in different columns to individually detect its concentration in the initial mixture. With this information composition of the material is calculated.

4. Lysosomal extracts constitute a useful strategy to determine the possible degradation of the molecular gate and cargo release of the nanoparticle, previous testing it in cell models, due to the fact that all nanoparticles will be endocytosed by the cells and will reach the lysosomes at the end of the endosomal pathway.
5. The digitonin concentration and treatment times are optimized to result in the first step in the total release of cytosolic content of the cell without disrupting lysosomes. Then, in the second step the high dose of digitonin will assure the total lysis of the lysosomes to extract its content.
6. In case of compounds nonsoluble in water or lacking of a fluorescent or absorbance UV-Visible spectra, an alternative to determine the proper aperture mechanism of the molecular gate is the substitution of the cargo molecule by a fluorescent dye for characterization purposes (i.e., Rhodamine B, safranin O, …). Besides, in case of using molecules unable to be detected by fluorescence or UV-Visible absorbance alternative techniques can be employed to detect the cargo release, such as HPLC, RMN, or mass spectroscopy analysis.
7. Nanoparticle localization is usually tracked taking profit of the cargo associated fluorescence and the possible colocalization of the LAMP1-GFP signal and the signal corresponding to the nanoparticle are chased as indicators of the lysosomal localization of the nanoparticle. Alternatively, 3D stacks can be also done to prove the localization of the nanoparticles inside the cytoplasm of the cell in the absence of lysosomal markers.
8. As stated before, compounds employed as cargo molecules lacking of fluorescence will be substituted in this particular

experiment by fluorescent dyes for characterization purposes. As an alternative method, flow cytometry can be used to determine the internalization of the nanoparticle by measuring the fluorescence associated to the cargo molecule. However, in this case it is not possible discard if the nanoparticles remain attached to the membrane of the cell or if they are in its cytoplasm.

9. WST-1 is one example of tetrazolium salts able to measure NAD(P)H-dependent cellular oxidoreductase enzymes indicating if a cell is metabolically active. However, it is has been demonstrated that cells treated with nanoparticles tend to excrete tetrazolium salts such as 3-(4,5-dimethylthiazol-2-yl)-2,5-diphenyltetrazolium bromide (MTT) [26]. For that reason, it is recommended the use of WST-1 which is unable to cross the plasmatic membrane, but it is reduced to a water-soluble formazan by plasma membrane electron transport.

References

1. Heidel JD, Davis ME (2011) Clinical developments in nanotechnology for cancer therapy. Pharm Res 28(2):187–199
2. Duncan R, Gaspar R (2011) Nanomedicine(s) under the microscope. Mol Pharm 8(6): 2101–2141
3. Li ZX, Barnes JC, Bosoy A, Stoddart JF, Zink JI (2012) Mesoporous silica nanoparticles in biomedical applications. Chem Soc Rev 41(7): 2590–2605
4. Mamaeva V, Sahlgren C, Linden M (2013) Mesoporous silica nanoparticles in medicine - recent advances. Adv Drug Deliv Rev 65(5): 689–702
5. Coll C, Bernardos A, Martinez-Manez R, Sancenon F (2013) Gated silica mesoporous supports for controlled release and signaling applications. Acc Chem Res 46(2):339–349
6. Kresge CT, Leonowicz ME, Roth WJ, Vartuli JC, Beck JS (1992) Ordered mesoporous molecular sieves synthesized by a liquid-crystal template mechanism. Nature 359: 710–712
7. Attard GS, Glyde JC, Goltner CG (1995) Liquid-crystalline phases as templates for the synthesis of mesoporous silica. Nature 378(6555):366–368
8. Beck JS, Vartuli JC, Roth WJ, Leonowicz ME, Kresge CT, Schmitt KD, Chu CTW, Olson DH, Sheppard EW, McCullen SB, Higgins JB, Schlenker JL (1992) A new family of mesoporous molecular-sieves prepared with liquid-crystal templates. J Am Chem Soc 114(27): 10834–10843
9. Hoffmann F, Cornelius M, Morell J, Froba M (2006) Silica-based mesoporous organic-inorganic hybrid materials. Angew Chem Int Ed 45(20):3216–3251
10. Stein A, Melde BJ, Schroden RC (2000) Hybrid inorganic-organic mesoporous silicates - nanoscopic reactors coming of age. Adv Mater 12(19):1403–1419
11. Vinu A, Hossain KZ, Ariga K (2005) Recent advances in functionalization of mesoporous silica. J Nanosci Nanotechnol 5(3):347–371
12. Buolamwini JK (2000) Cell cycle molecular targets in novel anticancer drug discovery. Curr Pharm Des 6(4):379–392
13. McClue SJ, Blake D, Clarke R, Cowan A, Cummings L, Fischer PM, MacKenzie M, Melville J, Stewart K, Wang SD, Zhelev N, Zheleva D, Lane DP (2002) In vitro and in vivo antitumor properties of the cyclin dependent kinase inhibitor CYC202 (R-roscovitine). Int J Cancer 102(5):463–468
14. Fischer PM, Gianella-Borradori A (2005) Recent progress in the discovery and development of cyclin-dependant kinase inhibitors. Expert Opin Investig Drugs 14(4):457–477
15. Bernardos A, Mondragon L, Aznar E, Marcos MD, Martinez-Manez R, Sancenon F, Soto J, Barat JM, Perez-Paya E, Guillem C, Amoros P (2010) Enzyme-responsive intracellular controlled release using nanometric silica mesoporous supports capped with “saccharides”. ACS Nano 4(11):6353–6368
16. Coll C, Mondragon L, Martinez-Manez R, Sancenon F, Marcos MD, Soto J, Amoros P, Perez-Paya E (2011) Enzyme-mediated controlled release systems by anchoring peptide sequences on mesoporous silica supports. Angew Chem Int Ed 50(9):2138–2140

17. de la Torre C, Mondragón L, Coll C, Sancenón F, Marcos MD, Martínez-Máñez R, Amorós P, Pérez-Payá E, Orzáez M (2014) Cathepsin-B induced controlled release from Peptide-capped mesoporous silica nanoparticles. Chem Eur J 20(47):15309–15314
18. Dietrich N, Thastrup J, Holmberg C, Gyrd-Hansen M, Fehrenbacher N, Lademann U, Lerdrup M, Herdegen T, Jaattela M, Kallunki T (2004) JNK2 mediates TNF-induced cell death in mouse embryonic fibroblasts via regulation of both caspase and cathepsin protease pathways. Cell Death Differ 11(3):301–313
19. Mondragon L, Mas N, Ferragud V, de la Torre C, Agostini A, Martinez-Manez R, Sancenon F, Amoros P, Perez-Paya E, Orzaez M (2014) Enzyme-responsive intracellular-controlled release using silica mesoporous nanoparticles capped with e-poly-l-lysine. Chem Eur J 20(18):5271–5281
20. Kruk M, Jaroniec M, Kim JH, Ryoo R (1999) Characterization of highly ordered MCM-41 silicas using X-ray diffraction and nitrogen adsorption. Langmuir 15(16):5279–5284
21. Radu DR, Lai CY, Jeftinija K, Rowe EW, Jeftinija S, Lin VSY (2004) A polyamido-amine dendrimer-capped mesoporous silica nanosphere-based gene transfection reagent. J Am Chem Soc 126(41):13216–13217
22. Kruk M, Jaroniec M, Sakamoto Y, Terasaki O, Ryoo R, Ko CH (2000) Determination of pore size and pore wall structure of MCM-41 by using nitrogen adsorption, transmission electron microscopy, and X-ray diffraction. J Phys Chem B 104(2):292–301
23. Brunauer S, Emmet PH, Teller E (1938) Adsorption of gases in multimollecular layers. J Am Chem Soc 60:309
24. Barrett EP, Joyner LG, Halenda PP (1951) The determination of pore volume and area distributions in porous substances. I. Computations from nitrogen isotherms. J Am Chem Soc 73:373
25. Araujo AS, Jaroniec M (2000) Thermogravimetric monitoring of the MCM-41 synthesis. Thermochim Acta 363(1-2):175–180
26. Fisichella M, Dabboue H, Bhattacharyya S, Saboungi ML, Salvetat JP, Hevor T, Guerin M (2009) Mesoporous silica nanoparticles enhance MTT formazan exocytosis in HeLa cells and astrocytes. Toxicol In Vitro 23(4): 697–703

Chapter 13

Animal Models for Studying the In Vivo Functions of Cell Cycle CDKs

Sanjiv Risal, Deepak Adhikari, and Kui Liu

Abstract

Multiple Cdks (Cdk4, Cdk6, and Cdk2) and a mitotic Cdk (Cdk1) are involved in cell cycle progression in mammals. Cyclins, Cdk inhibitors, and phosphorylations (both activating and inhibitory) at different cellular levels tightly modulate the activities of these kinases. Based on the results of biochemical studies, it was long believed that different Cdks functioned at specific stages during cell cycle progression. However, deletion of all three interphase Cdks in mice affected cell cycle entry and progression only in certain specialized cells such as hematopoietic cells, beta cells of the pancreas, pituitary lactotrophs, and cardiomyocytes. These genetic experiments challenged the prevailing biochemical model and established that Cdks function in a cell-specific, but not a stage-specific, manner during cell cycle entry and the progression of mitosis. Recent in vivo studies have further established that Cdk1 is the only Cdk that is both essential and sufficient for driving the resumption of meiosis during mouse oocyte maturation. These genetic studies suggest a minimal-essential cell cycle model in which Cdk1 is the central regulator of cell cycle progression. Cdk1 can compensate for the loss of the interphase Cdks by forming active complexes with A-, B-, E-, and D-type Cyclins in a stepwise manner. Thus, Cdk1 plays an essential role in both mitosis and meiosis in mammals, whereas interphase Cdks are dispensable.

Key words Cell cycle, Cdk1, Cdk2, Cdk4, Cdk6, Cyclins, Cyclin-dependent kinases, Mitosis

1 Introduction

The cell cycle is the biological process through which cells duplicate themselves. The universal cell cycle events are S phase (DNA replication) and M phase (mitosis), and these are under the control of Cyclin-dependent kinases (Cdks) [1]. Cdk activity during these cell cycle phases is regulated by the binding of regulatory molecules known as Cyclins. The temporal regulation of Cdks is a unique feature of the cell cycle machinery in eukaryotes and depends on the oscillations of Cyclin levels and the phosphorylation state of the Cdks [2]. Mammalian cells contain at least 20 different Cdks, but only a few subsets of Cdk–Cyclin complexes are directly involved in cell cycle progression. These include three interphase kinases (Cdk4, Cdk6, and Cdk2), a mitotic Cdk (Cdk1,

Mar Orzáez et al. (eds.), *Cyclin-Dependent Kinase (CDK) Inhibitors: Methods and Protocols*, Methods in Molecular Biology, vol. 1336, DOI 10.1007/978-1-4939-2926-9_13,

also called M-Cdk) and ten Cyclins of four different classes (the A-, B-, D-, and E-type Cyclins) [2, 3]. Experiments in yeast have contributed to an in-depth understanding of cell cycle regulation, and these processes have been found to be highly conserved in mammalian cells.

According to the long prevailing model of the cell cycle based on biochemical evidence (*see* Fig. 1a), stage-specific Cdk–Cyclin complexes orchestrate the various events during interphase in a sequential manner. In response to mitogen cues, cells initiate DNA synthesis and this is marked by specific binding of D-type Cyclins (D1, D2, and D3) to Cdk4 and Cdk6 resulting in their activation during G1 phase [4, 5]. This 'preparatory' phosphorylation leads to partial inactivation of the retinoblastoma protein (RB) and its homologues (p107 and p130), and facilitates the transcription of E2F-dependent genes such as *Cyclin E* [6]. Subsequently, E-type Cyclins (E1 and E2) bind to and activate Cdk2 [7]. Further phosphorylation of RB is carried out by the Cdk2–Cyclin E complex leading its complete inactivation. Additionally, several studies have indicated that the Cdk2–Cyclin E complex is essential for driving the G1–S transition [8]. During late S phase, Cyclin-A2 (Cyclin-A1 in germ cells) activates Cdk2 and the cell enters the G2 phase. At the end of G2 phase, A-type Cyclins activate Cdk1 to facilitate the onset of mitosis (the M phase). Furthermore, the phosphorylation of CDH1 (a component of the anaphase-promoting complex (APC)) by the Cdk2–Cyclin A complex causes its abrupt dissociation from the APC and leads to an increased level of Cyclin B that is required for cell cycle progression through the G2–M transition [9]. Nuclear envelope breakdown and A-type Cyclins degradation precedes the formation of the Cdk1–Cyclin B complex, which is responsible for driving M phase [10]. Cyclin binding alone is not sufficient to make Cdks fully functional and complete activation of Cdks requires their phosphorylation at a threonine residue (Thr161 in Cdk1, Thr160 in Cdk2) located adjacent to the kinase active site by *C*dk-*a*ctivating *k*inase (CAK). In mammalian cells, CAK phosphorylates the Cdks only after binding of Cyclins [11]. The regulation of the timing and coordination of crucial cell cycle events, therefore, depends on the finely tuned interactions of Cyclins (positive regulators), Cdk inhibitors (negative regulators), and both activating and inhibitory phosphorylations.

1.1 Regulation of Cdks by Cyclins

In eukaryotic cells, Cyclins can be classified into G1-, G1/S-, S-, and M-Cyclins based on their specific functions and temporal expressions [12]. These specialized proteins bind to and activate Cdks in various phases of the cell cycle, and the Cdk–Cyclin complexes phosphorylate specific targets to ensure that cell cycle events occur in a timely manner. During the cell cycle, the levels of Cdks are held constant while the levels of Cyclins undergo cyclical fluctuations. The Cyclins that directly control cell cycle events are

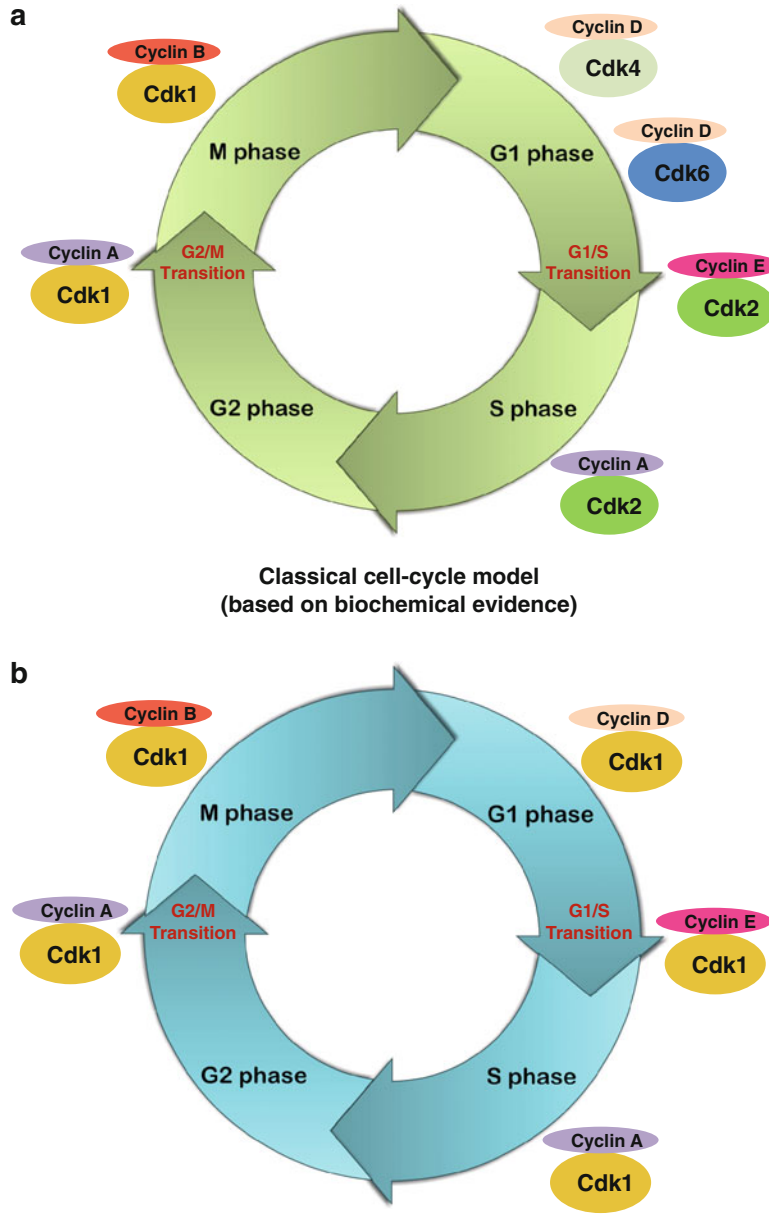

Fig. 1 Cell cycle models. (**a**) Diagram showing the classical cell cycle model (based on biochemical analysis) that shows stage-specific functions of Cdks during cell cycle progression. (**b**) The essential cell cycle model (based on genetic evidence) that shows Cdk1 is the only essential Cdk needed to drive all the cell cycle events by binding with different Cyclins in the absence of interphase Cdks

G1/S-, S-, and M-Cyclins, whereas the G1-Cyclins regulate cell cycle entry in response to extracellular cues. The D-type Cyclins typify the G1-Cyclins in mammals and their major catalytic partners are Cdk4 and Cdk6. Complexes of D-type Cyclins with Cdk4/6 are essential for exiting G1 and the initiation of S phase during the cell cycle [6]. Moreover, Cdk4/6-Cyclin D also regulates the expression of the E-type Cyclins. Levels of E-type Cyclins begin to rise in late G1 and decline in late S phase, which eventually initiates progression through the restriction point leading to DNA replication [2]. The commencement of S phase results in autophosphorylation of Cyclin E by the Cdk2–Cyclin E complex. The phosphorylated Cyclin E is then recognized by F-box protein FBW7 and is destined for proteasomal degradation [13]. This event allows A-type Cyclins (also known as S-Cyclins) to form complexes with Cdk2 to maintain DNA replication, and high levels of Cdk2 activity are maintained in S phase, G2 and early mitosis [14]. As the cell approaches mitosis, M-Cyclin (Cyclin B) comes into play and its activity peaks during metaphase. The major binding partner of Cyclin B is Cdk1 and the Cdk1–Cyclin B complex leads to mitotic spindle assembly and the alignment of sister chromatid on the metaphase plate [1, 15].

1.2 Regulation of Cdks by Cdk Inhibitors

The activity of the interphase and M-Cdks is regulated by the binding of Cdk inhibitors (CKIs). These polypeptide inhibitors of Cdks are categorized into two groups based on their specificities: the INK4 (*IN*hibitors of Cd*k4*) family and the CIP/KIP (*C*dk-*I*nteracting *P*rotein/*K*inase *I*nhibiting *P*rotein) family [11, 16]. The INK4 family includes four members ($p16^{INK4a}$, $p15^{INK4b}$, $p18^{INK4c}$, and $p19^{INK4d}$) that exclusively target Cdk4 and Cdk6. These highly conserved 15–19 kDa polypeptides are roughly 40 % homologous with each other, and it has been shown that mouse INK4 proteins share 90 % identity with those of humans [17]. INK4 proteins bind to Cdk4/6 and prevent phosphorylation of RB and thus promote cellular differentiation and inhibit inappropriate reentry into the cell cycle [18]. On the other hand, CIP/KIP family proteins ($p21^{CIP1/WAF1}$, $p27^{KIP1}$, and $p57^{KIP2}$) prefer to bind Cdk–Cyclin complexes involved in G1 and G1/S control, and their promiscuous nature allows them to interact with G1 Cdks [5, 17].

1.3 Regulation of Cdks by Phosphorylation

The activities of the major Cdks involved in cell cycle progression are modulated by phosphorylation at positive (activating phosphorylation) and negative (inhibitory phosphorylation) regulatory sites [19–22]. The activating phosphorylation of Cdk1, Cdk2, Cdk4, and Cdk6 is catalyzed by CAK, a complex of Cdk7, Cyclin H, and Mat1 (ménage à trois 1) [23, 24]. Cyclin H activates Cdk7 and Mat1 regulates the substrate specificity of the complex [25]. Studies of Cdk2 showed that threonine 160 (Thr161 in Cdk1) located in the

activation segment (T-loop) prevents binding of Cdk2 to its substrates. Phosphorylation of this segment enhances substrate binding by an additional 80- to 300-fold and leads to cell cycle progression [11, 12]. Conversely, further phosphorylation at threonine (Thr14) and tyrosine (Tyr15) of the Cdk2 and Cdk1 subunits inhibits the kinase activity of the Thr160/161-phosphorylated Cdk–Cyclin complexes [12, 19, 21, 22]. Crystallographic studies of Cdk2 showed that the inhibitory phosphorylation is Cyclin dependent, and that the phosphorylation alters the orientation of the catalytic site residues and the phosphates of ATP [12, 21]. The temporal regulation of mitosis entry by inhibitory phosphorylation is a unique feature of the cell cycle machinery [12, 26]. For example, inhibitory phosphorylation on Thr14 and Tyr15 of Cdk1 suppresses the activity of the Cdk1–Cyclin B complex during interphase. In mammalian cells, Wee1 and Myt1 kinases are responsible for the conserved Thr14 and Tyr15 phosphorylation activity. At the end of G2 phase, phosphatases abruptly dephosphorylate these residues leading to the activation of Cdk1 and subsequent entry of the cell into mitosis [27–29]. The tight coupling between activating and inhibitory phosphorylation of Cdk1 acts as a mitotic timer to prevent catastrophic mitotic failure [30].

2 Genetic Models for In Vivo Functional Studies of Cdks

The classical model of the cell cycle emphasizes the requirement of specific Cdks for each phase of cell cycle (*see* Fig. 1a). However, genetic experiments in cell cycle control in mice have challenged this concept and suggested that the functions of Cdks are cell-specific. Systematic loss-of-function studies in mice have given us a wealth of information regarding cell-specific roles of Cdks and their regulation at different cellular levels (Table 1).

2.1 Cdk4 and Cdk6 Knockout Mice

Two initially independent studies revealed the in vivo function(s) of Cdk4 in somatic cells [31, 32]. *Cdk4*$^{-/-}$ mice display normal viability with defects in some organs, a similar phenotype to that seen in *Cyclin D*$^{-/-}$ mice. The prominent phenotype of *Cdk4*$^{-/-}$ mice is both a small body size due to reduced cellularity compared to controls, and partial sterility. Despite a normal proliferation rate, *Cdk4*$^{-/-}$ *M*ouse *E*mbryonic *F*ibroblasts (MEFs) show delayed entry into S phase from their quiescence state. This is due to redistribution of p27, which attenuates Cdk2 activity. The double knockout of both *Cdk4* and *p27* demonstrated the importance of Cdk2 in normal S phase entry [32]. Additionally, pituitary hypoplasia and lactotroph (prolactin-producing cells) dysfunction occurs in *Cdk4*$^{-/-}$ mice [33]. In these types of cells, Cdk6 does not compensate for the loss of Cdk4 and might not even be expressed in these cells. In adult *Cdk4*$^{-/-}$ mice, degeneration of pancreatic beta cells

Table 1
Cdk mutant mouse models exhibiting cell-specific phenotypes

Mouse models	Phenotypes	References
Cdk1	Embryos die before E3.5	[48, 49]
Cdk2	Meiotic failure; Sterile	[42, 45]
Cdk4	Small body size due to reduced cellularity; Decreased pancreatic beta cells resulting in diabetes; Both sexes are infertile due to perturbed neuro-endocrine dysfunction	[31, 32]
Cdk6	Low cellularity in the thymus and spleen combined with mild anemia	[38]
Cdk4/6	Compromised maturation of erythroid precursor cells and severe anemia; Perhaps sterile, similar to $Cdk4^{-/-}$	[38]
Cdk2/4	Cardiomyocyte proliferation defects; Might be sterile, similar to $Cdk2^{-/-}$	[36]
Cdk2/6	Reduced body size; Hematopoietic defects; Male and female infertility	[38]
Cdk2/4/6	Heart and hematopoietic defects; Might be sterile, similar to $Cdk2^{-/-}$	[48]
Cdk1 (Oocyte-specific)	Normal body size; Female infertile; Meiotic maturation failure	[47]
Cdk2 (Oocyte-specific)	Normal body size; Female fertile; Normal meiotic profile	[47]

resulted in a reduced cellularity of the pancreas leading to the development of diabetes mellitus in 80 % of the mutant mice. Besides exhibiting endocrine dysfunctions, $Cdk4^{-/-}$ mice also display compromised fertility in both sexes. The male mutant suffer from testicular atrophy contributing to impaired spermatogenesis, whereas in females corpus luteum formation and ovulation are compromised rendering them infertile [31, 32]. The infertility in these mice is caused by perturbation of the neuro-endocrine axis in the absence of Cdk4 as opposed to developmental abnormalities of their gonads per se [31, 33]. The cell cycle inhibitor $p16^{INK4a}$ inhibits Cdk4 activity and prevents the phosphorylation of RB proteins [34]. Furthermore, the missense mutation of *Cdk4* that replaces arginine 24 with a cysteine (R24C) abrogates inhibition of Cdk4 by $p16^{INK4a}$ without hindering binding of Cdk4 to D-type Cyclins. Generation of $Cdk4^{R24C/R24C}$ mice corroborated the results from $Cdk4^{-/-}$ mice and highlighted the highly specific role of Cdk4 in pancreatic beta cell proliferation and the maintenance of glucose homeostasis [31].

The results with *Cdk4* knockout mice raised the question of whether or not *Cdk2* could compensate for the loss of *Cdk4* in the

mammalian cell cycle. This was based on the fact that both of these genes are involved in the G1–S transition and there is the general notion that the lack of individual Cdks is compensated for by other Cdks [3]. Experiments with the *Cdk4/Cdk2* double mutant showed the intricate roles these kinases play in mammalian cell cycle regulation. The predominant phenotype of these mutants is cardiac insufficiency due to their limited number of cardiomyocytes, which is caused by incomplete inactivation of the RB protein [36]. The diminished phosphorylation of RB resulted in suppression of E2F-dependent genes such as *Cdk1* and *Cyclin A2*. The subsequently reduced Cdk1 expression level and failure of *Cdk6* to compensate for the lack of *Cdk4* and *Cdk2* resulted in defective cell proliferation in the *Cdk4/Cdk2* double mutant. This shows that *Cdk4* and *Cdk2* are crucial for embryonic cardiomyocyte proliferation whereas these kinases appear to be dispensable in other cell types and these two kinases cooperate to drive G1–S transition with mitosis [35, 36].

Cdk6 is widely distributed in mammalian tissues but is most prominent in lymphoid tissues [37]. Genetic studies in mice have revealed its specific function in the expansion of differentiated hematopoietic cells of erythroid lineage. Deletion of *Cdk6* resulted in delayed G1 progression in lymphocytes, lower cellularity in the thymus and spleen, and mild anemia [38]. Nevertheless, the combined deletion of *Cdk2* and *Cdk6* had no effect on cell proliferation and revealed no synergism between Cdk6 and Cdk2 in driving cells through the G1–S transition. The phenotype of these mutants were similar to that of the *Cdk6* and *Cdk2* single mutants with limited hematopoietic defects and male and female sterility, respectively [38].

Whether or not any compensatory mechanism exists between Cdk4 and Cdk6 in the cell cycle has been highlighted by the study of the *Cdk4/Cdk6* double knockout. Cdk4 and Cdk6 are functionally similar kinases that bind D-type Cyclins but govern different stages of erythroid maturation [39]. The *Cdk4/Cdk6* double mutant exhibits late embryonic and postnatal lethality but normal cell proliferation kinetics. The cause of this phenotype is a lack of maturation of erythroid precursor cells that results in severe anemia. Based on the evidence from these genetic experiments, it can be assumed that these Cdks are dispensable in embryogenesis and are not involved in exiting cells from their quiescence state during cell cycle progression. In agreement with these observations, MEFs lacking both *Cdk4* and *Cdk6* showed normal proliferation and cell cycle profiles, which is similar to the phenotype of mice lacking the three D-type Cyclins [40]. In conclusion, Cdk4 and Cdk6 only play roles in cell cycle progression in specialized cells, such as hematopoietic cells [38, 41] and are dispensable in all other cell types.

2.2 Cdk2 Knockout Mice

Several lines of evidence indicate that Cdk2 governs the G1–S transition (in association with E-type Cyclins), S phase progression (in association with A-type Cyclins), progression to G2 phase, and, perhaps, mitotic entry [12, 42]. It has also been suggested that Cdk2 has specific roles in centrosome duplication [43], histone synthesis, and chromatin assembly [44]. These observations all portrayed Cdk2 as an essential regulator of the cell cycle for the majority of, if not all, somatic cells. However, deletion of *Cdk2* in mice has refuted this idea and demonstrated that this seemingly crucial cell cycle kinase is dispensable for cell proliferation and development [42, 45]. Surprisingly, *Cdk2*$^{-/-}$ mice are viable without any developmental anomalies, but display delayed S phase entry and dramatic meiotic failure [42, 45]. The obvious phenotype of *Cdk2*-deficient mice is infertility in both sexes with 100 % penetrance, emphasizing the essential role of Cdk2 in germ cell development beyond meiotic prophase I.

The germ cells of *Cdk2*$^{-/-}$ males are arrested at the pachytene stage of prophase I. This results in increased apoptosis of primary spermatocytes combined with defective synaptonemal complex formation [45]. On the other hand, the oocytes at embryonic day 14.5–18.5 (E14.5–E18.5) had normal meiotic profiles with dictyate stage progression, normal synapsis, and apoptosis. *Cdk2*$^{-/-}$ females displayed postnatal meiotic defects with improper distribution of synaptonemal complex protein 3 (a marker for the axial elements). Additionally, the ovarian morphology of prepubertal and adult mutant mice showed a depletion of functional oocytes along with an increase in apoptotic cells that resulted in ovarian atrophy [45]. Even when Cdk1 was expressed from the Cdk2 locus, male and female sterility could not be rescued in these genetically modified mice [46]. These studies indicate that Cdk2 is essential for cell cycle progression in germ cells in mice and that this function cannot be complemented by Cdk1. Deletion of *Cdk2* from growing oocytes in mice shows the dispensability of Cdk2 in meiotic maturation and metaphase II arrest [47], but any roles of Cdk2 in early germ cell development in mice still remain to be tested.

2.3 Cdk1 Knockout Mice

The idea of a minimally essential Cdk in mammalian cells, such as is found in yeast, emerged from the results showing the dispensability of all interphase Cdks in mice [3, 48]. The triple knockout *Cdk4*$^{-/-}$; *Cdk6*$^{-/-}$; *Cdk2*$^{-/-}$ MEFs show complete cell cycle progression, albeit with some delay in entry into different cell cycle stages. Moreover, the deletion of *Cdk4*, *Cdk6*, and *Cdk2* did not affect the expression levels of Cdk1, Cdk7, Cdk9 or Cyclins (D1, D2, E1, A2, and B1), and the phosphorylation of RB at all four serine residues that are targets for the interphase Cdks was normal [48]. It was found that Cdk1 binds to all Cyclins, phosphorylates RB in the absence of these interphase Cdks, and causes the cells to leave their quiescent state [42]. Thus, Cdk1 is the only essential Cdk for

cell division as *Cdk1*-null embryos fail to undergo even the early stages of development and die before E3.5, and *Cdk1*-null MEFs undergo premature senescence [48, 49].

A recent study used liver as an in vivo model to establish the function of Cdk1 in hepatocytes, which are terminally differentiated cell types that do not divide in adults [49]. The absence of Cdk1 in hepatocytes renders them unable to enter into mitosis, indicating that regeneration of liver can occur after partial hepatectomy without cell division [49]. To understand the underlying mechanism behind this, BrdU incorporation assays showed that *Cdk1*-null hepatic cells undergo some form of DNA replication. Moreover, loss of *Cdk1* in these cells does not affect DNA replication in a wild-type Cdk2 background, but these cells are arrested at G2 phase and fail to enter into mitosis [49]. Approximately 30 % of *Cdk1*-null cells undergo DNA re-replication. This is due to Cdk2 activity because knocking down of *Cdk2* in *Cdk1*-null cells significantly reduces the re-replication phenotype [49]. Furthermore, these studies also revealed that Cdk1 regulates Cdk2 activity by sequestering Cyclin A2 and preventing re-replication during late S phase. Concomitant deletion of *Cdk1* with partial hepatectomy resulted in polyploidy, perhaps because of re-replication. Thus, this study suggests another layer of regulatory mechanisms for Cdk1 during cell cycle progression [49].

The above-mentioned studies have provided a wealth of information regarding functions of different Cdks in dividing cells such as hematopoietic cells, pancreatic beta cells, and pituitary lactotrophs. However, such details regarding the specific requirements of Cdks in case of non-dividing cells like oocytes had been lacking. In mammals, growing oocytes are arrested at prophase I of meiosis. The resumption of meiosis takes place with the preovulatory surge of luteinizing hormones, which is sequentially marked by germinal vesicle (GV) breakdown (GVBD), chromosome condensation, spindle formation, and the completion of meiosis I [47, 50]. Moreover, spontaneous meiosis resumption takes place when oocytes are liberated into suitable culture medium where they undergo meiosis II arrest until fertilization [50, 51]. Oocytes are mitotically inactive cells, but oocytes arrested at the GV stage are considered analogous to somatic cells at the G2–M transition phase of mitosis [52]. Furthermore, Cdk1 orchestrates the G2–M transition in dividing cells as demonstrated by several studies [46, 48, 49]. Nonetheless, such studies have not been extended to non-dividing cells like oocytes. Recently, this issue has been addressed by generating an oocyte-specific knockout of *Cdk1* in mice [47]. This study revealed that Cdk1 is a central regulator for driving the resumption of meiosis in mouse oocytes as the deletion of *Cdk1* from oocytes causes permanent arrest at the GV stage and renders females infertile. In mouse oocytes, Cdk1 phosphorylates PP1 (protein phosphatase 1) and suppresses its phosphatase activity. This maintains

the phosphorylation of lamin A/C and eventually leads to GVBD and the resumption of meiosis [47]. Thus, the evidence provided by these recent studies suggests that Cdk1 is the only essential Cdk that is sufficient to drive both mitosis and meiosis [53].

3 Concluding Remarks

The Cdk family of serine/threonine kinases is made up of 20 proteins, of which only a few subsets have been shown to directly participate in cell cycle progression. The biological functions of these kinases are regulated by Cyclin binding, CKIs, and phosphorylation. More than two decades ago, a cell cycle model was proposed that was based solely on the biochemical analysis of egg extracts from different animal species. This cell cycle dogma claimed that specific Cdks are responsible for governing each phases of the cell cycle. However, genetic studies of deletions of different Cdks in mice challenges this biochemical cell cycle model. The interphase Cdks (Cdk4, Cdk6, and Cdk2) are not essential for cell cycle progression, but are stringently necessary for some specialized cells such as germ cells, hematopoietic precursor cells, pituitary lactotrophs, and pancreatic beta cells. Additionally, a new role for Cdk1 has emerged from these studies as a master regulator of the basic cell cycle machinery that can compensate for the absence of all interphase-Cdks in mammalian cells (*see* Fig. 1b). Moreover, Cdk1 has been found to be the only essential Cdk even for the resumption of meiosis in oocytes. Thus, both the mitosis and meiosis are driven by Cdk1. Further research is clearly needed towards delineating the regulatory mechanisms that ensure the precise spatial and temporal activation of Cdks in the specific cell types.

References

1. Nurse P (1990) Universal control mechanism regulating onset of M-phase. Nature 344(6266):503–508
2. Malumbres M, Barbacid M (2009) Cell cycle, CDKs and cancer: a changing paradigm. Nat Rev Cancer 9(3):153–166
3. Satyanarayana A, Kaldis P (2009) Mammalian cell-cycle regulation: several Cdks, numerous cyclins and diverse compensatory mechanisms. Oncogene 28(33):2925–2939
4. Massague J (2004) G1 cell-cycle control and cancer. Nature 432(7015):298–306
5. Sherr CJ, Roberts JM (1999) CDK inhibitors: positive and negative regulators of G1-phase progression. Genes Dev 13(12):1501–1512
6. Lundberg AS, Weinberg RA (1998) Functional inactivation of the retinoblastoma protein requires sequential modification by at least two distinct cyclin-cdk complexes. Mol Cell Biol 18(2):753–761
7. Harbour JW, Luo RX, Santi AD, Postigo AA, Dean DC (1999) Cdk phosphorylation triggers sequential intramolecular interactions that progressively block Rb functions as cells move through G1. Cell 98(6):859–869
8. Hochegger H, Takeda S, Hunt T (2008) Cyclin-dependent kinases and cell-cycle transitions: does one fit all? Nat Rev Mol Cell Biol 9(11):910–916
9. Sørensen CS, Lukas C, Kramer ER, Peters J-M, Bartek J, Lukas J (2001) A conserved cyclin-binding domain determines functional interplay between anaphase-promoting complex–Cdh1

and Cyclin A-Cdk2 during cell cycle progression. Mol Cell Biol 21(11):3692–3703

10. Malumbres M, Barbacid M (2005) Mammalian cyclin-dependent kinases. Trends Biochem Sci 30(11):630–641
11. Morgan DO (1995) Principles of CDK regulation. Nature 374(6518):131–134
12. Morgan DO (1997) Cyclin-dependent kinases: engines, clocks, and microprocessors. Annu Rev Cell Dev Biol 13:261–291
13. Koepp DM, Schaefer LK, Ye X, Keyomarsi K, Chu C, Harper JW, Elledge SJ (2001) Phosphorylation-dependent ubiquitination of cyclin E by the SCFFbw7 ubiquitin ligase. Science 294(5540):173–177
14. Pagano M, Pepperkok R, Verde F, Ansorge W, Draetta G (1992) Cyclin A is required at two points in the human cell cycle. EMBO J 11(3): 961–971
15. Sherr CJ, Roberts JM (2004) Living with or without cyclins and cyclin-dependent kinases. Genes Dev 18(22):2699–2711
16. Tanner FC, Boehm M, Akyürek LM, San H, Yang Z-Y, Tashiro J, Nabel GJ, Nabel EG (2000) Differential effects of the cyclin-dependent kinase inhibitors p27Kip1, p21Cip1, and p16Ink4 on vascular smooth muscle cell proliferation. Circulation 101(17):2022–2025
17. Roussel MF (1999) The INK4 family of cell cycle inhibitors in cancer. Oncogene 18(38): 5311–5317
18. Buchold GM, Magyar PL, Arumugam R, Lee MM, O'Brien DA (2007) p19Ink4d and p18Ink4c cyclin-dependent kinase inhibitors in the male reproductive axis. Mol Reprod Dev 74(8):997–1007
19. Kaldis P, Sutton A, Solomon MJ (1996) The Cdk-activating kinase (CAK) from budding yeast. Cell 86(4):553–564
20. Gould KL, Moreno S, Owen DJ, Sazer S, Nurse P (1991) Phosphorylation at Thr167 is required for Schizosaccharomyces pombe p34cdc2 function. EMBO J 10(11):3297–3309
21. De Bondt HL, Rosenblatt J, Jancarik J, Jones HD, Morgant DO, Kim S-H (1993) Crystal structure of cyclin-dependent kinase 2. Nature 363(6430):595–602
22. Kaldis P (1999) The cdk-activating kinase (CAK): from yeast to mammals. Cell Mol Life Sci 55(2):284–296
23. Desai D, Wessling HC, Fisher RP, Morgan DO (1995) Effects of phosphorylation by CAK on cyclin binding by CDC2 and CDK2. Mol Cell Biol 15(1):345–350
24. Fisher RP (2005) Secrets of a double agent: CDK7 in cell-cycle control and transcription. J Cell Sci 118(22):5171–5180
25. Yankulov KY, Bentley DL (1997) Regulation of CDK7 substrate specificity by MAT1 and TFIIH. EMBO J 16(7):1638–1646
26. Dunphy WG (1994) The decision to enter mitosis. Trends Cell Biol 4(6):202–207
27. Mueller PR, Coleman TR, Kumagai A, Dunphy WG (1995) Myt1: a membrane-associated inhibitory kinase that phosphorylates Cdc2 on both threonine-14 and tyrosine-15. Science 270(5233):86–90
28. Fattaey A, Booher RN (1997) Myt1: a Wee1-type kinase that phosphorylates Cdc2 on residue Thr14. Prog Cell Cycle Res 3:233–240
29. Lew DJ, Kornbluth S (1996) Regulatory roles of cyclin dependent kinase phosphorylation in cell cycle control. Curr Opin Cell Biol 8(6):795–804
30. Coulonval K, Kooken H, Roger PP (2011) Coupling of T161 and T14 phosphorylations protects cyclin B–CDK1 from premature activation. Mol Biol Cell 22(21):3971–3985
31. Rane SG, Dubus P, Mettus RV, Galbreath EJ, Boden G, Reddy EP, Barbacid M (1999) Loss of Cdk4 expression causes insulin-deficient diabetes and Cdk4 activation results in [beta]-islet cell hyperplasia. Nat Genet 22(1):44–52
32. Tsutsui T, Hesabi B, Moons DS, Pandolfi PP, Hansel KS, Koff A, Kiyokawa H (1999) Targeted disruption of CDK4 delays cell cycle entry with enhanced p27Kip1 activity. Mol Cell Biol 19(10):7011–7019
33. Moons DS, Jirawatnotai S, Parlow AF, Gibori G, Kineman RD, Kiyokawa H (2002) Pituitary hypoplasia and lactotroph dysfunction in mice deficient for cyclin-dependent kinase-4. Endocrinology 143(8):3001–3008
34. Sherr CJ (2001) The INK4a/ARF network in tumour suppression. Nat Rev Mol Cell Biol 2(10):731–737
35. Berthet C, Klarmann KD, Hilton MB, Suh HC, Keller JR, Kiyokawa H, Kaldis P (2006) Combined loss of Cdk2 and Cdk4 results in embryonic lethality and Rb hypophosphorylation. Dev Cell 10(5):563–573
36. Berthet C, Kaldis P (2006) Cdk2 and Cdk4 cooperatively control the expression of Cdc2. Cell Div 1:10
37. Meyerson M, Harlow E (1994) Identification of G1 kinase activity for cdk6, a novel cyclin D partner. Mol Cell Biol 14(3):2077–2086
38. Malumbres M, Ro S, Santamaría D, Galán J, Cerezo A, Ortega S, Dubus P, Barbacid M (2004) Mammalian cells cycle without the D-type cyclin-dependent kinases Cdk4 and Cdk6. Cell 118(4):493–504
39. Matushansky I, Radparvar F, Skoultchi AI (2000) Reprogramming leukemic cells to terminal differentiation by inhibiting specific

cyclin-dependent kinases in G1. Proc Natl Acad Sci 97(26):14317–14322

40. Kozar K, Ciemerych MA, Rebel VI, Shigematsu H, Zagozdzon A, Sicinska E, Geng Y, Yu Q, Bhattacharya S, Bronson RT, Akashi K, Sicinski P (2004) Mouse development and cell proliferation in the absence of D-cyclins. Cell 118(4): 477–491
41. Barrière C, Santamaría D, Cerqueira A, Galán J, Martín A, Ortega S, Malumbres M, Dubus P, Barbacid M (2007) Mice thrive without Cdk4 and Cdk2. Mol Oncol 1(1):72–83
42. Berthet C, Aleem E, Coppola V, Tessarollo L, Kaldis P (2003) Cdk2 knockout mice are viable. Curr Biol 13(20):1775–1785
43. Meraldi P, Lukas J, Fry AM, Bartek J, Nigg EA (1999) Centrosome duplication in mammalian somatic cells requires E2F and Cdk2-cyclin A. Nat Cell Biol 1(2):88–93
44. Ma T, Van Tine BA, Wei Y, Garrett MD, Nelson D, Adams PD, Wang J, Qin J, Chow LT, Harper JW (2000) Cell cycle-regulated phosphorylation of p220(NPAT) by cyclin E/Cdk2 in Cajal bodies promotes histone gene transcription. Genes Dev 14(18):2298–2313
45. Ortega S, Prieto I, Odajima J, Martin A, Dubus P, Sotillo R, Barbero JL, Malumbres M, Barbacid M (2003) Cyclin-dependent kinase 2 is essential for meiosis but not for mitotic cell division in mice. Nat Genet 35(1):25–31
46. Satyanarayana A, Berthet C, Lopez-Molina J, Coppola V, Tessarollo L, Kaldis P (2008) Genetic substitution of Cdk1 by Cdk2 leads to embryonic lethality and loss of meiotic function of Cdk2. Development 135(20): 3389–3400
47. Adhikari D, Zheng W, Shen Y, Gorre N, Halet G, Kaldis P, Liu K (2012) Cdk1, but not Cdk2, is the sole Cdk that is essential and sufficient to drive resumption of meiosis in mouse oocytes. Hum Mol Genet 21(11):2476–2484
48. Santamaria D, Barriere C, Cerqueira A, Hunt S, Tardy C, Newton K, Caceres JF, Dubus P, Malumbres M, Barbacid M (2007) Cdk1 is sufficient to drive the mammalian cell cycle. Nature 448(7155):811–815
49. Diril MK, Ratnacaram CK, Padmakumar VC, Du T, Wasser M, Coppola V, Tessarollo L, Kaldis P (2012) Cyclin-dependent kinase 1 (Cdk1) is essential for cell division and suppression of DNA re-replication but not for liver regeneration. Proc Natl Acad Sci 109(10):3826–3831
50. Adhikari D, Liu K (2009) Molecular mechanisms underlying the activation of mammalian primordial follicles. Endocr Rev 30(5):438–464
51. Mehlmann LM (2005) Stops and starts in mammalian oocytes: recent advances in understanding the regulation of meiotic arrest and oocyte maturation. Reproduction 130(6):791–799
52. Solc P, Schultz RM, Motlik J (2010) Prophase I arrest and progression to metaphase I in mouse oocytes: comparison of resumption of meiosis and recovery from G2-arrest in somatic cells. Mol Hum Reprod 16(9):654–664
53. Adhikari D, Liu K, Shen Y (2012) Cdk1 drives meiosis and mitosis through two different mechanisms. Cell Cycle 11(15)

Chapter 14

Evaluating Chemical CDK Inhibitors as Cell Death Inducers

Hiroshi Hirai and Yoko Nakatsuru

Abstract

The cell cycle of eukaryotic cells is regulated by a family of protein kinases called cyclin-dependent kinases (Cdks). We have reported the identification and biological characterization of a highly potent, small-molecule pan-Cdk inhibitor, which inhibited Cdk1, 2, 4, 5, 6, and 9 with equal potency in the nM range. This compound inhibited multiple events in the cell cycle and induced cell death in human cancer cell lines as well as in peripheral blood or purified resting lymphocytes ex vivo. We describe the materials and methods to determine antitumor efficacy in vivo xenograft models. Pharmacodynamic marker assays that have been performed using tumors and normal tissues are explained. Moreover, we briefly describe methods for determining the effects of chemical Cdk inhibitors on peripheral blood cells or lymphocytes ex vivo.

Key words Antitumor efficacy, Cdk inhibitor, Immunohistochemistry (IHC) assay, In vivo xenograft model, In vivo pharmacodynamics (PD) assay, Lymphocytes, Peripheral blood cells

1 Introduction

The cell cycle of eukaryotic cells is regulated by a family of protein kinases called cyclin-dependent kinases (Cdks). In mammalian cells, multiple cyclin/Cdk complexes participate in the progression of the cell cycle. Namely, cyclin D-Cdk4, cyclin D-Cdk6, cyclin E-Cdk2, and cyclin A-Cdk2 regulate the progression from the G0/G1 phase through to the S phase. The progression from the G2 to the M phase is regulated by another type of Cdk, the cyclin B-Cdk1 (Cdc2) complex. Cyclin B-Cdc2 phosphorylates and activates key regulators of the M phase [1–6].

In addition to cell cycle regulation, Cdks participate in various cellular processes. Cdk7-cyclin H and Cdk9-cyclin T complexes are components of the transcription factors TFIIH and Positive Transcription Elongation Factor b (P-TEFb), respectively. These factors phosphorylate the carboxy-terminal domain (CTD) of RNA polymerase II, which is important for the elongation of transcription [7–9]. Cdk5/p35 or p39 complexes have numerous functions in the nervous system, including neuritis outgrowth and neuron migration,

Mar Orzáez et al. (eds.), *Cyclin-Dependent Kinase (CDK) Inhibitors: Methods and Protocols*, Methods in Molecular Biology, vol. 1336, DOI 10.1007/978-1-4939-2926-9_14,

and in the metabotropic glutamate receptor and dopamine signaling pathways [10]. In addition, Cdk5 appears to have a prominent role in promoting insulin secretion in pancreatic β-cells [11].

We have reported the identification and biological characterization of a highly potent, small-molecule pan-Cdk inhibitor, Compound M [12]. This compound inhibited Cdk1, 2, 4, 5, 6, and 9 with equal potency in the nM range and was selective against kinases other than Cdks. Compound M inhibited multiple events in the cell cycle in vitro, including retinoblastoma protein (pRb) phosphorylation, E2F-dependent transcription, DNA replication (determined using bromodeoxyuridine (BrdU) incorporation), and mitosis completion (assayed using flow cytometry) in the 10-nM range. Moreover, this compound induced cell death, as determined by the induction of the subG1 fraction, and activated caspase-3 and annexin V. In a nude rat xenograft tumor model, an 8-h constant infusion of Compound M inhibited pRb phosphorylation and induced apoptosis in HCT116 human colorectal cancer cells at ~30 nM, leading to the inhibition of tumor growth. In our studies, the suppression of pRb phosphorylation in tumor cells was clearly correlated with tumor cell growth inhibition and cell death both in vitro and in vivo. Compound M inhibited pRb phosphorylation in both tumor and gut crypt cells. Thus, pRb phosphorylation may be a suitable pharmacodynamics (PD) biomarker in both tumors and normal tissues for monitoring target engagement and predicting the efficacy of Compound M.

Interestingly, pan-Cdk inhibitors induced cell death in peripheral blood or purified resting (non-stimulated) lymphocytes ex vivo. Cell death was induced very rapidly (after 4 h of incubation), suggesting that the acute immunosuppression observed in rodents might be due, at least in part, to direct cytotoxic effects of pan-Cdk inhibitors on resting lymphocytes [13].

In this section, we describe the materials and methods used to determine antitumor efficacy by monitoring the tumor size. In addition, we explain the PD marker assays that have been performed using tumors and normal tissues in xenograft models. Moreover, we briefly describe methods for determining the effects of Cdk inhibitors on peripheral blood cells or lymphocytes ex vivo.

2 Materials

2.1 Animal Experiments

1. Animals: Nude mice, nude rats, SCID-mice, and NOD-SCID mice are immunodeficient rodents that are generally used in animal xenograft cancer models (*see* **Notes 1–3**). In general, the animals were bred under the following housing conditions: temperature, 23 ± 2 °C; relative humidity, 55 ± 15 %; illumination, 12 h; diet, CE-2; and housing method, ~ 4 rats/cage. In the case of nude rats, female 6–7-week-old F344 nude rats with 100–150 *g* of body weight were generally used.

2. Cannulation and intravenous (IV) dosing: isoflurane for anesthetization, custom infusion kits (INSTECH Co. Ltd., KVAH95T).
3. Tumor volume measurements: a digital caliper.
4. Blood cell count: potassium-EDTA coated syringe, automated hematology analyzer (SF-3000; Sysmex).

2.2 Determination of pRb Phosphorylation in Xenograft Tumor Samples Using a Western Blot

1. Glycerophosphate buffer: 50 mM glycerophosphate, pH 7.5, 250 mM NaCl, 5 mM EDTA, 1 % NP-40, 0.1 % Triton X-100, 10 mM sodium fluoride, 2 mM sodium vanadate, and proteinase inhibitors (5 μg/mL of leupeptin, pepstatin, antipain, chymostatin, and E64).
2. Protein assay: BCA protein assay (Pierce).
3. Antibodies and other reagents: Anti-Rb antibody; MK-15-1 from MBL, Protein G agarose, Anti-phospho Rb antibody (Ser780); #9307S; Cell Signaling Technology.
4. 5× SDS Buffer: 625 mM Tris–HCl [pH 7.5], 10 % sodium dodecyl sulfate (SDS), 25 % β-mercaptoethanol, 5 % glycerol, and bromophenol blue (BPB).
5. Polyvinylidene fluoride (PVDF) membrane.
6. Reagents for immunoblotting: PBS containing 1 % Tween 20, Blocking solution; 5 % skim milk in PBS containing 1 % Tween 20, horseradish peroxidase (HRP)-linked anti-rabbit IgG, ECL system.

2.3 Determination of BrdU Incorporation in Xenografted Tumor by Using Immunohistochemistry (IHC) Assays

1. BrdU.
2. Target Retrieval Solution (DAKO).
3. MOM Mouse IgG Blocking Reagent (Vector Laboratories), MOM immunodetection kit (Vector Laboratories).
4. Antibodies: Anti-BrdU antibody; Cat #347580; Beckton Dickinson, Anti-phosphor-Rb (Ser807/811) Ab; #9308; Cell Signaling Technology, Anti-activated caspase 3 Ab; #9661; Cell Signaling Technology.
5. PBS containing 10 % normal goat serum and 3 % bovine serum albumin.
6. Goat anti-rabbit IgG H&L-biotin conjugate, VECTASTAIN Elite ABC kit (Vector Laboratories).

2.4 Isolation of Lymphocytes for Ex Vivo Experiments Using Peripheral Blood or Isolated Lymphocytes

1. Balanced salt solution; 0.13 M NaCl, 0.01 % glucose, 5.0 mM $CaCl_2$, 98 mM $MgCl_2$, 0.54 mM KCl, and 15 mM Tris–HCl (pH 7.6).
2. Ficoll-Paque Plus.
3. IOTest 3 Lysing Solution (Beckman Coulter).
4. For stimulation; 10 ng/mL of phorbol 12-myristate 13-acetate (PMA) and 1 μM of Ionomycin.

2.5 Cell Cycle and Cell Death Assays of Whole Peripheral Blood Cells or Isolated Lymphocytes

1. CycleTEST PLUS DNA Reagent Kit (Becton Dickinson).
2. Apo-ONE Homogeneous Caspase-3/7 Assay kit (Promega).
3. Lysis buffer (CelLytic™ M; Sigma-Aldrich), protease inhibitor cocktail, Halt Phosphatase Inhibitor Cocktail.

3 Methods

3.1 Determination of Antitumor Efficacy Using Animal Models (see Notes 4–8)

All the animal experiments were performed in accordance with good animal practices, as defined by the International Animal Care and Used Committee (IACUC). The inoculation of human cancer cell lines or the dosing of compounds was started at least 1 week after purchase for quarantine purposes. In our experiments, human colorectal cancer cell line, HCT-116 was used.

1. Grow HCT116 cells to a semi-confluent cell density. Then treat the cells with trypsin, resuspend them in DMEM containing 10 % FBS and collect them by centrifugation.
2. Wash the cells with phosphate buffered saline (PBS), and finally suspend in PBS at 1×10^8 cells/mL.
3. Anesthetize nude rats via isoflurane inhalation. HCT116 cells are subcutaneously transplanted into both flanks of each nude rat using a 27-G needle and a 1-mL syringe (1×10^7 cells/100 μL). Once the tumor had reached a size of ~200 mm^3 L, start dosing with the compounds. For the HCT116 cells, 7–10 days are required before the tumor size reached ~200 mm^3 (*see* **Note 4**).
4. Anesthetize tumor-bearing nude rats via isoflurane inhalation and insert a cannula into the subclavian vein using custom infusion kits. Immediately after cannula insertion, the rat is placed in a free-movement cage and saline will be administered by continuous IV infusion using a syringe pump for around 24 h (0.1 mL/h) to avoid blood clotting (*see* **Note 5**).
5. Randomize rats according to tumor volumes and distribute into treatment groups of 4–8 rats each, with each treatment group having an approximately equivalent range of tumor volumes, on the day before the start of drug administration.
6. Dissolve the compound in the vehicle and administer it into tumor-bearing nude rats by continuous IV infusion for 8 h.
7. Measure the tumor diameter using a digital caliper twice a week (*see* **Note 7**). The statistical analysis can be performed using a repeated measure ANOVA followed by the Dunnett test.
8. Obtain approximately 0.15 mL of blood using a potassium-EDTA coated syringe to perform white blood cell (WBC), red blood cell (RBC), and platelet (PLT) counts. Immunosuppression is a generally observed side effect of

antitumor agents (*see* **Note 3**). Collect the samples from the subclavian vein under isoflurane anesthesia on days 3 and 10. The cell counts can be determined using an automated hematology analyzer.

9. Measure the body weight and perform gross observations on each weekday during the experiment. Body weight changes (a decrease or suppression in the body weight increase) are a sign of general toxicity.
10. For measurement of drug concentrations, collect blood samples at the indicated times using a heparinized syringe via the subclavian vein. Prepare plasma samples from the blood samples using centrifugation and store at –80 °C until further assay. Measure the concentrations of the compounds using the LC/MS/MS method (*see* **Note 8**).

3.2 Determination of pRb Phosphorylation in Xenograft Tumor Samples Using a Western Blot (See Notes 9 and 10)

1. Dose compound M by a constant IV infusion in nude rats bearing an HCT116 xenograft tumor (*see* **Note 11**).
2. After 8 h, euthanize the animals and isolate the tumor tissues from the animals.
3. Suspend the tissues in glycerophosphate buffer and mince them using scissors.
4. Homogenize the tissue suspension in a Dounce homogenizer (ten strokes).
5. Centrifuge at 14,000 × *g* for 90 min at 4 °C, and store the resulting supernatant (cell lysate) at –80 °C.
6. Protein determination in the cell lysates can be performed using a BCA protein assay, according to the manufacturer's protocol.
7. Immunoprecipitate pRb in the supernatants with anti-Rb antibody. The cell lysates are incubated with the above mentioned anti-Rb antibody for 2 h at 4 °C.
8. Add protein G agarose and incubate the samples for additional 3 h at 4 °C with rotation.
9. Precipitate the bound pRb by centrifugation and elute in 5× SDS Buffer. Load and separate the proteins in 7.5 % SDS-PAGE and transfer to a PVDF membrane.
10. Block the membrane in blocking solution at room temperature for 1 h, and then probe with anti-phospho Rb antibody (Ser780) in blocking solution at 4 °C overnight.
11. Wash the membrane with PBS containing 1 % Tween 20 for three times.
12. Detect the bound antibody with HRP-linked anti-rabbit IgG, followed by the use of an ECL system.

3.3 Determination of BrdU Incorporation in Xenografted Tumor by Using IHC Assays (See Notes 9, 10, 12, 13)

1. Administered intravenously BrdU at 30 mg/kg into tumor-bearing nude rats via the tail vein.
2. Euthanize the animals 2 h after administration of the BrdU. Collect the target tissues, such as the tumor and small intestine.
3. Fix tissues in 10 % formalin for no more than 24 h and then embed in paraffin.
4. After deparaffinization, place the sections in Target Retrieval Solution and heat using a microwave for 20 min, then treat with 3 % H_2O_2 at room temperature for 10 min to inactivate the endogenous peroxidase.
5. For BrdU staining, block the sections with MOM Mouse IgG Blocking Reagent for 1 h.
6. Then, treat the sections with anti-BrdU antibody at 4 °C overnight.
7. The bound Abs are detected and developed using a MOM immunodetection kit according to the manufacturer's instructions.
8. For phospho-Rb and activated caspase 3 staining, maintain the sections at a sub-boiling temperature for 10 min. Then cool the slides on a bench top for 30 min.
9. Block the sections with PBS containing 10 % normal goat serum and 3 % bovine serum albumin.
10. Treat the sections with anti-phosphor-Rb (Ser807/811) Ab or anti-activated caspase 3 Ab at 4 °C overnight.
11. The bound Abs are detected using goat anti-rabbit IgG H&L-biotin conjugate and visualized using a VECTASTAIN Elite ABC kit according to the manufacturer's instructions.

3.4 Isolation of Lymphocytes for Ex Vivo Experiments Using Peripheral Blood or Isolated Lymphocytes

1. Dilute heparinized peripheral blood with an equal volume of balanced salt solution and layer on a Ficoll-Paque Plus in a centrifuge tube.
2. Centrifuge the tube at $400 \times g$ for 30 min at 20 °C.
3. Collect the cells in the middle layer and wash twice with balanced salt solution.
4. For isolation from the spleen, mince spleen cells isolated from the rat and filter the cells using a 100-μm nylon mesh.
5. Incubate the cells in IOTest 3 Lysing Solution for 10 min at room temperature to lyse contaminating erythrocytes and then wash with PBS.
6. Culture isolated splenocytes in RPMI 1640 containing 10 % heat-inactivated fetal calf serum (FCS), 100 U/mL penicillin, and 100 μg/mL streptomycin at $0.7–2.5 \times 10^6$ cells/mL.
7. For stimulation, add 10 ng/mL of PMA and 1 μM of Ionomycin.

3.5 Cell Cycle and Cell Death Assays of Whole Peripheral Blood Cells or Isolated Lymphocytes Treated with Cdk Inhibitors (See Note 14)

1. For flow cytometric analysis, dilute whole peripheral blood cells or isolated lymphocytes with RPMI 1640 containing 10 % heat-inactivated FCS, 100 U/mL penicillin, and 100 μg/mL streptomycin and expose to Cdk inhibitor with/without PMA and Ionomycin.
2. After 0–48 h (the incubation time depends on the experiments), collect the cells, fix and stain their nuclei with propidium iodide (PI) using the CycleTEST PLUS DNA Reagent Kit.
3. Collect the data in a fluorescence-activated cell sorter (FACS) Calibur flow cytometer and analyze using CellQuest software (Becton Dickinson). The S-phase population are calculated using ModFit LT software (Verity Software House).
4. For trypan blue exclusion assay, plate isolated lymphocytes at a density of 0.7×10^6 cells/mL in 96-well plates with various concentrations of Cdk inhibitor.
5. After 24 h, determine cell viability using trypan blue exclusion. Perform the assays in triplicate, and express the results as the mean plus or minus standard deviation.
6. For caspase 3/7 activation assay, plate isolated lymphocytes as **step 4**. After 8 h of exposure to inhibitors, caspase-3/7 activity is detected using the Apo-ONE Homogeneous Caspase-3/7 Assay kit according to the manufacturer's instructions.
7. For western blot analysis, culture isolated lymphocytes with inhibitors in the presence or absence of PMA-Ionomycin and resuspend in lysis buffer containing a protease inhibitor cocktail and the Halt Phosphatase Inhibitor Cocktail.
8. Sample tubes are kept at –80 °C for 15 min. Collect the supernatant after centrifugation at $15{,}000 \times g$ for 30 min.
9. Determine protein concentration using the BCA Protein Assay Kit. Load equal amounts of protein (10–20 μg) and separate in 7.5 % SDS-PAGE, then transfer to Immobilon-P membranes (Millipore).
10. Block the membranes were blocked with PBS containing 0.2 % Tween 20 and 5 % skim milk, and incubate with primary antibodies.
11. The bound antibodies are detected with anti-mouse/rabbit IgG-HRP and visualized using an ECL system.

4 Notes

1. The selection of the animal is, of course, dependent on the aim of the study. In general, not all human cancer cell lines are transplantable. The transplantability of cancer cells depends on the type of immunodeficiency in the animal model. For example, HCT116 is transplantable in both nude mice and rats, but

Colo205 is only transplantable in mice. We recommend testing to see whether a particular cell line of interest can grow within the planned animal model at the beginning of the study.

2. When testing small molecular compounds in vivo, the animal body weight is another important factor to consider when choosing between mice and rats. In general, as mice are smaller than rats, the total amounts of the required test compound will be smaller for mice than for rats. Moreover, nude mice are, in general, cheaper than nude rats.
3. In our studies, nude rats were used for two reasons: (1) we wanted to collect blood at several time points from a single animal during the course of the study, and (2) we wanted to dose the compound using an intravenous (IV) constant infusion. Inserting a cannula into mice is difficult because of the animal's relatively smaller size. Of note, a subcutaneously (SC) constant infusion can be performed in mice using an osmotic infusion pump.
4. For molecular targeted drug research, a specific human cancer cell line might be needed for in vivo studies. If such cells cannot be grown in animals, an appropriate model for performing in vivo experiments might be difficult to establish. To improve the transplantability or growth efficiency of cell lines, Matrigel (BD Biosciences) is often used. Matrigel is a solubilized basement membrane preparation extracted from the EHS mouse sarcoma. We suspended cells in 50 % Matrigel and 50 % PBS and inoculated animals. Co-inoculation with Matrigel improved the transplantability and growth efficiency of some cell lines.
5. In our experiment with Cdk inhibitor, Compound M, we chose a constant IV infusion to avoid high Cmax effects and to maintain a constant exposure level at a specific concentration. In this experiment, we used 0.1 % ascorbic acid-30 % polyethylene glycol (PEG) as the vehicle, which enables to dose up to around 8–10 h. If the test compound dissolves, 5 % glucose or saline are highly safe vehicles for continuous IV dosing over a period of several months.
6. Before the start of in vivo PD or efficacy experiments, the "target" plasma concentration (biological effective concentration) and treatment time for efficacy should be estimated. We estimated the in vivo target concentration based on the potency of the compound during in vitro cell-based experiments in addition to the serum protein binding ability of the compound. In the case of Compound M, we first performed in vitro PD (inhibition of pRb phosphorylation) and cell growth inhibition/cell death induction experiments to determine the effective concentrations in vitro. The serum protein binding of the

compound is also important for estimating these parameters. We performed an in vitro cell-based experiment in a medium containing 10 and 50 % serum and tested how the IC_{50} value shifts in the presence of high serum concentrations. Then, the infusion dose of the compound needs to be estimated; in other words, the dose of compound required for the infusion to enable the target concentration to be reached in animals must be determined. Before the start of PD and efficacy studies, we performed constant IV infusion dosing experiments to determine the correlation between the dose of the compound and the plasma concentration level in animals.

7. The tumor volume (mm^3) was calculated using the following formula:

$$\text{Tumor volume}\left(\text{mm}^3\right) = \text{length} \times \left(\text{width}\right)^2 \times 0.5.$$

The relative tumor volume was calculated using the following formula:

$$\text{Relative tumor volume} = V \,/\, V_0,$$

where V_0 equals the tumor volume on day 0 and V equals the tumor volume on different observation days (for example, days 0, 3, 6, 10 and 13). Also, the following parameters were also determined:

$$\%T \,/\, C = 100 \times \Delta T \,/\, \quad C \qquad if \;\; \Delta T > 0,$$

or

$$\%T \,/\, C = 100 \times \Delta T \,/\, \text{Ti} \qquad if \;\; \Delta T < 0,$$

where, ΔT equals the change in the mean relative tumor volume compared with the initial relative tumor volume for the treatment group, ΔC equals the change in the mean relative tumor volume compared with the initial relative tumor volume for the vehicle control group, and Ti equals the initial relative tumor volumes for the treatment group. Low positive $\%T/C$ values reflect the control of tumor growth, while negative values indicate tumor regression. According to the National Cancer Institute (NCI) guidelines, $\%T/C \leq 42$ % is considered to indicate significant antitumor activity, while $\%T/C < 10$ % is indicative of a highly active agent.

8. The biological consequences of dosing compounds in animals should be discussed with regard to not only the amount of the dosed compound, but also the actual exposure of the compound. Thus, determining the plasma or tissue concentrations of the compound is important for understanding the results.

9. In our studies, we used three PD markers: the phosphorylation of pRb, BrdU incorporation, and the induction of activated caspase-3. As the Rb protein is a direct substrate of Cdks, we can determine the inhibition of Cdk in cells by a decrease in its phosphorylation. BrdU incorporation and the activation of caspase-3 are markers of cell proliferation (cell cycle progression from G1 to S phase) and cell death, respectively. Thus, by monitoring these markers, we can determine the cellular biological consequences of Cdk inhibition: the inhibition of cell proliferation, and the induction of cell death. In our experiments, the inhibition of pRb phosphorylation and BrdU incorporation occurred within the same range of Cdk inhibitor plasma concentrations. Moreover, our Cdk inhibitor showed an antitumor efficacy at a dose that inhibited pRb phosphorylation. The suppression of pRb phosphorylation in tumor cells is clearly correlated with tumor cell growth and cell death in this model [12].
10. In general, biomarkers should ideally be tested for target engagement and biological effects. For example, in the case of receptor tyrosine kinases (RTKs), the autophosphorylation of RTK could be used to test for target engagement, while markers involved in the Ras/MAPK or PI3K pathway could be used to test for biological effects. These markers are important for understanding the mode of action and the mechanism of the biological effects of the test compounds.
11. Before starting the PD studies, we suggest performing a few experiments to optimize the assay conditions, i.e., to test the expression of the PD marker protein/mRNA in the tumor samples. The expression of PD markers at a quantitatively measurable level is essential for PD experiments. If the expression is insufficient, another PD marker or cell lines with a higher expression level of the marker protein should be considered. The stability of the PD markers is another important factor, because in some cases, the marker proteins are very unstable after the isolation of tumors from animals. For example, some phosphorylated substrate proteins are unstable and rapidly dephosphorylated or degraded after isolation. For this reason, we added proteinase inhibitor and phosphatase inhibitor cocktails to our tissue lysis buffer. Moreover, we performed experiments such as (1) the isolation of tumors from animals and incubation on ice or at 4 °C for different periods, followed by (2) the detection of PD markers at each time point to test stability. This strategy might be useful for determining the optimum assay condition. If the protein of interest is unstable, the protein should be solubilized from the tissues immediately after isolation.

12. There are pros and cons to both a western blot and an IHC assay. For a western blot, the protein of interest should be solubilized from the tumor tissues. However, xenograft tumors of human cancer cell lines are often inhomogeneous and often contain necrotic areas, which cause variations among samples. The formation of necrotic areas is dependent on the cancer cell line (xenograft tumors of some cancer cell lines tend to form a necrotic area, but others do not) and tumor size (larger tumors tend to contain larger necrotic areas). The selection of adequate cell lines and tumor sizes is important for western blot analyses. For immunohistochemistry, this point is not a concern, as necrotic areas can be visually distinguished from the tumors.
13. However, IHC is not suitable for quantitative or throughput analyses. A western blot has the advantage of allowing ~15 or 20 samples to be analyzed at once. However, for quantification, the band intensity must be scanned. If the PD marker can be detected using an ELISA, instead of a western blot, quantitative analyses with a good throughput are feasible.
14. Pan-Cdk inhibitors exhibited an antitumor efficacy while rapidly causing immunosuppression in a rodent tumor model at only 8 h after administration in mice. To understand why Cdk inhibitors caused such rapid immunosuppression, we tested the direct effects of inhibitors on isolated blood cells or lymphocytes in ex vivo experiments. Interestingly, pan-Cdk inhibitors induced cell death in peripheral blood or purified resting (non-stimulated) lymphocytes very rapidly (after 4 h of incubation), suggesting that the acute immunosuppression observed in rodents might be, at least in part, caused by direct cytotoxic effects of pan-Cdk inhibitors on resting lymphocytes [13]. Cell cycle related Cdks were not activated in resting lymphocytes; the phosphorylation of pRb was observed only after stimulation by PMA and Ionomycin. Instead, CTD of the largest subunit of RNA polymerase II is phosphorylated, indicating that Cdk7 or Cdk9 (which phosphorylate this domain) are activated in resting lymphocytes. Indeed a pan-Cdk inhibitor suppressed CTD phosphorylation in resting cells at a dose required for cell death induction. A Cdk4/6 inhibitor with selectivity against Cdk7 and 9 [14] did not induce cell death in resting lymphocytes. These results suggest that CTD phosphorylating activity, possibly arising from Cdk7 or 9, might be important for the survival of resting lymphocytes.

References

1. Sherr CJ (1996) Cancer cell cycles. Science 274:1672–1677
2. Sherr CJ (2000) The Pezcoller lecture: cancer cell cycles revised. Cancer Res 60:3689–3695
3. Pines J (1995) Cyclins and cyclin-dependent kinases: theme and variations. Adv Cancer Res 66:181–212
4. Sherr CJ, Roberts JM (1999) CDK inhibitors: positive and negative regulators of G1-phase progression. Genes Dev 13:1501–1512
5. Pavletich NP (1999) Mechanism of cyclin-dependent kinase regulation: structures of cdks, their cyclin activators, and CIP and INK4 inhibitors. J Mol Biol 287:821–828
6. Koepp DM, Haper JW, Elledge SJ (1999) How the cyclin became a cyclin: regulated proteolysis in the cell cycle. Cell 97:431–434
7. Falco GD, Giordan A (1998) CDK9 (PITALRE): a multifunctional cdc2-related kinase. J Cell Physiol 177:501–506
8. Palancade B, Bensaude O (2003) Investigating RNA polymerase II carboxyl-terminal domain (CTD) phosphorylation. Eur J Biochem 270: 3859–3870
9. Price DH (2000) P-TEFb, a cyclin-dependent kinase controlling elongation by RNA polymerase II. Mol Cell Biol 20:2629–2634
10. Dhavan R, Tsai L-H (2001) A decade of CDK5. Nat Rev Mol Cell Biol 2:749–759
11. Lilja L, Yang S, Webb D et al (2001) Cyclin-dependent kinase 5 promotes insulin exocytosis. J Biol Chem 276:34199–34205
12. Hirai H, Takahashi-Suzuki I, Shimomura T et al (2011) Potent anti-tumor activity of a macrocycle-quinoxalinone class pan-Cdk inhibitor in vitro and in vivo. Invest New Drugs 29:534–543
13. Kobayashi M, Takahashi-Suzuki I, Shimomura T et al (2011) Cell death induction in resting lymphocytes by pan-Cdk inhibitor, but not by Cdk4/6 selective inhibitor. Invest New Drugs 29:921–931
14. Hirai H, Shimomura T, Kobayashi M et al (2010) Biological characterization of 2-aminothiazole-derived Cdk4/6 selective inhibitor in vitro and in vivo. Cell Cycle 9:1590–1600

Chapter 15

Models for the Study of the Cross Talk Between Inflammation and Cell Cycle

Laura J. Hoodless, Calum T. Robb, Jennifer M. Felton, Carl S. Tucker, and Adriano G. Rossi

Abstract

Cyclin-dependent kinases (CDKs) have been traditionally associated with the cell cycle. However, it is now known that CDK7 and CDK9 regulate transcriptional activity via phosphorylation of RNA polymerase II and subsequent synthesis of, for example, inflammatory mediators and factors that influence the apoptotic process; including apoptosis of granulocytes such as neutrophils and eosinophils. Successful resolution of inflammation and restoration of normal tissue homeostasis requires apoptosis of these inflammatory cells and subsequent clearance of apoptotic bodies by phagocytes such as macrophages. It is believed that CDK7 and CDK9 influence resolution of inflammation since they are involved in the transcription of anti-apoptotic proteins such as Mcl-1 which is especially important in granulocyte survival.

This chapter describes various in vitro and in vivo models used to investigate CDKs and their inhibitors in granulocytes and particularly the role of CDKs in the apoptosis pathway. This can be performed in vitro by isolation and use of primary granulocytes and in vivo using animal models of inflammatory disease in rodents and zebrafish. Some of the methods described here to assess the role of CDKs in inflammation and apoptosis include flow cytometry and western blotting, together with imaging and quantification of apoptosis in fixed tissue, as well as in vivo models of inflammation.

Key words Apoptosis, Cyclin-dependent kinase, Cyclin-dependent kinase inhibitor, Inflammation, Macrophage, Neutrophil

1 Introduction

Inflammation is vital for pathogen clearance and subsequent repair of damaged tissue. Inflammatory leukocyte cells (especially neutrophils, eosinophils and monocytes) are involved in the destruction of pathogens and co-ordinate the inflammatory response and repair processes by, for example, release of inflammatory mediators. During the resolution phase of the inflammatory response, these cells usually undergo apoptosis and are cleared by phagocytic cells such as macrophages. Therefore, leukocyte apoptosis is thought to be important for effective resolution of inflammation, and for the

Mar Orzáez et al. (eds.), *Cyclin-Dependent Kinase (CDK) Inhibitors: Methods and Protocols*, Methods in Molecular Biology, vol. 1336, DOI 10.1007/978-1-4939-2926-9_15,

prevention of dysregulated inflammation and the development of chronic inflammatory diseases [1, 2].

Evidence indicates that cyclin-dependent kinases (CDKs) and their inhibitors (endogenous or pharmacological inhibitors) regulate inflammation by influencing processes such as apoptosis. Interestingly, CDKs, which are known to regulate the proliferation of cells undergoing the cell cycle, also regulate the function and longevity of terminally differentiated cells (e.g., neutrophils) [3]. Specific CDKs regulate transcription (especially CDK7 and CDK9), and it has been demonstrated that specific inhibitors that target CDK9 are important controllers of inflammation. Inhibition of these CDKs promotes apoptosis of neutrophils and eosinophils [4–7], and when CDK inhibitors are administered during established inflammation in vivo, resolution is enhanced [5, 6, 8]. Granulocytes, with their high expression of CDK7 and CDK9, are especially prone to undergo apoptosis when exposed to CDK9 inhibition [4], whereas CDK9 inhibition does not appear to have a major effect on macrophage apoptosis (6) but likely regulates macrophage production of inflammatory cytokines [9, 10].

A variety of models have been used to study CDKs and their inhibitors in innate inflammatory cells. Human neutrophils, eosinophils and monocytes can be readily isolated from peripheral blood. It is essential to isolate a pure cell population in a careful manner where the cells are unperturbed and remain unactivated [11–13]. This can be done using a variety of techniques and procedures and often include dextran sedimentation and/or hypotonic lysis of erythrocytes, discontinuous Percoll or Ficoll/Hypaque gradients, or the use of antibody cocktails followed by magnetic column separation methods [14]. Furthermore, highly purified populations can be obtained by flow-cytometric cell sorting [15]. When culturing these cells it is important to control for factors such as pH, temperature, oxygen tension, cell density, and serum concentration, which affect cell longevity and activation status [13, 14].

Furthermore, a number of mouse models have been used successfully to investigate CDKs in inflammation. Good examples of this include sterile and non-sterile models of inflammation; principally by eliciting an inflammatory response, treating the animals with CDK inhibitor compounds during established inflammation, and then assessing inflammatory parameters. Specific previously used mouse models include bleomcyin-induced lung inflammation and fibrosis, lung inflammation induced by intratracheal LPS, LTA/PepG, or *E. coli* administration [4, 5], carrageenan or OVA-induced pleurisy [8], and serum-induced arthritis [5].

Transgenic zebrafish which express fluorescent proteins under the control of inflammatory cell-specific promoters have also been successfully used to investigate CDKs during inflammation [16, 17]. These fish allow specific cell populations to be imaged continuously in vivo using fluorescence microscopy. The first study of this nature

was carried out in 2006 with the publication of a transgenic fish expressing green fluorescent protein (GFP) under control of the myeloperoxidase promoter, labeling neutrophils specifically [16]. This model has been used to image the effects of CDKi drugs in more detail in vivo [18, 19].

The use of these models has provided an insight into the role of CDKs in specific subtypes of innate leukocytes and inflammatory processes in general. This chapter outlines some of the methodologies used to investigate isolated inflammatory cell apoptosis and selected in vivo models of inflammation. The sections described below highlight only a limited perspective on what can be used and we emphasize that there are numerous other in vitro and in vivo techniques available to investigate the pleiotropic effects of CDKs in inflammation.

2 Materials

2.1 Culture and Treatment of Human Leukocytes In Vitro

1. Iscove's Modified Dulbecco's Medium (IMDM).
2. Penicillin–streptomycin (10 %).
3. Autologous serum (fetal bovine serum [FBS], 10 %).
4. 96-well flat bottomed plate.
5. Dynabeads® (Invitrogen).
6. Dulbecco's Phosphate-Buffered Saline (DPBS).
7. CDK inhibitor drug, such as *R*-roscovitine (Calbiochem, Merck Millipore).
8. GM-CSF, LPS, TNF-α, or IL-5.

2.2 Cytocentrifuge Preparations for Light Microscopy

1. Cytocentrifuge chambers, filter cards, glass slides, and coverslips.
2. Methanol, Quick-Diff™ stains.
3. DPX mounting medium.

2.3 Annexin V/ Propidium Iodide Staining

1. Annexin-V conjugated to fluorescein isothiocyanate (FITC).
2. Annexin binding buffer, consisting of Hank's balanced salt solution (HBSS) with 5 mM Ca^{2+}. (Stored at 4 °C.)
3. Propidium iodide, 1 mg/ml in sterile ddH_2O.
4. 96-well flat bottomed plate.

2.4 Hypodiploid Nuclei Staining Solution

2.4.1 Propidium Iodide Staining Solution

1. Propidium iodide: Add 250 µl of 10 mg/ml stock solution.
2. Sodium citrate: Add 2.2 ml of stock solution (2.2 g in 10 ml ddH_2O).
3. Triton X-100 in solution—50 µl.
4. Add ddH_2O up to 50 ml.

2.4.2 DAPI Staining Solution

DAPI (5 μg/ml) in DPBS (−/−) + 1 % IGEPAL (CA-630).

Storage: 2–8 °C, protect from light.

2.5 Alterations in Mitochondrial Permeability

MitoCapture™ Mitochondrial Apoptosis Detection Fluorometric Kit (Biovision, Milpitas, CA 95035 USA) containing MitoCapture™ reagent and MitoCapture™ incubation buffer.

2.6 Western Blotting for Intracellular Proteins That Regulate Apoptosis

1. Tris-buffered saline (TBS 10× stock):
   - NaCl (87.66 g).
   - Trizma base (24.22 g).
   - Distilled water (ddH_2O, 800 ml), pH adjusted to 7.4 with HCl then made to 1 l with ddH_2O. Dilute 1:10 with ddH_2O prior to use for 1× TBS.
2. Protease inhibitor buffer: 780 μl 1× TBS added to 20 μl protease inhibitor cocktail (Sigma-Aldrich), supplemented with:
   - β-glycerophosphate (60 μl of 3.33 M stock in H_2O).
   - Pepstatin A (40 μl of 0.75 μM stock in methanol).
   - 4-(2-aminoethyl)benzenesulfonyl fluoride hydrochloride (AEBSF; 20 μl of 400 mM stock in H_2O).
   - Aprotinin (20 μl of 0.15 μM stock in H_2O).
   - Leupeptin (20 μl of 20 mM stock in H_2O).
   - Sodium vanadate (20 μl of 1 M stock in H_2O, pH 10, boiled).
   - Benzamidine (20 μl of 0.5 M stock in H_2O).
   - Levamisole (20 μl of 2 M stock in H_2O).
3. 10 % Nonidet P-40 (NP-40) in 1× TBS.
4. BCA protein assay.
5. Sample Buffer (4× stock):
   - 50 % glycerol (4 ml).
   - 20 % sodium dodecyl sulfate (SDS) (4 ml).
   - Tris–HCl (2.5 ml of 1 M, pH 6.8).
   - 1 % (w/v in ethanol) bromophenol blue (20 μl).
   - β-mercaptoethanol (400 μl—use inside a fume hood).
6. Prestained molecular weight standard.
7. 12 % Precise Protein SDS gel.
8. Running buffer (10×):
   - Tris base (121 g).
   - Sodium dodecyl sulfate (SDS, 10 g).
   - Hepes (238 g).

- ddH_2O (800 ml). Once chemicals are dissolved, make up to 1 l (ddH_2O).
- Dilute 1:10 in ddH_2O for 1× solution as required.

9. Transfer buffer (10×):
   - Trizma base (30.3 g).
   - Glycine (144.12 g).
   - ddH_2O (800 ml). Once chemicals are dissolved, make up to 1 l (ddH_2O).
10. Transfer buffer (1×):
    - 10× transfer buffer stock (above, 100 ml).
    - Methanol (200 ml).
    - ddH_2O (700 ml).
11. Polyvinylidene difluoride (PVDF) membrane.
12. Blocking buffer:
    - TBS (1×).
    - 0.1 % Tween® 20.
    - 5 % dried milk powder.
13. Primary antibodies, diluted in 5 ml of blocking buffer (above):
    - CDK9 (1 in 1000, Santa Cruz Biotechnology).
    - GAPDH (1:10,000; Sigma-Aldrich).
    - Cleaved caspase-3 (1:1000, Cell Signaling, Danvers, MA, USA).
    - Cleaved caspase-9 (1:1000; Cell Signaling).
14. Secondary antibodies, diluted in 5 ml blocking buffer (above): corresponding horseradish-peroxidase-conjugated antibodies (1:2500).
15. ECL prime, light-sensitive film, X-ray film developer.

2.7 Flow Cytometry-Based Phagocytosis Assay

1. CellTracker™ dye (Life Technologies).
2. pHrodo™ dye (Life Technologies).

2.8 siRNA Transfection of Cell Lines

1. Nucleofector Solution (Lonza).
2. siRNA sequences (Dharmacon).
3. Amaxa Nucleofector Kit V (Lonza).

2.9 Reagents for Rodent Models

1. Bleomycin sulfate (0.033 mg; Apollo Scientific, Cheshire, UK).
2. *R*-roscovitine (Calbiochem, Merck Millipore).
3. Lipopolysaccharide (LPS), Lipotechoic Acid (LTA)/ Peptidoglycan (PepG).

2.10 Reagents for Zebrafish Models

1. 4.2 % (w/w) Tricaine/MS222 (Ethyl 3-aminobenzoate methanesulfonate salt) anesthetic. Recipe:
   - 400 mg Tricaine powder.
   - 97.9 mL ddH_2O.
   - ~2.1 ml 1 M Tris (pH 9).

   Adjust pH to ~7. Store this solution in the freezer.
2. *Embryo medium*:

   1.0 ml Hank's solution #1.

   0.1 ml Hank's solution #2.

   1.0 ml Hank's solution #4.

   1.0 ml Hank's solution #5.

   1.0 ml fresh Hank's solution #6.

   95.9 ml ddH_2O.

   Use about ten drops 1 M NaOH to pH 7.2.
   - *Hank's solution #1*

     8.0 g NaCl.

     0.4 g KCl.

     100 ml ddH_2O.
   - *Hank's solution #2*

     0.358 g Na_2HPO_4 anhydrous.

     0.6 g KH_2PO_4.

     100 ml ddH_2O.
   - *Hank's solution #4*

     0.72 g $CaCl_2$.

     50 ml ddH_2O.
   - *Hank's solution #5*

     1.23 g $MgSO_4 \times 7$ H_2O in 50 ml ddH_2O.
   - *Hank's solution #6*, made fresh

     0.35 g $NaHCO_3$.

     10 ml ddH_2O.
3. CDKi drugs previously used in zebrafish models for pharmacological manipulation:
   - *R*-roscovitine (Calbiochem) 20 μM.
   - Wogonin (Sigma-Aldrich) 50 μM.
4. Equipment for microinjection.
   - Morpholinos (Gene Tools LLC).
   - Microinjector such as Narishige IM-300 or World Precision Instruments PV-820.

- Borosilicate glass capillary tubes to make micropipette needles, for example Harvard Apparatus GC100TF-10.
- Needle puller, such as P-97 Flaming/Brown Micropipette Puller (Sutter Instruments); example of typical setting: Heat = ramp + 10; Pull 90; Velocity 70; Time 70; Air pressure 200.
- Micromanipulator, such as WPI Marzhauser M3301R.

3 Methods

3.1 In Vitro Methods

The first step required to study CDK in specific inflammatory cells in vitro is effective isolation of pure cell populations from human donors and it is desirable to attain purity of at least 97 %. All purification of cell populations, as well as subsequent treatments should ideally be carried out in sterile tissue culture conditions. In published work, CDK inhibitor compounds have been tested on the granulocyte populations, and then various apoptosis assays have been performed; the monocytes can be differentiated into macrophages and used for phagocytic assays.

3.1.1 Neutrophil Isolation

1. Approximately 40–160 ml of blood is collected in 50 ml BD Falcon tubes containing sterile sodium citrate (to final conc. 0.38 %).
2. Centrifuge at 300 × *g* for 20 min (making sure that there is no centrifuge brake applied) and remove platelet-rich plasma.
3. Separate leukocytes from erythrocytes by dextran sedimentation over 25–30 min using pre-warmed (37 °C) 0.6 % (wt/vol) dextran T500.
4. Aspirate the upper leukocyte-rich layer.
5. Adjust volume to 50 ml using pre-warmed 0.9 % saline.
6. Pellet leukocytes by centrifugation at 350 × *g* for 6 min.
7. Separate polymorphonuclear leukocytes from mononuclear leukocytes using a discontinuous isotonic Percoll gradient (9:1 percoll–10× Phosphate Buffered Saline [PBS] ratio). Gradients: 81, 70, 55 % Percoll in 1× PBS (without cations).
8. Layer 3 ml of 70 % isotonic Percoll on 3 ml of 81 % isotonic Percoll in a 15 ml polypropylene tube. Layer leucocytes resuspended in 3 ml 55 % Percoll on top.
9. Centrifuge gradients at 720 × *g* for 20 min. Mononuclear cells are located in the upper 55:70 % interface and polymorphonuclear leucocytes at the 70:81 % interface (*see* Fig. 1 for an example flow plot of forward and side scatter profiles of various leukocytes).
10. Calculate cell yield with a hemocytometer.

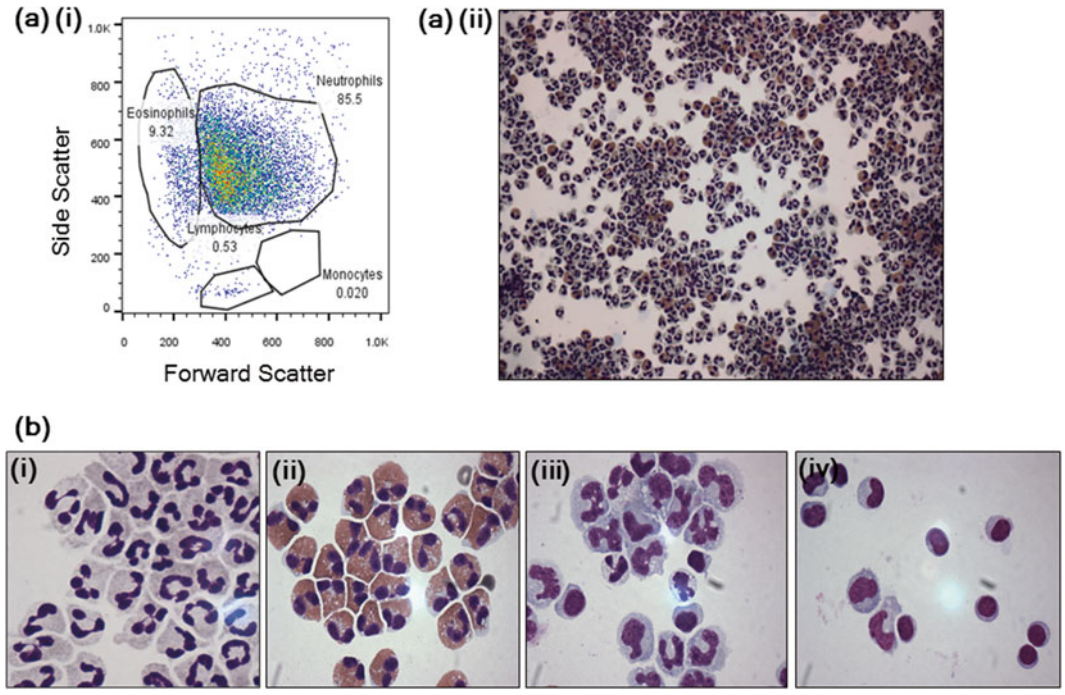

Fig. 1 (**a**) Representative (*i*) forward and scatter flow plot and (*ii*) microscopy images of granulocyte layer (taken at ×200 magnification). (**b**) Freshly isolated (*i*) neutrophils, (*ii*) eosinophils, (*iii*) monocytes, and (*iv*) lymphocytes (taken at ×1000 magnification). Images acquired by the authors

11. Wash leukocytes two more times in pre-warmed 1× PBS (without cations), by filling up the Falcon tube containing cells with 50 ml of 1× PBS, centrifuging at 300×*g* for 5 min and discarding the supernatant.
12. Using morphologic criteria and cell viability staining (e.g., trypan blue) a purity of at least 98 % neutrophils is recommended for subsequent assays.
13. Resuspend cells at 5×10^6 cells/ml in IMDM with 50 U/ml penicillin and 50 U/ml streptomycin (10 % Pen/Strep) plus 10 % autologous serum.
14. Newly isolated neutrophils can be cultured in flat-bottomed 96-well plates at 5×10^7 cells/ml in IMDM with 10 % autologous serum, 10 % Pen/Strep in a humidified, 5 % CO_2 atmosphere at 37 °C (*see* Fig. 1c(i)).

3.1.2 Eosinophil Isolation

To be carried out following isolation of the granulocyte layer (**steps 1–11**, above).

Pre-prepare up to 24 h before isolation.

1. 320×10^6 beads (from Dynabead kit, Invitrogen) are added to a 50 ml Falcon tube.

2. Wash in 50 ml Dulbecco's PBS.
3. Use magnet from the kit to attract beads and remove supernatant.
4. Add 45 ml of 3G8 hybridoma cell supernatant (this contains anti-CD16 antibody which binds to the beads) overnight at 4 °C (alternative sources of anti-CD16 antibody can be used).
5. Before use, wash 2× in PBS, and wash magnet.

1. Resuspend at 10×10^6 cells/ml in IMDM with 10 % serum, 10 % penicillin–streptomycin.
2. Place beads on magnet to allow removal of supernatant.
3. Add granulocyte cells to beads, incubate at 4 °C for 20 min.
4. Place beads on magnet and remove and keep supernatant.
5. Transfer supernatant to fresh tube of beads, incubate at 4 °C for 20 min.
6. Use magnet to remove beads, and transfer supernatant to a fresh 50 ml Falcon tube. Use the magnet to remove any excess beads.
7. Transfer supernatant to fresh tube and centrifuge at $230 \times g$ for 6 min.
8. Resuspend cells in 2 ml of media, and count using a hemocytometer. A purity of at least 97 % should be attained for future experiments. Culture in 96-well plates at 5×10^6 cells/ml in IMDM with 10 % serum, 10 % penicillin–streptomycin in a humidified, 5 % CO_2 atmosphere at 37 °C (*see* Fig. 1c(ii)).

3.1.3 Culture of Monocyte-Derived Macrophages

Human monocytes can be isolated using the blood isolation protocol described in Subheading 3.1.2, **step 9** (*see* Fig. 1c(iii) shows images of isolated monocytes). Separation of the monocytes from lymphocytes can then be carried out by adherence. Monocytes rapidly attach to tissue culture plastic, unlike lymphocytes. Non-adherent cells can be washed off after 1 h to leave a relatively homogenous cell population to culture. The monocytes should then be differentiated into macrophages. Differentiation of human-derived monocytes into macrophages in culture in vitro can be done in a variety of ways. One method involves culturing cells with autologous serum [20] or a combination of IL-4, IL-6, and GM-CSF [21]. Resuspend peripheral blood mononuclear cells at a concentration of 4×10^6 cells/ml, in IMDM with 10 % autologous serum and add 500 μl/well in a 48-well plate and incubate for 60 min at 37 °C.

1. Wash adherent cells 3–4 times with IMDM and incubate in 500 μl IMDM with 10 % autologous serum at 37 °C.
2. Culture monocytes for 5–7 days with media changed after day 3 in culture prior to use in subsequent experiments.

3.1.4 Treatment of Neutrophils/Eosinophils with CDK Inhibitor Compounds for the Assessment of Apoptosis

1. Add 75 μl of 5×10^6 cells/ml cell suspension to each well of a flat-bottomed 96-well plate.
2. Add 15 μl of apoptosis-modifying agents (at 10× required concentration) or buffer control (e.g., appropriate concentration of DMSO) and 60 μl of IMDM/10 % serum. If two agents are used in combination, use 45 μl of IMDM. Previously used compounds include *R*-roscovitine (20 μM) [5], AT7519 (0.01–1 μM) [6], and flavones such as apigenin, luteolin, and wogonin (1–100 μM) [19].
3. Cover and incubate the plate at 37 °C in an incubator at 5 % CO_2 for the desired length of time. Between 4 and 12 h is the best time to monitor apoptosis without high levels of necrosis (*see* **Note 1**).

3.1.5 Examination of CDKi on Stimuli-Induced Granulocyte Survival

Stimuli such as GM-CSF, LPS, and TNF-α cause survival signaling in neutrophils, delaying their eventual fate of apoptosis. The same is true of eosinophils when incubated with GM-CSF or IL-5 [22–25]. These survival factors will often be present in vivo during an inflammatory response, and adding them to cultures of neutrophils/eosinophils in combination with CDKi drugs is a useful experiment to determine whether CDKi-induced apoptosis can still effectively induce apoptosis in these conditions [7].

1. Add 75 μl of neutrophil/eosinophil cell suspension (5×10^6 cells/ml) to each well of a flat-bottomed 96-well plate.
2. Add 15 μl of GM-CSF (50 ng/ml) *or* LPS (100 ng/ml) *or* TNF-α (10 ng/ml) and 60 μl of IMDM/10 % serum, to increase neutrophil survival. For eosinophils, add GM-CSF (10 ng/ml) or IL-5 (1 ng/ml).
3. Cover and incubate the plate at 37 °C in an incubator at 5 % CO_2. This assay can be combined with CDKi drug treatment to assess whether CDK inhibition can overcome these survival factors.

3.1.6 Analyzing Inflammatory Cell Apoptosis After CDK Inhibition

It has previously been established that manipulating CDKs in inflammatory cells, such as neutrophils and eosinophils, results in apoptosis [4, 5, 8]. Assays for assessing neutrophil and eosinophil apoptosis, including imaging and flow-cytometric analysis methods, are outlined below. Apoptosis can also be assessed by western blotting (*see* Subheading 3.1.7). This is not exhaustive; other methods include Terminal deoxynucleotidyl transferase dUTP nick end labeling (TUNEL) staining, or running a DNA gel to check for a "ladder" pattern, characteristic of apoptotic DNA fragmentation.

Cytocentrifuge Preparation to Image Isolated Cells

The preparation of cytospins from isolated cell populations (treated or control) allows the confirmation of the purity of cell isolation, as well as assessment of apoptosis levels based on morphological

criteria such as shrunken cell morphology and rounded pyknotic nuclei (due to chromatin condensation).

1. Load 100 μl of cell suspension into a cytospin chamber.
2. Cytocentrifuge the chamber for 3 min at 30 × *g*.
3. Remove the slide and air dry for 5 min.
4. Fix the slide in methanol for 2 min then drain the slide.
5. Stain with an acid dye, e.g., Diff-Quik solution #1 for 2 min. Drain.
6. Stain with a basic dye, e.g., Diff-Quik solution #2 for 1 min.
7. Drain the slide then rinse with distilled water.
8. Allow the slide to dry, add a drop of DPX, and apply a coverslip.
9. View with 40× or 100× oil objectives using a light microscope. To assess apoptosis, count >300 cells per slide (*see* Fig. 2 for examples of viable, apoptotic and necrotic neutrophils after *R*-roscovitine treatment).

Flow-Cytometric Analysis

Phosphatidylserine is externalized to the outer surface of the cell membrane during the apoptotic process. This allows apoptotic cells to be recognized by surrounding phagocytic cells. Annexin V (AnnV) binds to phosphatidylserine in the presence of Ca^{2+}. Fluorescent conjugation (usually AnnV-FITC) allows its usage to identify apoptotic cells by flow cytometry. The distinction between viable, apoptotic and necrotic cells can also be made by including propidium iodide (PI) in the flow-cytometric assay. PI binds to nuclear material but cannot enter cells with an intact cell membrane. During necrosis the integrity of the cell membrane is lost, allowing PI to enter the cell and bind to nuclear material, labeling it fluorescently.

After CDK inhibitor treatment of cells (*see* Subheading 3.1.2)

1. Resuspend cells in the 96-well plates by gently pipetting, then pipette 50 μl of cell suspension from each well into a flow cytometry tube with 250 μl AnnV buffer.
2. Incubate tubes on ice for 5–10 min.
3. Immediately prior to analyzing the samples using a flow cytometer, add 1 μl of PI (1 mg/ml solution) to each sample.
4. Analyze samples on a flow cytometer using FL-1/FL-2 channel analysis. Viable cells are dual AnnV/PI negative; apoptotic cells are AnnV positive, PI negative; necrotic cells are dual AnnV/PI positive (*see* Fig. 3).

Measuring Mitochondrial Membrane Potential Using MitoCapture™

During intrinsic apoptosis pores form within the mitochondrial membrane. This leads to the loss of mitochondrial membrane potential ($\Delta\psi_M$) and allows the movement of proteins (especially cytochrome C) into the cytoplasm, resulting in caspase activation.

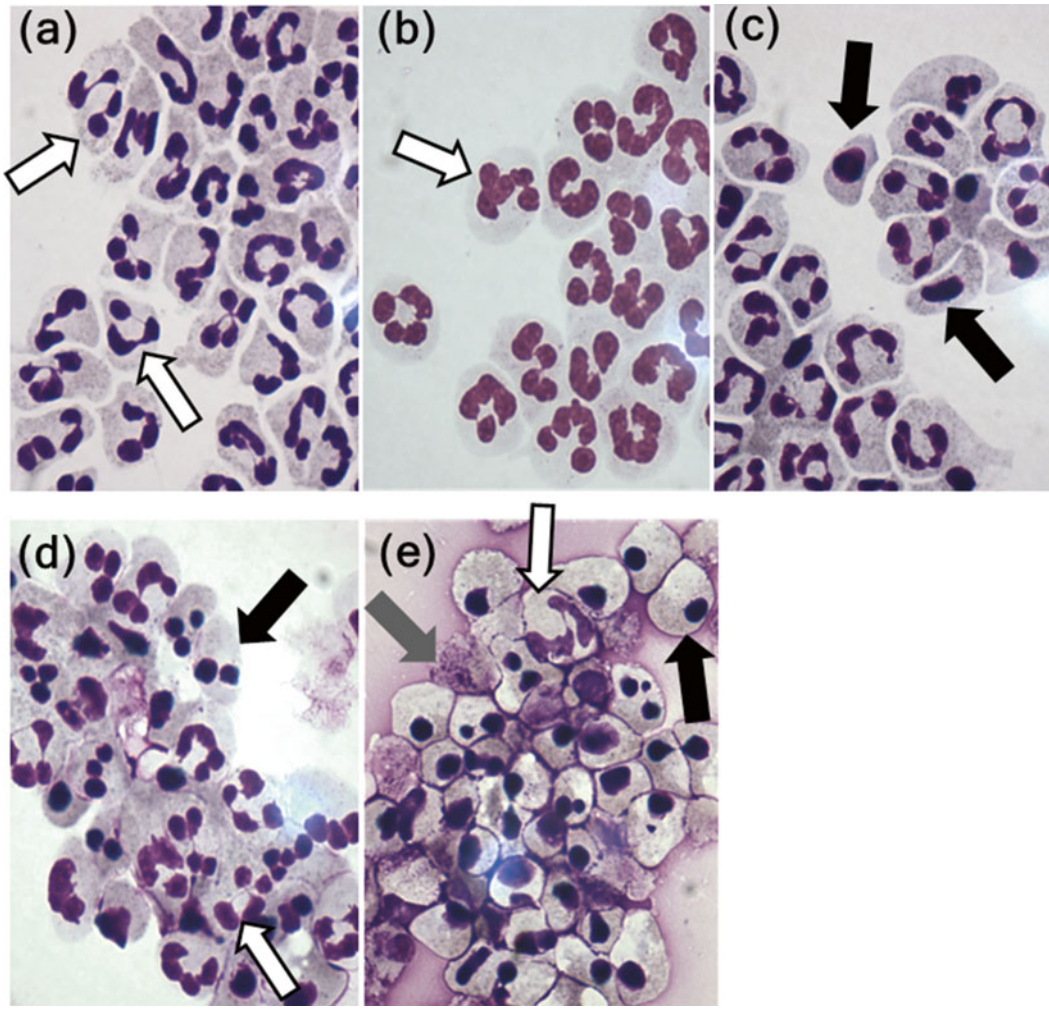

Fig. 2 (**a**) Freshly isolated neutrophils. (**b**) Untreated neutrophils after 6 h. (**c**) Neutrophils treated with the CDKi *R*-roscovitine after 6 h. (**d**) Untreated neutrophils after 24 h. (**e**) Neutrophils treated with *R*-roscovitine after 24 h. *White arrows* indicate viable cells, *black arrows* indicate apoptotic neutrophils with condensed nuclei, and *gray arrows* indicate necrotic neutrophils. Images (taken at 1000× magnification) acquired by authors

The changes in the mitochondrial membrane potential of cells can be measured using MitoCapture™. This is a cationic dye that accumulates in viable cells. It polymerizes within mitochondria and fluoresces in the red (FL-2) channel—indicated by a green (535 nm) to red (590 nm) fluorescence emission shift. During apoptosis, when $\Delta\psi_M$ is compromised, the dye stays in the cytoplasm and does not polymerize, instead fluorescing in the green (FL-1) channel. Mitochondrial depolarization can be quantified using flow cytometry by measuring increasing FL-1 green fluorescence, or by a fluorometric plate assay measuring decreased red/green fluorescence intensity ratio (*see* Fig. 4).

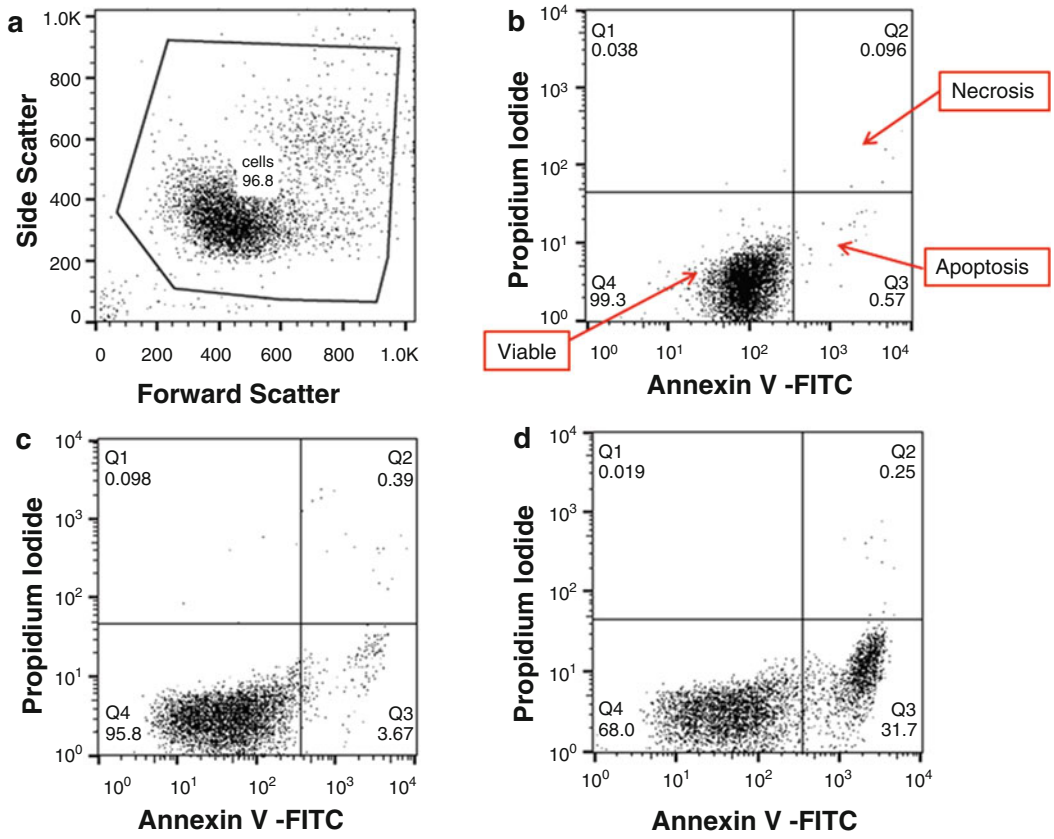

Fig. 3 (**a**) Gating on healthy cells by exclusion of cell debris. (**b**) Freshly isolated neutrophils with labeling of viable cells (Annexin V and propidium iodide [PI] negative), apoptotic cells (Annexin V positive, PI negative) and necrotic cells (Annexin V and PI double positive). (**c**) Untreated neutrophils after 6 h. (**d**) *R*-roscovitine-treated neutrophils after 6 h. Data obtained by the authors

1. For each sample dilute 0.5 µl MitoCapture™ reagent in 500 µl pre-warmed (37 °C) MitoCapture™ Incubation buffer in a 1.5 ml Eppendorf tube. (NB this protocol relies on the use of a MitoCapture™ mitochondria permeability detection kit.)
2. Suspend neutrophils/eosinophils (at least 97 % purity) at 4×10^6 cells/ml in IMDM (10 % autologous serum).
3. In a 96-well flat-bottomed plate add 75 µl of cell suspension, 15 µl of apoptosis-modifying agents (at 10× of the working concentration) or vehicle control, and 60 µl IMDM with 10 % autologous serum to each well. (NB if two agents are used only 45 µl of IMDM is required for total volume of 150 µl.)
4. Cover and incubate at 37 °C in a 5 % CO_2 incubator for the duration of the experiment.
5. Add 150 µl of cell suspension to 500 µl diluted MitoCapture™ reagent.

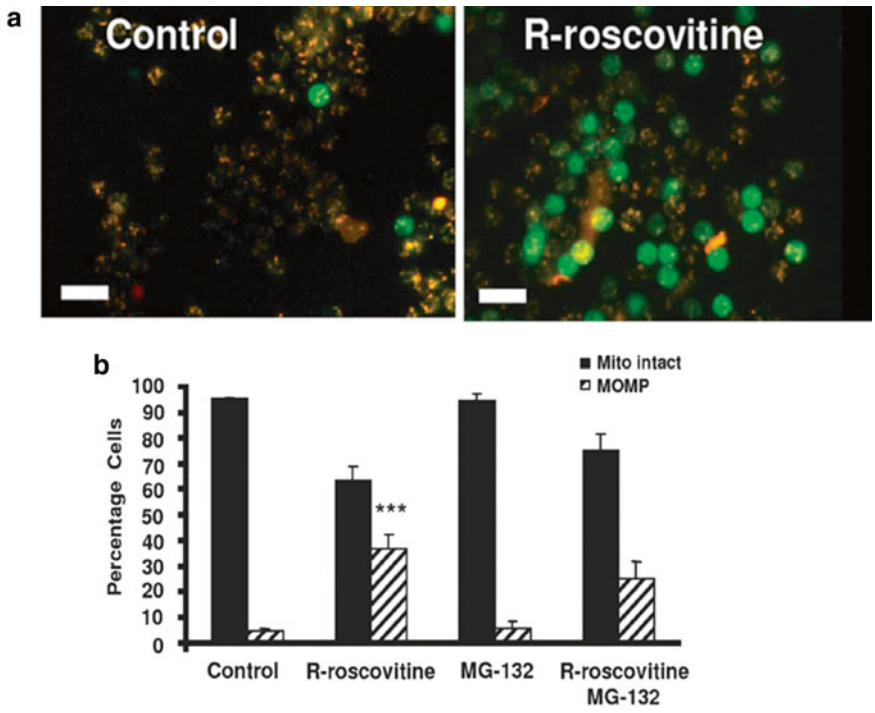

Fig. 4 Analyzing mitochondrial membrane integrity using Mitocapture dye. Two hour incubation in medium (control), the CDKi R-roscovitine (20 μM) and/or proteasome inhibitor MG-132 (50 μM). (**a**) Orange fluorescence occurs in viable neutrophil mitochondria, and green fluorescence is present in neutrophils which have lost mitochondrial outer membrane potential (MOMP). (**b**) Cells can be counted and quantified as depicted in the graph. Images taken at ×320, scale bar corresponds to 20 μm. Adapted from Leitch et al., 2012 (Cell Death and Differentiation, open access)

6. Incubate on shaking heat block at 37 °C, 300 × *g* for 15 min.
7. Centrifuge at 300 × *g* for 5 min and discard supernatant.
8. Resuspend cells in 300 μl MitoCapture™ Incubation buffer.
9. Analyze using a flow cytometer, with increased fluorescence in FL-1 channel indicating loss of $\Delta\psi_M$ and increased apoptosis.

Assessment of Hypodiploid Peak to Measure Apoptosis

Another flow cytometry method to investigate granulocyte apoptosis is the measurement of hypodiploid peaks. This is carried out by staining DNA in cells. Apoptotic DNA has a different fluorescence histogram profile compared to viable cell DNA.

Propidium iodide staining

1. Neutrophils are isolated from peripheral blood as normal (*see* Subheading 3.1.1) and plated down at 5×10^6 cells/ml in IMDM + 1 % P/S + 10 % autologous serum in a 96-well flat-bottomed cell culture plate with low evaporation lid. Induce apoptosis using conventional methods (Subheading 3.1.2).

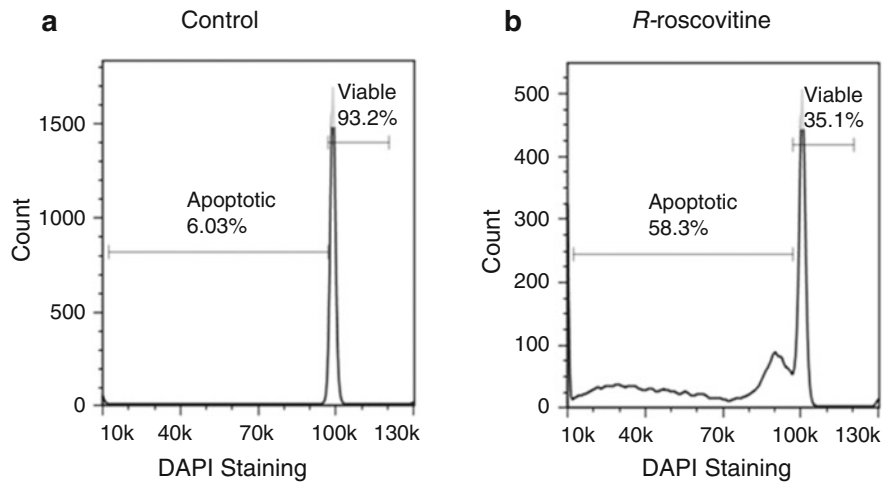

Fig. 5 Assessing neutrophil apoptosis via hypodiploid peak measurement by gating on a fluorescence histogram. Apoptotic DNA forms a broad peak below the narrow peak of viable (G1 phase) DNA. In (**b**) *R*-roscovitine (20 μM) treated neutrophils, levels of apoptosis are higher than in (**a**) Control (untreated) neutrophils after 6 h

2. At desired time point (e.g., 6 and 20 h)—aspirate neutrophil suspension and add 50 μl cells to 250 μl PI staining solution. Incubate for 30 min, protected from light.
3. Neutrophil apoptosis assessed at the sub-G1 peak region (broad hypodiploid peak) below the narrow peak of viable DNA (G0/G1 peak). Measure propidium iodide-stained DNA on a fluorescence histogram—gate the sub-G1 peak regions to give the percentage of apoptosis (*see* Fig. 5).

DAPI (4′,6-diamidino-2-phenylindole) Staining

1. Neutrophils are isolated from peripheral blood as normal (*see* Subheading 3.1.1) and plated down at 5×10^6 cells/ml in IMDM + 1 % P/S + 10 % autologous serum in a 96-well flat-bottomed cell culture plate with low evaporation lid. Induce apoptosis using conventional method (Subheading 3.1.2).
2. At a desired time point (e.g., 6 and 20 h) aspirate neutrophil cell suspension and add 100 μl neutrophils to 100 μl DAPI solution in a FACS tube. Incubate for 1–2 min at room temperature (protected from light). Do not leave cells in DAPI solution for longer than 1–2 min, and add cells to DAPI as you run each sample on a flow cytometer, i.e., add DAPI to each tube one at a time and run immediately.
3. Neutrophil apoptosis is assessed at the sub-G1 peak region (broad hypodiploid peak) below the narrow peak of viable DNA (G0/G1 peak). Measure DAPI-stained DNA on a fluorescence histogram—gate the sub-G1 peak regions to give the percentage of apoptosis (*see* Fig. 5).

3.1.7 Confocal Imaging of Isolated Granulocytes

This protocol describes immunostaining of isolated granulocytes, allowing imaging of, for example, CDK7 and CDK9; or other molecules/complexes downstream (e.g., RNA Polymerase II). Appropriate controls for these studies are: unlabelled cells, cells with primary antibody only; and cells with secondary antibody only. Combine with 4′,6-diamidino-2-phenylindole (DAPI) staining to allow cellular structure to be imaged (*see* Fig. 6).

1. Pellet cells at (2.5×10^6 cells/ml) by centrifugation at $300 \times g$ for 4 min.
2. Resuspend cells and transfer to coverslips.
3. Fix cells for 20 min in 3 % paraformaldehyde (PFA).
4. Wash and quench with 50 mM glycine.
5. Resuspend cells in 50 μl of 10 % serum (from the same animal as secondary antibody) and block for 1 h.
6. Remove supernatant and gently place coverslips onto 100 μl of primary antibody diluted to the appropriate concentration for 1 h.
7. Wash then incubate with 50 μl of appropriate fluorescent conjugated secondary antibody and DAPI/PI nuclear stain (2 μl in 1 ml) for 1 h.
8. Wash in PBS, then finally in ddH_2O.

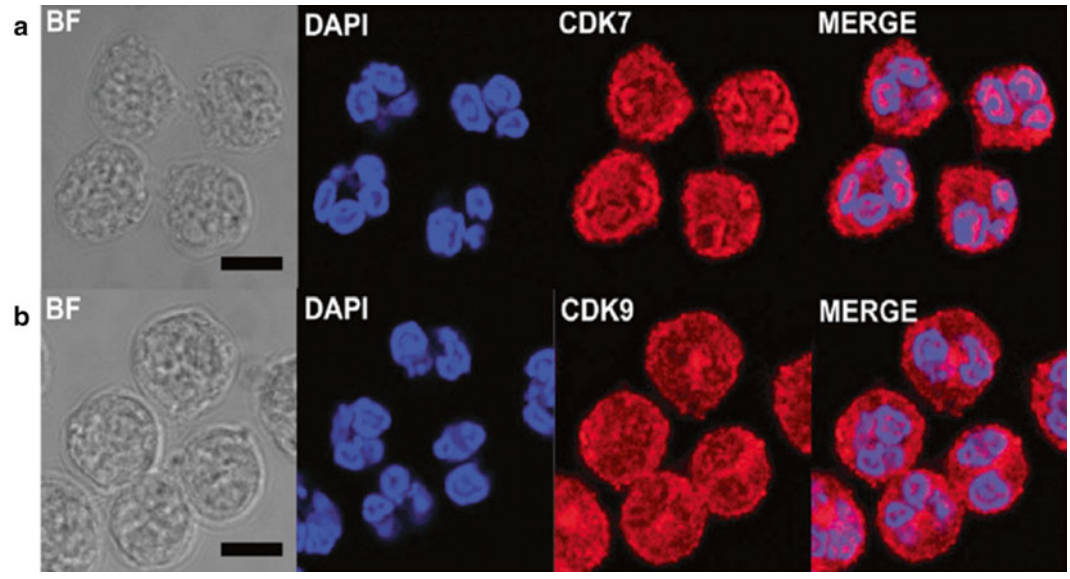

Fig. 6 Red immunofluorescent staining for CDK7 (**a**) and CDK9 (**b**) in conjunction with DAPI (*blue*) nuclear staining, demonstrating nuclear co-localization in the merged image. ×630 oil immersion lens. Representative image from $n = 3$ experiments. Scale bar = 5 μm scale. Adapted from Leitch et al., 2012 (Cell Death and Differentiation, open access)

9. Transfer coverslips to slides and mount with mowiol mounting solution and seal with nail varnish prior to visualization on a confocal microscope.

3.1.8 Western Blotting for CDK Expression

Western blotting is used as a method of assessing protein levels in a sample of cells. In this context it can be used to assess CDK levels with/without treatment, as well as the expression of proteins downstream of CDKs, using CDK-specific primary antibodies. Western blotting can also be used to assess apoptosis, for example, by using an antibody against cleaved caspase 3; which is expressed at increased levels during apoptosis (*see* Fig. 7).

1. Suspend cells at a concentration of 4×10^6 cells/ml in IMDM with 10 % autologous serum. Add 750 μl of the cell suspension into a 2 ml Eppendorf tube. Incubate with 150 μl of CDK inhibitor agents and 600 μl IMDM (10 % autologous serum) to give a total volume of 1500 μl.
2. Incubate the cells at 37 °C in a shaking heat block for the required time.
3. Centrifuge the Eppendorf tubes for 1 min at 16,000 × *g* and discard supernatants.
4. Resuspend the pellet of cells in 90 μl protease inhibitor buffer, incubate for 10 min on ice (*see* **Note 2**).
5. Add 10 μl 10 % NP-40 (diluted in TBS) to each Eppendorf, vortex, and incubate for a further 10 min on ice.
6. Centrifuge for 20 min at 16,000 × *g* at 4 °C. Transfer the supernatant, which contains the soluble protein fraction, into a 500 μl Eppendorf tube. Samples can be frozen at −20 °C until use.
7. Calculate protein concentration of each sample using a BCA protein assay (e.g., Thermo Scientific) according to manufacturer's instructions.
8. Transfer the required volume containing 30 μg of protein into fresh Eppendorf tubes and make up to 30 μl total volume with PBS and 8 μl of sample buffer (4× concentration).

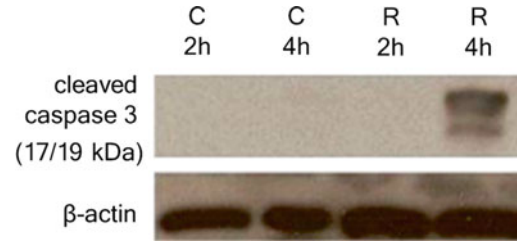

Fig. 7 Western blot of lysed neutrophils for cleaved caspase-3 after incubation with media alone (*C*) or *R*-roscovitine (20 μM) for 2 or 4 h. Adapted from Leitch et al., 2012 (Cell Death and Differentiation, open access)

9. Heat samples at 95 °C for 5 min.
10. Load samples onto a 12 % polyacrylamide gel, alongside molecular weight standards. Run at 110 V until the dye front reaches the bottom of the gel (approximately 60 min).
11. Transfer proteins onto a PVDF membrane (pre-activated for 30 s in 100 % methanol) at 80 V for 1 h at 4 °C.
12. Wash the membrane in TBS/0.1 % Tween® 20 for 5 min on a rocking platform.
13. Add the membrane to a 50 ml Falcon tube. Block for 1 h at room temperature with 10 ml of 5 % dried milk powder in TBS/0.1 % Tween® 20 on a rocking platform.
14. Wash the membrane three times in TBS/0.1 % Tween® 20 for 5 min.
15. Incubate with primary antibody overnight at 4 °C. Generally a 1:1000 concentration of antibody (diluted in 5 ml of TBS/0.1 % Tween® 20 containing 5 % dried milk powder) is a good starting point; but antibody concentration may need to be adjusted as required.
16. Wash membrane in TBS/0.1 % Tween® 20 each for 5 min (repeat three times).
17. Incubate for 2 h with the appropriate secondary antibody diluted 1:2500 (in 5 ml TBS/0.1 % Tween® 20 containing 5 % dried milk powder).
18. Wash membrane three times in TBS/0.1 % Tween® 20 for 5 min.
19. Develop the membrane using an enhanced chemiluminescence kit according to the manufacturer's instructions, and developing on film using a developer.
20. Strip and reprobe blot with β-actin or GAPDH as a loading control.

3.1.9 Assessing Phagocytic Uptake of Apoptotic Cells

It is important that apoptotic cells are cleared by phagocytic cells such as macrophages to ensure that the cells do not become necrotic and cause tissue damage. With this in mind, several assays have been developed to examine phagocytic clearance of apoptotic cells; for example flow cytometry or microscopic assessment. This allows assessment of the effect of CDK inhibition on phagocytosis

Plate Assay for Phagocytosis of Apoptotic Granulocyte

Assessing macrophage phagocytosis of apoptotic neutrophils can be conducted using a serum-free phagocytosis assay, modified from the original assay described by Newman et al. [26]. This method uses adherent human monocyte-derived macrophages; it has also been carried out using murine peritoneal and bone marrow-derived monocytes. Opsonins can also be added depending on the required nature of the assay (e.g., C1q).

1. This method accepts the use of adherent macrophages in 48-well plates, cultured in sterile conditions.
2. Suspend 10^8 fresh peripheral blood neutrophils (≥97 % purity) in 20 ml of IMDM/10 % autologous serum (*see* **Note 3**). Add the neutrophil suspension into a 75 cm^2 cell culture flask. Keep the flask on its end in an incubator for 20 h at 37 °C in a 5 % CO_2 incubator.
3. Dispense the neutrophil suspension into a 50 ml conical polypropylene tube. Wash 2× in warm IMDM (50 ml IMDM per wash) by centrifugation at 220 × *g* for 5 min, then discarding the supernatant. After each wash, carefully resuspend the neutrophil pellet in 1 ml of warm (37 °C) IMDM using a Pasteur pipette to prevent cell clumping.
4. Count the cells using a hemocytometer, then resuspend the neutrophils at 4×10^6 cells/ml in warm (37 °C) IMDM (without serum).
5. Remove non-adherent cells from the macrophage monolayer with warm IMDM.
6. Overlay the macrophage monolayer with 0.5 ml (2×10^6 cells) of the neutrophil suspension in serum-free IMDM. Incubate for 60 min at 37 °C in a 5 % CO_2 incubator.
7. Wash each well with ice-cold PBS (without cations). An inverted microscope can be used to check that non-ingested neutrophils have been mostly removed.
8. Repeat the wash as necessary to remove non-ingested neutrophils, continually checking with the microscope to ensure that the macrophage monolayer is not disturbed.
9. Fix each well with 2.5 % glutaraldehyde for 30 min, then rinse with PBS.
10. Stain for neutrophil myeloperoxidase (MPO) by addition of 0.1 mg/ml dimethoxybenzidine and 0.03 % (v/v) H_2O_2 in PBS, for 60 min at room temperature.
11. Count the percentage of MPO-negative macrophages that have phagocytosed one or more apoptotic MPO-positive neutrophils, by examination of at least 5 fields (a minimum of 400 cells) with an inverted microscope. Calculate the mean percentage phagocytosis of duplicate/triplicate wells.

Flow Cytometry-Based Phagocytosis Assay

Induction of granulocyte apoptosis requires effective clearance by phagocytes such as macrophages. One way of measuring this in vitro is by use of a fluorescent chloromethyl dye which crosses cell membranes to label the cytoplasm of live neutrophils or eosinophils. CellTracker™ dyes can also be used in conjunction with a pH sensitive succinimidyl ester (pHrodo™) for definitive discrimination of apoptotic cell phagocytosis. pHrodo™ dyes

fluoresce brightly only in acidic conditions (for example within the phagolysosome). Hence this assay works on the basis that macrophages display dual pHrodo™ and Cell Tracker™ fluorescence upon phagocytosis of apoptotic CellTracker™-green labeled neutrophils/eosinophils.

1. This method accepts the use of adherent monocyte-derived macrophages in Costar® 48-well TC-treated microplates.
2. Suspend neutrophils/eosinophils (≥97 % purity) at 20×10^6 cells/ml in IMDM (+10 % autologous serum) in a 15 ml Falcon conical polypropylene tube. Add 2 μg/ml of 10 mM 5-chloromethylfluorescein diacetate (CellTracker™ Green), pipette gently, and incubate at 37 °C for 30 min.
3. Centrifuge at $220 \times g$ for 5 min and wash cell pellet in PBS, spin again at $220 \times g$ for 5 min.
4. Resuspend cells at 4×10^6 cells/ml in IMDM (10 % autologous serum). Transfer the cell suspension into Costar® 75 cm^2 cell culture flask and incubate for 20 h at 37 °C (5 % CO_2).
5. Transfer the cells into a 50 ml Falcon® conical polypropylene tube and wash twice in warm IMDM (50 ml volume per wash, $220 \times g$ for 5 min) and discard the supernatant. Following each wash, resuspend the cell pellet in 1 ml of warm IMDM to avoid cell clumping. Resuspend the aged neutrophils/macrophages at 1×10^6 cells/ml in warm HBSS (37 °C).
6. Incubate cells with 20 ng/ml pHrodo™ (30 min, room temperature).
7. Centrifuge at $220 \times g$ for 5 min and wash cell pellet in PBS, spin again at $220 \times g$ for 5 min (pellet should be red if pHrodo™ staining has worked correctly).
8. Resuspend cells at 4×10^6/ml in warm IMDM (serum free).
9. Rinse the macrophages with warm IMDM to wash off non-adherent cells.
10. Pipette 500 μl (2×10^6 cells) of labeled, aged neutrophils/eosinophils in IMDM (serum-free) on top of the macrophage monolayer. Incubate for 60 min at 37 °C in a 5 % CO_2 atmosphere (*see* **Note 4**).
11. Remove the neutrophil/eosinophil suspension from the plate and wash macrophages with PBS three times.
12. Incubate the macrophages with 500 μl of 0.25 % trypsin/1 mM ethylenediaminetetraacetic acid solution for 10 min at 37 °C followed by 10 min at 4 °C.
13. Collect the detached macrophages by pipetting vigorously and place in a flow cytometer tube on ice

14. Analyze samples immediately by flow cytometry. Apoptotic cells and macrophage populations are identified by their distinct forward and side scatter characteristics. Divide the number of dual CellTracker/pHrodo positive events in the macrophage gate by the total macrophage number, in order to calculate the percentage of macrophages that have internalized apoptotic cells.

3.1.10 Transfection of Cell Lines with siRNA to Knockdown Genes of Interest

This technique can be used to knockdown specific genes to reveal their role during inflammation and resolution. It is often carried out in cell lines (e.g., the neutrophil-like HL-60 cell line, and the eosinophil-like EOL-1 cell line), as primary granulocytes are generally not amenable to genetic manipulation due to their short lifespan. The efficacy of knockdown can be determined using western blotting (Subheading 3.1.7). Here this technique is described for HL-60 cells.

1. Culture HL-60 cells (ATCC, Middlesex, UK) in RMPI-1640 (PAA) supplemented with 10 % heat-inactivated fetal bovine serum, 2 mM L-glutamate, penicillin (100 U/ml), and streptomycin (100 U/ml) at 2–5 × 1–5 cells/ml at 37 °C in 5 % CO_2.
2. Resuspend cells at 4×10^6 cells/ml in PBS (without cations).
3. Aliquot 1 ml of cells into a 1.5 ml Eppendorf tube.
4. Centrifuge and resuspend in 100 μl Nucleofector solution (Lonza) and 200 nM Mcl-1 siRNA or scrambled sequence siRNA (Dharmacon, Rockford, IL).
5. Using Nucleofector Kit V; transfer cells into an Amaxa Nucleofector™ cuvette and transfect by electroporation (Amaxa (Cambridge, UK) at setting T-019.
6. After transfection, transfer cells into 12-well plates containing 2 ml of the culture medium for 4 h. Afterwards, transfer to 6-well plates containing 10 ml culture media.
7. Centrifuge cells at 300 × *g* for 5 min. Resuspend in PI staining buffer.
8. HL-60 cell survival and apoptosis can be assessed by changes in forward and side scatter profiles, or assessment of hypodiploid peak [27] (Subheading 3.1.5).

3.2 In Vivo Rodent Models

A large variety of mouse models exist which can be used to investigate inflammation and resolution; both sterile and non-sterile, e.g., bleomycin sulfate-induced, LPS-induced, or infection with *E. coli*. This is caused by administration of an inflammatory stimulus to the mouse that can be manipulated by treatment with compounds such as CDK inhibitor drugs. Here we describe some previously used models (*see* Fig. 8).

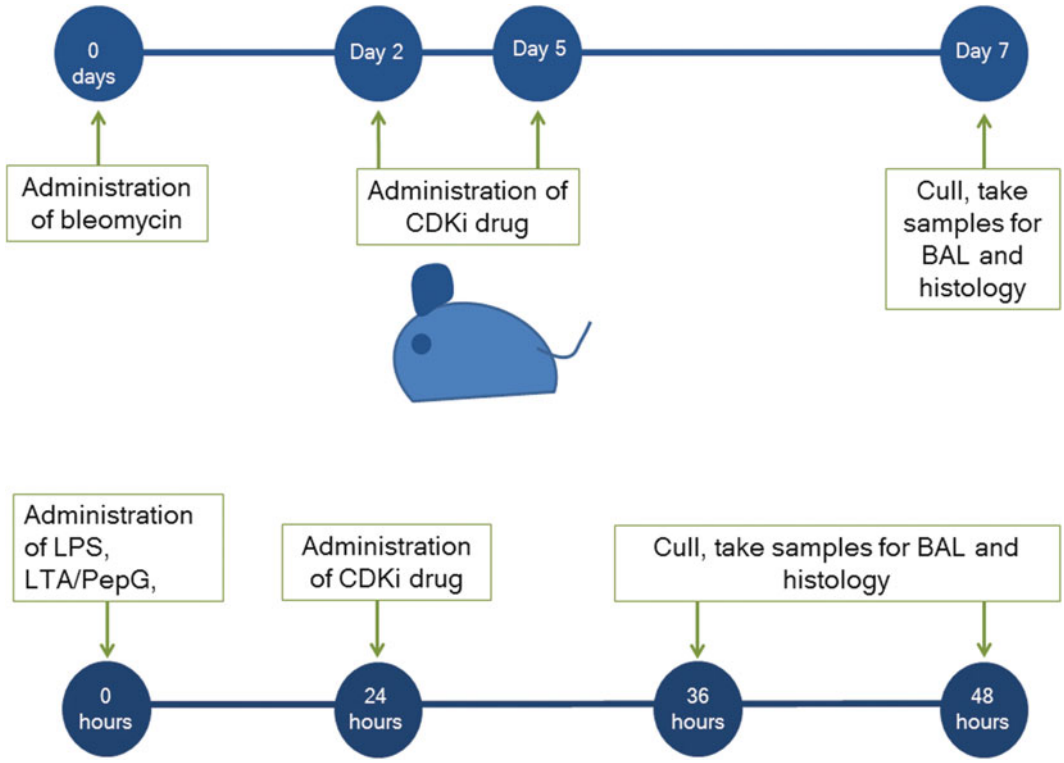

Fig. 8 Diagrammatical representation of the typical time-courses of bleomcyin and LPS, LTA/PepG-induced inflammation, and when CDKi treatment can be given

3.2.1 Bleomycin Sulfate-Induced Lung Inflammation

This model has previously been performed in C57BL/6J mice, weighing at least 20 g, kept under pathogen free conditions (*see* **Note 5**).

1. Anesthetize mouse using an appropriate anesthetic, such as isofluorane (according to standard operating procedures).
2. Suspend mice upright and rest teeth on a rigid wire, allowing tongue to be protruded.
3. Place 50 μl of 0.033 mg bleomcyin sulfate onto the oropharynx.
4. Cover the mouse nose briefly, to cause aspiration of the solution, while retaining tension on the tongue.
5. Allow mouse to recover from anesthesia.
6. On day 2 and day 5 after the bleomycin sulfate treatment, treat the mice intratracheally with 50 μl of 0.05 % DMSO as a vehicle control, or 10 mg/kg of CDK inhibitor compound (e.g., *R*-Roscovitine).
7. Euthanize mice 7 days after bleomycin/saline administration (e.g., with a 200 μl intraperitoneal injection of sodium pentobarbitone [200 mg/ml]).

3.2.2 Lipopolysaccharide (LPS) or Lipotechoic Acid (LTA)/Peptidoglycan (PepG)-Induced Lung Inflammation

Use female C57Bl6 mice, 8–12 weeks old, kept under pathogen-free conditions.

1. Induce anesthesia in animals by inhalation of isoflurane.
2. For LPS: Inject 1 μg *E. coli*-derived LPS (0.127:B8) intratracheally (i.t.) in 50 μl sterile saline.
   For LTA/peptidoglycan: Inject combined *S. Aureus*-derived lipotechoic acid (50 μg) and peptidoglycan (150 μg).
3. At 24 h after LPS or LTA/PepG treatment; inject 30 mg/kg of CDK inhibitor compound intraperitoneally (i.p.) in 200 μl sterile saline.
4. Euthanize animals after appropriate time point as described below for lavage and histology with a 200 μl intraperitoneal injection of sodium pentobarbitone (200 mg/ml).

3.2.3 Bronchoalveolar Lavage (BAL) and Histology

1. Open the diaphragm via the peritoneal cavity, remove the rib cage.
2. Cannulate the lungs via the trachea in situ. Tie a fine cannula in place with a single suture. Perform BAL by carrying out three washes of 0.8 ml ice-cold sterile 0.9 % saline.
3. Centrifuge the retrieved samples at 180 × *g* for 5 min at 4 °C.
4. Remove supernatant and resuspend cell pellet in 0.5 ml sterile 0.9 % saline.
5. Count cell numbers with a nucleocounter.
6. Prepare cytocentrifuge slides and stain with Diff Quick™ (*see* Subheading 3.1.4).
7. Count at least 300 cells per slide and express results as total number of neutrophil/macrophages in total lavage volume.
8. Sections of lung tissue can be prepared by histological methods (without BAL, so tissue integrity is not disturbed). Embed the lung sections in paraffin and stain with hematoxylin and eosin. Figure 9 shows that in *R*-roscovitine-treated animals, lung tissue has less inflammatory cell infiltrate after bleomycin-induced lung injury.

3.3 Zebrafish as an In Vivo Animal Model to Investigate CDKs

It may seem a strange peculiarity that zebrafish are being used for medical research but there are numerous human diseases being investigated through the use of zebrafish. For the 2465 human conditions with an associated human sequence, it has been determined that 1608 (65 %) have at least one candidate zebrafish protein [28]. The zebrafish genome is said to regulate 26,241 zebrafish protein-coding genes; for further details *see* Kettleborough et al. [29]. Furthermore, the human genome shows at least 70 % of human genes have at least one orthologous gene in zebrafish [30].

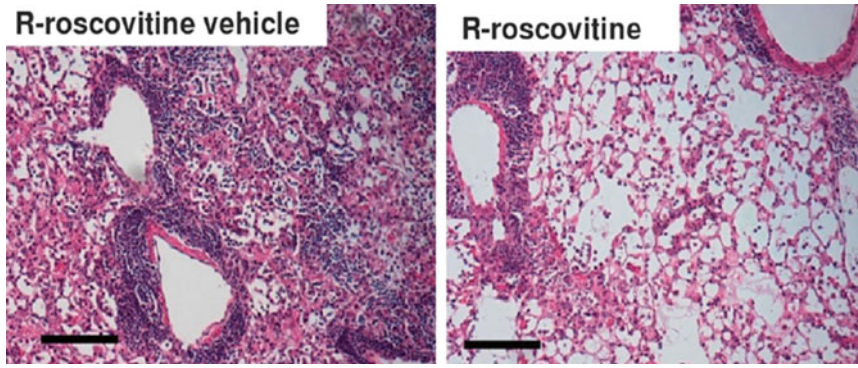

Fig. 9 Histological images (hematoxylin and eosin staining) of mouse lung tissue of R-roscovitine vehicle (control) and R-roscovitine-treated mice, taken at magnification ×100. Scale bar: 100 μm. Adapted from Leitch et al., 2012 (Cell Death and Differentiation, open access)

The zebrafish is an innovative animal model to investigate inflammatory disease and resolution [31], as the zebrafish embryo is optically clear, and transgenic lines exist with specific fluorescent inflammatory cells. This allow the unique opportunity for continuous in vivo observations of cell populations during the inflammatory response. The zebrafish is genetically tractable and with systems such as Tol2 transgenesis it is becoming relatively simple to generate new transgenic lines [32]. Zebrafish produce a large number of eggs that rapidly develop to adulthood (approximately 3 months) independently of the mother; therefore experiments can be rapid and high throughput when compared to mouse models.

Fish with specific fluorescent protein expression in inflammatory cells, such as neutrophils and macrophages, have been generated and characterized [16, 17, 33, 34]. The zebrafish only possesses innate inflammatory cells such as neutrophils, eosinophils, and macrophages at this early developmental stage (<10 dpf), allowing innate inflammation to be investigated without the interference of the adaptive immune response [35]. Transgenic lines can be crossed to image cell-cell interactions (*see* Fig. 10).

Transection and wounding of the fish tailfin is a previously described sterile inflammatory model which has allowed investigation of the mechanisms of CDKi-induced neutrophil apoptosis [19, 36]. Wounding results in rapid neutrophil/macrophage recruitment to the injury site (within hours), which can be imaged and manipulated in various ways, both pharmacologically and genetically. Other inflammatory models have been established in the zebrafish; such as wounding of the brain [37], wounding of the vasculature [38], and infection models caused by microinjection of bacteria [39].

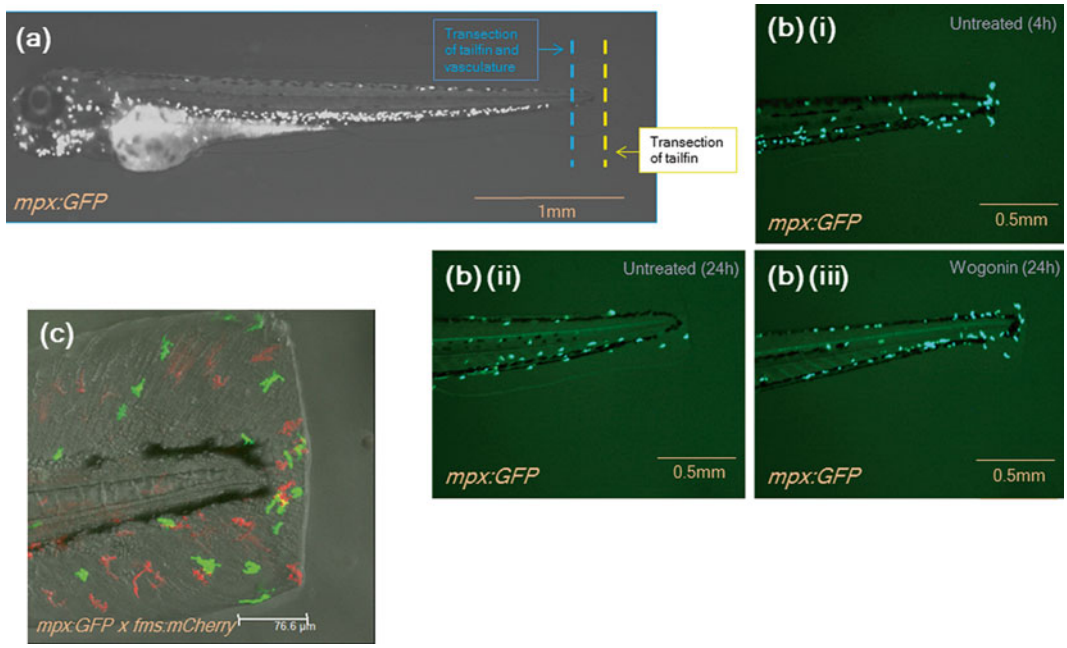

Fig. 10 (**a**) Zebrafish embryo showing transection of tailfin and the more severe tailfin and vasculature transection (4×). (**b**) Injury site of *mpx:GFP* embryo with a wounded tailfin, after (*i*) 4 h, (*ii*) 24 h and (*iii*) 24 h with CDKi drug treatment (Wogonin, 50 μM, 8×). (**c**) Example of double transgenic mpx:GFP × fms:mCherry, after tailfin transection. Images acquired by the authors

There exist various ways to manipulate genes of interest in the zebrafish embryo, including morpholinos, transcription activator-like effector nucleases (TALENs) and clustered regularly interspaced short palindromic repeats (CRISPRs). Morpholinos, as well as pharmacological interventions, have been used in this model to target the ERG gene, which attenuates the neutrophil inflammatory response to wounding [40].

3.3.1 Transection of the Zebrafish Tailfin

This technique can be carried out in transgenic zebrafish embryos with fluorescently labeled neutrophils and macrophages to image inflammation at the injury site; the use of such transgenic reporters allows continuous assessment of the inflammatory response.

1. Fish at 3 days post fertilization are anesthetized using 4.2 % (w/w) Tricaine MS222 diluted in E3 embryo medium. This is typically done in a small petri dish (50 mm).
2. A Pastette transfer pipette is used to transfer the embryo to the top of a petri dish lid. Excess water is removed using tissue paper.
3. The tailfin wounding assay can be performed using a sterile scalpel. This can be done by (a) fully transecting the tailfin,

without damaging the caudal vein of the fish (*see* Fig. 10) [19]; (b) by fully transecting the tailfin and also damaging the caudal vein [16]; or by causing a smaller "nick" wound to the ventral fin rather than a full transection [40]. The fin nick can also be done with a 19-G needle. Injury can also be carried out using a laser [41].

4. The fish can then be placed in fresh E3 embryo medium to recover, and imaged at the required time point by placing them back under anesthesia (as in **step 1**).
5. The fish can be imaged in a petri dish of embryo medium/4.2 % v/v Tricaine MS222 anesthetic under a standard fluorescent microscope. They can also be mounted on a slide to image for confocal microscopy.
6. Each fish can be placed in an individual well of a plate to allow it to be tracked over time. The use of double transgenic lines, e.g., Tg(*mpx*:*eGFP*) and Tg(*fms*:*mCherry*) (*see* Fig. 10c), allows simultaneous tracking of neutrophils and macrophages, respectively. Typically the peak of neutrophilic inflammation is 4–6 h and resolves over 24–48 h. Still images can be taken at regular intervals and the number of cells in the area of the inflammatory response counted at each time point (*see* Fig. 10). Time Lapse movies can be made with appropriate software. These can be analyzed with software such as Volocity, which can be used to track the migratory behavior of the cells (e.g., speed, directionality, distance traveled).

3.3.2 Pharmacological Manipulation of Zebrafish Inflammatory Response

At 4–6 h post transection (peak neutrophil inflammatory response) the embryo can be treated with CDKi compounds, as described [18, 19].

1. The compound is made up to stock concentration (often in <1 % DMSO, unless it can be dissolved in saline) then can be diluted in E3 embryo medium to desired concentration in each well of the plate, as a bath solution. This is usually similar concentrations to those used in vitro cell culture concentrations. A typical concentration would be 20 μM [18]. Alternatively, compounds can be given via microinjection (*see* **Note 6**).
2. Assessment of the inflammatory response can be made, as detailed in Subheading 3.3.1 (**step 5**).

3.3.3 Genetic Manipulation of Zebrafish Inflammatory Responses

Specific, stable, heritable knockdown techniques have been developed which are relatively simple to carry out in zebrafish; such as TALEN and CRISPR technologies [42, 43]. In addition, transient gene knockdown can be caused by microinjection of synthetic oligonucleotide morpholino sequences [44], which bind to genes of interest and prevent their transcription or translation. Here is a

brief description of the technique of microinjecting procedure, used to microinject morpholino, TALEN or CRISPR sequences into newly laid zebrafish eggs; or plasmids to create transgenic fish.

1. Set up pair-mating crosses of fish the night before, with a divider between the male and female. Remove divider the next morning when lights are turned on, or as eggs are required.
2. Pre-prepare micropipette needles. Use capillary tubes pulled in a needle puller.
3. Load injection solution into the micropipette needle. Attach to needle holder of an injection rig (consisting of microinjector [such as a Narishige IM-300 or WPI PV-820] and needle holder), connected to a nitrogen cylinder, and micromanipulator.
4. Prior to commencing injections, the micropipette needle must be calibrated so that the injection volume, injected into mineral oil is known; this will allow the calculation of injected DNA (*see* Fig. 11).
5. Inject solution into the developing cell of the egg, when it is at the 1-cell stage (around 15 min after the egg harvest). Subsequently the cell should generally be orientated away from the needle; this will prevent damage to the cell mass (*see* Fig. 11). Targeted morpholino (fluorescently labeled) synthetic oligonucleotides which can be used for gene knockdown, can be injected from 1-cell up to and including the 8–16 cell stages, into the area of cytoplasmic streaming beneath the cell mass.
6. Store injected eggs in a petri dish in embryo medium at 28.5 °C. Morpholino efficacy can be detected by western blotting (for ATG targeting morpholinos) or RT-PCR (for splice site-targeting morpholinos). TALEN or CRISPR embryos must undergo a full genotyping process.

In summary; various methods exist to investigate the cross talk between inflammation, apoptosis and cyclin-dependent kinases. There are various models available to researchers to unpin the role of specific molecules, ranging from isolated primary human cells, cell lines (which are easier to manipulate at the genetic level than primary cells), in vivo models such as zebrafish (allowing simple genetic and pharmacological manipulation, and real time imaging in vivo) and mouse inflammatory models (in which human-like diseases can be modeled and treated). CDKs have been known for some time to play a role in the cell cycle; however, they are increasingly being recognized as having important roles to play in the transcription of important cell proteins; notably Mcl-1 in neutrophils and eosinophils, an anti-apoptotic member of the Bcl-2 family.

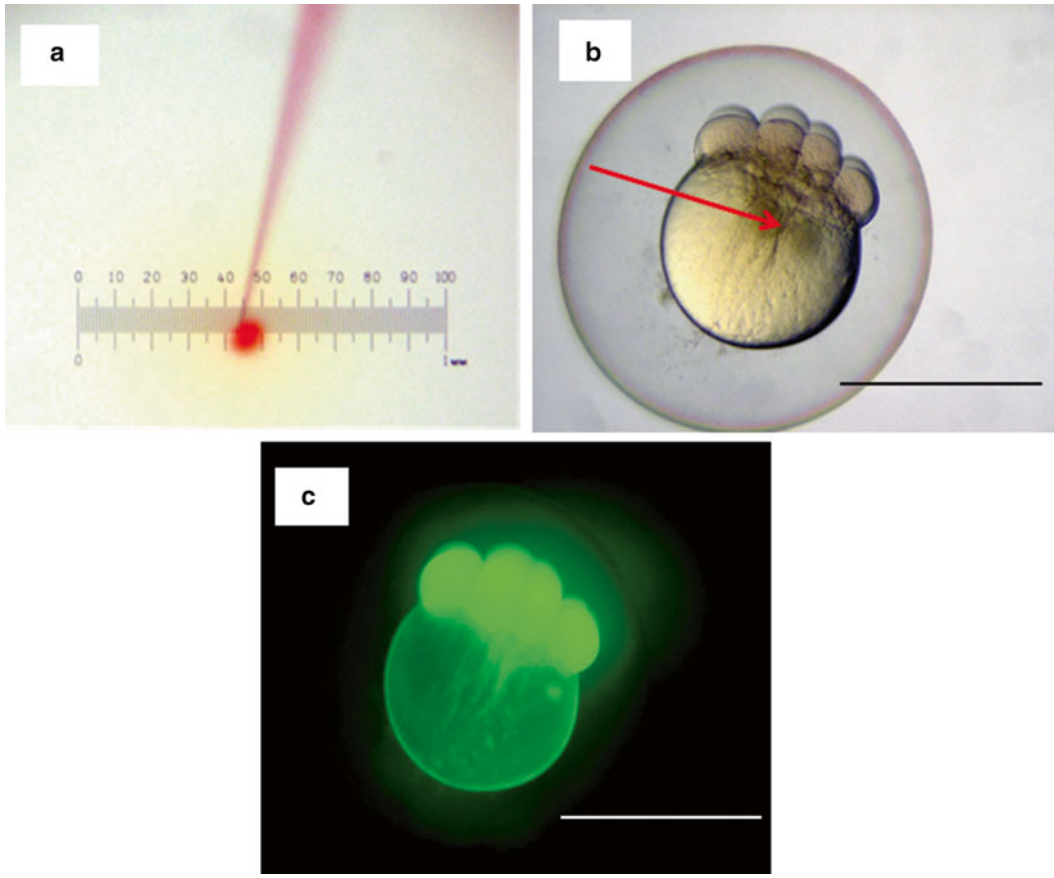

Fig. 11 Microinjection into zebrafish eggs. (**a**) Calibration of micropipette delivered bolus size. Bolus size of 100 μm diameter (on a 1 mm graduated scale) with radius of 50 μm (or 0.05 mm). The bolus therefore has a volume is 0.00052 μl or 0.5 nl. Delivered DNA concentration can subsequently be calculated. (**b**) Bright-field image of an 8-cell stage with cytoplasmic streaming injection site indicated by *red arrow*. (**c**) Successful injections will be observed with the cell mass fluorescing and therefore predict morpholino knockdown. Scale bar 0.5 mm. Images acquired by the authors

4 Notes

1. Cells which have undergone apoptosis later proceed to secondary necrosis; hence later time points such as 24 h post-CDKi treatment make it more difficult to assess apoptosis levels.
2. From this point onwards it is important that all steps are carried out on ice, due to the high level of proteases present in neutrophils and eosinophils.
3. Neutrophils should be washed in HBSS prior to assay, to ensure they are free of serum opsonins such as Protein S.
4. This is an excess number of apoptotic neutrophils/eosinophils in order to determine macrophage phagocytic capacity and

therefore is not a surrogate marker of eosinophil/neutrophil apoptosis.

5. Different strains of mice exhibit different types of inflammatory response.
6. The compound administration can also occur via microinjection into the embryo, into an area such as the yolk sac, to better ensure uptake [45].

References

1. Leitch AE, Duffin R, Haslett C, Rossi AG (2008) Relevance of granulocyte apoptosis to resolution of inflammation at the respiratory mucosa. Mucosal Immunol 1(5):350–363
2. Fox S, Leitch AE, Duffin R, Haslett C, Rossi AG (2010) Neutrophil apoptosis: relevance to the innate immune response and inflammatory disease. J Innate Immun 2:216–227
3. Leitch AE, Haslett C, Rossi AG (2009) Review: cyclin-dependent kinase inhibitor drugs as potential novel anti-inflammatory and pro-resolution agents. Br J Pharmacol 158: 1004–1016
4. Leitch AE, Lucas CD, Marwick JA, Duffin R, Haslett C, Rossi AG (2012) Cyclin-dependent kinases 7 and 9 specifically regulate neutrophil transcription and their inhibition drives apoptosis to promote resolution of inflammation. Cell Death Differ 1–12
5. Rossi AG, Sawatzky DA, Walker A, Ward C, Sheldrake TA, Riley NA, Caldicott A, Martinez-Losa M, Walker TR, Duffin R, Gray M, Crescenzi E, Martin MC, Brady HJ, Savill JS, Dransfield I, Haslett C (2006) Cyclin-dependent kinase inhibitors enhance the resolution of inflammation by promoting inflammatory cell apoptosis. Nat Med 12(9): 1056–1064
6. Lucas CD, Dorward DA, Tait MA, Fox S, Marwick JA, Allen KC, Robb CT, Hirani N, Haslett C, Duffin R, Rossi AG (2013) Downregulation of Mcl-1 has anti-inflammatory pro-resolution effects and enhances bacterial clearance from the lung. Mucosal Immunol 10
7. Leitch AE, Riley NA, Sheldrake TA, Festa M, Fox S, Duffin R, Haslett C, Rossi AG (2010) The cyclin-dependent kinase inhibitor *R*-Roscovitine down-regulates Mcl-1 to override pro-inflammatory signalling and drive neutrophil apoptosis. Eur J Immunol 40: 1127–1138
8. Alessandri AL, Duffin R, Leitch AE, Lucas CD, Sheldrake TA, Dorward DA, Hiriani N, Pinho V, de Sousa LP, Teixeira MM, Lyons JF, Haslett C, Rossi AG (2011) Induction of eosinophil apoptosis by the cyclin-dependent kinase inhibitor AT7519 promotes the resolution of eosinophil-dominant allergic inflammation. PLoS One 6(9):1–10
9. Smallie T, Ricchetti G, Horwood NJ, Feldmann M, Clark AR, Williams LM (2010) IL-10 inhibits transcription elongation of the human TNF gene in primary macrophages. J Exp Med 207(10):2081–2088
10. Wang S, Fischer PM (2008) Cyclin-dependent kinase 9: a key transcriptional regulator and potential drug target in oncology, virology and cardiology. Trends Pharmacol Sci 29(9): 302–313
11. Haslett C, Guthrie LA, Kopaniak MM, Johnston RB, Henson PM (1985) Modulation of multiple neutrophil functions by preparative methods or trace concentrations of bacterial lipopolysaccharide. Am J Pathol 119:101–110
12. Youssef PP, Mantzioris BX, Roberts-Thomson PJ, Ahern MJ, Smith MD (1995) Effects of ex vivo manipulation on the expression of cell adhesion molecules on neutrophils. J Immunol Methods 186:217–224
13. Macey MG, McCarthy DA, Vordermeier S, Newland AC, Brown KA (1995) Effects of cell purification methods on CD11b and L-selectin expression as well as the adherence and activation of leucocytes. J Immunol Methods 181: 211–219
14. Hu Y (2012) Isolation of human and mouse neutrophils ex vivo and in vitro. Methods Mol Biol 844:101–113
15. Dorward DA, Lucas CD, Alessandri AL, Marwick JA, Rossi F, Dransfield I, Haslett C, Dhaliwal K, Rossi AG (2013) Technical advance: autofluorescence-based sorting: rapid and nonperturbing isolation of ultrapure neutrophils to determine cytokine production. J Leukoc Biol 94(1):193–202
16. Renshaw SA, Loynes CA, Trushell DMI, Elworthy S, Ingham PW, Whyte MKB (2006)

A transgenic zebrafish model of neutrophilic inflammation. Blood 108(13):3976–3978

17. Gray C, Loynes CA, Whyte MKB, Crossman DC, Renshaw SA, Chico TJA (2010) Simultaneous intravital imaging of macrophage and neutrophil behaviour during inflammation using a novel transgenic zebrafish. Thromb Haemost 105(5):811–819
18. Loynes CA, Martin JS, Robertson A, Trushell DMI, Ingham PW, Whyte MKB, Renshaw SA (2010) Pivotal advance: pharmacological manipulation of inflammation resolution during spontaneously resolving tissue neutrophilia in the zebrafish. J Leukoc Biol 87:203–212
19. Lucas CD, Allen KC, Dorward DA, Hoodless LJ, Melrose LA, Marwick JA, Tucker CS, Haslett C, Duffin R, Rossi AG (2013) Flavones induce neutrophil apoptosis by down-regulation of Mcl-1 via a proteasomal-dependent pathway. FASEB J 27(3):1084–1094
20. Michlewska S, Dransfield I, Megson IL, Rossi AG (2009) Macrophage phagocytosis of apoptotic neutrophils is critically regulated by the opposing actions of pro-inflammatory and anti-inflammatory agents: key role for TNF-α. FASEB J 23:844–854
21. Chomarat P, Banchereau J, Davoust J, Palucka AK (2000) IL-6 switches the differentiation of monocytes from dendritic cells to macrophages. Nat Immunol 1(6):510–514
22. Walker A, Ward C, Dransfield I, Haslett C, Rossi AG (2003) Regulation of granulocyte apoptosis by hemopoietic growth factors, cytokines and drugs: potential relevance to allergic inflammation. Curr Drug Targets Inflamm Allergy 2(4):339–347
23. Felton JM, Lucas CD, Rossi AG, Dransfield I (2014) Eosinophils in the lung – modulating apoptosis and efferocytosis in airway inflammation. Front Immunol 5(302):1–11
24. Yamaguchi Y, Hyashi YI, Sugama Y, Miura Y, Kasahara T, Kitamura S, Torisuj M, Mita S, Tominaga A, Takatsu K, Suda T (1988) Highly purified murine interleukin 5 (IL-5) stimulates eosinophil function and prolongs in vitro survival. J Exp Med 167:1737–1742
25. Farahi N, Uller L, Juss JK, Langton AJ, Cowburn AS, Gibson A, Foster MR, Farrow SN, Marco-Casanova P, Sobolewski A, Condliffe AM, Chilvers ER (2011) Effects of the cyclin-dependent kinase inhibitor *R*-Roscovitine on eosinophil survival and clearance. Clin Exp Allergy 41(5):673–687
26. Newman SL, Henson JE, Henson PM (1982) Phagocytosis of senescent neutrophils by human monocyte-derived macrophages and rabbit inflammatory macrophages. J Exp Med 156(2):430–442
27. Nicoletti I, Migliorati G, Pagliacci MC, Grignani F, Riccardi C (1991) A rapid and simple method for measuring thymocyte apoptosis by propidium iodide staining and flow cytometry. J Immunol Methods 139(2):271–279
28. Coutinho P (2005) Models of human genetic diseases. BMC Bioinformatics 2005:6 (Suppl 4:P7)
29. Kettleborough RN, Busch-Nentwich EM, Harvey SA, Dooley CM, de Bruijn E, van Eeden F, Sealy I, White RJ, Herd C, Nijman IJ, Fényes F, Mehroke S, Scahill C, Gibbons R, Wali N, Carruthers S, Hall A, Yen J, Cuppen E, Stemple DL (2013) A systematic genome-wide analysis of zebrafish protein-coding gene function. Nature 496(7446):494–947
30. Howe K, Clark MD, Torroja CF, Torrance J, Berthelot C, Muffato M, Collins JE, Humphray S, McLaren K, Matthews L, McLaren S, Sealy I, Caccamo M, Churcher C, Scott C, Barrett JC, Koch R, Rauch GJ, White S, Chow W, Kilian B, Quintais LT, Guerra-Assunção JA, Zhou Y, Gu Y, Yen J, Vogel JH, Eyre T, Redmond S, Banerjee R, Chi J, Fu B, Langley E, Maguire SF, Laird GK, Lloyd D, Kenyon E, Donaldson S, Sehra H, Almeida-King J, Loveland J, Trevanion S, Jones M, Quail M, Willey D, Hunt A, Burton J, Sims S, McLay K, Plumb B, Davis J, Clee C, Oliver K, Clark R, Riddle C, Elliot D, Threadgold G, Harden G, Ware D, Begum S, Mortimore B, Kerry G, Heath P, Phillimore B, Tracey A, Corby N, Dunn M, Johnson C, Wood J, Clark S, Pelan S, Griffiths G, Smith M, Glithero R, Howden P, Barker N, Lloyd C, Stevens C, Harley J, Holt K, Panagiotidis G, Lovell J, Beasley H, Henderson C, Gordon D, Auger K, Wright D, Collins J, Raisen C, Dyer L, Leung K, Robertson L, Ambridge K, Leongamornlert D, McGuire S, Gilderthorp R, Griffiths C, Manthravadi D, Nichol S, Barker G, Whitehead S, Kay M, Brown J, Murnane C, Gray E, Humphries M, Sycamore N, Barker D, Saunders D, Wallis J, Babbage A, Hammond S, Mashreghi-Mohammadi M, Barr L, Martin S, Wray P, Ellington A, Matthews N, Ellwood M, Woodmansey R, Clark G, Cooper J, Tromans A, Grafham D, Skuce C, Pandian R, Andrews R, Harrison E, Kimberley A, Garnett J, Fosker N, Hall R, Garner P, Kelly D, Bird C, Palmer S, Gehring I, Berger A, Dooley CM, Ersan-Ürün Z, Eser C, Geiger H, Geisler M, Karotki L, Kirn A, Konantz J, Konantz M, Oberländer M, Rudolph-Geiger S, Teucke M, Lanz C, Raddatz G, Osoegawa K, Zhu B, Rapp A, Widaa S, Langford C, Yang F, Schuster SC, Carter NP, Harrow J, Ning Z, Herrero J, Searle SM, Enright A, Geisler R, Plasterk RH, Lee C, Westerfield M, de Jong PJ, Zon LI, Postlethwait

JH, Nüsslein-Volhard C, Hubbard TJ, Roest, Crollius H, Rogers J, DL. S (2013) The zebrafish reference genome sequence and its relationship to the human genome. Nature 496(7446): 498–503

31. Lieschke GJ, Currie PD (2007) Animal models of human disease: zebrafish swim into view. Nat Rev Genet 8:353–367
32. Kwan KM, Fujimoto E, Grabher C, Mangum BD, Hardy ME, Campbell DS, Parant JM, Yost HJ, Kanki JP, Chien CB (2007) The Tol2kit: a multisite gateway-based construction kit for Tol2 transposon transgenesis constructs. Dev Dyn 236(11):3088–3099
33. Ellett F, Pase L, Hayman JW, Andrianopoulos A, Lieschke GJ (2010) mpeg1 promoter transgenes direct macrophage-lineage expression in zebrafish. Blood 117(4):e49–e56
34. Hall C, Flores MV, Storm T, Crosier K, Crosier P (2007) The zebrafish lysozyme C promoter drives myeloid-specific expression in transgenic fish. BMC Dev Biol 7(42)
35. Henry KM, Loynes CA, Whyte MKB, Renshaw SA (2013) Zebrafish as a model for the study of neutrophil biology. J Leukoc Biol 94:1–10
36. Renshaw SA, Loynes CA, Elworthy S, Ingham PW, Whyte MKB (2007) Modeling inflammation in the zebrafish: how a fish can help us understand lung disease. Exp Lung Res 33: 549–554
37. Sieger D, Moritz C, Ziegenhals T, Prykhozhij S, Peri F (2012) Long-range Ca^{2+} waves transmit brain-damage signals to microglia. Dev Cell 22(6)
38. Jagadeeswaran P, Carrillo M, Radhakrishnan UP, Rajpurohit SK, Kim S (2011) Laser-induced thrombosis in zebrafish. Methods Cell Biol 101:197–203
39. Prajsnar TK, Cunliffe VT, Foster SJ, Renshaw SA (2008) A novel vertebrate model of Staphylococcus aureus infection reveals phagocyte-dependent resistance of zebrafish to non-host specialized pathogens. Cell Microbiol 10(11):2312–2325
40. Brown SB, Tucker CS, Ford C, Lee Y, Dunbar DR, Mullins JJ (2007) Class III antiarrhythmic methanesulfonanilides inhibit leukocyte recruitment in zebrafish. J Leukoc Biol 82(1):79–84
41. Enyedi B, Kala S, Nikolich-Zugich T, Niethammer P (2013) Tissue damage detection by osmotic surveillance. Nat Cell Biol 15: 1123–1130
42. Auer TO, Del Bene F (2014) CRISPR/Cas9 and TALEN-mediated knock-in approaches in zebrafish. Methods 14
43. Hruscha A, Krawitz P, Rechenberg A, Heinrich V, Hecht J, Haass C, Schmid B (2013) Efficient CRISPR/Cas9 genome editing with low off-target effects in zebrafish. Development 10
44. Moulton JD, Yan YL (2008) Using morpholinos to control gene expression. Curr Protoc Mol Biol 26(28):21–29
45. Milan DJ, Peterson TA, Ruskin JN, Peterson RT, MacRae CA (2003) Drugs that induce repolarization abnormalities cause Bradycardia in zebrafish. Circulation 107:1355–1358

Chapter 16

Metabolomic Applications to the Characterization of the Mode-of-Action of CDK Inhibitors

Martina Palomino-Schätzlein and Antonio Pineda-Lucena

Abstract

Cyclin-dependent kinases (CDKs) regulate cell cycle progression, and some of them are also involved in the control of cellular transcription. Dysregulation of these critical cellular processes, due to the aberrant expression of some of these proteins, is common in many neoplastic malignancies. Consequently, the development of chemical compounds capable of inhibiting the biological activity of CDKs represents an attractive strategy in the anticancer area. CDK inhibition can trigger apoptosis and could be particularly useful in hematological malignancies, which are more sensitive to inhibition of cell cycle and apoptosis induction. Over the last few years, a number of pharmacological inhibitors of CDKs (CDKIs) belonging to different chemical families have been developed, and some of them have been tested in clinical trials. Given the complexity of the role of CDKs in cell functioning, it would be desirable to develop new tools that could facilitate a better understanding of the new insights into CDK functions and the mode-of-actions of CDKIs. In this context, this chapter describes an experimental approach to evaluate the metabolic consequences of CDKIs at the cellular level based on metabolomics by NMR. More specifically, a description of a strategy to characterize the biochemical effects of CDKIs acting on mammalian cells is provided, including protocols for the extraction of hydrophilic and lipophilic metabolites, the acquisition of 1D and 2D metabolomic Nuclear Magnetic Resonance (NMR) experiments, the identification and quantification of metabolites, and the annotation of the results in the context of biochemical pathways.

Key words Cancer, CDK inhibitor, Metabolomics, Mode-of-action, Pathway analysis

1 Introduction

Cyclins are important regulators of cell cycle in both normal and transformed eukaryotic cells. Cyclins regulate the cyclin-dependent kinases (CDKs), which have a variety of functions within the cell including the regulation of cell cycle [1, 2]. Because control of cell cycle is an attractive target in cancer therapy [3, 4], inhibitors of CDKs (CDKIs) are being explored as a novel therapeutic class. Although regulation of cell cycle was the original motivation for the identification of CDK inhibitors [5], new insights into the mechanism of CDK inhibitor-mediated cytotoxicity have revealed roles of CDKs unrelated to cell cycle but important for the maintenance

Mar Orzáez et al. (eds.), *Cyclin-Dependent Kinase (CDK) Inhibitors: Methods and Protocols*, Methods in Molecular Biology, vol. 1336, DOI 10.1007/978-1-4939-2926-9_16,

of the cancer cell [6]. The complex and multifaceted role of CDKs in cell functioning would benefit from the introduction of new experimental approaches capable of providing a holistic view of the interplay between the different biological activities associated to CDKs. Furthermore, the progressive development of new CDKIs requires a much better understanding of the mode-of-action of these compounds [7]. In this context, it becomes necessary to introduce new tools capable of providing an in-depth insight about the different biochemical pathways involved in the response to this new class of chemotherapeutic agents.

Metabolomics, a comprehensive tool for monitoring biological systems, impacts on a number of important areas including drug discovery and development [8]. Metabolomics involves the analysis of small molecules present in biological samples and can lead to an improved understanding of small molecule's actions and to a better selection of pharmaceutical targets. This experimental approach has the possibility of transforming our knowledge of inhibitors' action through the examination of chemical-induced metabolic pathways associated to both the efficacy and the development of adverse drug reactions. The application of metabolomic approaches is particularly relevant in oncology [9]. The reason for that is that metabolic requirements of cancer cells are different from those of most normal differentiated cells. Because the metabolome captures the state of a cell, being a direct measure of protein activity, any observed changes in the metabolome as a result of the treatment with inhibitors would provide information on the inhibitor's activity and selectivity [10, 11].

An experimental approach for evaluating the cell metabolome of mammalian cells using metabolomics by NMR is described in this chapter. A description is provided of the procedures involved in the extraction of hydrophilic and lipophilic metabolites from cell cultures in the absence/presence of CDKIs, the acquisition of 1D ^{1}H-NMR metabolomic experiments leading to the measurement of the metabolic content of mammalian cells, and the chemical characterization of these metabolites. Furthermore, bioinformatic approaches for annotating and interpreting the results obtained in the absence/presence of CDKIs are also described.

2 Materials

2.1 Reagents

1. Sterile cell culture plates.
2. Sterile culture media for mammalian cell culture with filtered inactivated FBS.
3. Mammalian cell line.
4. CDKI stock solution in DMSO (aliquots stored at –20 °C).
5. Sterile cell scraper (BD Falcon).

6. Phosphate Buffered Saline (PBS): 137 mM NaCl, 2.7 mM KCl, 10.6 mM Na_2HPO_4, 1.4 mM KH_2PO_4, pH 7.4, filtered.
7. Methanol, LC-MS grade.
8. Liquid nitrogen.
9. Chloroform, LC-MS grade.
10. Water, LC-MS grade.
11. 3-(trimethylsilyl)-2,2′,3,3′-tetradeuteropropionic acid or TSP-d4 (Eurisotop).
12. D_2O 99 % D (Eurisotop).
13. NMR phosphate buffer: 100 mM NaH_2PO_4, 0.1 mM TSP-d4, pH = 7.4, solution in D_2O.
14. $CDCl_3$ 99 % D, with 0.0.3 % (v/v) tetramethylsilane (TMS), in capsules (Eurisotop).
15. NMR tubes, 5 mm, quality ≥100 MHz (Norell).

2.2 Equipment

1. Standard equipment for human cell culture.
2. Multiscan reader for 96-well plates.
3. Centrifuge for 15 ml tubes up to 13,000 × *g*.
4. Centrifuge for 1.5 ml tubes up to 13,000 × *g*.
5. Vortex.
6. Lyophilizer.
7. Speed vacuum concentrator.
8. Glass pipettes.
9. NMR spectrometer 400–600 MHz (Bruker).
10. NMR probe with inverse detection, nuclei: ^{1}H and ^{13}C (Bruker).

3 Methods

The analysis of the metabolic changes experienced by a mammalian cell culture in the presence of CDKIs requires a precise combination of cell biology approaches, advanced analytical methods and bioinformatics tools [12]. Cells will be exposed to an effective dose of the CDKI, and the growth and harvest conditions have to be optimized for the metabolite quantification by NMR [13], as first described (*see* Subheading 3.1) (Fig. 1). Afterwards, hydrophilic and lipophilic metabolites are extracted from the harvested pellet using a combination of different solvents (*see* Subheading 3.2). Frozen extracts are then prepared for NMR analysis and optimized 1D and 2D experiments are acquired and processed [14] (*see* Subheading 3.3). Finally, efforts are directed to the assignment of all relevant metabolites [15] and the identification of the metabolic pathways associated to the metabolic changes (*see* Subheading 3.4).

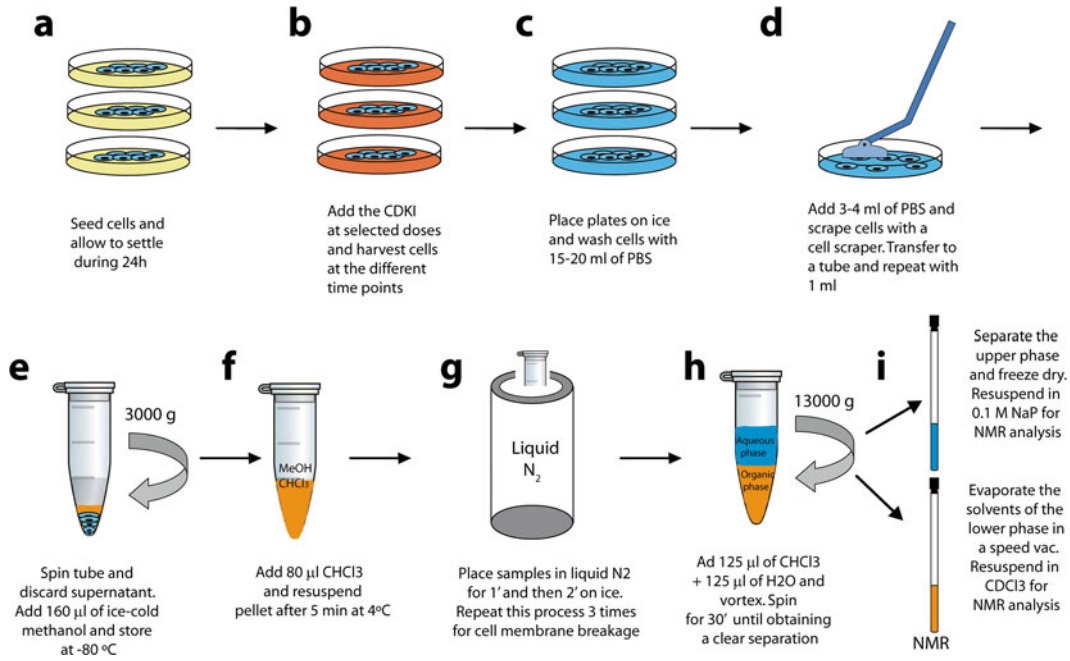

Fig. 1 Summary of the main steps that have to be carried out to obtain a metabolic extract in the presence of a CDKI including: cell culture (*a–b*), cell harvesting (*c–e*), metabolite extraction (*f–h*), and NMR sample preparation (*i*)

3.1 Cell Culture in the Presence of CDKIs

There are two key factors that have to be taken into account when studying the effect of a CDKI on a cell culture, the dose and the time point. Therefore, the cytotoxic effect of the CDKI should be first evaluated using a dose–response curve at different time points (*see* **Note 1**). An optimal way to perform the study is to choose at least two different time points and two different doses. This will facilitate the analysis of the effect of the inhibitor over time and the evaluation of the potential differences between doses (i.e., high and low cytotoxicity).

Depending on the cell type, cells may be either grown as a suspension or as adherent cell culture, with a slightly different harvesting protocol, as stated below. The number of cells that are finally harvested for each NMR sample should be between 1 and 20 million cells (*see* **Note 2**). The reliability of the final results required at least three independent cell cultures, each of them with 2–3 replicates, for each condition.

3.1.1 Cell Growth and Treatment

1. Seed cells in sterile p150 plates (*see* **Note 3**) at a concentration that has been optimized to have a 95–100 % confluence at the final time point.

2. Allow cells to settle for 24 h. In the case of adherent cells, it should be checked that cells are now well attached to the plate. This will be the initial time point.
3. Treat cells at the time points and doses previously defined with the CDKI of interest, previously filtered with a 0.2 μm filter. Control cells should be treated with the filtered vehicle at the same time points. Particular attention must be paid to avoid contamination of the cells during the treatment with the CDKI.

3.1.2 Cell Harvesting of Adherent Cells

1. Place plates on ice, remove the culture medium (*see* **Note 4**) and wash cells quickly with 15–20 ml of PBS.
2. Add small amount (3–4 ml) of PBS to the plates and scrape cells from the bottom of the plate with a cell scraper. Transfer the resulting cell suspension to a 15 ml tube. To collect the remaining cells, add again 1 ml of PBS to the plates, resuspend the remaining cells and add this suspension to the tube.
3. Spin the cell suspension at 3000 × *g* for 5 min at 15 °C and remove the PBS.
4. Add 160 μl of ice-cold methanol to the pellet to ensure that the metabolism is completely quenched [16].
5. Snap-freeze tubes in liquid nitrogen and store them at −80 °C (*see* **Note 5**).

3.1.3 Cell Harvesting of Cells in Suspension

1. Transfer the cell suspension to plastic tubes, centrifuge at 3000 × *g* and 15 °C, and remove the medium (*see* **Note 4**).
2. Add 15 ml of PBS to the pellets and vortex the tubes for 10 s. Spin tubes at 3000 × *g* for 5 min at 15 °C, and remove the PBS.
3. Add 160 μl of ice-cold methanol to the pellet to ensure that the metabolism is completely quenched.
4. Snap-freeze tubes in liquid nitrogen and store them at −80 °C (*see* **Note 5**).

3.2 Cell Extraction

Once cells have been collected, an extraction of the intracellular metabolites from the frozen pellets is performed. The optimal method for this procedure is the so-called chloroform-methanol extraction [17], based on the combination of polar and nonpolar solvents to extract hydrophilic metabolites (e.g., sugars, amino acids, organic acid, nucleotides) as well as lipophilic compounds (e.g., fatty acids, phospholipids, steroids). It is critical to follow the time periods described in the procedure and to ensure that cells are kept at a temperature ≤4 °C during the whole extraction procedure to achieve reproducible results.

1. Place frozen pellets corresponding to ten million cells (*see* **Note 6**) on ice and allow them to thaw for 5 min.
2. Add 80 μl chloroform previously cooled to 4 °C.

3. After 30 min, homogenize samples with a vortex, resuspend the pellet with a pipette and transfer the suspension to an eppendorf tube.
4. For uniform cell breakage, place the samples in liquid nitrogen for 1 min and then allow them to thaw on ice for 2 min. Repeat this step two more times (*see* **Note 7**).
5. Add 125 µl of distilled water and 125 µl of chloroform (both at 4 °C) and vortex the samples.
6. Spin samples at 13,000 × *g* for 20 min at 4 °C to obtain two phases (*see* **Note 8**):
   - An upper methanol/water phase (with hydrophilic metabolites, aqueous phase).
   - A lower chloroform phase (with lipophilic compounds, organic phase).
7. Transfer each phase into a separate tube:
   - Aqueous phase (top) is collected with a micropipette of 200 µl.
   - Organic phase (bottom) is collected with a glass pipette.
8. Spin each phase separately at 13,000 × *g* for 2 min at 4 °C and discard the remaining solvent from the other phase with a pipette.
9. Freeze the aqueous phase with liquid nitrogen and lyophilize it overnight to remove water and methanol.
10. Remove the solvents from the organic phase using a speed vacuum concentrator at room temperature (1 h).
11. Store sample extracts at −80 °C until sample preparation for NMR experiments.

3.3 NMR Experiments

To perform the NMR analysis of the metabolic profile of the cell extracts obtained in the presence of the CDKI, the cell extracts have to be dissolved in suitable NMR solvents. Most of the time, these solvents are deuterated to avoid the presence of extra signals in the ^{1}H NMR spectra. Aqueous solutions are usually buffered at a physiological pH value (by default 7.4) to avoid pH differences between samples, which may result in signal shifts in the spectra. Once NMR samples have been prepared, 1D spectra are acquired for all samples. It is critical to acquire all NMR experiments with the same parameters to facilitate a reliable comparison of the metabolites in different conditions.

After acquisition, NMR spectra have to be processed (*see* **Note 9**). A fundamental step is the referencing of all spectra to a specific signal (TSP and TMS at 0 ppm are normally used, but also other signals such as specific metabolites that are present in all samples may be used) to ensure that spectra are perfectly aligned before they are integrated.

3.3.1 Preparation of NMR Samples

1. Place samples on ice and allow them to thaw for 5 min.
2. Add 600 µl of phosphate NMR buffer to the aqueous phase and vortex the samples. Spin at 12,000 × *g* for 5 min. Transfer 550 µl of the supernatant into a 5 mm NMR tube (*see* **Note 10**).
3. Dissolve the organic extract in 600 µl of deuterated chloroform with 0.03 % TMS. Vortex the sample and then centrifuge at 12,000 × *g* for 5 min. Transfer 550 µl of the supernatant into a 5 mm NMR tube with a glass pipette.
4. NMR samples should be prepared the same day they are analyzed, and stored at 4 °C before the spectrum acquisition.

3.3.2 Acquisition of NMR Spectra

1. Place the sample inside the magnet and adjust the temperature to 27 °C. Allow the sample to equilibrate for 5 min.
2. Tune and match the probe for ^{1}H (and ^{13}C in the case of acquiring also 2D heteronuclear experiments).
3. Lock the sample for D_2O (aqueous phase) or $CDCl_3$ (organic phase).
4. Adjust the field homogeneity until obtaining a linewidth <1Hz for the TSP (aqueous samples) or the TMS (organic samples) signal.
5. Determine the ^{1}H 90° pulse.
6. For aqueous samples, acquire a 1D ^{1}H-NMR spectrum with presaturation over a region of 25 Hz and optimize the value of the center of the spectrum to minimize the water signal.
7. Acquire 1D NOESY spectra for all samples (*see* **Note 11**). Record an appropriate number of free induction decays (FIDs) providing a good signal to noise (S/N) ratio in minimal experimental time. Total experiment time should not exceed 30–60 min.
8. Select 1–2 representative samples from each sample group and acquire a 2D Total Correlation Spectroscopy (TOCSY) experiment and 2D Heteronuclear Single Quantum Correlation (HSQC) experiment (*see* **Note 12**).

3.3.3 Processing of NMR Spectra

1. Transform all spectra applying an exponential function with a 0.5 Hz line broadening factor (*see* **Note 13**).
2. Correct the phase of each spectrum with the manual phase option.
3. Reference the spectra to the TSP (aqueous samples) or the TMS (organic samples) signal at 0 ppm.

3.4 Analysis of Metabolomic Data

A comprehensive understanding of the metabolic consequences of the addition of CDKIs to a cell culture requires a thorough analysis of all the metabolites present in the aqueous and organic phases

obtained after the extraction procedure. This information is also required for performing statistical and quantitative analysis of the data. Therefore, the analysis of the metabolomic data generated in previous steps involves the assignment, quantification and characterization, in terms of their involvement in different biological pathways, of all the metabolites identified in the absence/presence of CDKIs.

3.4.1 Assignment of Relevant Metabolites

Metabolite assignment is usually performed using a combination of different approaches, including Analysis of Mixtures (AMIX 3.9.7; Bruker BioSpin, Karlsruhe, Germany), the SBASE compound library (BBIOREFCODE 2.0.0 database), the standard spectra database in HMDB 3.0 (http://www.hmdb.ca), as well as other existing public databases and literature reports. Ambiguities in the assignment of metabolites associated to severe overlapping of signals in the 1D ^{1}H-NOESY experiments are usually resolved using 2D ^{1}H-^{1}H-TOCSY and ^{1}H-^{13}C-HSQC. The assignment of key metabolites can be confirmed by a spiking procedure, based on the addition of the candidate metabolite to a sample and the acquisition of an NMR spectrum to confirm that the signals match the proposed assignment. Figure 2 shows as an example the assignment of MCF7 cells.

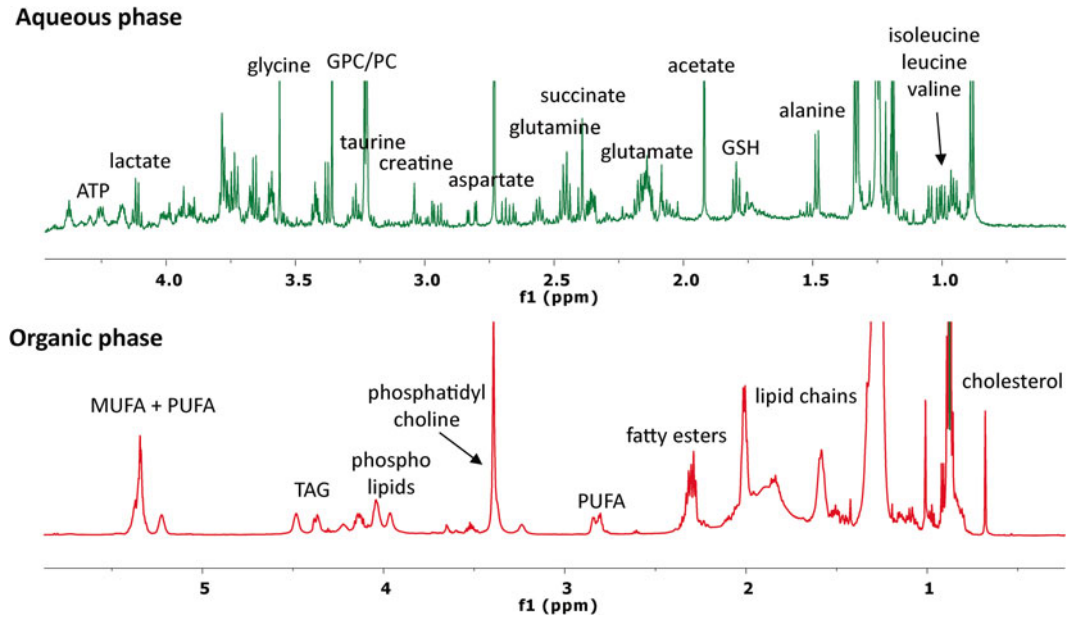

Fig. 2 1D ^{1}H-NMR spectrum obtained from the aqueous and organic extracts of MCF7 cells acquired with a 600 MHz NMR spectrometer with a TCI cryoprobe at 27 ºC in the absence of a CDKI. NMR assignment for some of the metabolites detectable in both phases is indicated. *GPC* glycerophosphocholine, *PC* phosphocholine, *GSH* reduced glutathione, *ATP* adenosine triphosphate, *MUFA* monounsaturated fatty acids, *PUFA* polyunsaturated fatty acids

3.4.2 Statistical and Quantitative Analysis

Once the metabolites detectable in the different extracts have been assigned, spectral regions corresponding to the different metabolites are automatically integrated. The statistical and quantitative analysis comprises the following steps:

1. Use the variable size bucketing module in AMIX 3.9.7 (*see* **Note 14**) to obtain the exact integral value corresponding to the NMR signal of each selected metabolite in each NMR spectrum (*see* **Note 15**).
2. Calculate an average fold change for each metabolite included in the analysis. This value is calculated as the ratio of average value in the cell culture exposed to the CDKI to that in the absence of the compound, indicating an overall change direction of the metabolite in both situations.
3. Perform an analysis of the statistical significance of the differences between the means of the two groups using the nonparametric Mann–Whitney *t* test. A *p*-value <0.05 (confidence level 95 %) is considered statistically significant.

3.4.3 Identification of Relevant Metabolic Pathways

Based on the results obtained in the previous steps, a molecular pathway and network analysis is performed to identify the key biological pathways that could likely explain the observed differences of the metabolic profiles in the presence of CDKIs. The analysis is carried out using Ingenuity Pathway Analysis (IPA; http://www.ingenuity.com), a web-based software application that identifies biological pathways and functions relevant to biomolecules of interest. This process consists of the:

1. Evaluation of the systematic influence of the treatment with CDKIs. This step is performed using MetaMapp [18] and the Cytoscape plug-in Metscape [19], and by uploading onto an IPA server the metabolites identified as statistically significant, as well as their change directions.
2. Evaluation of canonical pathways and molecular interaction networks based on the knowledge sorted in the Ingenuity Pathway Knowledge Base.
3. Display the ratio of the number of metabolites that map to the canonical pathway divided by the total number of molecules that map to the pathway.
4. Calculation of a *p*-value based on Fischer's exact test to determine the probability of the association between the metabolites and the canonical pathways.
5. Calculation of network scores with the right-tailed Fischer's exact test. The higher a score is, the more relevant the submitted metabolite is to the network.

This analysis should facilitate the identification of the most relevant molecular pathways associated to the response to CDKIs.

4 Notes

1. A typical cell viability assay can be performed with MTS (3-(4,5-dimethylthiazol-2-yl)-2,5-diphenyl-tetrazolium bromide). To carry out this experiment, cells are seeded into sterile 96-well microtiter plates at 25,000 cells/cm^2. Cells are allowed to settle for 24 h before the inhibitor, previously filtered with 0.2 μm filter, is added. Cells are treated with at least ten different concentrations of inhibitor within a range of 1:100. After 72 h of incubation, 10 μl MTS–PMS (20:1) are added to each well, and the cells are incubated for 2 further hours. Then, plates are read spectrophotometrically at 490 nm using a plate reader. Data are represented as the percentage of viable cells after the treatment, taken as 100 % of cell viability the untreated cells.
2. The number of cells that are required for each NMR sample depends on the cells size and has therefore to be optimized in each case. A factor that has to be taken into account is the kind of NMR spectrometer used for the analysis. If a strong field (600–800 MHz) equipment or cryoprobe is available, samples from 1 million or even 0.5 million cells will provide high quality spectra. However, lower fields (300–500 MHz) NMR spectrometers would require at least five million cells to obtain an adequate signal to noise ratio in a reasonable acquisition time.
3. In general, P150 plates are an optimal choice for metabolomic analysis by NMR. The amounts of PBS indicated at the cell harvesting step are adjusted for these plates. In the case of cells grown in suspension, these steps are adjusted to a T75 dish with 15 ml of medium. When smaller or bigger plates are used, the PBS volume should be slightly increased/decreased in order to achieve an efficient washing.
4. In some studies, the analysis of the metabolic profile of the culture medium can provide valuable information about the metabolites that are generated/consumed by the cells [20]. Therefore, it is advisable to store 1 ml of culture medium from each plate/flask at −80 °C, in case it may be needed later. Medium samples can be directly measured by NMR after mixing 300 μl of medium with 300 μl of PBS NMR buffer in an NMR tube.

   For adherent cell cultures, the culture medium should be always checked for the presence of cells in suspension resulting from detachment due to the treatment. If this is the case, then the culture medium should be treated following the procedure described in Subheading 3.1.3 and put together with the pellet of the adhered cells.
5. Cell pellets can be stored at −80 °C up to 6 months before performing the metabolite extraction. If several batches of cells

are grown, it is advisable to freeze the pellets, and extract and analyze all at the same time to reduce the variability associated to different extraction or NMR acquisition days.

6. The solvent volumes described in the extraction procedure are optimized for a pellet of ten million cells. When working with a significantly different number of cells, solvent volumes should be recalculated. This is important for two reasons; if an insufficient solvent volume is used, not all metabolites may be extracted, and if too much solvent volume is used, more cell proteins may be solubilized.
7. For a complete extraction of the metabolites, cell and organelle walls have to be completely broken during the extraction procedure. This breakage may already have taken place when cells are thawed after storage at −80 °C. Still it is important to carry out at least 1–2 freeze–thaw cycles to ensure a homogeneous cell breakage and higher reproducibility in the final data.
8. If no clear separation is observed, samples may be centrifuged again, but ensure that the same centrifugation time is applied for all samples.
9. If spectra are acquired using Bruker NMR spectrometers, than the software used for spectra acquisition and processing is TopSpin. Spectra integration can then be carried out with the complementary software AMIX, also from Bruker. Another suitable option for processing and integration is the program MestReNova, which reads raw data from different kind of NMR spectrometers.
10. It is advisable to use NMR tubes with a quality of at least 100–200 MHz to ensure that good field homogeneity and water suppression can be obtained for the NMR experiments.
11. Although the relaxation time filtered CPMG (Carr–Purcell–Meiboom–Gill) experiment is widely used for metabolomic samples, in the case of cell extracts, that do not contain many protein signals, a 1D NOESY spectrum is often sufficient for capturing the metabolic profile. Suitable parameters for this experiment are:
    - A NOESY mixing time of 10 ms.
    - A calibrated ^{1}H 90° pulse.
    - A relaxation delay of 3–4 s in order to ensure full relaxation and thus increase the reliability of the quantification of the metabolites.
    - An acquisition time of 2 s corresponding to a digitalization of 64 k data points and a spectral width of 30 ppm.
    - The same receiver gain (rg) value should be applied for all spectra, optimal values are between 64 and 256. Higher rg

values provide a better signal to noise ratio, but may cause baseline and phase problems when working with concentrated samples.

12. Suitable parameters for 2D experiments of cell extract samples are 256–512 increments in the indirect dimension and 32–96 transients in the direct dimension. In the case of the HSQC experiment, the sensibility enhanced variant with adiabatic pulses in ^{13}C provides an improved signal to noise ratio. TOCSY spectra can be recorded using standard MLEV or DIPSI pulse sequences with mixing times (spin-lock) of 60–80 ms.
13. When working with more diluted samples, also higher linebroadening factors (1–2 Hz) can be applied to achieve a better signal to noise ratio in the final spectrum. However, it should be taken into account that spectra transformed with higher linebroadening factors may suffer from a loss in resolution.
14. The variable size option of AMIX requires a pattern file with the regions of all assigned metabolites to be previously created.
15. The integration modes in AMIX allows the normalization of the signal integrals to total spectrum intensity (this option is useful to avoid the influence of dilution effects when samples of different cell concentration are analyzed) or to the intensity of a specific reference signal, for example the TSP signal (this option allows the calculation of the exact concentration of each metabolite in the sample).

References

1. Hirama T, Koeffler H (1995) Role of the cyclin-dependent kinase inhibitors in the development of cancer. Blood 86:841–854
2. Murray AW (2004) Recycling the cell cycle: cyclins revisited. Cell 116:221–234
3. Malumbres M, Barbacid M (2009) Cell cycle, CDKs and cancer: a changing paradigm. Nat Rev Cancer 9:153–166
4. Shapiro GI (2006) Cyclin-dependent kinase pathways as targets for cancer treatment. J Clin Oncol 24:1770–1783
5. Fischer PM, Gianella-Borradori A (2005) Recent progress in the discovery and development of cyclin-dependent kinase inhibitors. Expert Opin Investig Drugs 14:457–477
6. Bose P, Simmons GL, Grant S (2013) Cyclin-dependent kinase inhibitor therapy for hematologic malignancies. Expert Opin Investig Drugs 22:723–738
7. Blachly JS, Byrd JC (2013) Emerging drug profile: cyclin-dependent kinase inhibitors. Leuk Lymphoma 54:2133–2143
8. Nicholson JK, Lindon JC (2008) Systems biology: metabonomics. Nature 455:1054–1056
9. Spratlin JL, Serkova NJ, Eckhardt SG (2009) Clinical applications of metabolomics in oncology: a review. Clin Cancer Res 15:431–440
10. Wei R (2011) Metabolomics and its practical value in pharmaceutical industry. Curr Drug Metab 12:345–358
11. Powers R (2014) The current state of drug discovery and a potential role for NMR metabolomics. J Med Chem 57:5860–5870
12. Zhang A, Sun H, Xu H et al (2013) Cell metabolomics. OMICS 17:495–501
13. Aranibar N, Borys M, Mackin NA et al (2011) NMR-based metabolomics of mammalian cell and tissue cultures. J Biomol NMR 49:195–206

14. Barding GA Jr, Salditos R, Larive CK (2012) Quantitative NMR for bioanalysis and metabolomics. Anal Bioanal Chem 404:1165–1179
15. Wishart DS, Jewison T, Guo AC et al (2013) HMDB 3.0 – the human metabolome database in 2013. Nucleic Acids Res 41:D801–D807
16. Teng Q, Huang W, Collette TW et al (2009) A direct cell quenching method for cell-culture based metabolomics. Metabolomics 5: 199–208
17. Beckonert O, Keun HC, Ebbels TM et al (2007) Metabolic profiling, metabolomic and metabonomic procedures for NMR spectroscopy of urine, plasma, serum and tissue extracts. Nat Protoc 2:2692–2703
18. Barupal DK, Haidiya PK, Wohlgemuth G et al (2012) MetaMapp: mapping and visualizing metabolomic data by integrating information from biochemical pathways and chemical and mass spectral similarity. BMC Bioinformatics 13:99
19. Gao J, Tarcea VG, Karnovsky A et al (2010) Metscape: a cytoscape plug-in for visualizing and interpreting metabolomic data in the context of human metabolic networks. Bioinformatics 26:971–973
20. Duarte TM, Carinhas N, Silva AC et al (2014) ^{1}H-NMR protocol for exametabolome analysis of cultured mammalian cells. Methods Mol Biol 1104:237–247

INDEX

Mar Orzáez et al. (eds.), *Cyclin-Dependent Kinase (CDK) Inhibitors: Methods and Protocols*, Methods in Molecular Biology, vol. 1336, DOI 10.1007/978-1-4939-2926-9, © Springer Science+Business Media, LLC 2016

E

F

G

H

I

K

L

M

N

P

R

S

T

U

V

W

X

Z